2012

Molecular and Functional Characterization of Pyramidal Cell Types in the Frontal Cortex of Mouse Brain

Prerana Shrestha

MOLECULAR AND FUNCTIONAL CHARACTERIZATION OF PYRAMIDAL CELL TYPES IN THE FRONTAL CORTEX OF MOUSE BRAIN

A Thesis Presented to the Faculty of

The Rockefeller University

in Partial Fulfillment of the Requirements for the

degree of Doctor of Philosophy

by

Prerana Shrestha

June 2012

MOLECULAR AND FUNCTIONAL CHARACTERIZATION OF PYRAMIDAL CELL TYPES IN THE FRONTAL CORTEX OF MOUSE BRAIN

Prerana Shrestha, Ph.D.

The Rockefeller University 2012

Mammalian neocortex is the most complex structure in the brain. Considered the seat of executive function, the neocortex subserves diverse cognitive processes such as decision-making, motor planning, sensory discrimination and memory consolidation. The cellular heterogeneity of the neocortex makes it difficult to understand the molecular and cellular substrate of cognition during normal brain function and disease related dysfunction. A deep understanding of the contribution of the neocortex to behavior can best be achieved with reproducible access to genetically defined and functionally coherent cell populations. Using BAC modification strategy, we targeted distinct cell types in the neocortex for expressing effector molecules such as EGFP-tagged ribosomal protein L10 and Cre recombinase. We generated bacTRAP transgenic mice for six pyramidal cell types in the neocortex distinct by marker expression, areal/laminar topography, connectivity and cell morphology. These include corticocortical neurons in upper layer 2 of neocortex defined by genes Ntf3, Pdyn and Wfs1, corticostriatal neurons in layer 5a of lateral cortex expressing Etv1 and corticothalamic neurons in layer 6 of neocortex defined by Ntsr1 and Syt6.

We generated translation profiles of actively translated mRNAs in the targeted cell types with affinity purification of tagged polysomes and carried out quantitative comparative analysis of the cell types using the Specificity Index algorithm to identify cell type specific molecular repertoire. Besides the molecular profile and cellular morphology, pyramidal cell types can be characterized by connectivity and function at the level of circuitry as well as global behavior. Using Cre-inducible viral transduction of fluorophore (EGFP or mCherry), we were able to map the circuit of focal populations of three cell types defined by Ntsr1, Syt6 and Wfs1 in the visual cortex and anterior cingulate cortex respectively.

We then applied viral mediated silencing of neural transmission using viral tethered toxins that target voltage gated calcium channels (VGCCs) Cav2.1 and Cav2.2. We found that the Wfs1 cell type in the anterior cingulate cortex is necessary for the affective pain circuitry. Compared to control mice, the Wfs1 silenced mice exhibited a significantly reduced aversion to formalin-paired context in the formalin-conditioned place aversion paradigm but have intact pain sensitivity. Anterior Cingulate has previously been shown to be connected to the emotional center of the brain, the amygdale, and neural responses during pain perception have been recorded in the ACC. Hence we present supportive evidence that layer 2 Wfs1 cells in the anterior cingulate cortex are important for mediating affective pain.

In addition, we investigated a candidate gene, Wfs1, enriched in the translational profile for Ntf3 cell type in the neocortex and studied behavioral phenotype of mice harboring cortex specific deletion of Wfs1. The Wfs1 Cortex KO mice were anhedonic and were impaired in their preference for sucrose, which is normally considered more pleasurable than water. The KO mice also exhibited compulsive responding in the three-choice operant conditioning task.

In conclusion, this dissertation presents evidence that BAC transgenesis can be applied to genetically access pyramidal cell types in the neocortex for molecular profiling as well as functional characterization using silencing viruses and conditional alleles. We also showed direct utility of TRAP data in elucidating cortex specific contribution to the complex neurological disorder, Wolfram Syndrome. Therefore, a combination of specific gene driver selection, BAC transgenesis methods and functional modulatory strategies can give us valuable insight into the underlying neuronal circuitry in the cortex responsible for distinct behavioral outputs, physiology and pathophysiology.

For my late grandfather Meher Sundar Shrestha

ACKNOWLEGEMENTS

Like Henry Drummond said, “The people who influence you are the people who believe in you”. I have been fortunate in my life to come across remarkable and generous individuals who have given me inspiration to move ahead in life while at the same time believing in me even when I myself was in doubt. Pursuing a doctorate requires not just a passion for science but a lot of perseverance, determination and encouragement from people you respect and luck. At this juncture in my life, having completed the requirements for the Ph.D., I look back and find so many people I should be grateful to.

First, I would like to thank my advisor, Prof. Nathaniel Heintz. Nat has been a great mentor who was always available and helpful with his scientific insight and allowed me the freedom to pursue big ideas in his lab. I am really grateful to Nat for giving me his time and guidance throughout my student life at Rockefeller. I would like to thank my thesis committee members Prof. Timothy Ryan (Chair), Prof. Robert Darnell, Prof. Nathaniel Heintz and Prof. Gordon Fishell for taking their time to guide me through my thesis, helping me see the big picture and figuring out how to fit the pieces of work into one coherent thesis.

I would not have been able to accomplish any of these if I had not had the support of my mother Maiya Shrestha and my father Mangal Shrestha, who have always been there for me and just a phone call away. My father, a photographer in Nepal, always told me to pursue any career that I want but be really good at it. My mother, a storekeeper and home-maker, supported me in all my endeavors with unfaltering love and encouragement, even from thousands of miles away.

I am blessed to have great siblings in Manish Shrestha, Madhup Shrestha and Hima Shrestha, and for their support, I will forever be grateful.

I would like to thank my previous mentors Prof. John Blenis, Sharon Lebowitz, Dr. Francine Blei and Prof. Pam Baker for instilling confidence and giving me valuable advices to pursue science as a career. I would like to thank my dear friends Rana Anjum, Maria Joachim, Kamal Thapa, Miriva Magar, Sarana Shrestha and Pratikshya Bohra for their friendship and standing by me throughout my Ph.D. years. I would also like to thank my labmates and friends Jenna Rimberg, Miho Nakajima, Pinar Ayata, Dr. Eric Schmidt, Dr. Erika Andrade, Dr. Elizabeth Heller, George Skabardonis, Dr. Joseph Doyle, Dr. Joseph Dougherty, Dr. Skirmantas Kriacionis, Dr. Noah Gray and Dr. Ines Ibanez-Talon for their scientific advices and good times in the lab. I would also like to thank Cristian Rosario and Marta Delgado in the Dean's Office for their help during the preparation of this dissertation.

Finally, my husband Dr. Sameer Raj Maskey having got his Ph.D. in Computer Science from Columbia understood the rigor of graduate school and was there for me throughout the ups and downs of science. I am grateful for his love and honesty that helped me grow as a person and as a scientist.

TABLE OF CONTENTS

LIST OF FIGURES:

CHAPTER 1:

GENETIC TARGETING OF SPECIFIC PYRAMIDAL CELL TYPES IN NEOCORTEX BY BAC ENGINEERING

1.1 Molecular classification of pyramidal cell types in the neocortex

1.1.1 History of Molecular markers for Neocortex

Mammalian neocortex is a complex structure consisting of a host of heterogeneous cell types that subserve a diverse array of cognitive functions including decision-making, motor planning, sensory discrimination and consolidation of long term memory. For a long time, the heterogeneity of cell types has eluded our understanding of the molecular substrate of different cognitive functions and pathophysiology. Classical neuroanatomical studies by Santiago Ramon Y Cajal (Ramon, 1899) and Raphael Lorente de No (Lorente de No, 1934) were pioneering efforts into defining the diverse neuronal cell types in the cerebral cortex using Golgi stains to reveal the morphological parameters of the neurons. Even today, we use some of the same nomenclature such as pyramidal, stellate, granular etc. that these pioneers used in their study. Continued efforts have been underway for the last century to define and characterize cell types in the neocortex. Researchers have used antibodies to label different cell types by histological methods as well as injected retrograde and anterograde tracing dyes directly into the brain to fill up axons of the neuronal cell types (Lund et al., 1975; Rockland and Pandya, 1979). These approaches gave insight into the classification of some classes of neurons and the direction of the cortical feedback and feedforward pathways but paucity of markers for cortical cell types limited the identification and analysis of neuronal classes. In the last ten years, there has been a lot of progress in the identification of markers for different cell types in the neocortex mainly with the large scale efforts into mapping the expression of thousands of genes in the CNS including Gene Expression Nervous System Atlas (GENSAT), Allen Brain Atlas (ABA) and BGEM (Gong et

al., 2003; Hatten and Heintz, 2005; Lein et al., 2007). While ABA and BGEM are large-scale efforts at producing digital atlas of gene expression by in situ hybridization of gene specific probes, GENSAT is a large-scale effort at generating BAC transgenic mouse lines that express EGFP reporter under the transcriptional control of gene specific promoter. These digital atlases have uncovered a wealth of information for screening potential gene candidates for definition of distinct cell types in different brain regions including neocortex. As such the discovery of cell types in the neocortex is ongoing.

In some regions of the brain, such as the retina and the spinal cord, major subtypes of neurons have already been defined on the basis of similarities in morphological and physiological properties (Jessell, 2000; Livesey and Cepko, 2001). The classification of neurons in these structures has benefited from their relatively tractable histological structure and more importantly, the identification of molecular markers to genetically access the different neuronal classes. In comparison, the mammalian neocortex is much more complex with an estimate of at least a thousand cell types and there are not many validated molecular markers of cell types in the neocortex. It is well established that neurons in the neocortex are divided broadly into two major classes – pyramidal cells and interneurons (Bannister, 2005; Shepherd, 2004). Pyramidal cells, also known as the projection neurons, represent roughly 70% of the total cell population in the neocortex. They project to local and distant targets in the brain and use glutamate as their main neurotransmitter and thus are excitatory by definition. Interneurons are also referred to as inhibitory non-pyramidal cells represent about 20% of the cells in the neocortex (Molnar and Cheung, 2006). The interneurons project locally and use GABA as the main neurotransmitter.

During development, these different classes of neurons arise from different neuroepithelial compartments – the pyramidal cells are generated in the cortical neuroepithelium and migrate radially to reach the cortex following usually an inside-out gradient while most interneurons originate from basal telencephalon and migrate to the cortex through tangential migration (Marin and Rubenstein, 2001; Parnavelas, 2000; Rakic, 1988). Theses neuronal classes can be further subdivided into distinct cell types based on the following criteria 1. Cytoarchitectonics (topographical distribution of the cells in the cortex) 2. Cellular morphology (e.g. size and shape of soma) 3. Hodology (projection of the axons) 4. axodendritic morphology (shape, orientation and length of the cellular processes) 5. electrophysiological behavior and 5. molecular signature (combinatorial array of molecules expressed in the cells). Different groups of researchers have used each or a combination of these criteria to identify different groups of neurons in the neocortex. A remarkable study by Yuste and colleagues showed that multidimensional cluster analysis of different morphological parameters of the cell soma and processes reveal at least five classes of neurons within the deep layer 5 of visual cortex (Tsiola et al., 2003). Other research groups have used the criterion of hodology to define and characterize the gene expression profile of pyramidal cell classes by injecting retrograde fluorescent microbeads into the target projection site and isolating the back-labeled cells in the cortex (Arlotta et al., 2005). Still others have defined cell classes in the neocortex by their electrophysiological behavior and isolated transcripts from single cells to correlated gene expression profile (Sugino et al., 2006).

1.1.2 Organization of the Neocortex

The neocortex, although cellularly heterogeneous, has relatively well-defined cytoarchitectonic topography. There is wide consensus on the laminar structure of the neocortex along the radial axis but the fine areal structure along the tangential axis is still being redefined. Cajal (Ramon, 1899) first described the laminar structure in the human neocortex and Lorente de No (Lorente de No, 1934) followed it up with excellent neuroanatomical analysis of the cortical layers in mouse neocortex (Fig 1.1). The mammalian neocortex can be divided into six layers whereupon the layer 4 defines the major input layer for thalamocortical input and layer 5 defines the major output layer that sends long distance subcortical and callosal projections. The superficial layers 2 and 3 are involved in corticocortical connectivity and provide two-thirds of the input to all neurons in the cortex, while the deepest layer 6 is primarily important for sending feedback to the thalamus (Shepherd, 2004). Generally the time of neurogenesis in the ventricular zone regulates the laminar location of neurons. The 'inside-out' gradient of cortical neurogenesis was first reported in 1961 (Angevine and Sidman, 1961) and it laid out the framework that cells that leave the cell cycle earlier form the deeper cortical layers where as the cells that are born later form progressively more superficial layers. However, birthdating results suggest that laminar fates are more closely related to molecular phenotypes than the birthdays. For instance, as study (Hevner et al., 2003) showed that several different molecular kinds of neurons are borne on the same day of corticogenesis, yet they occupy a different laminar location based on the expression of the molecular marker.

In the last several decades, laminar fate has dominated the classification of cortical architecture and different pyramidal cell groups, however it has become increasingly clear that more precise definitions are needed for at least two reasons – 1. Different cell types occupy the same laminar fate and 2. The laminar structure varies across the cortex in terms of the thickness of each layer and cytoarchitectonics within the layer. For the same reason, we decided to focus on cell populations in distinct functionally and hodologically defined regions within the neocortex. These regions, parcellated along the tangential axis and referred as cortical 'areas' (a term that came into practice since Korbinian Brodmann used it in his classic papers in 1909), can be categorized into three main divisions – sensory cortices, including primary somatosensory cortex, primary auditory cortex and primary visual cortex, motor cortices including the primary motor cortex, and association cortices that includes the prefrontal cortex and secondary motor cortex (Fig 1.1). In the case of human cortex, Brodmann areas 1, 2 and 3 belong to the primary somatosensory cortex, area 4 to primary motor cortex, area 17 to primary visual cortex and areas 41 and 42 to primary auditory cortex. Similarly, higher order functions of the association cortical areas are also consistently localized to the same Brodmann areas by neurophysiological, functional imaging and other methods. In the same vein, Lorente de No (Lorente de No, 1933) divided the mouse neocortex into different cortical areas and in the decades that followed, researchers modified the designated parcellations of the neocortex, the current well-accepted nomenclature and areal divisions being the Franklin and Paxinos Atlas for mouse brain (Paxinos and Franklin, 2004) (Fig 1.1).

Arealization of the cortex is a crucial event during embryonic development because the areas form the bases for distinct cortical functions such as sensory processing, motor output planning

and goal direction behavior. The cortical areas are specified during development, presumably according to the protomap hypothesis where cues that specify particular areas act on cortical progenitor cells. It is proposed that the same families of signaling molecules that pattern other parts of the embryo also establish the spatial coordinates of the protomap (Rash and Grove, 2006; Sur and Leamey, 2001). Morphogens such as Fgf family members, BMPs, Wnt proteins, as well as transcription factors including Emx2, Pax6, Otx1, Etv1 and COUP-TF1/ Nr2f1 are candidate mediators of the protomap formation (Sur and Leamey, 2001). Areas were first identified by cytoarchitecture, including layer organization, which reciprocally differs by area. For instance, the prominent layer IV in S1 consists of columnar units called barrels that guide thalamic axons to their target. Also, neuronal projections are pruned during development according to their areal identity. For instance, corticospinal projections initially arise from a large part of the neocortex including visual cortex, but are pruned back to become area-specific to the more rostral parts. The cortical areas develop in a rostrolateral to caudomedial gradient and while some transcription factors such as Tbr1 may be essential for early specification, they may not useful as markers in adults due to decreased laminar specificity and overall expression. Other developmental transcription factors such as Etv1 and Rorb remain highly laminar specific throughout the postnatal period and into adulthood, and serve as good markers for their respective cell types (Hevner et al., 2003).

1.2 Prefrontal Cortex in Mice

The anterior part of the neocortex, also known as the prefrontal cortex (PFC) is the most expanded neocortical region in primates. Long after Brodmann studies, the prefrontal cortex was

considered unique to the primates since it was defined by the presence of the granular layer IV. However, this granularity-based definition came into question when it was found that primary motor cortex in rats is granular but the homologous region is agranular in primates. Over time, the criterion for the definition of prefrontal cortex was modified to be the cortical region that receives afferents from the mediodorsal thalamus (Rose and Woolsey, 1949). But this definition was inadequate because the prefrontal cortex receives projections not only from the mediodorsal thalamus but from a host of other thalamic nuclei as well, as evident from many tracer studies. The current bench standard is the set of criteria laid out by Uylings (Uylings et al., 2003), which includes the pattern of specific neuronal connections, the functional i.e. electrophysiological and behavioral properties, embryological development and cytoarchitectonic features for closely related species. The rodent neocortex is about 1000 times smaller than a human neocortex (Rakic, 2009), so the cytoarchitectonic feature comparison begs the question of whether all the correlates of human PFC are present in the rodents. The primate PFC is divided into three major divisions – dorsolateral, medial and orbital regions, each with a categorical cognitive function.

The defining function of PFC is goal directed behavior – involving an executive system that plans and selects behavioral patterns (Coutureau and Killcross, 2003). Much of the information about the functions of different subregions of PFC comes from lesioning studies in humans, primates and rodents. One of the first documented case studies of PFC damage was that of Phineas Gage, a railway construction worker who suffered a massive frontal lobe damage in an explosion that plummeted an iron rod into his skull (Damasio et al., 1994). While he was touted as a miraculous survivor of the accident with core behaviors and motor abilities intact, it was soon realized that his personality had altered and he had become more indecisive and socially

abusive. In the years that followed, lesions in different PFC regions gave insight into their functions (Coutureau and Killcross, 2003; Gourley et al., 2010; Killcross and Coutureau, 2003; Ostlund and Balleine, 2007a, b; Ragozzino et al., 1999).

In mice, there are three distinct regions in the PFC – 1. medial PFC, 2. anterior Cingulate and 3. orbitofrontal cortex (Fig 1.2) (Van De Werd et al., 2010). The functional connectivity suggest that the homologous correlate of primate dorsolateral PFC, important for working memory, consolidation of fear extinction memory and extradimensional shift of attention, is the medial PFC which is further subdivided into prelimbic cortex (PL) and infralimbic cortex (IL) (Uylings et al., 2003; Van De Werd et al., 2010). Damage to the anterior cingulate cortex (ACC) is characterized by deficits in behavioral disinhibition, pain perception and motor sequencing of behavior (Bussey et al., 1996; Muir et al., 1996; Rushworth and Behrens, 2008). On the other hand, damage to the orbitofrontal cortex (OFC) results in impairments in behavioral inhibition, social behavior, stimulus-reward association and odor and taste related working memory (Gourley et al., 2010).

Often diseases of the human neocortex show restricted lamina or cell type specific degeneration. For instance, the size of layer III large pyramidal cells are reduced in Schizophrenia patients, while Reelin expression deficits are mainly found in superficial layers. Also cortical lamination deficits have been observed in lissencephaly, different forms of heteropia, autism and intractable epilepsy (Arion et al., 2007). The dysfunction of PFC is implicated in a host of neurodegenerative diseases such as Frontotemporal Dementia, Depression, Addiction, Attention Deficit Hyperactivity Disorder (ADHD), Tourette Syndrome

and Schizophrenia (Sotres-Bayon et al., 2004). Thus to understand the pathophysiology of these neocortical disorders, it is important to investigate the key molecular players that define the cell types affected in different disorders. Till date, there are very few molecular markers known for pyramidal cells in the PFC. Several morphogens and transcription factors have been characterized to play an essential role in cortical area specification during embryonic development but most of those genes are not necessary for adult neuronal circuitry and maintainence in the neocortex.

We have taken the approach of bacterial artificial chromosome (BAC) transgenesis to access and characterize distinct cell types within the PFC. The precise and efficient engineering of BACs can facilitate a variety of studies that cannot be readily accomplished using conventional approaches (Hatten and Heintz, 2005; Heintz, 2000, 2001; Yang et al., 1997). The targeted BAC can be used to specifically express large marker genes, recombination enzymes, toxins, tract-tracing proteins, dominant-activating or dominant negative alleles or multiple combinations of these elements using internal ribosome entry sites (IRES). These modifications are introduced into the BAC by homologous recombination as described in previous lab publications. To achieve proper expression of a BAC transgene, a BAC should be chosen with the gene centered on its insert, and ~50 kb of 5'- and 3'- flanking DNA. As the carrying capacity of BACs is several hundred kilobases, and an average mammalian gene is < 50 kb, it is possible to choose a BAC that contains all the regulatory sequences necessary for accurate expression of the transgene.

RESULTS

1.3 Screen for Pyramidal Cell Type Markers in the Prefrontal Cortex

Studies on the function and connectivity of PFC have for the large part based on anatomy and lesioning of cellularly heterogeneous region within PFC. The cellular heterogeneity of PFC complicates the interpretation of the functional perturbations resulting from lesioning. So far, there have not been any studies undertaken to characterize distinct cell types in the prefrontal cortex, owing both to the lack of good molecular markers and a paucity of transgenic mice that target specific cell types in the PFC. In order to select molecular markers for cell types enriched in the PFC, we digitally screened candidate genes in the online gene expression databases including GENSAT GFP-reporter mouse database (Gong et al., 2003) (www.gensat.org) and Allen Brain Atlas In Situ Hybridization database (Lein et al., 2007) (www.brain-map.org) as well as consulted published literature on cortical pyramidal cell markers. We scored genes qualitatively in these online resources for three measures: 1. genes enriched in the prefrontal cortex, 2. genes with a negative rostrocaudal (RC) gradient and 3. genes with laminar expression in the Neocortex. The score of a given gene was higher if it had matching expression pattern when probed in the ABA ISH database as well as the GENSAT reporter mouse database. We shortlisted the candidates for gene drivers with a total of 16 genes for prefrontal cortex, 3 genes for RC gradient and 2 genes for laminar expression pattern (Fig 1.3). Out of the shortlisted candidates, we carried out the bacterial artificial chromosome (BAC) transgenesis for 11 genes namely Cxcl11, Drd4, Epha2, Hspb8, Htr2a, Irx3, Ntf3, Pdyn, Etv1 and Syt6, based on specificity of expression and interesting gene function.

Following the established BAC homologous recombination strategy, BACs containing most of the regulatory sequences for the selected genes were modified with EGFP tagged ribosomal protein L10 transgene. Instead of a typical reporter EGFP or the likes, we modified the BACs with EGFP-L10 so that we could not only analyze the neuronal anatomy of cell types expressing the reporter but also extract cell type specific transcripts for detailed analysis of the molecular profile of the cell type. Once the BAC transgenic founder mice were generated, they were individually characterized by histochemical methods and evaluated for how well the pattern of reporter expression matches the expected endogenous gene expression. It is beyond the scope of this dissertation to discuss the details of all the candidate genes for which BAC modifications were attempted without success. Possible explanations are: position effect from the genomic site of integration, low BAC copy number combined with transcription inefficiency of the promoter, high BAC copy number leading to ectopic expression or that the regulatory sequences are distant from the gene and not included in the corresponding BAC. However, modification of four BACs corresponding to four different genes led to mouse transgenic lines that recapitulated the endogenous gene expression pattern. These genes are: 1. Neurotrophin-3 (Ntf3), 2. Prodynorphin (Pdyn), 3. Ets Variant 1 (Etv1) and Synaptotagmin 6 (Syt6). These different BAC transgenic lines target distinct cell types in nonoverlapping areas in the neocortex. Ntf3 and Pdyn specify gene drivers for layer II corticocortical pyramidal cells in the orbitofrontal cortex (OFC) and Prelimbic Cortex (PL)/ Anterior Cingulate (ACC) respectively. Etv1 specifies the gene driver for layer Va corticostriatal pyramidal cells in the rostrolateral cortex where as Syt6 specifies the gene driver for layer VI corticothalamic pyramidal cells in the rostromedial cortex.

1.4 Genetic access to Prodynorphin Cell Type, Layer II Pyramidal Cells in the Anterior Cingulate Cortex (ACC)

Prodynorphin (Pdyn), also known as Preprodynorphin, is the precursor for all six members of the dynorphin family of opioid peptides including alpha-neoendorphin, beta-endorphin, dynorphin A, dynorphin A-17, dynorphin B, and dynorphin B-29 (Sharifi et al., 2001). The dynorphins bind preferentially to the Oprk1 kappa receptors and to a lesser extent at mu Oprm and delta Oprd receptors. Dynorphins have potent effects on mood and reward and drugs of abuse such as cocaine have been shown to modulate dynorphin activity in the striatum. The levels of dynorphin are also regulated by levels of the neurotransmitter dopamine (Hurd et al., 1999) as well as complex seizures (Romualdi et al., 1999a; Romualdi et al., 1999b). Loss of Pdyn results in deficits in stress induced analgesia (Clarke et al., 2003). The Prodynorphin gene (ID: 18610) is located in chromosome 2 and is flanked by immediate neighboring genes, Sir-alpha at 5' end and Gm14046 at 3' end. The in situ hybridization images in the Allen Brain Atlas database showed a strong expression of Pdyn mRNA in Layer II cells in the medial PFC and Anterior Cingulate Cortex (Fig 1.4). Apart from the cortical expression, Pdyn mRNA was also highly enriched in the Caudate Putamen as well as the Hypothalamus. This pattern of Pdyn gene expression concurs with the literature. Expression profile for Pdyn-EGFP BAC transgenic mice at the GENSAT database agrees well with the cortical Pdyn RNA distribution. Additionally since the reporter EGFP fills up the entire cell body including the axonal projections, it can be figured out the Pdyn positive neurons in layer II of PFC define corticocortical projection neurons.

We used the same Pdyn BAC RP23-358G23 for the EGFP-L10 modification as the one used for generation of EGFP BAC transgenic mice (GENSAT). The chosen Pdyn BAC incorporates 199,507 bp of genomic DNA at the plus strand of Chr 2: 129,470,806 – 129,670,312 bp. An 800 bp region immediately upstream of translational start codon was PCR amplified and cloned into a building shuttle vector next to the EGFP-L10 transgene. The Pdyn A box-EGFP-L10 transgene cassette was the basis for E.coli based homologous recombination where upon the A box was used as a homology region. The modified Pdyn EGFPL10 BAC was injected into the pronuclei of fertilized mouse oocytes, which then randomly integrated into the mouse genome in a concatenated form with variable copies of the BAC. We got one good founder CP12 for Pdyn EGFPL10 BAC transgenic mice, which expressed the transgene EGFP-L10 in the pyramidal cells residing in the top of layer II in the PFC (Fig 1.4). Using relative qPCR with an EGFP-L10 Knock-In mouse as a baseline (single copy), we determined that CP12 founder line has 4 ± 0.85 SEM copies of the Pdyn EGFP-L10 BAC (Fig 1.4). As expected for the distribution of ribosomes, the EGFP-L10 i.e. the reporter fused to the essential ribosomal protein L10, is localized to the cytoplasm in the cell body and in the nucleolus but is largely absent in the neuronal processes and nucleoplasm. Besides the neocortex, the reporter is also expressed in the medium spiny neurons of the caudate putamen of the ventral striatum and in the arcuate nucleus of the hypothalamus. Given the relative sparse distribution of the Pdyn cell type and medium levels of expression of the transgene, we decided to characterize the cell type but did not include the cell type for the comparative analysis of the distinct areal pyramidal cell types.

1.5 Genetic access to Neurotrophin-3 Cell Type, Layer II Pyramidal Cells in the Medial PFC and Orbitofrontal Cortex (OFC)

Neurotrophin-3 (Ntf3), first discovered in 1990, is a member of the neurotrophin family of growth factors that serve multiple functions both in the developing and adult nervous system (Segal, 2003). Although originally defined as neuronal survival factors, neurotrophins elicit many biological effects including proliferation, synaptic modulation and axonal pathfinding (Farinas et al., 1994; Klein, 1994; Nickl-Jockschat and Michel, 2011; Poo, 2001; Russo et al., 2009; Schnell and Schwab, 1993; Topic et al., 2008). Ntf3 forms a small 27 KDa polypeptide that undergoes homodimerization and binds preferentially to tyrosine receptor kinase C (TrkC) and also to p75NTR with low affinity. Substrate binding leads to TrkC dimerization and therefore to trans-autophosphorylation at two tyrosine residues in the cytoplasmic domain of the receptor, activating the intracellular signaling cascades, mainly Ras/ Raf/ ERK cell proliferation pathway and PI3K cell survival pathway (Nickl-Jockschat and Michel, 2011). Both Ntf3 and TrkC are highly expressed in multiple tissues during embryonic development (Farinas et al., 1994). Mice lacking Ntf3 have severe deficits in sensory and sympathetic populations, since Ntf3 is essential for survival of sympathetic and sensory neurons during embryogenesis, which later become dependent on other neurotrophins such as nerve growth factor (NGF) or brain derived neurotrophic factor (BDNF) (Farinas et al., 1994; Poo, 2001). Ntf3 has been implicated in neurological disorders such as Depression and Autism (Nickl-Jockschat and Michel, 2011). It is reported that levels of Ntf3 in the Dentate Gyrus of hippocampus decrease upon exposure to long term immobilization stress (Duman and Monteggia, 2006). Also, recent studies indicate that an Autism susceptibility gene Caps2, which is enriched in synaptic vesicles of parallel fibers in

granule cells, is associated with Ntf3 along with BDNF, and induced overexpression of Caps2 leads to an increase in the depolarization-induced release of Ntf3 and Bdnf (Nickl-Jockschat and Michel, 2011). The Ntf3 gene (ID: 18205) is located in chromosome 6 (126,043,000 - 126,125,000) and is flanked by neighboring genes Ano2 at the 3' end and Kcna5 at the 5' end. The in situ hybridization images in the Allen Brain Atlas database at first glance seemed to have no signal for the Ntf3 mRNA in the neocortex but only in the Dentate Gyrus. However upon closer inspection, a higher enrichment of the probe was visible in layer II of the medial PFC and OFC and in the Infralimbic Cortex (IL) in slightly caudal sections. But the laminar expression of Ntf3 was much more compelling in a paper by Miyashita et al (Miyashita et al.) where they did colorimetric ISH of Ntf3 in rat neocortex. Likewise, GENSAT database supported the expression pattern of Ntf3 in layer II of neocortex and it was evident that the Ntf3 cell type defines corticocortical pyramidal cells with their apical dendrites reaching out to the molecular layer I (Fig 1.6).

We used the same Ntf3 BAC RP23-79E22 for the EGFP-L10 modification as that used for generation of Ntf3 EGFP BAC transgenic mice (GENSAT). The selected Ntf3 BAC incorporates 170,202 bp of genomic DNA at the minus strand of Chr 6: 125,999,011-126,169,212). A 711 bp region immediately upstream of translational start codon (TSC) was PCR amplified using the Forward primer (5' - GGCGCGCCTAGACAGCTTGAACTAACTGTG) and Reverse primer (3' – CTGCTGGGTAAGGAGAGGAGCCTT) and cloned into the shuttle vector pS296 next to the EGFP-L10 transgene. The Ntf3 A box-EGFP-L10 was then homologously recombined from the shuttle vector to the Ntf3 BAC right before the Ntf3 TSC in recombination competent E. Coli

cells. The modified Ntf3 –EGFPL10 BAC was injected into the pronuclei of fertilized mouse oocytes, which then randomly integrated into the mouse genome in variable tandem repeats. We got four founders - PS1045, PS1046, PS1049 and PS1052 – for Ntf3 EGFPL10 BAC transgenic mice, which expressed the transgene EGFPL10 in the neocortical cell type in a BAC dosage dependent manner. Out of six founders, we decided to characterize the neuronal anatomy of three of the founders – PS1045, PS1046 and PS1049 since they recapitulated the expression pattern of Ntf3 in a subregion of PFC (PS1045), accurately as the endogenous pattern (PS1046) or provided an illustration of the correlation of high BAC dosage to ectopic expression in the cortex (PS1049). Using relative qPCR with an EGFP-L10 Knock-In mouse as a baseline (single copy), we determined that PS1045 founder line has 15 ± 0.912 (Mean ± SEM) copies, PS1046 has 4 ± 0.912 copies, PS1049 has 7 ± 0.959 copies and PS1052 has 6 ± 0.629 copies of Ntf3 EGFP-L10 BAC (Fig 1.4).

1.5.1 Characterization of Ntf3 EGFP-L10 BAC Transgenic Founder Line PS1045

The Ntf3 founder line PS1045 represented the highest copy (15 ± 0.912) BAC transgenic line among the four founders. However, the expression pattern of EGFP-L10 in the PS1045 line was remarkably restricted in the neocortex to medial OFC and Anterior Cingulate Cortex (ACC). It is possible that the genomic integration site of the concatenated BACs in this line influences the neocortical expression of the transgene outside of the PFC. The high copy number of the BAC in this line is reflected in strong direct EGFP epifluorescence. Besides the PFC, the reporter is also expressed in layer II of Piriform Cortex, medial Olfactory Bulb, Dentate Gyrus and dorsal Septum as evident in the global CNS expression profile carried out with DAB

immunostaining in whole brain sections (Fig 1.7). Only the Ntf3 cell type in the medial PFC and OFC were of interest, so during further analysis by tissue extraction, the Piriform Cortex together with the subcortical regions were excised out. The Ntf3 cell type in the CNS defines a neuronal population, as evident from the colocalization of NeuN and GFP when double immunostained with their respective antibodies in the PFC, ACC and Dentate Gyrus (Fig 1.8).

1.5.2 Characterization of Ntf3 EGFP-L10 BAC Transgenic Founder Line PS1046

The Ntf3 PS1046 Founder line has 4 ± 0.912 copies of BACs integrated randomly into the mouse genome. This line recapitulates the neocortical expression of Ntf3 more faithfully compared to the endogenous gene expression. The whole brain DAB-immunostaining shows that in this line, the reporter EGFP is expressed in the superficial layer II of the medial OFC, Infralimbic and Prelimbic Cortex (Fig 1.9). The PS1045 line in comparison did not have any reporter expression in the Prelimbic Cortex (PL). Apart from the PFC, the EGFP reporter was expressed in the layer II of Piriform Cortex, Septum, Reticular nucleus in the Thalamus and Dentate Gyrus. As previously stated, we were interested in characterizing the Ntf3 cell type only in the PFC, so for molecular profile analysis of these lines, the OFC and PL/ILC were the only brain regions dissected out for transcript isolation. Ntf3 cell type in this founder line defines pyramidal cells as evident from co-labeling of EGFP with the Neuronal marker NeuN and mutually exclusive labeling of GABA and EGFP (Fig 1.10). In this line, the hippocampus has EGFP expressed not only in the Dentate Gyrus but also in the CA1 region.

1.5.3 Characterization of Ntf3 EGFP-L10 BAC Transgenic Founder Line PS1049

The Ntf3 PS1049 founder line has the second highest of the BAC copy numbers (7 ± 0.959) among the Ntf3 founders after PS1045. This line has expression in pyramidal cells residing not only in the superficial layer II of the neocortex (not restricted to the PFC) but also in the deep layer VI (Fig 1.11). High enrichment of the reporter in the Anterior Cingulate is detectable. Besides the neocortex, this line has EGFP expression in the entire hippocampus spanning CA1, CA2, CA3 and Dentate Gyrus. The EGFP positive cells colabel with NeuN indicating that in spite of the ectopic expression of the reporter in the deeper cortical layers, they still target projection neurons. This line serves as a good example of BAC dosage related ectopic expression of the transgene in some BAC transgenic founder lines.

1.5.4 Hodology of Ntf3 cell type in the Ntf3 EGFP-L10 BAC Transgenic Mice

The cellular distribution of the EGFP-L10 protein follows the distribution of the ribosomes, sites of active protein translation, in the cells. Ribosomes are predominantly localized to the cytoplasm and nucleolus, but are scarce in the dendrites and axons. For this reason, the EGFP-L10 in the targeted cell types was largely absent from the processes, making it difficult to ascertain where these cells project. Although comparison of the corresponding Ntf3 EGFP line can yield inference for the hodology of the cell type, we sought to gather direct evidence for the projections of Ntf3 cell type in the EGFP-L10 transgenic mice. Hence, we took advantage of the Alexa Fluor 590 conjugated Cholera Toxin-B (CTB) subunit which acts as a transneuronal retrograde tracer and stereotaxically injected it into the layer V of PFC (Coordinates: +2.5 mm,

+0.25 mm, -1.6 mm). Four days following the intracranial administration, the CNS tissue was harvested and analyzed by histochemical methods using antibodies against CTB and EGFP. We found that there is a considerable overlap between retrogradely traced CTB positive neurons and Ntf3 EGFP-L10 pyramidal cells in the ventromedial PFC (Fig 1.12). Since a small area of the layer V of neocortex was injected with CTB, it is not experimentally feasible to retrogradely label all Ntf3 cells. The results of the aforementioned CTB injection show that a representative population of the Ntf3 cell type project to deeper layer V in the ipsilateral cortex. We however, cannot conclude whether the Ntf3 cell type project callosally to the contralateral cortex.

1.6 Genetic access to Ets Variant 1 (Etv1) Cell Type, Layer V Pyramidal Cells in the Lateral Neocortex

Ets Variant 1 (Etv1) gene, also known as Er81, is a member of the ets family of transcription factors that includes more than 30 members. Etv1 was mapped at position 7p22 and submitted to a 722 translocation in a human Ewing's sarcoma. Etv1 belongs to the PEA3 group within the Ets transcription factors that consists of three members, Pea3, Etv1 and Etv5, all of which are over 95% identical in the Ets domain. The signature ETS domain is a domain of 85 amino acids, which binds to sites containing 5'-GGAA/T-3' motif (Coutte et al., 1999). The transcriptional activity of Etv1 is regulated by both Ras-dependent and other kinase pathways, suggesting its role in oncogenic mechanisms. Etv1 is developmentally regulated i.e. during embryogenesis, Etv1 plays a role in the specification of a sublineage of layer V projection neurons and is expressed in a prominent rostrolateral high to caudomedial low gradient in cortical progenitors (Tuoc and Stoykova, 2008). Prior studies have shown that Etv1 is a

downstream target of another transcription factor Pax6, in the absence of which cortical progenitors for layer V fail to express Etv1. In the mouse cortex, Etv1 transcripts are first detected at E13 in the Ventricular Zone (VZ) of the rostrolateral pallium and the expression is maintained in a subset of pyramidal cells in the lower part of layer V in later embryonic stages and in the mature brain. Contrary to other transcription factors such as RORb and Coup-TFII, which are expressed by the cortical progenitors during early embryonic development but gradually lost as the thalamocortical afferents establish functional connections with the cortex around E18.5-P0, Etv1 gene is stably expressed from development through adulthood suggesting its role for cortical specification in adult CNS (Yoneshima et al., 2006). Outside of neocortex, Etv1 is expressed in the motorneurons of the spinal cord and it plays a role in the formation of functional connections with Ia sensory afferents (Arber et al., 2000; Molnar and Cheung, 2006).

The Etv1 gene (ID: 14009) is located in Chromosome 12 at 39,506,845 – 39,594802 (87,958 bp) and is flanked by neighboring genes Gm4257 at the 3' end and LOC100417196 at the 5' end. The in situ hybridization images for Etv1 in the Allen Brain Atlas show that the gene is expressed in layer V of the neocortex without any areal restriction or graded expression in the rostrolateral cortex (Fig 1.13). It is possible that since the Pea3 group of transcription factors share such a high homology to each other (95% in Ets domain), the RNA probe used for ISH is cross-reacting with the two other Pea3 family members Etv5 and Pea3, in stead of specifically detecting Etv1. It has been previously shown that Etv5 is expressed preferentially in the medial cortex in layer V, which would seem to complement the expression pattern of Etv1 (Coutte et al., 1999). Other researchers have utilized ISH methods to elucidate the restricted expression pattern of Etv1 in layer V in the neocortex of rodents as well as humans (Yoneshima et al.,

2006). The GENSAT Etv1-EGFP expression data indicates that the transgene is expressed by layer V corticostriatal pyramidal cells with a negative rostrocaudal (i.e. high rostral low caudal) gradient (Fig 1.13). In adult Etv1-EGFP mice, there was a preferential expression of the reporter in the rostrolateral cortex similar to the reported expression pattern in the literature. Groh et al (Groh et al., 2009) characterized the electrophysiological behavior and neuronal morphology of the Etv1 cell type and compared them to another layer V pyramidal cell type defined by Glt25d2. They showed that Etv1 is expressed in the slender pyramidal cells with thin apical dendrites in layer Va that retain their morphology in at least two different cortical areas along the rostrocaudal axis, somatosensory cortex and visual cortex. By retrograde tracer injection, they confirmed that the Etv1 cell type projects to the ipsilateral striatum and to some extent contralateral striatum, which concurs with the EGFP staining pattern for the Etv1 BAC transgenic line. Etv1 cell type was further shown to have a resting membrane potential of -68 mV and to have a high adaptation index between successive spikes, representing the spike frequency adaptation feature.

We used the same Etv1 BAC RP23-250K4 for EGFP-L10 modification as the one used by GENSAT to generate the EGFP BAC Transgenic mice. The selected Etv1 BAC contains 178, 997 bp of genomic DNA at the plus strand of Chromosome 12 (39,430,275 – 39,609,271). A 489 bp region immediately upstream of translational start codon (TSC) was PCR amplified using the Forward primer (5' – TATGTCTCTCCAGATAATTGCA) and Reverse Primer (3' – AGGAGCAGAATGGATGGATTTTAT) and cloned into the shuttle vector pS296 next to the EGFP-L10 transgene. The Etv1 A box-EGFP-L10 was then homologously recombined from the shuttle vector to the Etv1 BAC right before the Etv1 TSC in the recombination competent E.

Coli cells. The modified Etv1- EGFP-L10 BAC was injected into the pronuclei of fertilized mouse oocytes, which then randomly integrated into the mouse genome in variable tandem repeats. We got five founders for Etv1 EGFP-L10 transgenic mice – PS476, PS477, TS88, PS3020 and PS3021. Out of six founders, we decided to characterize the neuronal anatomy of three founders namely PS476, PS477 and TS88 since they recapitulated the expression pattern of Etv1 in layer V of neocortex more faithfully compared to other founders, eventually focusing on PS476 as the representative line for transcript profiling. Using relative qPCR with an EGFP-L10 Knock-In mouse as a baseline (single copy), we determined that PS476 founder line has 9 ± 0.817 copies, PS477 founder line has 2 ± 0.792 copies, TS88 has 5 ± 0.780 copies, PS3020 has 1 ± 0.448 copy and PS3021 has 1 ± 0.565 copy of Etv1 EGFP-L10 BAC (Fig 1.4). The last two founders PS3020 and PS3021 did not have any detectable expression of the transgene which suggests that a single copy of the EGFP-L10 BAC under the transcriptional regulation of Etv1 promoter is not sufficient to produce detectable fluorescence. Out of the remaining founders, PS477 had the reporter expressed not only in layer V but also in scattered cells in layer VI, the latter being ectopic. TS88 on the other hand had laminar expression of the reporter in layer V, but there were contaminating astrocytes in the cortex that expressed EGFP-L10. PS476 founder line better recapitulated the endogenous pattern of Etv1 expression, so we used this line for further analysis.

1.6.1 Characterization of Etv1 EGFP-L10 BAC Transgenic Founder Line PS476

The Etv1 PS476 founder line has the highest copy number of the BAC (9 ± 0.817) among the Etv1 founders. This line has the reporter expressed in a tight band of small pyramidal

cells in layer V of the lateral neocortex. It is remarkable that the medial cortical regions, which include association areas such as medial PFC (PL, IL, MOFC), Cingulate (Cg1), caudal Secondary Motor Cortex (M2) and Retrospenial Cortex (RS) completely lack the expression of the reporter in this line. On the other hand, the reporter is expressed strongly in the layer V of ventrolateral OFC and in the lateral neocortex spanning the rostrocaudal axis. Global CNS DAB histology profile for Etv1 shows expression of the reporter in Frontal Association Cortex (FrA), rostral M2, Insular cortex, Primary Motor Cortex (M1), Primary Somatosensory Cortex (S1), Secondary Somatosensory Cortex (S2), Primary Visual Cortex (V1), Secondary Visual Cortex (V2), Auditory Cortex (Au), Ectorhinal Cortex (Ect) and Temporal Association Cortex (TeA) (Fig 1.14). Besides neocortex, the EGFP reporter in this line was also expressed specifically in the Posterior Thalamic Nucleus (Po). Thus, this line can be valuable for studying the neuronal anatomy and characteristics of the Po thalamic nucleus. The Etv1 cell type defines an excitatory neuronal subtype in the neocortex as revealed with the histochemistry with antibodies to NeuN and GABA, where the GFP positive cells completely colabel with NeuN but are exclusive of GABA (Fig 1.15).

1.6.2 Hodology of Etv1 cell type in the Etv1 EGFP-L10 BAC Transgenic Mice

Although we can infer the projection target of the Etv1 cell type from the corresponding Etv1 EGFP line generated with the same BAC, we wanted to produce a direct evidence for the projections of the Etv1 EGFP-L10 cell type. Hence, as described earlier for Ntf3 EGFP-L10 line, we stereotaxically injected Alexa Fluor 590 conjugated CTB retrograde tracer into the ventral striatum at the globus pallidus (Coordinate: : -0.10 mm, +1.75 mm, 4.0 mm). There was a

considerable overlap of EGFP and CTB in the layer 5 Etv1 cell type in ventral auditory Cortex (AuV) and ectorhinal cortex (Ect), indicating that a representative population of these cells project to the ventral striatum. Note however that there are many cells that do not overlap for EGFP and CTB expression, which is not surprising given that the CTB is taken up by axons of all neurons that project to the site of injection (ventral striatum). For instance, strong CTB labeling is visible in the layer VI neurons in the medial retrospenial cortex (RS), medium spiny neurons in the striatum itself and scattered neurons in the entorhinal cortex (Ent) (Fig 1.16). On the other hand, the site of injection is small enough to exclude the axons of many EGFP-L10 neurons that project presumably to the striatum but do not project to the injection site. Our results are in good agreement with Groh et al (2010) where they showed that Etv1 GFP BAC transgenic mice project to the ventral striatum using CTB retrograde tracer as well.

1.7 Genetic access to Synaptotagmin 6 (Syt6) Cell Type, Layer VI Pyramidal Cells in the Rostromedial Neocortex

Synaptotagmin 6 (Syt6) is a member of the family of synaptotagmins. Synaptotagmins are a family of membrane-trafficking proteins that are characterized by an N-terminal TMR, a variable linker and two C-terminal C2 domains. Syt6 is a class 3 synaptotagmin characterized by disulfide bonds on cysteine residues at N terminus and may function as calcium sensor for exocytosis (Sudhof, 2002). Syt6 is localized to the plasma membrane and has a 10 fold higher Ca2+ affinity than Syts 1 and 2 (Butz et al., 1999). Vertebrates express at least 13 synaptotagmins that are synthesized exclusively or predominantly in neurons and neuroendocrine cells. The release of neurotransmitters by Ca2+ triggered synaptic vesicle

exocytosis is a key event in interneuronal communication, and Syt6 by the virtue of its high affinity to Ca2+ and presence on the plasma membrane in the active zones might play a role in the modulating the efficiency of neurotransmitter release.

The Syt6 gene (ID: 54524) is located in the plus strand of chromosome 3: 103,370,173 – 103,448,041 (77,869 bp) and is flanked by neighboring genes Trim33 at the 5 end and Atg4a at the 3' end. The in situ hybridization images in Allen Brain Atlas database have a relatively weak signal, upon the application of the gene expression filter, for the Syt6 probe except at the dorsomedial habenula. But a closer inspection of the ISH images indicates that the Syt6 RNA is enriched in the layer VI of the neocortex with a high medial and low lateral expression levels (Fig 1.17). The GENSAT Syt6 EGFP BAC transgenic mouse is in excellent agreement with the graded expression in the neocortex. Pyramidal cells in the neocortex expressing the EGFP reporter under Syt6 promoter have long apical dendrites extending all the way to the molecular layer I and send projections to the thalamus. The Syt6 cell type has graded expression in both rostro caudal, also known as anterior-posterior, axis and medial-lateral axis, and basically is restricted to the rostromedial neocortex layer VI.

We used the same Syt6 BAC RP23-184N6 for the EGFP-L10 modification as that used for generation of Syt6 EGFP BAC transgenic mice (GENSAT). The chosen Syt6 BAC incorporates 223,019 bp of genomic DNA at the plus strand of Chromosome 3 (103,266,515 – 103,489,533). A 617 bp region immediately upstream of translational start codon was PCR amplified using the Forward primer (5' – GGCGCGCCGTCTTGGGGTCTTATA) and Reverse primer (3' – ACACTCAGGCCAGCGGAGTAGTGGCTCGAA) and cloned into the shuttle vector pS296

next to the EGFP-L10 transgene. The Syt6 A box – EGFP-L10 was then homologously recombined from the shuttle vector to the Syt6 BAC right before the Syt6 translation start codon in recombination competent E.Coli cells. The modified Syt6 – EGFP-L10 BAC was injected into the pronuclei of fertilized mouse oocytes, which then randomly integrated into the mouse genome in variable tandem repeats. We got four founders – PS718, PS3011, PS3013 and PS3016 - for Syt6 EGFP-L10 BAC transgenic mice, which expressed the transgene EGFP-L10 in a BAC dosage dependent manner. Using relative qPCR with an EGFP-L10 Knock-In mouse as a baseline (single copy), we determined that PS718 has 4 ± 0.921 (Mean ± SEM) copies, PS3011 has 4 ± 0.888 copies, PS3013 has 21 ± 0.964 copies and PS3016 has 5 ± 0.863 copies of Syt6 EGFP-L10 BAC (Fig 1.4). Out of these transgenic founder lines, PS3014 founder line expressed the reporter only in the dorsomedial habenula but not in neocortex where as PS718 and PS3011 expressed the reporter in a subset of endogenous Syt6 cell type when compared with the GENSAT Syt6 EGFP transgenic line and ISH data. Both PS718 and PS3011 have equal copies (4) of Syt6 EGFP-L10 BAC and express the reporter in a restricted region of Layer VI of rostromedial cortex in Secondary Motor Cortex (M2) and Anterior Cingulate Cortex (ACC) (Fig 1.18). PS3013 founder line has the highest copies of Syt6 EGFP-L10 BAC (21) and is discussed in detail below.

1.7.1 Characterization of Syt6 EGFP-L10 BAC Transgenic Founder Line PS3013

The Syt6 PS3013 founder, with the highest copies of BACs (21) among the Syt6 EGFP-L10 founders, expresses the reporter with brighter epifluorescence and better recapitulates the endogenous Syt6 expression in the neocortex. A subpopulation of pyramidal cells in the layer VI

express EGFP-L10 in a high rostral to low caudal as well as high medial to low lateral expression gradient (Fig 1.18). The Syt6 cell type represents a class of excitatory neurons as evident from co-labeling of the cells with NeuN and absence of co-labeling with GABA (data not shown). The transgene is expressed in layer VI of prelimbic cortex (PL), infralimbic cortex (IL), anterior cingulate cortex (ACC), secondary motor cortex (M2) and retrospenial agranular cortex (RSA) also known as posterior cingulate cortex, all of which are association cortices. The anterior cingulate cortex has been shown to be important for motor sequencing of behavior and pain perception where as the retrospenial cortex is important for spatial navigation (Harker 2004, Aggleton 2004, Pothuizen 2008), fear motivated behavior and classical conditioning (Radwanska 2010) . The retrospenial cortex receives signals from the anterior thalamic nuclei and parietal cortex and highly processed hippocampal input from CA1, subiculum and postsubiculum. Both ACC and RSC are also involved in emotionally driven behaviors, so it is possible that Syt6 cells are important for such behaviors.

1.7.2 Hodology of Syt6 cell type in the Syt6 EGFP-L10 BAC Transgenic Mice

That Syt6 cell type defines a class of corticothalamic projection neurons can be inferred from the digital images of the GENSAT Syt6 EGFP BAC Transgenic mice. For definitive evidence, we stereotaxically injected Alexa Fluor 590 conjugated CTB retrograde tracer into the posterior thalamic nucleus (coordinates: (-2.18 mm, +0.75 mm, 3.5 mm) in Syt6 EGFP-L10 mice. Histological analysis of the CNS tissue of the surgerized mice indicated a considerable overlap of Syt6 cell type and CTB retrograde tracer labeled cells in the prefrontal cortex, primary motor cortex and retrospenial granular cortex (Fig 1.19). This directly confirms that

Syt6 pyramidal cells project to the thalamus and are thus important component of the corticothalamic feedback loop. However, the retrograde tracer experiments also show that the Po thalamic nucleus receives projections from non-Syt6 positive cells in the prefrontal cortex, somatosensory cortex and retrospenial cortex. Similarly, a fraction of the Syt6 cell type project to the area surrounding the injection site in the Po nucleus, thus not all Syt6 cell type are labeled with CTB.

PERSPECTIVES:

1.8 Chapter Summary

Using the BAC transgenesis strategy established in our lab, we were able to genetically access four distinct neocortical pyramidal cell types defined by the gene drivers Pdyn, Ntf3, Etv1 and Syt6 (Fig 1.20). The targeted cell types are distinguished by parameters such as the cytoarchitectonic areal distribution, laminar restriction, neuronal morphology and the projection targets. The gene drivers thus serve not only as molecular markers for pyramidal cells in the neocortex but provide a means to genetically access the cell types reproducibly for reporter expression, molecular profile as well as functional perturbation by relevant modifications of the corresponding BACs. We illustrated that two different modifications - EGFP and EGFP-L10 - of a common BAC were able to reproducibly target the transgene into the same cell type, reinstating the ability of BACs to carry most or all of the regulatory sequences necessary for a faithful expression of the inserted transgene in spite of random genomic integration. The gene drivers Pdyn, Ntf3, Etv1 and Syt6 provided genetic access to subpopulations of excitatory projection neurons in the neocortex such as 1. Corticocortical layer II pyramidal cells in Anterior

Cingulate (Pdyn - green), 2. Corticocortical/ Transcallosal layer II pyramidal cells in Medial PFC (Ntf3 - purple), 3. Corticostriatal layer Va pyramidal cells in Lateral Neocortex (Etv1 - yellow) and 4. Corticothalamic layer VI pyramidal cells in Rostromedial Neocortex (Syt6 – pink). For future studies, it would be invaluable to record firing patterns of these different cell types, however it can be inferred from Groh et al (2010) that at least one of our investigated cell types: the Etv1 cell type exhibits spike frequency adaptation. In the next chapter, we will compare three of these cell types – Ntf3, Etv1 and Syt6 in terms of their molecular profile and evaluate the host of unique molecules, gene ontologies and pathways that might underlie the characteristics and function of these various neocortical cell types.

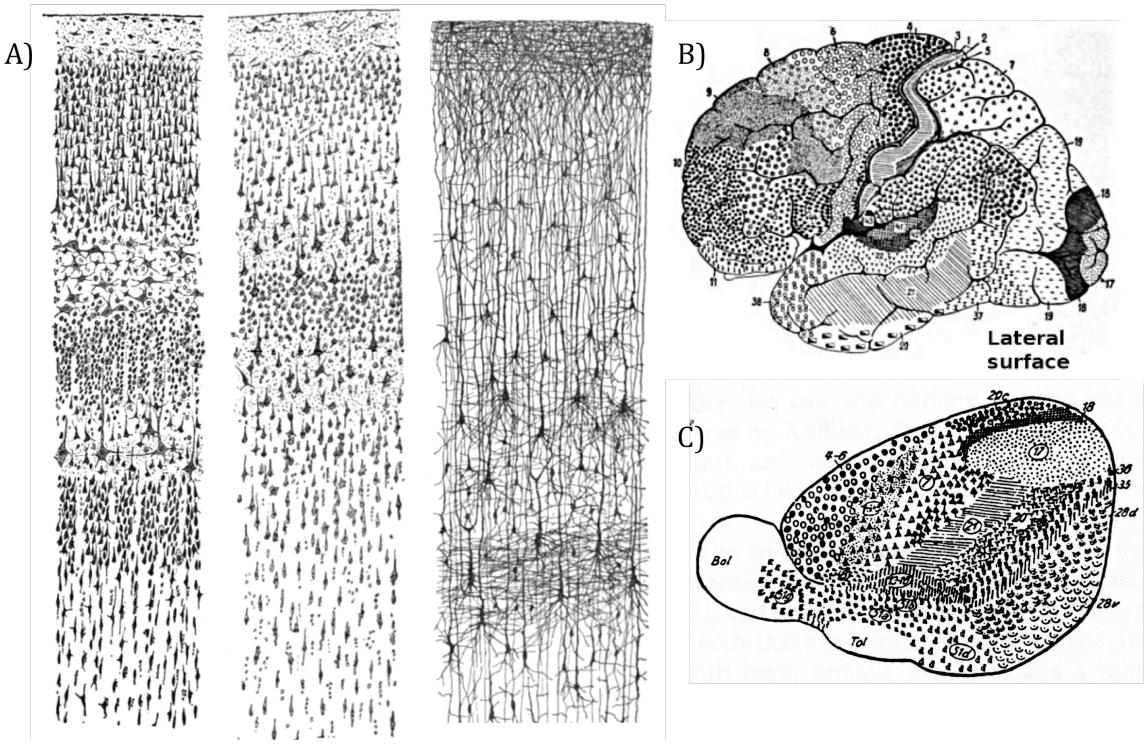

Figure 1.1: Classical studies in cortical cytoarchitecture: A) Santiago Raman Y Cajal (1905) first described the laminar structure of neocortex in human cerebral cortex. B) Korbinian Brodmann (1909) divided the human cerebral cortex into distinct numbered areas, referred to as Brodmann areas, corresponding to sensory, motor, executive and visual areas. C) Lorente de No (1938) divided the mouse neocortex into different cortical areas according to cytoarchitectonics and function.

A) Prefrontal Cortex Areas

PFC Area	Subregions	Function
medial PFC	Prelimbic Cortex (PL), Infralimbic Cortex (IL)	Consolidation of Fear Extinction Memory, Visual Working Memory (WM) , Extradimensional Shift of Attention
dorsal PFC	Anterior Cingulate Cortex (ACC)	Behavioral Disinhibition, Pain perception, Motor sequencing of Behavior
orbitofrontal Cortex (OFC)	medial OFC, lateral OFC	Behavioral Inhibition, Social behavior, Stimulus-Reward association, Odor and Taste related WM

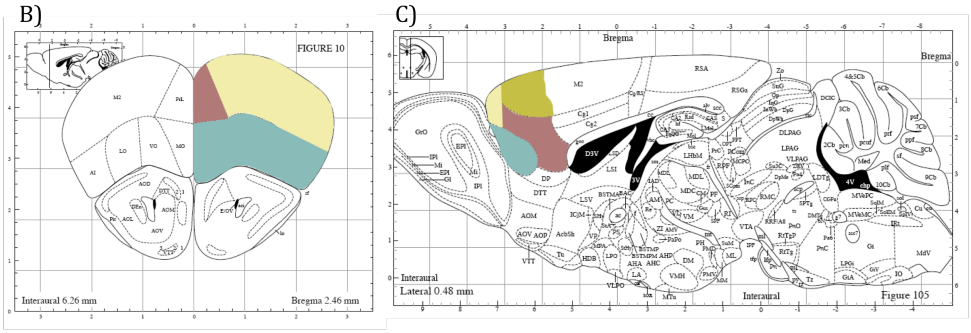

Figure 1.2: Prefrontal cortex (PFC) subdivisions in Mouse: A) Areal subdivisions within PFC include medial PFC (further consists of prelimbic cortex and infralimbic cortex), dorsal PFC (consists of anterior cingulate cortex) and orbitofrontal cortex (OFC that consists of medial OFC and lateral OFC). B) Coronal section of the mouse brain at Bregma 2.46 mm (Franklin and Paxinos, 2006) illustrating different PFC divisions: red – medial PFC, yellow – dorsal PFC and blue – OFC. C) Mid-sagittal section of the mouse brain with the same PFC divisions colored in the respective hues.

Cortical Areal Markers

Prefrontal Cortex

Gene Symbol	NCBI ID	Reference	Annotation	Gene Description	bacTRAP
Abcb1b	18669	GENSAT - GFP	L5	ATP-binding cassette, sub-family B (MDR/TAP), 1B	NA
Chrm4	12672	"	L5	cholinergic receptor, muscarinic 4	NA
Crabp1	12903	"	L5	cellular retinoic acid binding protein I	NA
Cxcl11	56066	"	L2/3	chemokine (C-X-C motif) ligand 11	3 Founders; No expression
Drd4	13491	"	L5	dopamine receptor D4	8 Founders; 1 with inaccurate expression
Epha2	13836	"	L2/3	Eph receptor A2	4 Founders; 1 with inaccurate expression
Epha7	13841	"	L5	Eph receptor A7	NA
Hsbp8	80888	"	AI	heat shock protein 8	3 Founders; No expression
Htr2a	15558	GENSAT - GFP, Cre		5-hydroxytryptamine (serotonin) receptor 2A	4 Founders; 1 with incomplete expression in IG
Irx3	16373	GENSAT - GFP	L2/3	Iroquois related homeobox 3 (Drosophila)	3 Founders; No expression
Npy2r	18167	"	L2 and 5	neuropeptide Y receptor Y2	NA
Ntf3	18205	Miyashita et al, 2010	L2/3;ILC	neurotrophin 3	5 Founders; 2 with accurate expression
Nts	67405	GENSAT - GFP		neurotensin	3 Founders; No expression
Pdyn	18610	GENSAT - GFP, ABA ISH	L2	prodynorphin	1 Founder with accurate expression
Prss12	19142	GENSAT - GFP	VOFC	protease, serine, 12 neurotrypsin (motopsin)	NA
Sez6	20370	"	L5	seizure related gene 6	NA

Genes with Rostrocaudal gradient

Gene Symbol	NCBI ID	Reference	Annotation	Gene Description	bacTRAP
Etv1	14009	GENSAT - GFP, Cre	L5; Lateral Cx	ets variant gene 1	5 Founders; 2 with accurate expression
Syt6	54524	"	L6; Medial Cx	synaptotagmin VI	9 Founders; 2 with accurate expression
Wfs1	22393	GENSAT - GFP, ABA ISH	L2; Absent in A1, V1	Wolfram syndrome 1 homolog (human)	NA

Genes with laminar expression

Gene Symbol	NCBI ID	Reference	Annotation	Gene Description	bacTRAP
Coch	12810	ABA ISH	L2/ 3	coagulation factor C homolog (Limulus polyphemu	NA
Tnnc1	21924	ABA ISH	L3 and L5	troponin C, cardiac/slow skeletal	NA

Figure 1.3: Screening for candidate genes to genetically access neocortical cell types. Candidate genes are shortlisted for Prefrontal Cortical expression (16 genes), rostrocaudal gradient in the neocortex (3 genes) and laminar expression in the neocortex (2 genes)

a)

Pdyn TRAP EGFP Copy Number

Sample ID	Founder	RQ	SEM
KI EF1a-EGFPL10	EGFPL10 KI	1	0.000
Pdyn CP12 NA	Pdyn CP12	4	0.850

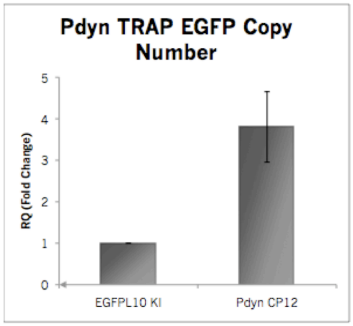

b)

Ntf3 TRAP EGFP Copy Number

Sample ID	Founder	RQ	SEM
KI EF1a-EGFPL10	EGFPL10 KI	1	0.000
Ntf3 PS1045 T4	PS1045	15	0.912
Ntf3 PS1046 E202	PS1046	4	0.912
Ntf3 PS1049 E474	PS1049	7	0.959
Ntf3 PS1052 D866	PS1052	6	0.629

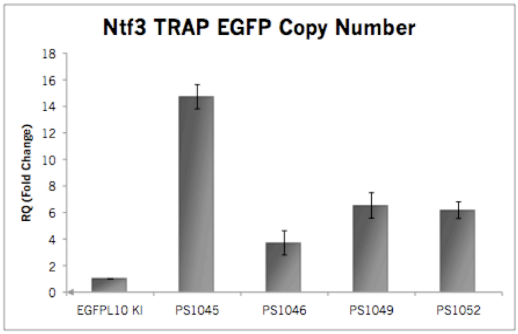

c)

Etv1 TRAP EGFP Copy Number

Sample ID	Founder	RQ	SEM
KI EF1a-EGFPL10	EGFPL10 KI	1	0.000
Etv1 PS476 D494	PS476	9	0.817
Etv1 PS477 C709	PS477	2	0.792
Etv1 PS3019 FF	PS3019	5	0.780
Etv1 PS3020 FF	PS3020	1	0.448
Etv1 PS3021 FF	PS3021	1	0.565

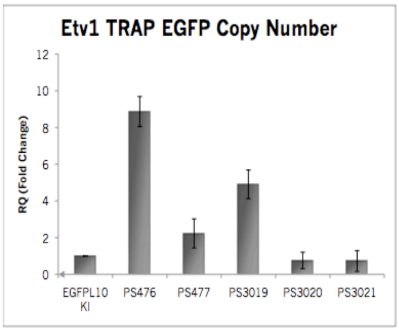

d)

Syt6 TRAP EGFP Copy Number

Sample ID	Founder	RQ	SEM
KI EF1a-EGFPL10	EGFPL10 KI	1	0.000
Syt6 PS3011 FF	PS3011	4	0.888
Syt6 PS3013 FF	PS3013	21	0.964
Syt6 PS3014 FF	PS3014	4	0.921
Syt6 PS718 FF	PS718	5	0.863

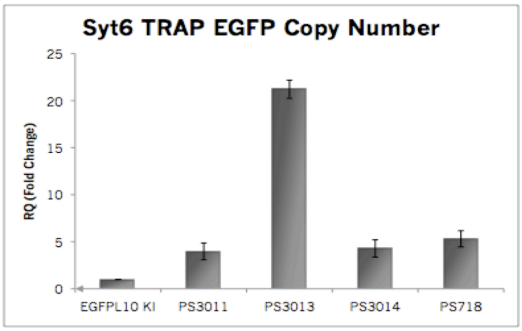

Figure 1.4: Copy number of EGFP-L10 BACs in different founder lines. Quantitative PCR analysis with EGFP primers reveals BAC dosage for Pdyn CP12 (a) as wel as TRAP founders for Ntf3 (b), Etv1 (c) and Syt6 (d). The Knock-in line EF1a-EGFP-L10 was used as a control for representing a single copy of EGFP.

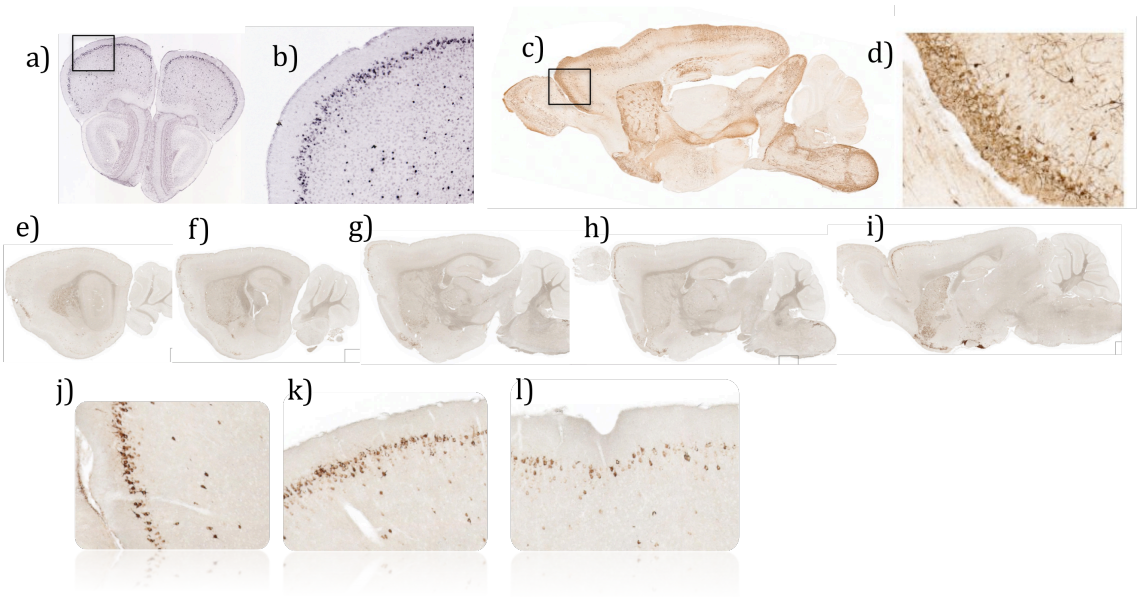

Figure 1.5: Neuroanatomy of the Prodynorphin (Pdyn) in the mouse brain. Digital *in situ* hybridization data in Allen Brain Atlas (ABA) reveals slight enrichment of Pdyn RNA in layer 2 of dorsal PFC (a; enlarged inset: b) in coronal sections. GENSAT BAC transgenic mice for Pdyn EGFP reporter concur with PDYN expression in layer II of neocortex and additionally indicated corticocortical projection (c; enlarged inset: d). The Pdyn TRAP line CP12 expresses the reporter EGFP-L10 in the superificial layer 2 of frontal cortex. Sucortical expression is detected in the striatum in both Pdyn EGFP (c) and Pdyn CP12 TRAP (g, h, i) mice.

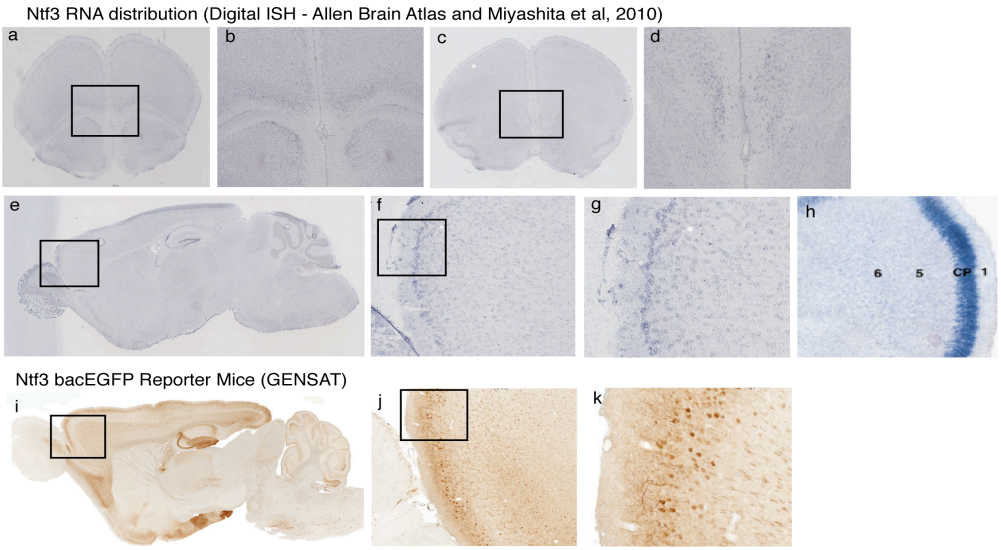

Figure 1.6: Expression pattern of Neurotrophin-3 (NTF3) in the mouse brain. Digital *in situ* hybridization data in Allen Brain Atlas (ABA) reveals slight enrichment of Ntf3 RNA in ventromedial PFC (a, b) and infralimbic cortex (c, d) in coronal sections. ISH on sagittal sections reveal enrichment in superficial layer II (e, f and g). The layer II restricted expression is better evident in Miyashita et al (2010) paper (h). GENSAT BAC transgenic mice for Ntf3 EGFP reporter concur with NTF3 expression in layer II of neocortex and additionally indicated corticocortical projection (I, j and k)

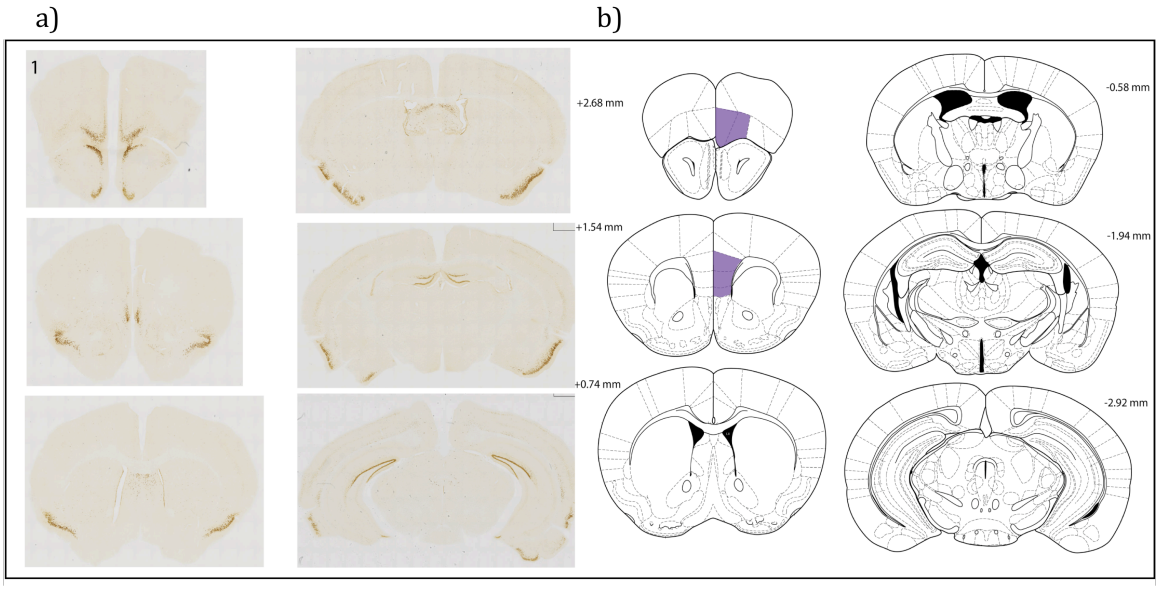

Figure 1.7: Global CNS expression pattern of EGFP-L10 in Ntf3 PS1045. DAB immunostaining of coronal brain sections of Ntf3 PS1045 reveal restricted PFC expression in layer II of ventromedial PFC and infralimbic cortex (a). Other areas of the brain that express EGFP-L10 include layer II of piriform cortex, superficial layer of medial olfactory bulb, dentate gyrus and septum (a). Schematic brain diagrams from Franklin and Paxinos (2005) are shown in (b) to mark the PFC area of interest where Ntf3 PS1045 expresses the reporter.

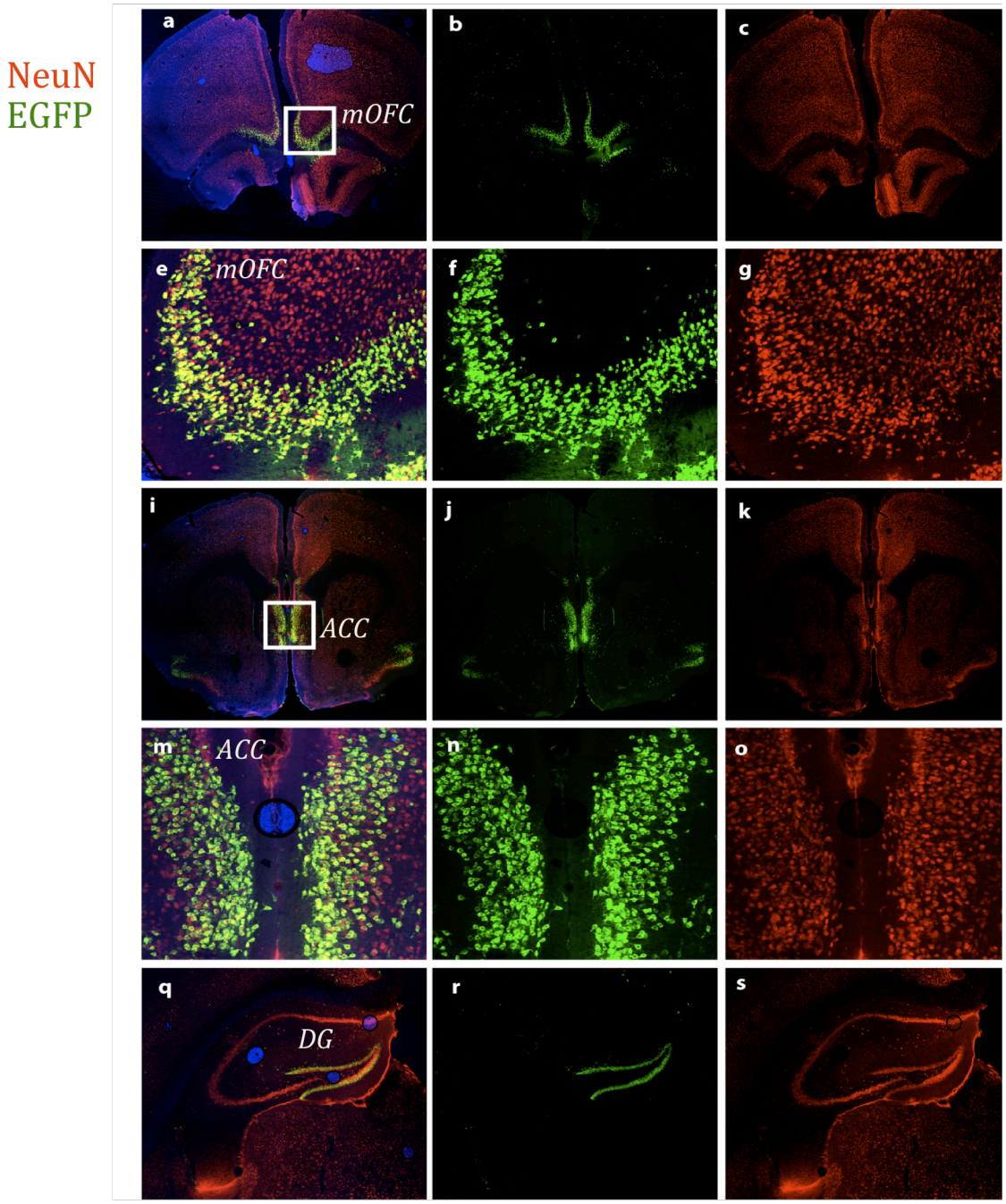

Figure 1.8: Immunohistochemistry of TRAP line Ntf3 PS1045: EGFP and NeuN co-immunostaining reveal complete colocalization of EGFP with NeuN, indicating a neuronal identity (a, e, I, m, q). Strong EGFP/NeuN staining is detected in the ventromedial PFC (a, b, c; enlarged inset: e, f, g), anterior cingulate cortex (I, j, k; enlarged inset: m, n, o) and dentate gyrus (q, r, s).

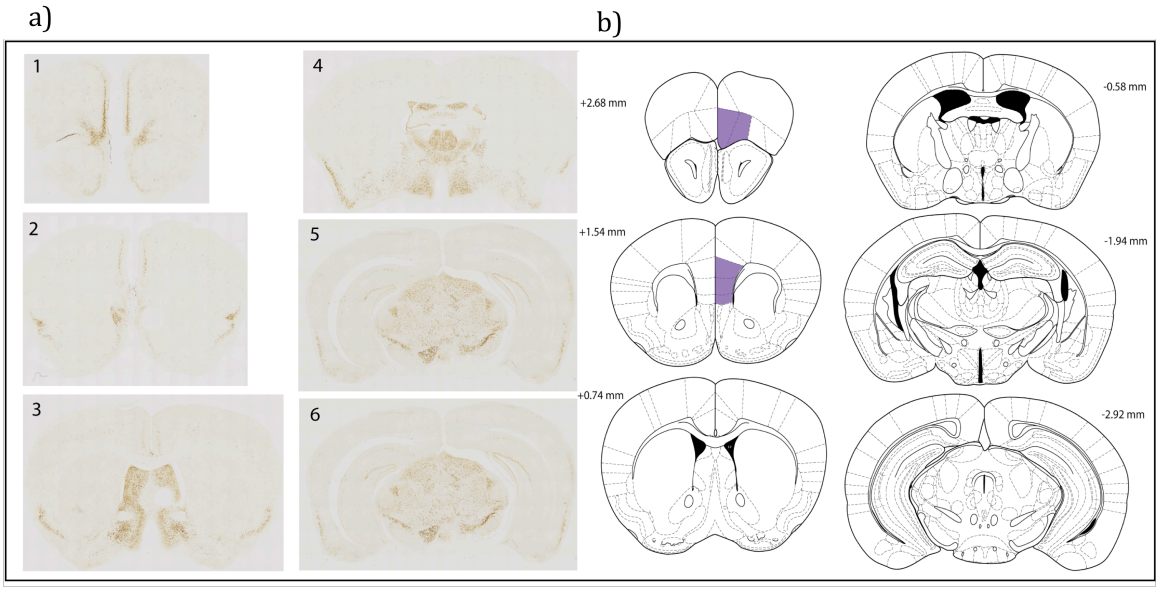

Figure 1.9: Global CNS expression pattern of EGFP-L10 in Ntf3 PS1046. DAB immunostaining of coronal brain sections of Ntf3 PS1046 reveal restricted PFC expression in layer II of medial PFC (a). Other areas of the brain that express EGFP-L10 include layer II of piriform cortex, superficial layer of medial olfactory bulb, dentate gyrus, septum and thalamus (a). Schematic brain diagrams from Franklin and Paxinos (2005) are shown in (b) to mark the PFC area of interest where Ntf3 PS1046 expresses the reporter.

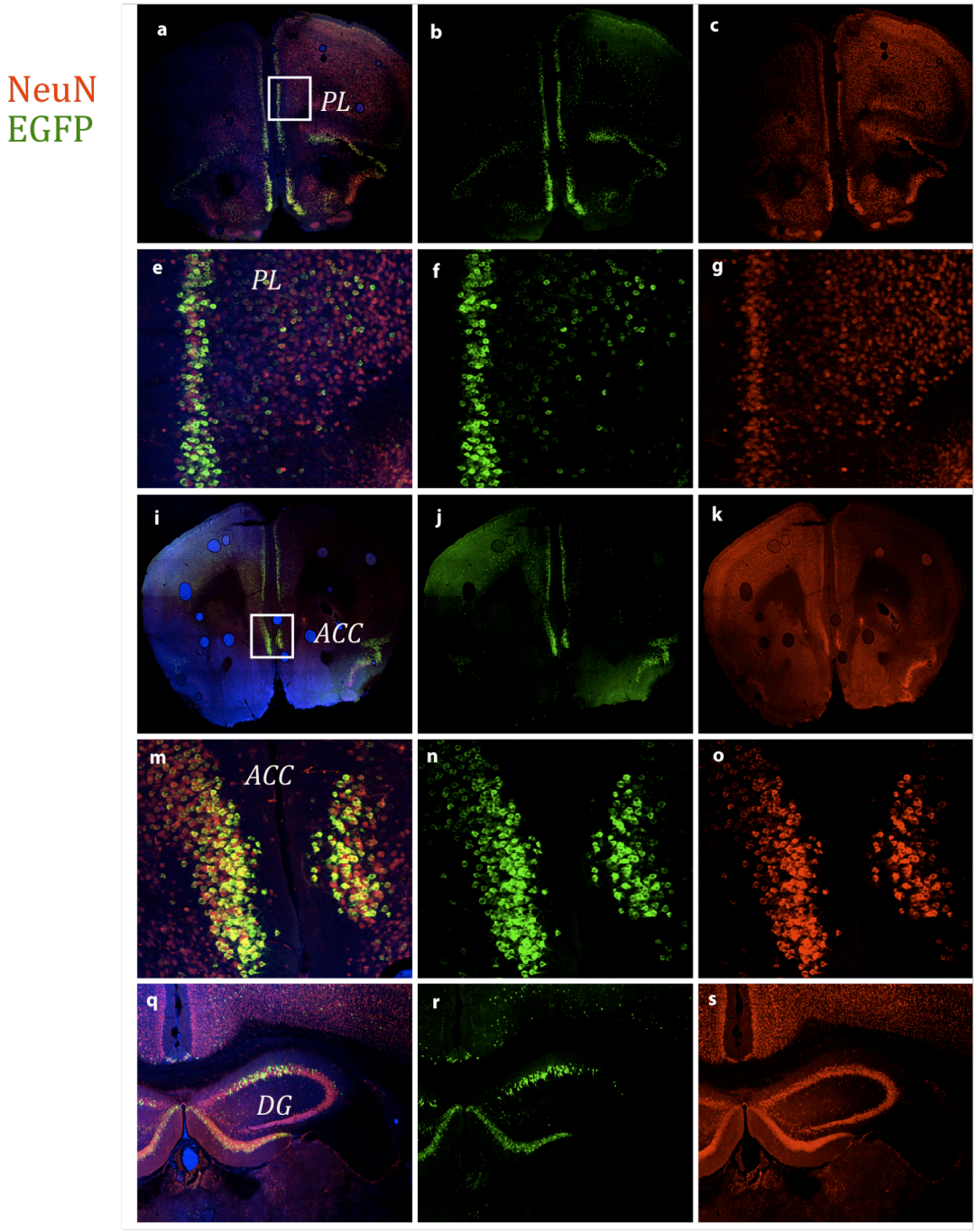

Figure 1.10: Immunohistochemistry of TRAP line Ntf3 PS1046: EGFP and NeuN co-immunostaining reveal complete colocalization of EGFP with NeuN, indicating a neuronal identity (a, e, i, m, q). Strong EGFP/NeuN staining is detected in the medial PFC (a, b, c; enlarged inset: e, f, g), anterior cingulate cortex (I, j, k; enlarged inset: m, n, o) and dentate gyrus (q, r, s).

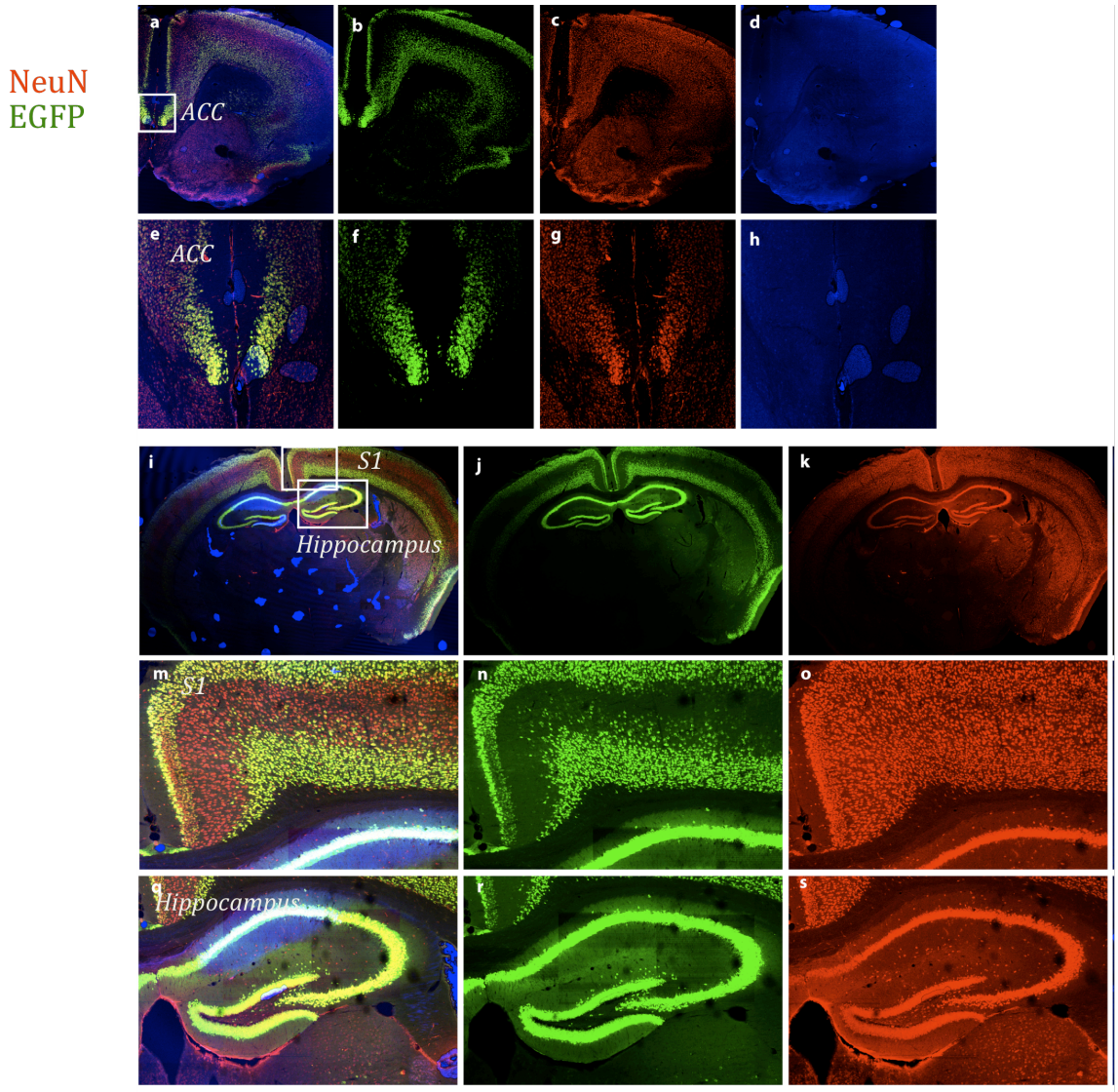

Figure 1.11: Immunohistochemistry of TRAP line Ntf3 PS1049: EGFP and NeuN co-immunostaining reveal complete colocalization of EGFP with NeuN, indicating a neuronal identity (a, e). Strong EGFP/NeuN staining is detected in the layer II and VI of ACC (a, b, c, d; enlarged inset: e, f, g), primary somatosensory cortex (S1: m) and the whole hippocampus (o)

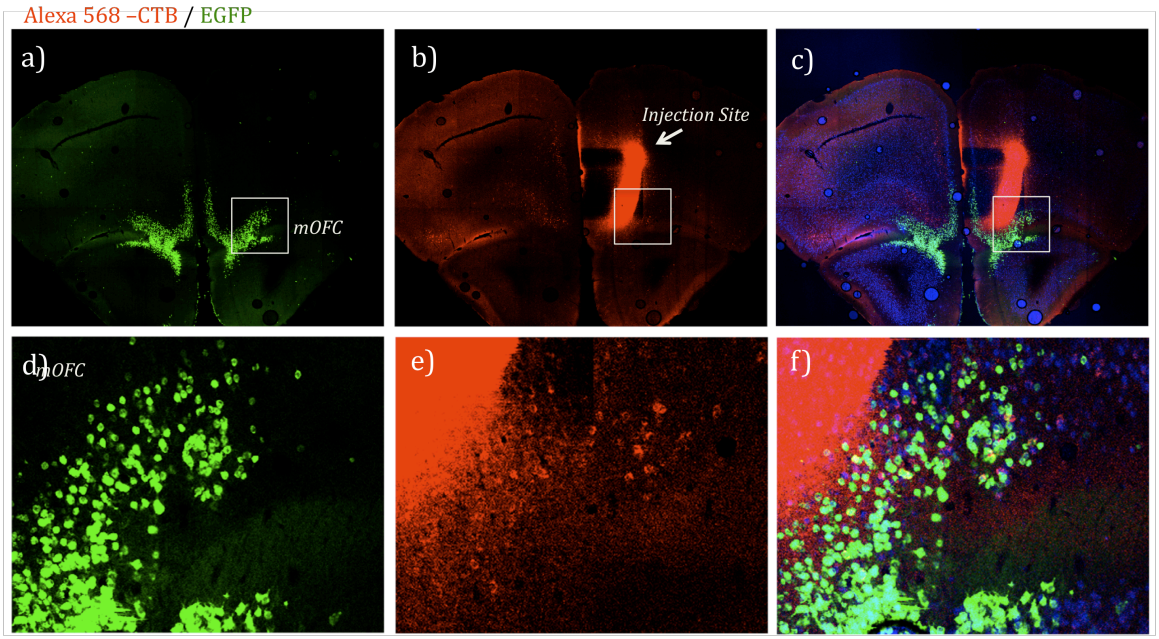

Figure 1.12: Hodology of Ntf3 cell type in Ntf3 TRAP line. Retrograde transneuronal tracer Cholera Toxin B (CT-B) conjugated to Alexa Fluor 568 was injected into layer 5 of PFC (b) Colabeled neurons, positive for both EGFP and CT-B, were present in layer II of ipsilateral ventral orbital PFC, indicating that Ntf3 defines corticocortical cell type.

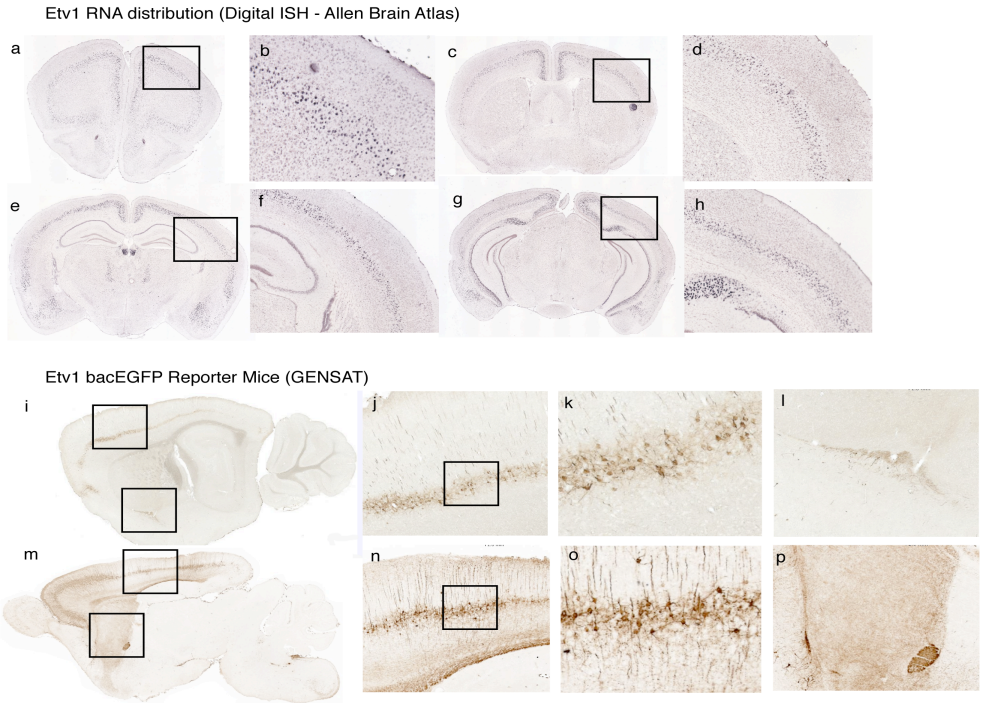

Figure 1.13: Expression pattern of Ets variant 1 (Etv1) in the mouse brain. Digital *in situ* hybridization data in Allen Brain Atlas (ABA) reveals slight enrichment of Etv1 RNA layer 5 of neocortex (a, c, e, g; enlarged insets: b, d, f, h) in coronal sections. GENSAT BAC transgenic mice for Etv1 EGFP reporter concur with Etv1 expression in layer 5 of neocortex and additionally indicated corticostriatal projection (i, m; enlarged insets: j, k, l, n, o, p).

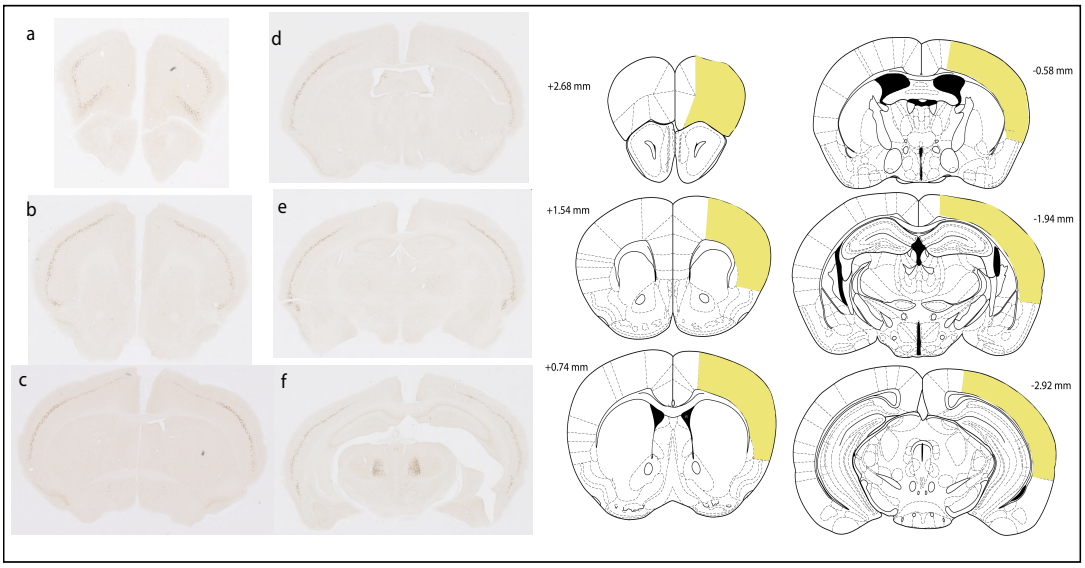

Figure 1.14: Global CNS expression pattern of EGFP-L10 in Etv1 PS476. DAB immunostaining of coronal brain sections of Etv1 PS476 reveal restricted PFC expression in layer 5 of lateral neocortex (a-f). Subcortically, EGFP in this line is also expressed in the thalamus (f). Schematic brain diagrams from Franklin and Paxinos (2005) are shown in right panel to mark the neocortical area of interest where Etv1 PS476 expresses the reporter.

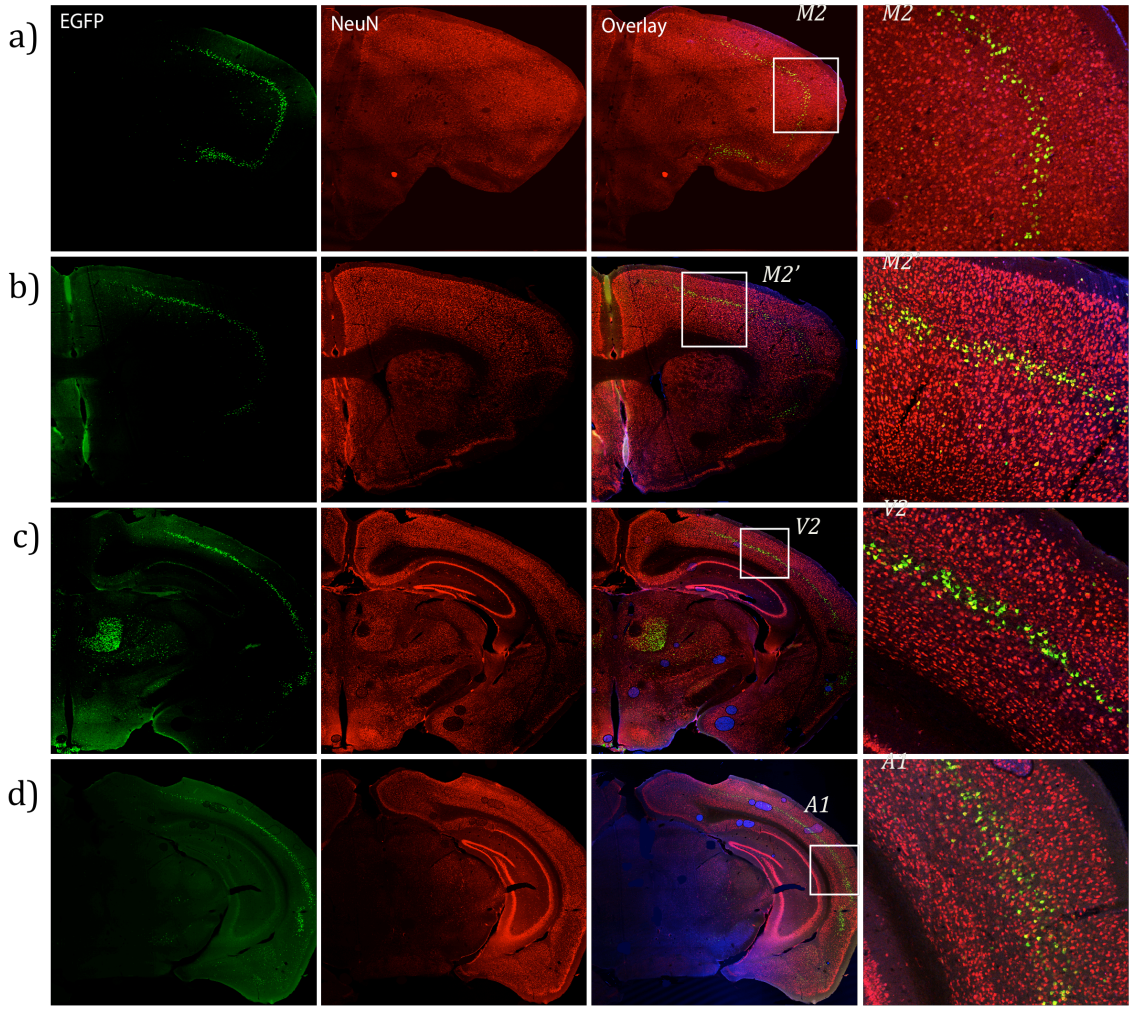

Figure 1.15: Immunohistochemistry of TRAP line Etv1 PS476: EGFP and NeuN co-immunostaining reveal complete colocalization of EGFP with NeuN, indicating a neuronal identity (a, e). Strong EGFP/NeuN staining is detected in the layer 5 of lateral neocortex (a, b, c, d; enlarged inset: M2, M2', V2, A1). Subcortical expression of EGFP is detected in the thalamus.

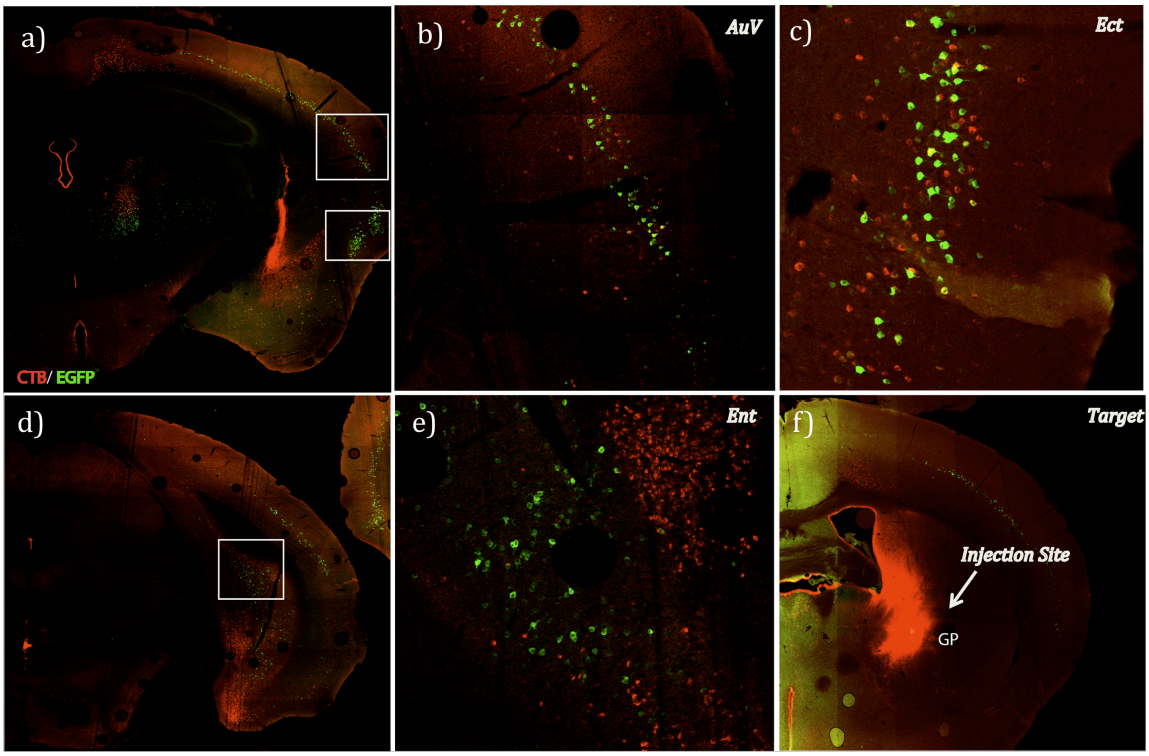

Figure 1.16: Hodology of Etv1 cell type in Etv1 TRAP line. Retrograde transneuronal tracer Cholera Toxin B (CT-B) conjugated to Alexa Fluor 568 was injected into ventral striatum with coordinates: -0.10 mm, +1.75 mm, 4.0 mm (f). Colabeled neurons, positive for both EGFP and CT-B, were present in layer 5 of auditory cortex and ectorhinal cortex (a; enlarged insets: b, c) indicating that Etv1 defines corticostriatal cell type. Striatal projecting neurons were also labeled in layer 6 of medial cortex (a) and entorhinal cortex, CTB+ cells in both regions were EGFP negative.

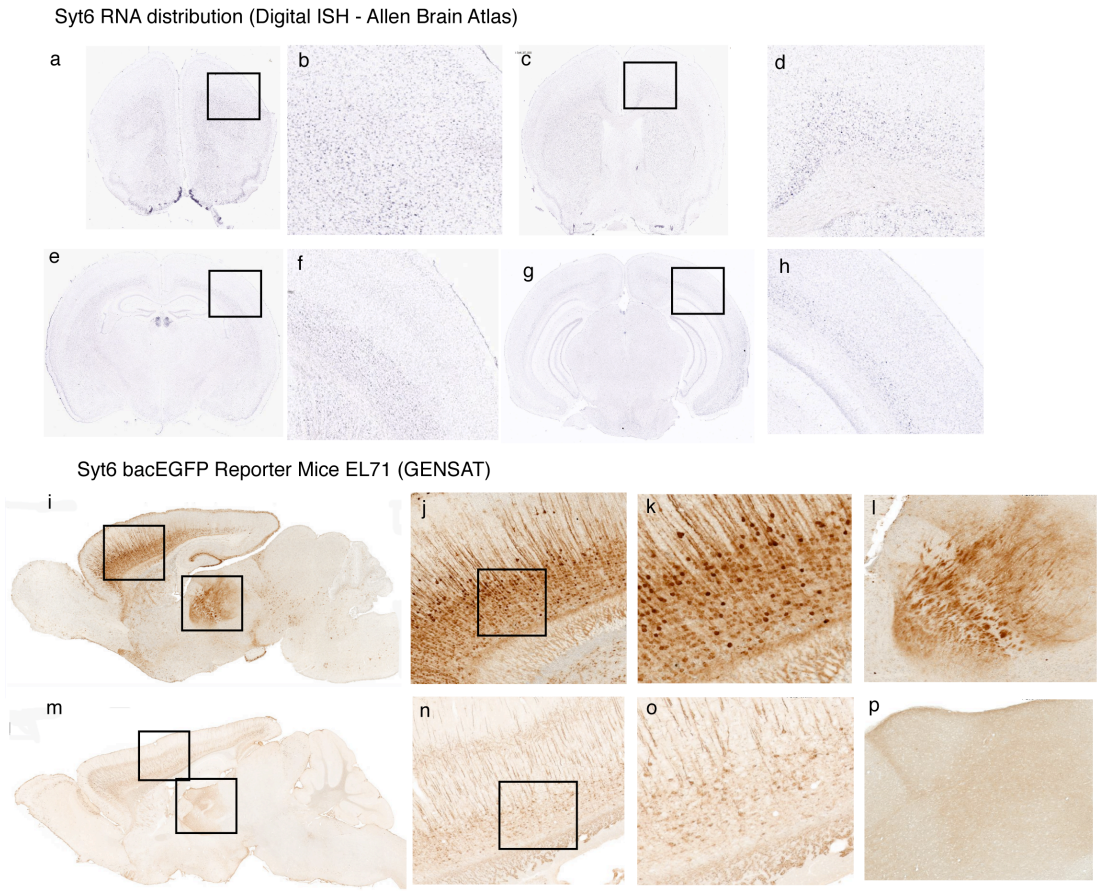

Figure 1.17: Expression pattern of Synaptotagmin 6 (Syt6) in the mouse brain. Digital *in situ* hybridization data in Allen Brain Atlas (ABA) reveals slight enrichment of Syt6 RNA in layer 6 of rostromedial neocortex (a, c, e, g; enlarged insets: b, d, f, h) in coronal sections. GENSAT BAC transgenic mice for Syt6 EGFP reporter concur with Syt6 expression in layer 6 of rostromedial neocortex and additionally indicated corticothalamic projection (i, m; enlarged insets: j, k, l, n, o, p).

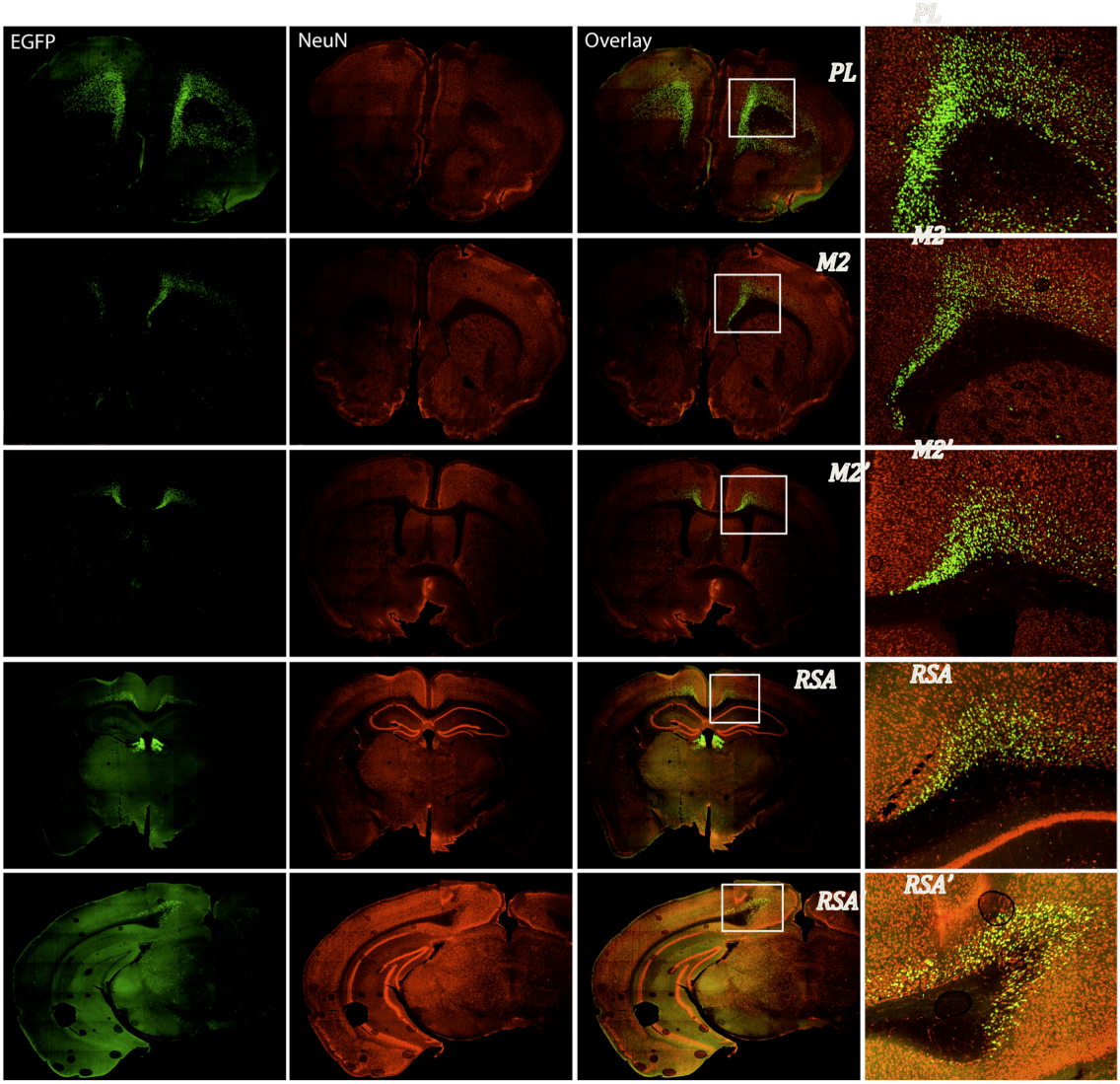

Figure 1.18: Immunohistochemistry of TRAP line Syt6 PS3013: EGFP and NeuN co-immunostaining reveal complete colocalization of EGFP with NeuN, indicating a neuronal identity (a-e). Strong EGFP/NeuN staining is detected in the layer 6 of rostromedial neocortex (a, b, c, d, e; enlarged inset: PL, M2, M2', RSA, RSA'). Subcortical expression of EGFP is detected in the dorsomedial habenula.

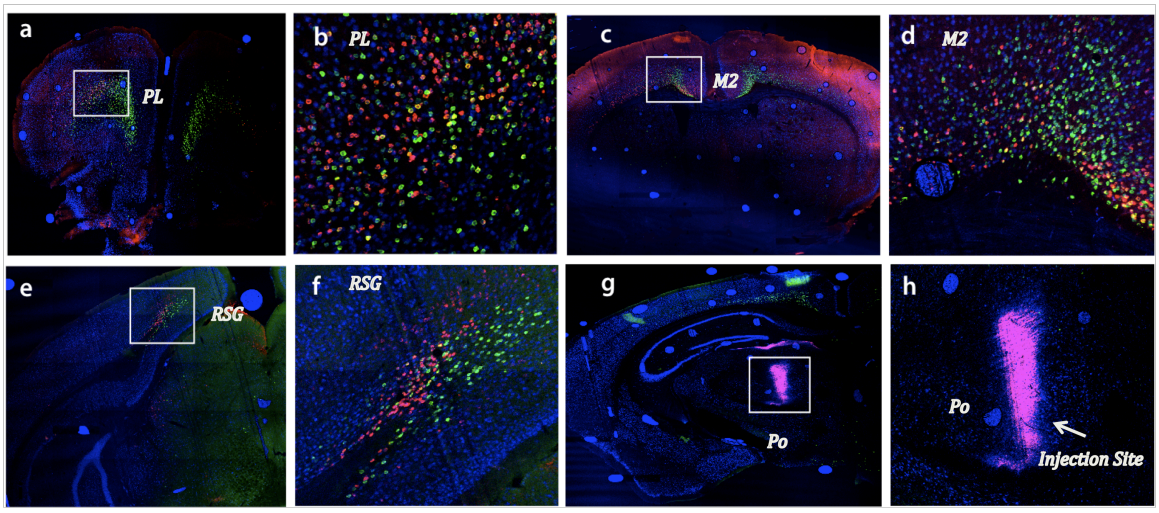

Figure 1.19: Hodology of Syt6 cell type in Syt6 TRAP line. Retrograde transneuronal tracer Cholera Toxin B (CT-B) conjugated to Alexa Fluor 568 was injected into posterior thalamic nucleus (Po) with coordinates: -2.18 mm, +0.75 mm, 3.5 mm (g; enlarged inset: h). Colabeled neurons, positive for both EGFP and CT-B, were present in layer 6 of prelimbic cortex in PFC (a, enlarged inset: b), secondary motor cortex M2 (c, enlarged inset: M2) and retrospenial granular cortex RSG (e; enlarged inset: f) indicating that Syt6 defines corticothalamic cell type.

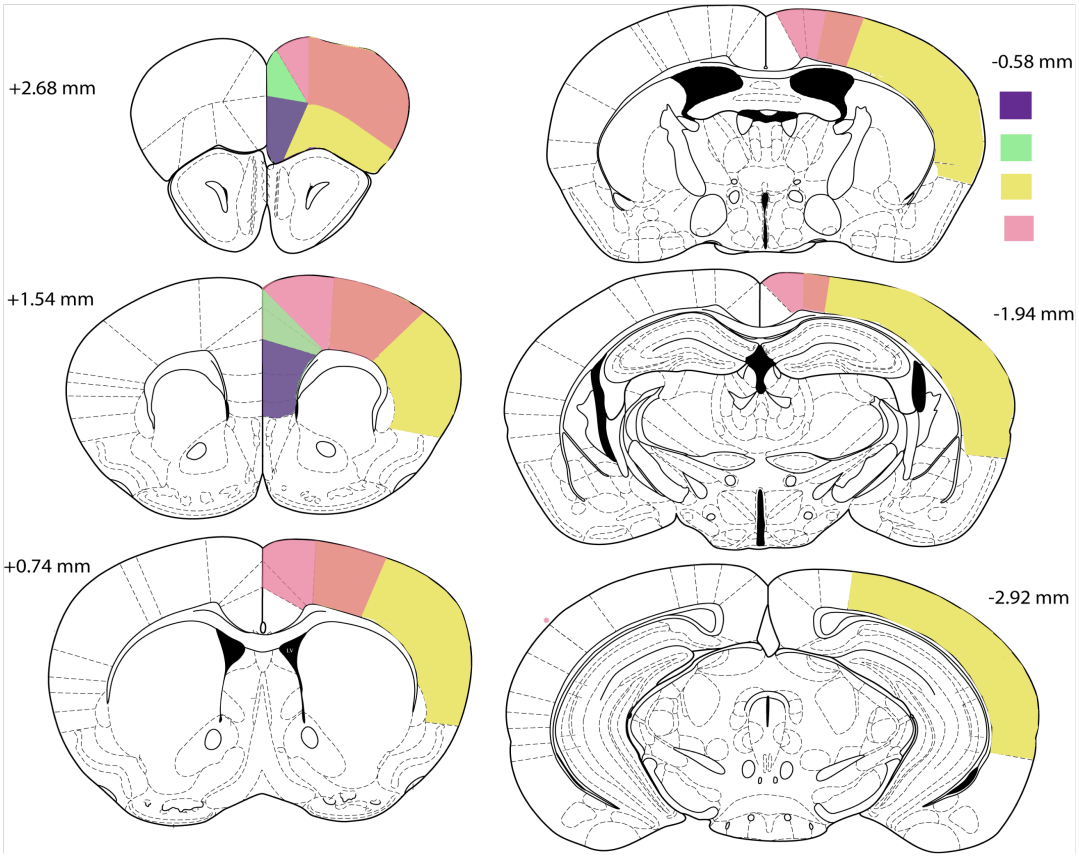

Figure 1.20: Color-coded schematic diagram of distinct TRAP lines. The bac TRAP transgenic lines allow genetic access to distinct cortical pyramidal cell types including Ntf3+ layer 2 medial PFC cell type (purple), Pdyn+ layer 2 dorsal PFC cell type (green), Etv1+ layer 5 lateral neocortex cell type (pink) and Syt6+ layer 6 rostromedial neocortex cell type (yellow).

CHAPTER 2: TRANSLATIONAL PROFILE OF GENETICALLY DEFINED PYRAMIDAL CELL TYPES IN THE NEOCORTEX

2.1 Overview of Genomic Analysis of Cell Types in the CNS

Single gene expression pattern in the CNS is investigated using staining methods such as *in situ* hybridization assay for locating the RNA and immunohistochemistry for locating the protein or by reporter gene assays in transgenic mice using epifluorescent molecules such as EGFP. Analysis of the CNS expression pattern of single gene is valuable for studying the distribution of the neurons that express the gene and the cellular projection and morphology in case of reporter gene assay with soluble EGFP. However, single gene expression pattern does not reveal any information on how the single gene may interact with the collective gene repertoire in the cells. Identification of gene interactions and unique effector molecules can be achieved with powerful genomic tools such as microarrays and RNA-seq that enables coincident detection of the entire molecular repertoire in defined cell types. Such studies of comprehensive cellular gene expression can provide insights into suites of genes that contribute to development and disease (Hatten and Heintz, 2005; Luo et al., 2008).

Traditionally, genomic studies were carried out on crudely extracted tissue of the CNS. However the extraordinary complexity and cellular homogeneity of the mammalian CNS significantly limited the power of the microarray for gene expression analyses. Since many distinct neuronal and non-neuronal cells are highly intermixed, microarray analyses of a given brain region presented only a composite view of gene expression while diluting out less abundant genes and masking genes that are differentially expressed in apposing cell types in the same tissue. Hence critical and significant gene expression alterations within a single neuronal cell type often eluded detection in microarray analyses using complex brain tissues. Over the last

decade, however, there have been massive efforts at microarray analyses of defined cell types in the CNS. Current existing methodologies that have been used for genomic analysis of cell types include laser capture microdissection (LCM) (Chung et al., 2005; Rossner et al., 2006), Fluorescence Activated Cell Sorting (FACS) (Arlotta et al., 2005), Immunopanning (PAN) (Cahoy et al., 2008), Manual dissection of Single neurons (Sugino et al., 2006) and lastly the strategy developed in our lab – Translating Ribosome Affinity Purification (TRAP) (Doyle et al., 2008; Heiman et al., 2008). Among these, LCM, FACS and PAN strategies all rely on acute physical dissociation of target cell populations which introduces potential stressors in the intervening steps between tissue extraction and mRNA isolation. Potential stressors include antibodies, enzymes and other reagents used for immunopanning or to digest tissue, non-physiological variations in temperature and other aspects of the cellular environment as well as mechanical stress of physical dissociation of the tissue. These potential stressors can induce transcriptional response of Immediate Early Genes (IEGs) and Apoptosis related genes, as an adaptive response upon loss of tissue intrinsic signals. Also, the LCM method is faced with the technical challenge associated with RNA purification from fixed tissue. Circumventing these problems, the TRAP methodology developed in our lab (Heiman et al., 2008) employs a direct and rapid affinity purification strategy for isolation of polysomal RNA from genetically targeted cell types.

2.2 Translating Ribosome Affinity Purification Methodology

The TRAP methodology is based on the simple idea that the messenger RNAs once transcribed and shuttled into the cytoplasm associate with ribosomes for the initiation of protein

synthesis. Tagging a key ribosomal subunit with an epitope permits pull down of the actively translated mRNAs that are associated with the ribosomal translation machinery. This idea has been previously applied in other organisms such as yeast (Inada et al., 2002), plants (Zanetti et al., 2005) and worms (Kunitomo et al., 2005). However, in these instances the researchers pulled down the ribosome associated mRNAs from the tissue in non-cell type specific manner. Our lab (Heiman et al., 2008) presented the novel approach of incorporating the ribosome-RNA pull down with BAC transgenesis. Heiman et al (Heiman et al., 2008) screened different epitopes and ribosomal subunits for generating the fusion peptide and settled on EGFP for epitope which doubles as a reporter and L10, the essential peptide that forms part of the 60S large ribosomal subunit, for the tagged protein. The use of EGFP as the affinity tag greatly facilitates anatomic studies of candidate bacTRAP mouse lines, as discussed in Chapter 1, and also enables electrophysiological characterization of the cell types. The EGFP-L10 modification was incorporated into relevant BACs by bacterial homologous recombination dependent on recombination competence introduced by exogenous RecA gene. Briefly, first the BACs for candidate genes are selected for central localization of the gene in the BAC so that the BAC contains regulatory sequences in both 5'- and 3'- Untranslated regions (UTRs). Then a short homology region, A box (usually 500 bp – 1kb), is defined as the genomic sequence immediately preceding the translation start codon and is cloned into the specialized shuttle vector pS296. The shuttle vector already has the coding sequence for EGFP-L10 fusion incorporated into its backbone. The modified shuttle vector pS296-A box is then used for homologous recombination of the A box – EGFP-L10 cassette into the BAC vector under RecA mediated recombination competence. The modified BAC vector is positively selected for by using a dual antibiotic medium since the homologous recombination renders antibiotic resistance

to both Ampicillin and Choramphenicol. This is followed with validation of the modified BAC by PCR based methods and by Southern Blotting with radiolabeled A box probe. Next, the validated BAC is purified by Cesium Chloride gradient taking utmost care to retain the integrity of the BAC and then injected into fertilized oocytes of super-ovulating FVB female mice. The newborn litter from the injections is screened for germline transmission of the BAC as well as expression of the reporter in the targeted cell type. The transgenic mice that successfully target the reporter into endogenous population expected for the gene driver are designated as founders and characterized in further detail for neuronal anatomy and BAC copy number analysis.

The bacTRAP transgenic mice are then subjected to the novel polysomal immunoprecipitation protocol that forms the crux of the TRAP methodology. After the bacTRAP transgenic mice are euthanized by CO2 asphyxiation, relevant CNS tissue is dissected out in a chilled medium containing glucose, nuclease inhibitors and cycloheximide followed by homogenization in a detergent buffer supplemented with magnesium, nuclease inhibitors and cycloheximide. Polysomes are then affinity purified using monoclonal EGFP antibodies conjugated to Protein L. Finally the RNAs bound to the polysomes are extracted and subjected for genomic analyses. The buffer conditions during the polysome extraction and purification steps are crucial in stabilizing the polysomes and in preventing the redistribution of the affinity tag within the mRNA pool, which obviates the problems inherent in using less stable mRNA binding proteins.

The pool of cell type specific RNAs obtained with TRAP methodology is representative of the active translatome at the time of tissue processing. Existing strategies to analyze the

transcripts can be categorized into three groups: 1) Single transcript enrichment analysis by quantitative RT-PCR, 2) Genomic analysis by oligonucleotide-based microarrays and 3) Genomic analysis by ultra high throughput sequencing (RNA-seq). The RT-PCR method is useful for validating the enrichment of individual candidate genes but it is not amenable to quantitate the copy number of all the transcripts (Geschwind, 2000; Mori et al., 1998). The two genomic analyses – microarray and RNA-seq – are coincident detection methods that allow simultaneous enrichment analysis for thousands of genes and thus present an opportunity to generate a relatively comprehensive gene expression profile of targeted cell types (Geschwind, 2000; Mortazavi et al., 2008). But both methods have their benefits and limitations. The microarrays are currently the most widely used methodology for transcriptome analysis and allow coincident detection of enrichment for 40,000 oligonucleotide cDNA probes, however they face limitations such as incomplete coverage of all possible genes in the genome, inability to detect low abundance genes (less than 5 copies) and splice variants. The sequencing methods (RNA-seq) on the other hand involve direct ultra high-throughput sequencing of cDNA (Mortazavi et al., 2008; Wang et al., 2009). The resulting sequence reads are individually mapped to the source genome and counted to obtain the number and density of reads corresponding to RNA from each known exon, splice event or new candidate gene. While RNA-seq gives a substantially higher coverage of the genome and enables detection of splice variants, it necessitates extensive sequencing (> 40 million reads) of a sample to detect and quantify RNAs from all biologically relevant abundance classes and to map RNA splice choices for transcripts of high and moderate abundance. Additionally, while there are well established analytical platforms designed for the microarray data, such as Gene Spring and dChip algorithm (Bunney et al., 2003), the tools for analyzing the extensive sequence data from the samples are

just being developed, such as Enhanced Read Analysis of Gene Expression (ERANGE) (Mortazavi et al., 2008). RNA-seq is also not free of ambiguities caused by gene sequences that are closely related to each other which could be attributed to multireads of the same gene. In the current study, we have used microarrays to analyze the translational profile of cortical pyramidal cell types.

2.3 Microarray Analysis of Cell Type Specific Transcripts in the Neocortex

Cortex researchers have employed a variety of methods to analyze the transcripts in defined neocortical cell types. As discussed earlier, the existing methodologies for transcriptome analysis besides TRAP are: LCM, FACS, PAN and Manual dissection (MAN). Rossner et al (Rossner et al., 2006) used Thy-1 transgenic mice in which genetically defined cells were labeled with a nuclear variant of EGFP and employed LCM to extract RNA from layer V of the somatosensory cortex in freeze-dried sections. Arlotta et al (Arlotta et al., 2005) injected green fluorescent microbeads into the projection targets such as spinal cord, corpus callosum and tectum and isolated the retrogradely labeled corticofugal neurons by FACS purification. Cahoy et al (Cahoy et al., 2008) used EGFP transgenic mice and extracted the relevant cell types, Aldhl1 astrocytes, by acute dissociation and immunopanning (PAN) purification protocols. On the other hand, Sugino et al (Sugino et al., 2006) used Thy-1 EGFP transgenic mice and also mice injected with retrograde fluorescent microbeads in the mediodorsal thalamus that labeled cells in the cingulate cortex. They dissected the tissue and manually (MAN) sorted the fluorescently labeled neurons for RNA extraction. Comparison of these methodologies with TRAP revealed that while all of these methods are highly reproducible, they differ in the level of

contamination from transcripts induced by the procedural stressors and from other cell types, a total of 12 genes, including interneuron markers, astrocyte markers and oligodendrocyte markers (Okaty et al., 2011). When Okaty et al (2011) analyzed the data from the Purkinje cell type, the LCM and FACS purified samples had the highest indices for contaminants from the stressors where as the contamination index for non-pyramidal cell genes was high for all methods except MAN. It is important to note however that the TRAP methodology is not directly comparable to the rest of the transcriptome analysis methods since TRAP gives a snapshot of the translational profile of a given cell type where as the other methods present aggregate transcription profile of the cells. Additionally, it is possible that the reporter is present in trace amounts in non-Purkinje cells leading to the presence of contaminating transcripts in the translational profile. From another perspective, it is possible that not all 12 of the selected negative genes are truly non-Purkinje cell markers.

In this study, we have used the TRAP methodology for affinity purification of polysomes specific to genetically defined pyramidal cell types in the neocortex and analyzed the translational profiles for enriched transcripts and overrepresented gene ontologies and biological pathways (Fig 2.1). Following the RNA isolation from the cortical tissue, we assessed the quality of the RNA using a Picochip with the Bioanalyzer – whereupon the electropherograms were analyzed for the relative measures of ribosomal RNAs 20S and 16S, and the RNA Integrity Number (RIN) was used as a metric for the transcript quality (data not shown). Good quality transcript replicates were then subjected to Affymetrix Two Cycle RNA Amplification. Briefly, the RNA pool was reverse transcribed to cDNA, which was then PCR amplified and subjected to a first round of In Vitro Transcription (IVT). This IVT RNA was again reverse transcribed to

cDNA, which finally undergoes the second round of IVT with Biotin-labeled nucleotides. On average, about 40-80 ug Biotin-labeled RNA was obtained after the two-cycle amplification and 20 ug of the yield was fragmented to small oligomers and hybridized on to the Mouse Genome 430 2.0 microarrays. Finally the chips were scanned for the intensities of the Biotin immunofluorescence and the expression values for each of the 40,000 oligo probes were compared with the whole cortical tissue as control using the scientific software GeneSpring 7.2.

RESULTS:

2.4 Translational Profile of Pdyn Cell Type, a subset of Layer II ACC enriched pyramidal cells

Pdyn is expressed in the superficial layer II cells in the Anterior Cingulate Cortex (ACC) and likewise, the Pdyn EGFP-L10 mice, also referred to as Pdyn bacTRAP mice, express the transgene in the layer II ACC cells. Pdyn CP12 bacTRAP mice however also express the transgene in few scattered cells in the middle layers of the caudal cortex and strongly in the subcortical regions such as striatum and hypothalamus. Hence we had to empirically determine the optimal dissection methods and starting tissue material for Pdyn CP12 in order to prevent contaminating transcripts from the striatum and caudal cortex. We defined frontal pole as the region of the anterior cortex immediately preceding the start of the corpus callosum and thus manually dissected out the frontal cortex from the mouse brain. Given the sparse distribution of the Pdyn Cell Type in the superficial ACC, we pooled together 12 cortices from a cohort of 6 adult mice to enrich the polysomes specific for Pdyn Cell Type. With this optimization protocol,

we obtained an average RNA yield of 10.2 ng/ ul from each biological replicate of 6 gender balanced adult mice. Replicate bacTRAP sample, referred to as Immunoprecipitated RNA (IP) from here on, for Pdyn CP12 gave nearly identical genome wide translational profiles (average Pearson correlation coefficients of 0.96). Using the Genespring software, Pdyn CP12 ACC IP samples were then plotted against an average of six pooled RNA samples from the whole cortex (average Pearson Correlation Coefficient of 0.93) (Fig 2.2).

The Pdyn probe (1416266_at) was enriched in the Pdyn ACC IP by a fold change (FC) of 19.34 compared to the whole cortical tissue. For the data quality assessment, known negative non-pyramidal cell markers were plotted on the Pdyn IP vs Whole Cortex graph. They include the astrocyte genes (Aqp4, Gfap, AldhL1, Lpd and S100b), glial genes (Mag, Mbp, Galc, Slc1a3, Cnp1, Cklsf5 and Olig2) and interneuron genes (E130115E03Rik, Slc6a1, Viaat, Calb2, Cort, Vip, Gad1, Gad2, Npy, Htr3a, Sst and Pva). Most of the non-pyramidal cell markers were depleted in the Pdyn CP12 ACC IP, however there were some genes from this list (Slc1a3, Mag and AldhL1) that were enriched (FC > 1.5) in the IP indicating that Pdyn might be expressed at low levels in some glial cells, although this was not visually detectable by immunofluorescence. We further examined the expression levels of annotated pyramidal cell markers and found that Wfs1 (1448411_at, FC = 3.128), Npnt (1452106_at, FC = 1.523), 2900052E22Rik (1428986_at, FC = 6.410), and Ntsr (1420799_at, FC = 1.759) were enriched in the Pdyn ACC IP. We next looked at the Top 1000 genes that were highly enriched in the Pdyn ACC IP and scored for specific or enriched expression in layer II of neocortex by consulting the digital ISH database at Allen Brain Atlas (ABA). Some of the Layer II enriched genes based on ABA data include Wfs1, Spint2, Npy1r, Lypd1, Kcns2, Kcna5, Gpr83, Efcbp2, Dpy19l3, and D330017J20Rik.

2.5 Translational Profile of Ntf3 Cell Type, a subset of Layer II medial PFC enriched pyramidal cells

Ntf3 is expressed in Layer II pyramidal cells of the medial PFC, as discussed in Chapter 1. Similarly, at least two founders of Ntf3 bacTRAP mice, PS1045 and PS1046, express the transgene EGFP-L10 in the endogenous cell populations in the PFC. Both of these lines however, also express the transgene in the piriform cortex, olfactory bulb and septum. Hence, care was taken to dissect out the subcortical regions as well as the piriform cortex during cortical tissue harvest. Given that the EGFP-L10 expression was very specifically restricted to a small population of tightly packed cells in the mPFC, we pooled together a cohort of 4 mice (8 cortices) for each of the three biological replicates of Ntf3 PFC IP. The average RNA yield for each IP replicate was 16.8 ng/μl for Ntf3 PS1045 and 27.19 ng/μl for Ntf3 PS1046. The Ntf3 PS1045 IP replicates gave nearly identical genomic translational profiles (average Pearson correlation coefficient of 0.974). Likewise the Ntf3 PS1046 IP replicates also had a high correlation coefficient of 0.966. The IP replicates were then plotted against Whole Cortex Tissue RNAs using GeneSpring 7.2.

2.5.1 Translational Profile of Ntf3 PS1045 Cell Type in the medial PFC

We first looked at the enrichment for the driver probe Ntf3. Both probes for Ntf3, 145660803_at and 1434802_a_at, were highly enriched in the Ntf3 PS1045 Cortex IP when compared to the whole cortex RNA. For the data quality assessment, known negative non-

pyramidal cell markers were plotted on the Ntf3 IP vs whole cortex graph (Fig 2.3). Most of the negative non-pyramidal cell markers were depleted in the Ntf3 PS1045 cell type except some genes such as the glial genes Cnp1 (1437341_x_at, 1418980_at), Hprt (1448736_a_at), Anxa5 (14255667_a_at), Slc1a3 (1452031_at), Mag (1460219_at) and astrocyte gene Lpd (1422428_at). It is possible that there is low, but visibly undetectable, level of expression of the transgene in the glial cells in PS1045 but on the other hand, it is also possible that some of these genes may not be exclusively glial and may actually be present in endogenous pyramidal cells that express Ntf3. Among annotated pyramidal cell markers, there were several genes enriched in the PS1045 Cortex IP such as Snap25 (1416828_at) – a pan-neuronal marker, Itpka (1424037_at), Neurod6 (1418047_at), Pdlim1 (1416554_at), 2900052E22Rik (1428986_at), Ntsr (1420799_at) and Pdyn (1416266_at) – also a layer II pyramidal cell marker as previously discussed. It is also noted that pyramidal cell markers Etv1 (1422607_at) and Npnt (1452107_a_at) are depleted in the Ntf3 cell type, indicating that these markers define mutually exclusive pyramidal cell types in the neocortex. We also looked at excitatory neuronal markers vGlut1 and vGlut2, and they were both enriched in Ntf3 PS1045 Cortex IP with FC of 2.11 for vGlut1 and 1.56 for vGlut2, reaffirming that the Ntf3 Cell Type is a cohort of excitatory pyramidal cells (Fig 2.3). For further data analysis, we applied a filter on the expression level – a threshold of 50 and looked at the Top 1000 genes that were most differentially enriched in the Ntf3 PS1045 Cortex IP. We then compared our list of genes with the ABA ISH annotated list for fine structure cortical layer 2. Our results indicated that the following ABA annotated Layer II genes are enriched in the Ntf3 PS1045 Cortex IP – Enpp2, Gucy1a3, Cyld, AW125753, Calb1, 6330514A18Erik, Igsf11, Smoc2, Hrh2, Ankrd6 and D8Ertd82e. On the other hand, the following ABA annotate Layer II genes were depleted in the Ntf3 PS1045 Cell Type – Kitl,

Ddit4l, Dusp18, Acvr1c, Pip5k1a, Syn3 and Pvrl3, which indicate that even within layer II, pyramidal cells are heterogeneous and form multiple distinct genetic cohorts.

2.5.2 Translational Profile of Ntf3 PS1046 Cell Type in the medial PFC

The Ntf3 PS1046 bacTRAP line defines a cohort of Layer II pyramidal cells in the medial prefrontal cortex and extends to the dorsal anterior cingulate as opposed to Ntf3 PS1045 cell type which is restricted to ventromedial PFC. Three biological replicates for Ntf3 PS1046 cortex IPs were imported together into Genespring 7.2, GC-RMA normalized and compared to the whole cortex RNAs that were imported separately (Fig 2.4). The scatterplot of PS1046 IP vs whole cortex showed a similar distribution as Ntf3 PS1045 cortex IP vs whole cortex. The driver probes for Ntf3 (1450803_at and 1434802_a_at) were both highly enriched in the Ntf3 PS1046 cortex IP respectively. All the negative non-pyramidal cell markers (all 24 of them) were depleted in the Ntf3 PS1046 Cortex IP suggesting that in this bacTRAP line, the Ntf3 cell type are targeted accurately with no contamination from the non-pyramidal cell types.

Among the annotated pyramidal cell markers, there were several genes enriched in the PS1046 IP such as Itpka (1424037_at), Wfs1 (1448411_at), 2900052E22Rik (14289886_at) and Ntsr (1420799_at) (Fig 2.4). On the other hand, several pyramidal cell markers were depleted in the Ntf3 cell type including Neurod6 (1418047_at), Etv1 (1450684_at and 1422607_at), Ctgf (1416953_at), Slc17a6 (1428379_at), Npnt (1452107_a_at and 1452106_at), Drd1a (1455629_at and 1456051_at) and Hsd11b1 (1449038_at). The latter result indicates the cellular heterogeneity in the neocortex among pyramidal cells. Next we looked at the excitatory

projection neuron markers, namely vGlut1 and vGlut2, of which vGlut1 is enriched in the Ntf3 PS1046 IP with a FC of 1.88 but vGlut2 is slightly depleted with an average FC of 0.505. For further data analysis, we applied a filter on the expression level – a threshold of 50 and looked at the Top 1000 genes that are most differentially enriched in the Ntf3 PS1046 Cortex IP. We then compared our list of genes with the ABA ISH annotated list for fine structure cortical layer 2. Our results indicated that the following ABA annotated Layer II genes are enriched in the Ntf3 PS1046 Cortex IP – 6330514A18Rik, Smoc2, Ptgs2, Rps6ka2, Palmd and Otof where as the following ABA annotated Layer II genes are depleted – Acvr1c, Enpp2, Pip5k1a, Calb1, Ddit4l, Pdzrn3, Tdg, Dusp18, Gucy1a3, Pvrl3, Pde7b and Rragd. It is interesting to note that compared to Ntf3 PS1045 cortex IP, Layer II markers Gucy1a3, Enpp2 and Calb1 have opposite trend in expression i.e. they are depleted in PS1046 IP but enriched in PS1045 IP. It is possible that these genes are enriched in the ventromedial PFC Ntf3 cell type (PS1045 and PS1046) but not enriched in the dorsomedial PFC (PS1046), so the regionally graded distribution of these genes may counterbalance each other in the case of Ntf3 PS1046.

The list of top 1000 highly enriched genes in Ntf3 PS1045 cortex IP and Ntf3 PS1046 cortex IP were directly compared using a Venn diagram (Fig 2.5). The comparative analysis revealed that there are 136 genes in common between PS1045 IP and PS1046 IP including the driver gene Ntf3. But remarkably, there are 865 genes exclusively enriched in PS1045 IP and 868 genes exclusively enriched in PS1046 IP. The first reasoning could be that the cell types targeted in PS1045 and PS1046 are fundamentally more different than similar due to different genomic site of integration of the BACs in each case. Alternative explanation could be that the mutually exclusive genes define molecular markers for the dorsal ACC layer II (PS1046) and the

ventral OFC (PS1045) since the transgene expression in these areas are different in the two bacTRAP lines. For further comparative cell type analysis, we decided to

2.6 Translational Profile of Etv1 Cell Type, a subset of Layer Va Lateral Cortex enriched pyramidal cells

Etv1 is expressed in Layer Va pyramidal cells of the lateral cortex, as discussed in Chapter 1. Out of the three founders for Etv1, PS476, PS477 and TS88, we decided to characterize the translational profile of PS476 cortex because the other two bacTRAP transgenic lines had ectopic expression in non-layer V pyramidal cells (PS477) and non-pyramidal cells (TS88). The latter bacTRAP line TS88 has the transgene expressed at low levels in astrocytes and so, the translational profile for this line has contaminating transcripts from the astrocytes (Doyle 2008). Etv1 PS476 bacTRAP line has a remarkably restricted transgene expression in a thin band of small layer Va pyramidal cells, as described in Chapter 1. Besides the neocortex, the PS476 bacTRAP line has transgene expression in CA1 region of the hippocampus and posterior nucleus of Thalamus. We dissected 8 cortices from 4 adult mice, which were then pooled together for each of the three biological replicates with an average RNA yield of 12 ng/μl. The Etv1 IP replicates gave nearly identical genomic translational profiles (average Pearson Correlation Coefficient of 0.93) (Fig 2.6).

We first looked at the enrichment for the driver probe Etv1. The Affy probe for Etv1 is enriched in the PS476 Cortex IP by a FC of 2.2 compared to the Whole Cortex RNA. For the data quality assessment, known negative non-pyramidal cell markers were plotted on the PS476

IP vs Whole Cortex graph (Fig 2.6). Most of the negative markers were depleted in Etv1 Cell Type except AldhL1 (1424400_a_at) and H2-K1 (1425545_x_at). Examination of the AldhL1 microarray data for cortex revealed that the Etv1 probe is similarly enriched in this Cell Type. This could either indicate that a subpopulation of AldhL1 cell type is Etv1 positive pyramidal cells, or conversely a subpopulation of Etv1 cell type is AldhL1 positive astrocytes. Immunofluorescence with EGFP antibody did not reveal expression of the transgene in astrocytes, so it is more likely that a subpopulation of AldhL1 cell type are Etv1 positive pyramidal cells. Among annotated pyramidal cell markers, there were several genes enriched in the PS476 cortex IP such as S100a10 (1456642_x_at and 1416762_at) – a layer V corticostriatal pyramidal cell marker, Hsd11b1 (1449038_at) – a layer V lateral cortex pyramidal cell marker and Emx1 (1441777_at) – a marker for cortical pyramidal cells. It is also noted that pyramidal cell markers Ctgf (1416953_at), Drd1a (1455629_at and 1456051_at), Npnt (1452107_s_at), Scara3 (1427020_at), Ntf3 (1434802_a_at) and Pdyn (1416266_at) are depleted from the Etv1 PS476 Cortex IP. Of these, Ctgf and Drd1a are known Layer VI markers whereas Ntf3 and Pdyn, as described earlier, define Layer II pyramidal cells in the neocortex. This suggests that the gene drivers we have utilized so far - Etv1, Ntf3 and Pdyn - define non-overlapping Cell Types in the neocortex. We also looked at excitatory neuronal markers vGlut1 and vGlut2, and we found that vGlut1 was present in PS476 Cortex IP with a FC of 1.138 but vGlut2 was slightly depleted with a FC of 0.826. Since Etv1 defines such a narrow band of small pyramidal cells in layer Va, and 70% of the cell types in neocortex are pyramidal and excitatory, this result indicates that the vGluts are enriched more in the whole cortex than the Etv1 positive Cell Type. Previous results already confirm that Etv1 Cell Type defines long distance corticostriatal

projection neurons (from the CTB retrograde tracer injections) and that they have adapting firing pattern (Groh 2010) described for pyramidal cells.

For further data analysis, we applied a filter on the expression level – a threshold of 50 and looked at the Top 1000 genes that were most differentially enriched in the Etv1 PS476 Cortex IP. We then compared our list of genes with the ABA ISH annotated list for fine structure cortical layer V. Our results indicate that that following ABA annotated Layer V genes are enriched in Etv1 PS476 Cortex IP – Hsd11b1 and Chst8, whereas the following ABA annotated Layer V genes are depleted – 9630015D15Rik, Ler3, Cxcl1, Rspondin, Thbd, Adamts2, Cyp39a1, Grik2, Matn2, 2310046M24Rik and B430320C24Rik. The following genes from the Top 1000 list were Layer V specific in the ABA ISH database even though there were not structurally annotated - Lamc2, Anxa6, Pcnt2, Ldhd, Susd2, Slc1a1, S100a10, 28104890O6Rik, A630065K24Rik, Coch, Sult1a1, Cyp26b1, Opn3, Twist1 and Whrn.

2.7 Translational Profile of Syt6 Cell Type, a subset of Layer VI Rostromedial Cortex enriched pyramidal cells

Syt6 is expressed in Layer VI pyramidal cells of the rostromedial cortex, as discussed in Chapter 1. Out of 5 founders for Syt6, we decided to characterize the translational profile for two bacTRAP lines PS3011 and PS3013, since they recapitulated the endogenous Syt6 expression. PS3013 has a higher copy number of the BAC than PS3011 so expectedly PS3013 had many more cells in the Layer VI labeled with the transgene compare to PS3011 and seems to completely cover the Syt6 expression in the neocortex. Besides the neocortex, both PS3011 and

PS3013 have the transgene expressed in dorsomedial habenula. We dissected 6 cortices from 3 adult mice which were then pooled together for each of the three biological replicates with an average RNA yield of 15 ng/µl for PS3011 cortex IP and 21.64 ng/ ul for PS3013 cortex IP. The Syt6 IP replicates gave nearly identical genomic translational profiles (average Pearson Correlation Coefficient of 0.944 for PS3011 and 0.956 for PS3013.

2.7.1 Translational Profile of Syt6 PS3011 Cell Type in the Rostromedial Cortex

We first looked at the enrichment for the driver probe Syt6. Unfortunately, both the Affy probes for Syt6 were below threshold of expression in the Syt6 PS3011 cortex IP. Upon inspection in other cortical pyramidal cell lines generated in the lab, the Syt6 probes always were expressed at low levels, which indicated that the probes did not hybridize well to the Syt6 transcript. For the data quality assessment, known negative non-pyramidal cell markers were plotted on the Syt6 PS3011 IP vs Whole Cortex graph (Fig 2.7). Most of the negative non-pyramidal cell markers were depleted in the PS3011 Cell Type except some genes such as the glial genes Slc1a3 (145031_at), Lpd (1422428_at), Mag (1460219_at) and blood cell genes H2-K1 (1425545_x_at, 1451784_x_at and 1451931_x_at). It is possible that Syt6 is expressed at low levels in the blood vessels and glial cells. Among annotated pyramidal cell markers, only Pdyn (1416266_at) was the only gene with borderline enrichment. The following pyramidal cell markers were depleted from the PS3011 cortex IP – S100a10 (14566642_x_at), Ctgf (14166953_at), Srf (1418255_s_at), Etv1 (1422607_at), Slc17a6 (14268379_at) and Drd1a (14556629_at and 1456051_at). While Etv1 and S100a10 are known markers for layer V corticostriatal pyramidal cells, Ctgf and Drd1a both label subpopulations of Layer VI pyramidal

cells with non-overlapping projections to the cortex and striatum respectively. So it is not surprising that these markers are not enriched in Syt6 PS3011 cell type. We also looked at excitatory neuronal markers vGlut1 and vGlut2, and they were not enriched with vGlut1 FC of 1.126 and vGlut2 FC of 0.355. For further data analysis we applied a filter on the expression level – a threshold of 50 and looked at the Top 1000 genes that were most enriched in the Syt6 PS3011 Cortex IP. We then compared our list of genes with the ABA ISH annotated list for fine structure cortical layer VI. Our results indicated that Pcnt2 was the only ABA annotated Layer VI gene enriched in the Syt6 PS3011 Cortex IP, whereas Atf6 was strongly depleted.

2.7.2 Translational Profile of Syt6 PS3013 Cell Type in the Rostromedial Cortex

We first looked at the enrichment for probes for the driver Syt6. On average, the four Syt6 probes were slightly enriched in PS3013 Cortex IP by 1.54, however when checked individually, one of the Syt6 probes (1426106_a_at) was enriched in the PS3013 Cortex IP by a FC of 3.128 while the other probes were expressed at low levels (Fig 2.8). Among the annotated pyramidal cell markers, there were several genes enriched in the PS3013 Cortex IP such as 2900052E22Rik (1428986_at), Scara3 (1427020_at) and Slc17a6 (1418610_at). However, some negative non-pyramidal cell markers are also enriched in PS3013 Cortex IP such as Anxa65 (1425567_a_at), Cnp1 (1418980_a_at), Slc1a3 (1452031_at and 1426341_at) , AldhL1 (1424400_a_at), Mag (1460219_at) and Gfap (1426509_a_at). We also looked at excitatory neuronal markers vGlut1 and vGlut2, and both of them were enriched with an average FC of 3.702 for vGlut1 and 1.721 for vGlut2 respectively. For further data analysis, we applied a filter on the expression level – a threshold of 50 and looked at the Top 1000 genes that were most differentially enriched in the

Syt6 PS3013 Cortex IP. We then compared our list of genes with the ABA ISH annotated list for fine structure layer VI. Our results indicated that the following Layer VI genes annotated by ABA are enriched in the Syt6 PS3013 IP: Cdh2, Crh, Rgs20, Rai14, Fstl1, Aacs, Cdh2, Moxd1, Shb, 6330500D04Rik, P4ha2, Sema5b, BC029169, Trh, Col23a1 and Pde6g. In addition, we manually annotated genes in our Top 1000 list and enlisted several more Layer VI genes in the list namely: Atf6, Pcnt2, Arhgap25, Slc17a6 and Cyr61.

The list of Top 1000 highly enriched genes in Syt6 PS3011 cortex IP and Syt6 PS3013 cortex IP were directly compared using a Venn diagram (Fig 2.9). The comparative analysis revealed that there are 308 genes in common between PS3011 IP and PS3013 IP. But remarkably, there are 720 genes exclusively enriched in PS3011 IP and 724 genes exclusively enriched in PS3013 IP. The PS3013 bacTRAP line has considerably more pyramidal neurons in Layer VI labeled with EGFP compared with PS3011 so the 724 genes exclusively enriched in PS3013 are likely genes important for the cellular identity in non-PS3011 cell type. In the same vein, it is likely that the 720 genes that are exclusively enriched in PS3011 likely define genes that are enriched highly in the PS3011 Layer VI cell type, but their enrichment in the aggregate Syt6 cell type is counterbalanced by relative depletion in the PS3011 negative Layer VI cell type.

2.8 Comparative Quantitative Translational Profile of Three Distinct Pyramidal Cell Types in Neocortex: Ntf3, Etv1 and Syt6

The TRAP methodology allows comprehensive translational profiling of individual genetically defined cell types in the CNS. So far, we have compared cell type specific RNAs to

the whole cortex RNAs in order to identify genes that are differentially expressed in the genetically targeted cell type in relation to the background neocortical tissue. However, this sort of analysis of individual cell type reveals a mixed repertoire of expressed genes that includes both unique cell type markers as well as genes that for example may be important for the entire class of pyramidal cells. Also, IP vs whole cortex alone does not give a sense of how likely a particular ratio is to appear by chance, and at what threshold a gene should be considered enriched. Our lab has generated many bacTRAP transgenic mice targeting different categories of cell types in the CNS, including pyramidal cells, interneurons, glial cells, astrocytes and oligodendrocytes. Concurrent comparison of different cell types in the neocortex can give us valuable information on the unique molecules that render the cellular identity and function in each cell type. Standard tools for identifying statistically significant differences between samples such as the empirical Limma module of Bioconductor with FDR multiple testing correction can be applied to the TRAP data, but this method results in a large list of statistically significant genes e.g. TRAP data comparison of Purkinje cells versus Astrocytes resulted in > 60% of probesets reaching statistical significance ($p < 0.05$) (Dougherty et al., 2010). This number of statistically significant changes demonstrates the limited utility of such methods for selecting small numbers of targets for biological follow-up studies from such dramatically different cell types. To address this issue, our lab (Dougherty et al., 2010) has devised a Specificity Index (SI) analytical approach that is specifically designed to provide a robust framework for comparative quantitative analysis of data obtained from large numbers of cell types. The SI uses a permutation based statistical approach to compensate for any irregularities in the distributions of the data, allowing direct comparison of P-values across samples with quite varied distributions. The SI analysis needs to be tailored to the biological question at hand.

The SI is an R-based generic algorithm for assessing the specificity of a given RNA in one sample relative to all other samples analyzed. For each cell type, the SI is calculated in three steps as described in Fig 2.10. First following GCRMA normalization within replicates and global normalization across samples, the IP was compared to the total to filter out the non-specific background by setting a simple threshold based on negative controls. Second, for the remaining probesets, this filtered IP was iteratively compared to each other (unfiltered) sample in the dataset and a ratio was calculated for each probeset. To prevent extreme outliers from skewing the subsequent analysis, and to make the analysis more robust for difficult to normalize datasets, the probesets were ranked from highest to lowest ratio within each comparison. Third, for each probeset, its ranks across all comparisons were averaged to give the SI. Thus, the SI is a measure of the specificity of expression for each probeset in a given cell type relative to all other cell types included in the analysis: how highly ranked on a gene list is this probeset, on average, in this cell type compared to all others. Previously Dougherty et al (Dougherty et al., 2010) evaluated the scrambled list of 150 enriched genes (by statistical significance) in six cell types using chi-squared tests. The evaluation revealed that SI outperforms IP/Whole Cortex especially for those cases where the TRAP'ed cell type makes up a significant fraction of the total, such as Neurod1 positive granule cells in the Cerebellum. In the case of Layer V cortical projection neurons (Glt25d2), SI or IP/Whole Cortex both yielded ~50% more than the amount of specific patterns expected by chance. Thus for cortical pyramidal cells, it is useful to carry out both IP/Whole Cortex and SI analyses to make a list of genes that are specific to the cell type relative to the whole tissue as well as to all other cell types being analyzed.

2.8.1 Selection of Cell Types for Comparative Quantitative SI Analysis of Cortical Pyramidal Cells

SI is a relative measure that is influenced by the composition of the entire dataset, so it is important to consider which datasets to include for the specific experimental question being addressed. We wanted to ask the question – what are the unique genes expressed in the different cortical cell types genetically defined by Ntf3, Etv1 and Syt6 Neuroanatomical studies revealed that these gene drivers define laminarly, areally and hodologically distinct cortical pyramidal cell types (Chapter 1). IP/ Whole Cortex comparisons for each cell type showed that relative to the whole tissue, there are many laminar markers enriched in the cell types in accordance with the expression pattern of the EGFP-L10 transgene. We further wanted to find out the exclusive genes in each cell type relative to the other cell types using the SI algorithm, so that we could probe further into the biological pathway most relevant to the cell type as well as pick candidates for further analysis. Besides the cell types of interest (Ntf3, Etv1 and Syt6: Fig 2.11), it is important to select negative i.e. non-pyramidal cell types for subtracting background transcripts. Following are the negative cell types we selected for this purpose –

a. Non pyramidal cell type 1: Interneuron line Pnoc GM64

Prepronociceptin (Pnoc) is the precursor for the opioid peptide nociceptin that binds preferentially to the OPRL receptor (Opioid Peptide Receptor Like 1) (Xuei et al., 2008). Pnoc defines a subpopulation of interneurons in the neocortex, and the bacTRAP line Pnoc GM64 targets the endogenous population of Pnoc positive interneurons in the cerebral cortex. TRAP data for Pnoc Cortex IP was collected as described earlier and compared against the Whole

Cortex (Fig 2.12). The Affy probe for the driver - Pnoc was highly enriched in the Cortex IP. The scatter plot of IP/Whole Cortex revealed a different gene distribution than the pyramidal cell type scatter plots, with higher scatter in the Whole Cortex and fewer genes enriched in the IP. This is not surprising since compared to pyramidal cells, which constitute majority of cells in the neocortex, interneurons constitute only 20% of all the cells. In Pnoc bacTRAP mice, the majority of EGFP-L10 positive cells in the superficial layers of the cerebral cortex were multipolar and GABA positive, although some cells in deeper layers of cortex were GABA negative and appeared to have a single apical dendrite (Doyle et al., 2008).

b. Non pyramidal cell type 2: Interneuron line Lypd6 JP48

LY6/ PLAUR domain containing 6 (Lypd6) is a gene member of the LY6 protein superfamily defined on the basis of the LU protein domain (Zhang et al.). Lypd6 is a gene driver for a subpopulation of interneurons in the neocortex and the bacTRAP line Lypd6 JP48 accurately targets the EGFP-L10 transgene to the endogenous population in the prefrontal cortex. The Affy probe for the driver – Lypd6 was highly enriched in the Cortex IP. The scatter plot of IP/Whole Cortex revealed a wider scatter of the probesets in both Whole Cortex and Lypd6 IP (Fig 2.12), which indicated that there are more differentially expressed genes in Lyd6 compared to the whole cortex.

c. Non neuronal cell type 1: Astrocyte line AldhL1 JD130

AldhL1, short for Aldehyde dehydrogenase 1 family, member L1, is a marker for astrocytes. Cahoy et al (Cahoy et al., 2008) indicated that AldhL1 labels more astrocytes than GFAP, so is a pan-astrocyte marker because it better labels both the astrocyte cell body and

processes throughout both grey and white matter. The AldhL1 bacTRAP line Fthfd JP48 accurately targets the EGFP-L10 transgene to the endogenous astrocyte population in the neocortex. The scatterplot of Fthfd IP/Whole Cortex revealed a wide scatter of the probesets in both directions, indicating that AldhL1 Cortex IP has more differentially expressed genes compared to the average of the Whole Cortex (Fig 2.13). The Affy probes for Fthfd (1424400_a_at and 1424401_at) are both highly enriched in the Fthfd Cortex IP in the IP/Whole Cortex comparison. We further looked at the distribution of astrocyte markers in the AldhL1 cortex IP and found that the following genes were enriched in the IP: Anxa5 (1425567_a_at), Cbfb (14606716_a_at), Aqp4 (1434449_at, 1447745_at, 1447745_at and 1425382_a_at), Alad (1424877_a_at), Slc1a3 (14390672_at, 1452031_at, 1426341_at and 1426340_at), Lpd (1422428_at), Cklfs5 (1430600_at), Ccnd3 (1415907_at), Cnp1 (1449296_a_at), Gp1bb (1422977_at), Entpd2 (1418259_a_at), Efemp2 (1417018_at), Gfap (1426508_at and 1426509_a_at), S100b (1419383_at), Masp1 (1419677_at and 1425985_a_at), Pros1 (1426246_at), Relb (14167856_at) and Icosl (1419212_at).

c. Non neuronal cell type 2: Oligodendrocyte Line Olig2 JD97

Olig2, short for Oligodendrocyte Transcription Factor 2, is a marker for oligodendrocyte progenitors as well as mature oligodendrocytes (Zhou and Anderson, 2002). Olig2 JD97 bacTRAP line targets these oligodendrocytes accurately as revealed by immunohistochemical staining with anti-Olig2 (Doyle et al., 2008). The scatterplot of Olig2 IP/Whole Cortex revealed a wide scatter of the probesets in both directions, indicating that Olig2 Cortex IP has more differentially expressed genes compared to the average of the Whole Cortex (Fig 2.14). Olig2 driver probeset (1416232_at) is highly enriched in the Olig2 Cortex IP along with the following

oligodendrocyte markers: Mbp (1433532_a_at, 1419646_a_at, 1436201_x_at and 1456228_x_at), Igbp1 (142000_s_at), Cbfb (1460716_a_at), Cnp1 (1418980_a_at), Slc1a3 (1452031_at, 1426340_at and 1419383_at), Sp3 (1431804_a_at), Mag (1460219_at), Cklfs5 (1430600_at and 1429798_a_at), S100b (1419383_at), Serpind1 (1418680_at), Ifi30 (1422476_at), Pros1 (1426246_at) and Cxcl12 (1467574_at). Interestingly, the Affy probesets for Etv1 (1450684_at and 1445315_at) are both slightly enriched in the Olig2 Cortex IP.

Together with these negative cell types, the cortical pyramidal cell types were compared to each other. IP replicates for the cortical tissue from following bacTRAP lines were used for the SI analysis: 1) Ntf3 PS1046, 2) Etv1 PS476, 3) Syt6 PS3013, 4) Pnoc GM64, 5) Lypd6 JP48, 6) AldhL1 JD130 and 7) Olig2 JD97. Briefly, for each cell type, the IP replicates were GCRMA normalized and compared to the Whole Cortex by setting the threshold for expression at 50. Then the SI analysis was carried out as described previously (Dougherty et al., 2010). The statistically significant ($p < 0.05$) genes in each cell type were compiled and then analyzed for overrepresented GO ontologies, biological networks and pathways. The SI is influenced by both the variations in the number of transcripts that are enriched I each cell type being analyzed, and the purity and recovery of TRAP mRNA collected for each cell type. The range of the rankings is dependent on the number of probesets in the comparison, and that number depends on the number of genes expressed and the level of filtering in each particular cell type. Hence, raw SI values are not directly comparable across cell types. For each SI, a P-value is calculated by permutation testing: for each IP, the filtered expression values are randomly shuffled many times and SIs are calculated for all probesets, to determine the frequency of a particular SI value appearing (Dougherty et al., 2010).

2.8.2 Comparative Quantitative Analysis of Ntf3 PS1046 Translational Profile

The comparative SI analysis for Ntf3 PS1046 Cortex IP revealed 238 genes that were significantly enriched ($p < 0.05$) compared to the other six cell types. Some of the biologically and statistically significant genes are described in Figure 2.15. The Ntf3 Cortical Cell Type genes that were identified with the SI algorithm include the driver Ntf3, ion channels (e.g. Kcnh3, Kcnip2, Kcnip4, Cacnb2, Cacnb3, Cacng3), cell surface proteins and receptors (e.g. Baiap2, Grik5, Grm1, Oxtr), transcription factors (Col9a2), calcium binding proteins (Wfs1, CamkV), opioids (Penk1), signal transduction molecules (Ras10a, Rin1, Sh3bgr, Rgs13) and other neuronal genes (Ngb, Neurod1 etc.). To determine the functional classes of the genes distinguishing the Ntf3 Cell Type, we performed an over-representation analysis using the Gene Ontology (GO) database. Go terms are nested functional categories that summarize the known molecular functions and biological processes associated with each gene, as well as its cellular localization. We used the BiNGO plugin with the Cytoscape software for generating an interactive platform to assess overrepresented GO categories (Maere et al., 2005). The hypergeometric test, in which sampling occurs without replacement, was used together with the Benjamini and Hochberg FDR correction to assign P value to the statistically overrepresented GO categories. The GO terms pertinent to Biological Pathways that were overrepresented in the Ntf3 Cell Type are: signaling, nervous system development, signal transmission, generation of neurons, regulation of transmission of nerve impulse, neuron differentiation, calcium ion transport, small GTPase mediated signal transduction, regulation of nervous system development and cation transport. These biologically relevant GO categories and the list of

genes under each category are listed in Fig 2.16. We then used the web-based DAVID software to analyze the biologically relevant KEGG pathways unique to each of the three cell types (Huang da et al., 2009). The KEGG pathways (Kanehisa et al., 2004) overrepresented in the Ntf3 Cell Type are shown in Fig 2.16. They include: calcium signaling (Cacna1h, Camk2d, Itpka, Mylk, Oxtr, Prkcc, Grm1 and Ntsr), MAPK signaling pathway (Rac3, Bdnf, Cacna1h, Cacnb2, Cacnb3, Cacng3, Mapk8ip1, Ntf3 and Prkcc), axon guidance (Epha6, Rac3, Rnd1, Ablim2, Pak6 and Unc5a), neuroactive ligand receptor interaction (Gabra2, Grin2b, Grik5, Oxtr, Mas1, Adra2c, Grm1 and Ntsr) and long-term potentiation (Camk2d, Grin2b, Prkcc and Grm1).

2.8.3 Comparative Quantitative Analysis of Etv1 PS476 Translational Profile

The comparative SI analysis of Etv1 PS476 Cortex IP revealed 264 genes that were significantly enriched ($p < 0.05$) compared to the other six cell types. Some of the biologically and statistically significant genes are described in Figure 2.17. The Etv1 Cortical Cell Type genes that were identified with the SI algorithm include Layer V markers (Dkkl1, Coch, Ptgr3, Crhr1, Depdc8), ion channels (Kcnj8), cell surface receptors (Grm2, Trpc3, Tacr3, Hrh3) and transcription factors (Lrrc24). Even though the driver gene Etv1 was enriched in the Etv1 IP/Whole Cortex comparison, it was ranked very low in the comparative SI analysis. This could be because Etv1 was also expressed by Olig2 cell types, and was eliminated as a unique marker for the Etv1 cortex cell type. To determine the functional classes of genes distinguishing the Etv1 cell type, we performed an over-representation analysis of the Gene Ontologies using the BiNGO plugin with the Cytoscape software. The analysis involved a hypergeometric test with Benjamini and Hochberg FDR correction. The GO terms related to Biological Pathways that

were overrepresented in the Etv1 cell type are: synaptic transmission, neuron projection development, neuron projection morphogenesis, calcium ion transport, axonogenesis, neuron differentiation, axon guidance and behavior (Fig 2.18).

We then used the web-based DAVID software to analyze the biologically relevant pathways unique to each of the three cell types. The KEGG pathways overrepresented in the Etv1 Cell Type are shown in Fig 2.18. They include: calcium signaling pathway (Htr7, Ptk2b, Cacna1a, Cacna1h, Camk4, Cckbr, Chrm1, Ptger3, Tacr3, Tnnc1), neuroactive ligand-receptor interaction (Htr7, Cckbr, Chrm1, Crhr1, Grm2, Hrh3, Ptger3, Sstr2, Tacr3) , MAPK signaling pathway (Cacna1a, Cacna1h, Cacna2d3, Dusp1, Dusp5, Map3k6, Nr4a1, Pdgfb) and Sphingolipid Metabolism (Glb1, Neu2, Sgpp2).

2.8.4 Comparative Quantitative Analysis of Syt6 PS3013 Translational Profile

The comparative SI analysis for Syt6 PS3013 cortex IP revealed 269 genes that were significantly enriched ($p < 0.05$) compared to the other six cell types. Some of the biologically and statistically significant genes are described in Figure 2.19. The Syt6 cortical cell type genes that were identified with the SI algorithm include ion channels (Kcnab3), transcription factors (Zfp692, Dffb, Rbm25, Ncoa5, Atf6), and cell surface receptors (Lime1, Tmem89). To determine the functional classes of genes that distinguish the Syt6 cell type, we performed an over-representation analysis using the Gene Ontology (GO) database in the BiNGO plugin. The hypergeometric test together with Benjamini and Hochberg FDR correction assigned P value to the statistically significant GO categories related to Biological Pathways which were as follows:

nervous system development, brain morphogenesis, regulation of synaptic transmission and transcription (Fig 2.20).

We then used the web-based DAVID software to analyze the biologically relevant KEGG pathways unique to the Syt6 cell type. They are described in Fig 2.20. The KEGG pathways overrepresented in the Syt6 cell type are: axon guidance (Rock2, Efnb2, Sema3a, Sema3e and Sema4c) and MAPK signaling pathway (Bdnf, Cacnb2, Chuk, Fgf14, Hspa1a, Mapt and Mapk11) (Fig 2.20).

2.9 Hierarchical Clustering of the Cortical Cell Types

To reveal the hierarchical relationships among the cortical cell types, we clustered all replicates of five cortical IPs (3 for cortical pyramidal cell types and 2 non neuronal cell types) and whole cortex according to their relative Euclidean distances to render a dendrogram. For hierarchical clustering, we first created an experiment in Genespring with all the 26 samples (3 replicates each of 7 cortical samples and 5 replicates of Whole Cortex). Second, we made a list of Top 1000 enriched probesets for the cortical cell type in question e.g. Ntf3. Then we subtracted out genes that were also among the Top 1000 genes enriched in Etv1 or Syt6 Cell Types. Third, we filtered this list to focus on biologically relevant molecules mainly transcription factors, receptors and ion channels, so our final list for Ntf3 Cell Type had 651 probesets. We then conducted a hierarchical clustering on replicates of six different samples using a combined gene and condition tree. The primary branch point on the resulting taxonomic tree reflects the basic division between glutamatergic pyramidal cells from non-neuronal cells including AldhL1 positive astrocytes and Olig2 positive oligodendrocytes. Glutamatergic

pyramidal cells form the majority of cells (~70%) in the neocortex, where as astrocytes and glia only form less than 10%. So it is not surprising that the replicates of whole cortex RNA branch together with the pyramidal cell types and are distant from the astrocytes and glia. The heat map of the unsupervised hierarchical cluster enables easy visualization of the differential expression of probesets for biologically relevant molecules across different cell types in the cortex. For Ntf3 cell type, some of the genes that are differentially enriched include: Acta2 (1416454_s_at), Tpm2 (1425028_a_at), Ntf3 (1434802_s_at), 1200008D14Rik (1449799_s_at), Baiap2 (1425656_a_at), 1700025B16Rik (1446928_at), Aes (1420619_a_at) and Tp53i11 (14436919_at) (Fig 2.21).

We applied the same procedure for Etv1 and Syt6 cell types. For Etv1 cell type, some of the genes that are differentially enriched include: 231006566K19Rik (1449860_at), Xlkd1 (1429379_at), Tbx2 (1422545_at), Enpep (1448649_at), Abcc9 (1435752_s_at), Cbr2 (1418509_at), Kcnj8 (1418142_at), Cd163 (1419144_at), Gpr105 (1424733_at), Gja7 (1449094_at), Mrc1 (145430_at), Nodal (1422058_at), Foxc1 (1419486_at) and Ncf2 (1448561_at) (Fig 2.22).

Finally for the Syt6 cell type, the following genes were differentially enriched: Kpna4 (1417975_at), Pfkp (1430634_a_at), Api5 (1439214_a_at), Haghl (1433650_at), 2610007K22Rik (1439037_at), Myef2 (1425349_a_at), Rg9mtd2 (1427375_at), Stk11 (1448062_at), Tde1 (1448847_at), Arpm1 (1429788_at), Tbcc (1451423_at), 1110021E09Rik (1428674_at), Fboxo6a (1430541_at), and 4732496O19Rik (1421035_a_at) (Fig 2.23).

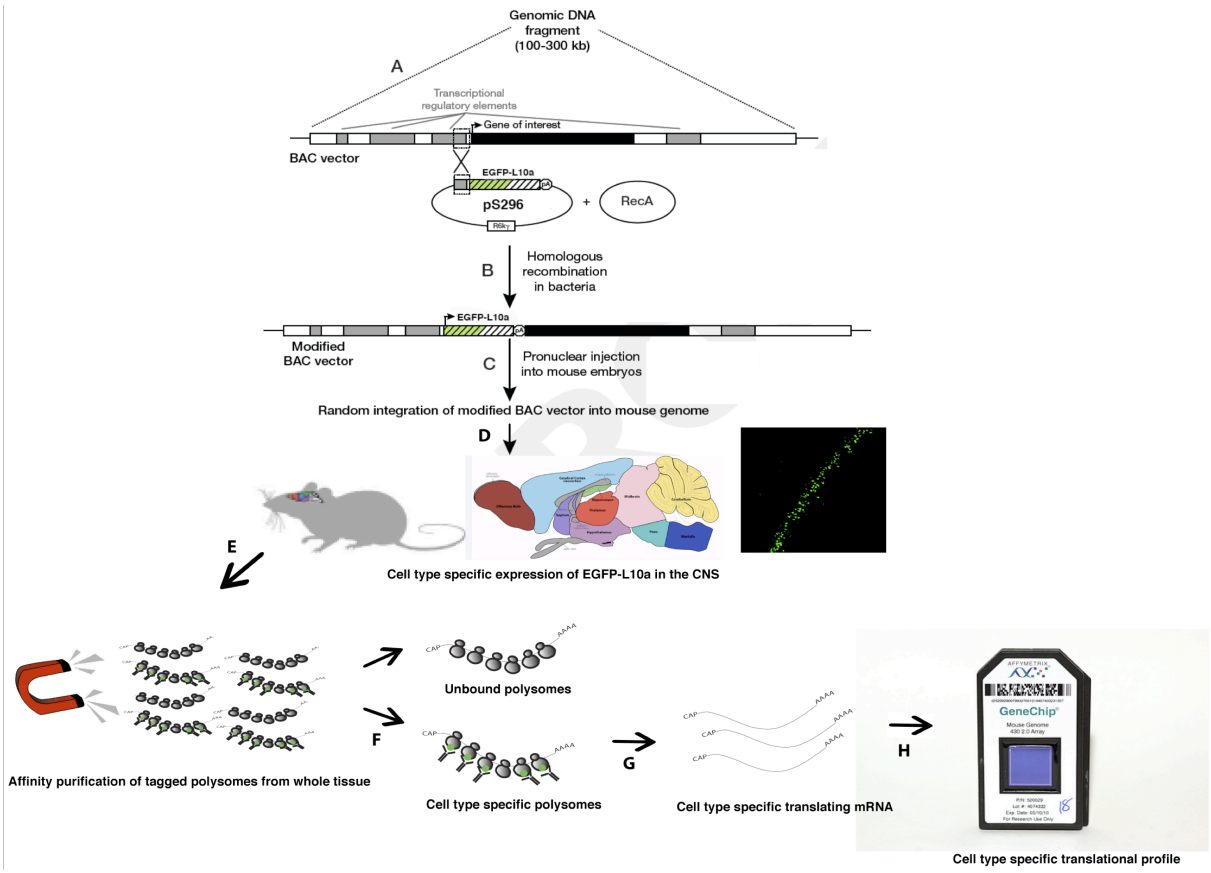

Figure 2.1: Scheme of Translating Ribosome Affinity Purification strategy. Bacterial Artificial Chromosome (BAC), centered around the gene of interest and incorporating most or all of the transcriptional regulatory sequences (A), is modified using a homology region 'A box' shared with the TRAP shuttle vector pS296. RecA plasmid transformation renders the BAC carrying *E.coli* competence for recombination (B). The modified BAC vector with the EGFP-L10a recombined immediately after the promoter is injected into the pronucleus of mouse oocytes (c). The modified BAC gets randomly integrated into the mouse genomes in variable tandem copies. Progeny of the injected mice are screened for germline transmission of EGFP and such BAC 'founder' lines are characterized for EGFP neuroanatomy (D). After cell type specific expression of EGFP-L10a in the brain for selected founder lines was confirmed, cortical tissue of adult mice was subjected to polysomal immunoprecipitation (E) using anti-EGFP to pull down tagged polysomes. Cell type specific polysomes (tagged) were affinity purified (F) and subjected to RNA extraction (G). The extracted RNA was amplified and labeled before being hybridized on to the Mouse Genome 430 2.0 microarray chips, whereupon label signals are quantified and analyzed to generate cell-type specific translational profile.

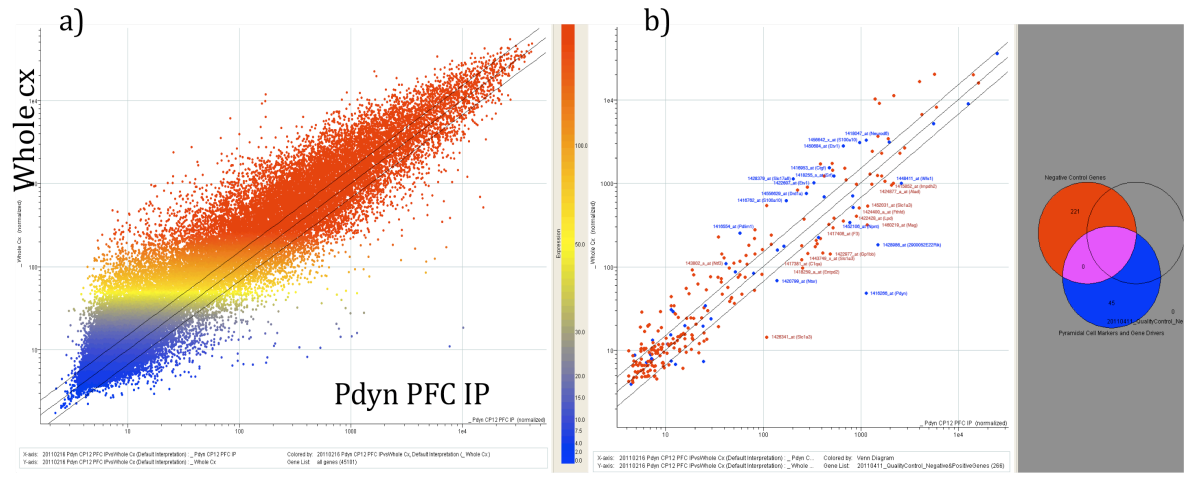

Figure 2.2: Translation profile of Prodynorphin Pdyn CP12 PFC cell type. Fluorescence signals of all 40,000 probesests for Pdyn CP12 PFC IP replicates were averaged and plotted against total cortex input (whole cx) in an X-Y scatterplot (a). Pyramidal cell marker probesets (in blue) were examined for their distribution in the scatterplot together with non-pyramidal cell type marker genes (in red) (b).

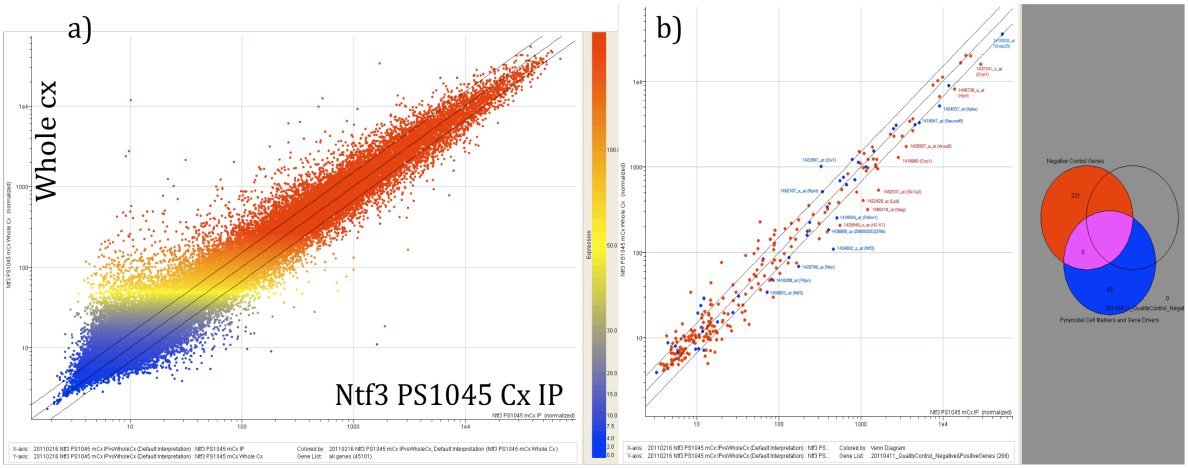

Figure 2.3: Translation profile of Neurotrophin-3 Ntf3 PS1045 cortex cell type. Fluorescence signals of all 40,000 probesests for Ntf3 PS1045 cortex IP replicates were averaged and plotted against total cortex input (whole cx) in an X-Y scatterplot (a). Pyramidal cell marker probesets (in blue) were examined for their distribution in the scatterplot together with non-pyramidal cell type marker genes (in red) (b).

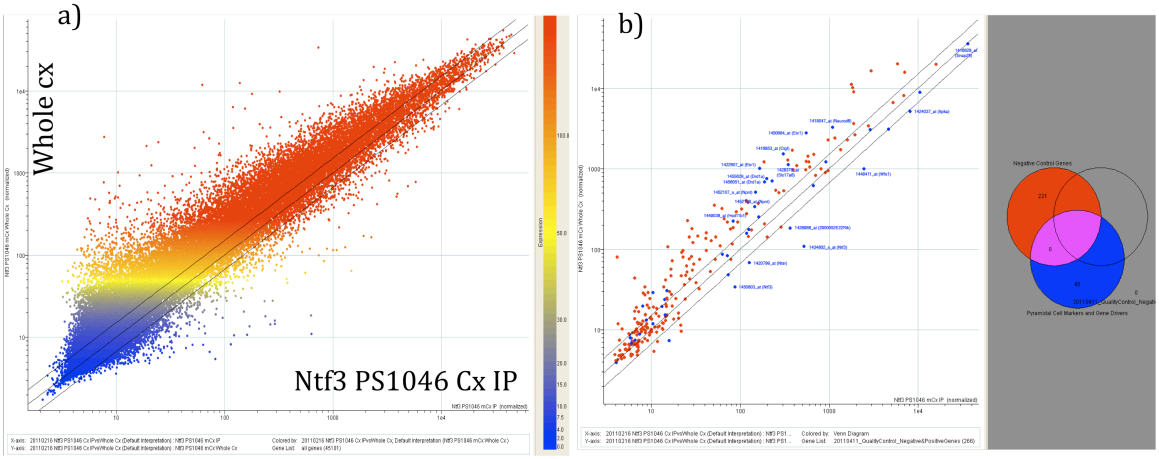

Figure 2.4: Translation profile of Neurotrophin-3 Ntf3 PS1046 cortex cell type. Fluorescence signals of all 40,000 probesests for Ntf3 PS1046 cortex IP replicates were averaged and plotted against total cortex input (whole cx) in an X-Y scatterplot (a). Pyramidal cell marker probesets (in blue) were examined for their distribution in the scatterplot together with non-pyramidal cell type marker genes (in red) (b).

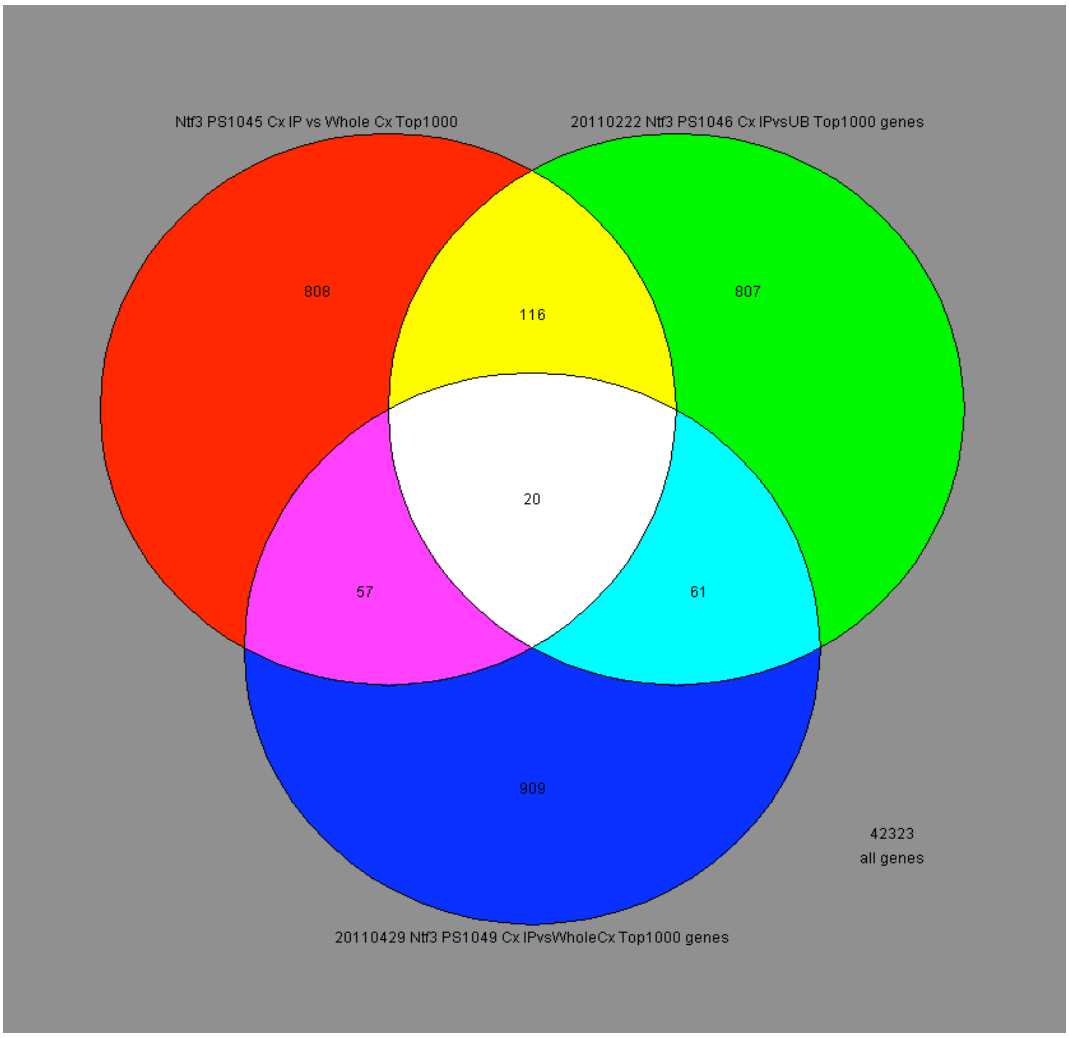

Figure 2.5: Venn Diagram comparing three founder lines for Ntf3 TRAP. Top 1000 most highly enriched genes in cortex IP (vs whole cx) of Ntf3 PS1045, Ntf3 PS1046 and Ntf3 PS1049 were compared to each other. There were 20 genes common among all three lists, 116 genes common between PS1045 and PS1046, 57 genes common between PS1045 an PS1049 and 61 genes common between PS1046 and PS1049. The number of genes that were exclusive for each of the TRAP founder line was 808 (PS1045), 807 (PS1046) and 909 (PS1049) respectively.

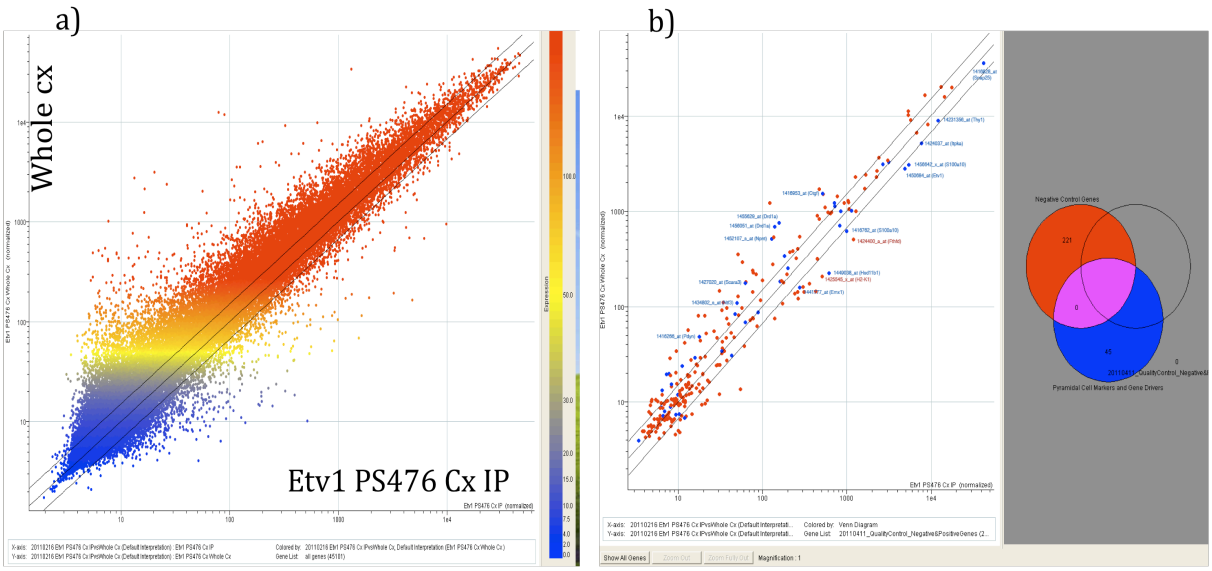

Figure 2.6: Translation profile of Ets variant gene 1 Etv1 PS476 cortex cell type. Fluorescence signals of all 40,000 probesests for Etv1 PS476 cortex IP replicates were averaged and plotted against total cortex input (whole cx) in an X-Y scatterplot (a). Pyramidal cell marker probesets (in blue) were examined for their distribution in the scatterplot together with non-pyramidal cell type marker genes (in red) (b).

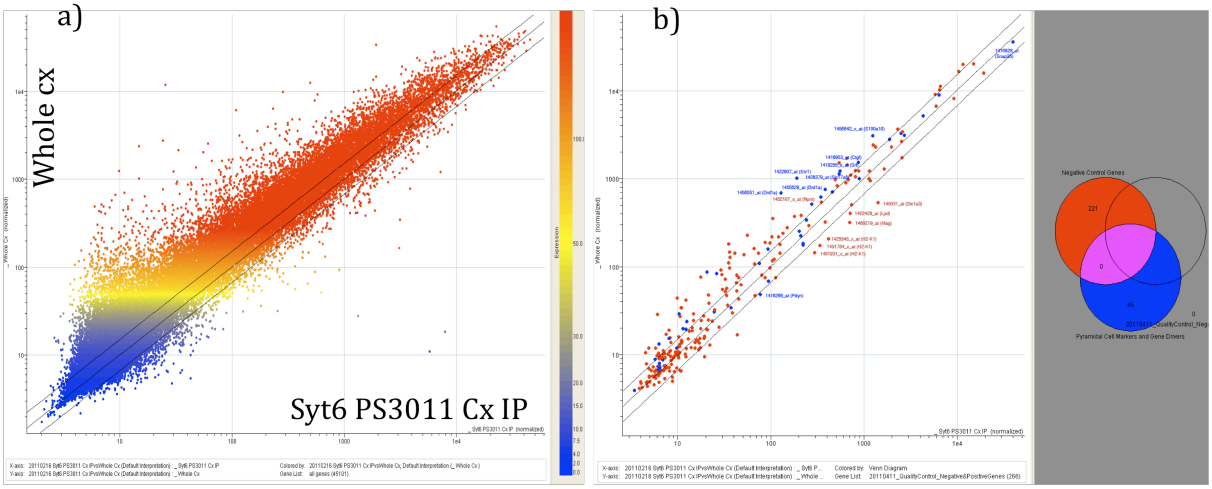

Figure 2.7: Translation profile of Synaptotagmin 6 Syt6 PS3011 cortex cell type. Fluorescence signals of all 40,000 probesests for Syt6 PS3011 cortex IP replicates were averaged and plotted against total cortex input (whole cx) in an X-Y scatterplot (a). Pyramidal cell marker probesets (in blue) were examined for their distribution in the scatterplot together with non-pyramidal cell type marker genes (in red) (b).

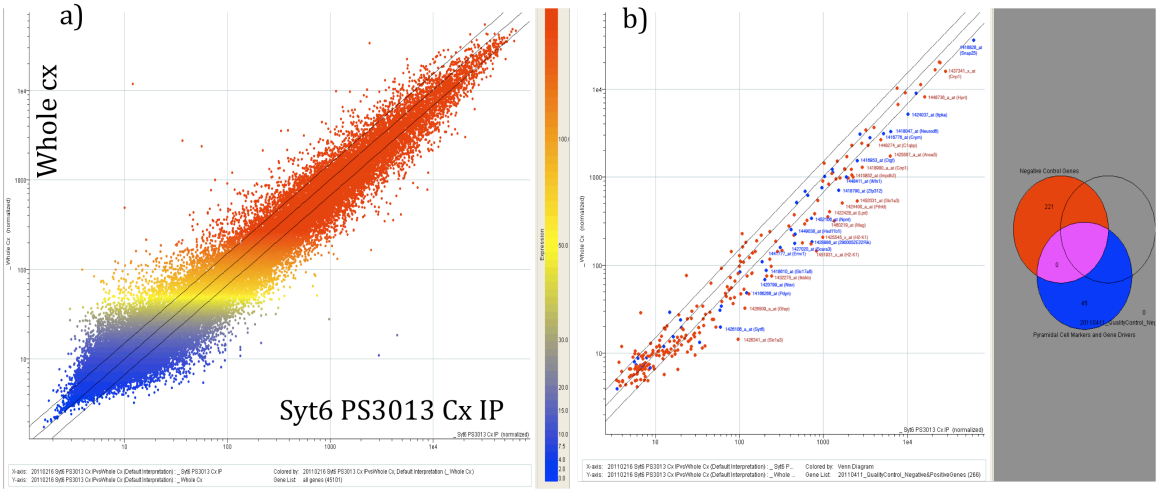

Figure 2.8: Translation profile of Synaptotagmin 6 Syt6 PS3013 cortex cell type. Fluorescence signals of all 40,000 probesests for Syt6 PS3013 cortex IP replicates were averaged and plotted against total cortex input (whole cx) in an X-Y scatterplot (a). Pyramidal cell marker probesets (in blue) were examined for their distribution in the scatterplot together with non-pyramidal cell type marker genes (in red) (b).

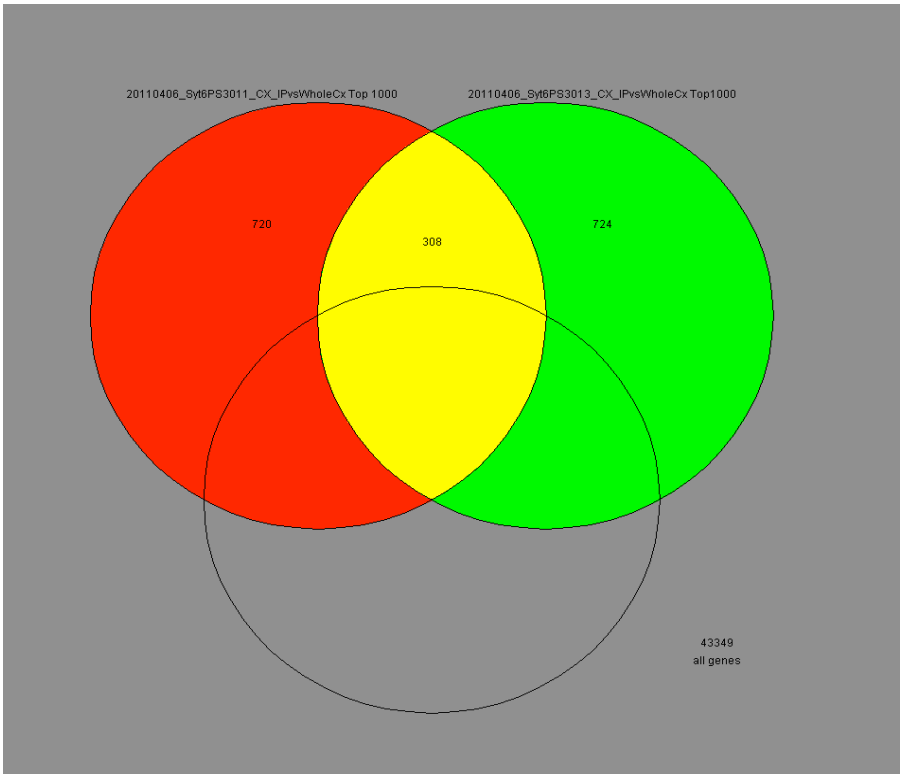

Figure 2.9: Venn Diagram comparing two founder lines for Syt6 TRAP. Top 1000 most highly enriched genes in cortex IP (vs whole cx) of Syt6 PS3011 and Syt6 PS3013 were compared to each other. There were 368 genes between the two lists whereas 720 genes and 724 genes were exclusive to Syt6 PS3011 and PS3013 TRAP lines respectively.

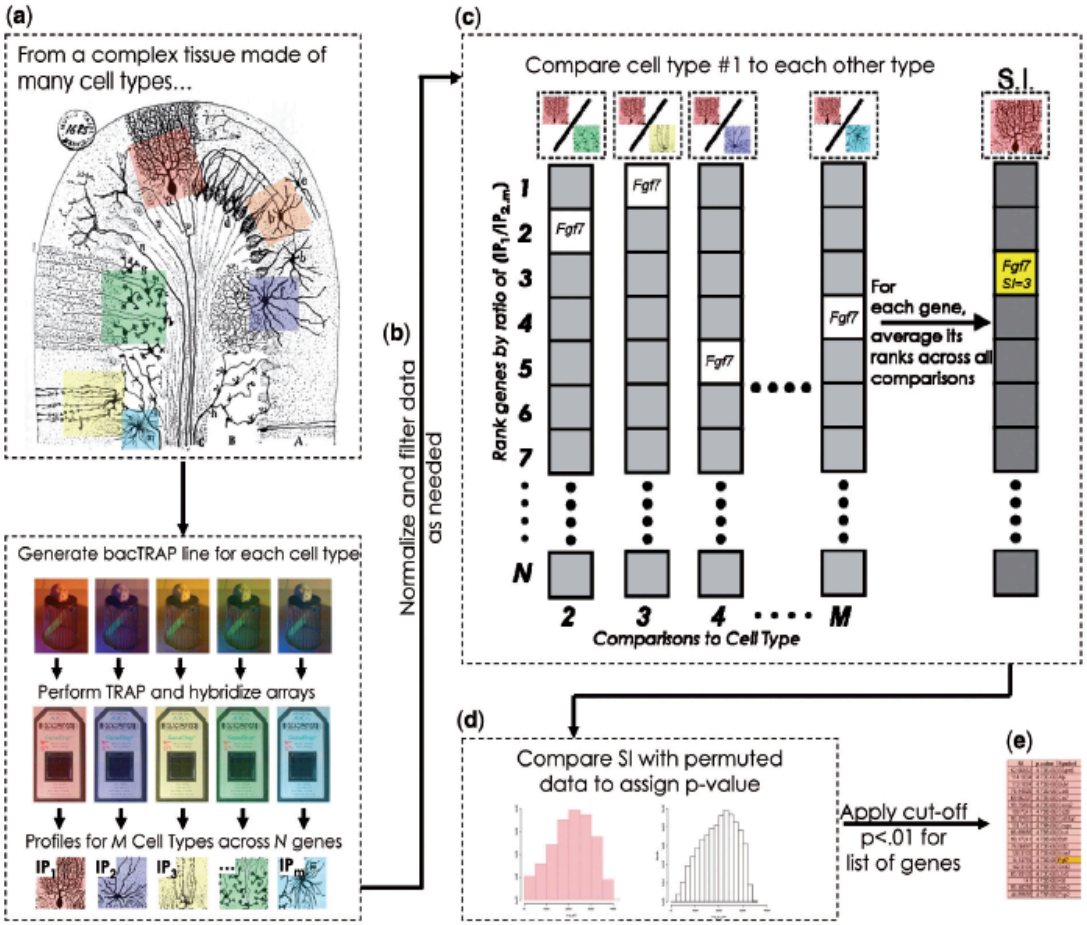

Figure 2.10: Quantitative comparative analysis of TRAP data using Specificity Index (SI) Algorithm. Cellularly heterogenous tissue such as cerebellum (illustration) or neocortex can be analyzed for cell type specific translational profiles by generating bacTRAP transgenic lines for different cell types within the tissue (color-coded). The polysomes from these lines are subjected to IP and bound RNA (IPs) are hybridized to arrays and profiles for M cell types across N genes are generated after subracting background by comparing with whole cortex input (a). The TRAP data for each cell type are normalized and filtered as needed, before being iteratively compared to each other on a gene by gene basis. Ratios of enrichment vs every other cell type is calculated for any given gene and ranks assigned based on the descending order of ratio in the list. For each gene, ranks are averaged across cell comparisons (c) and probabilities computed by permutation for the gene having the rank for each cell type (d). Finally a threshold of $p < .05$ is applied to get the list of genes that are significantly enriched in each cell type. (Dougherty et al, 2010)

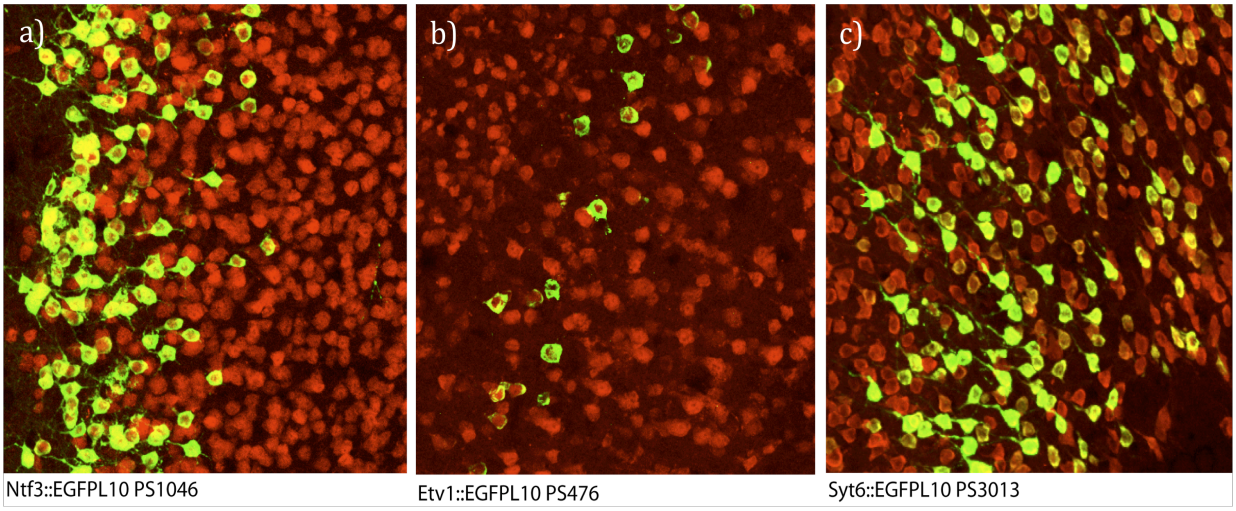

Figure 2.11: Cell somatic neuroanatomy of distinct cortical pyramidal cell types. High magnification of Z stacked images for relevant cortical areas revealed relative cell body size, shape, density and position within the cortex for Ntf3 PS1046 (layer 2 PFC: a), Etv1 PS476 (layer 5 lateral PFC: b) and Syt6 PS3013 (layer 6 medial PFC: c)

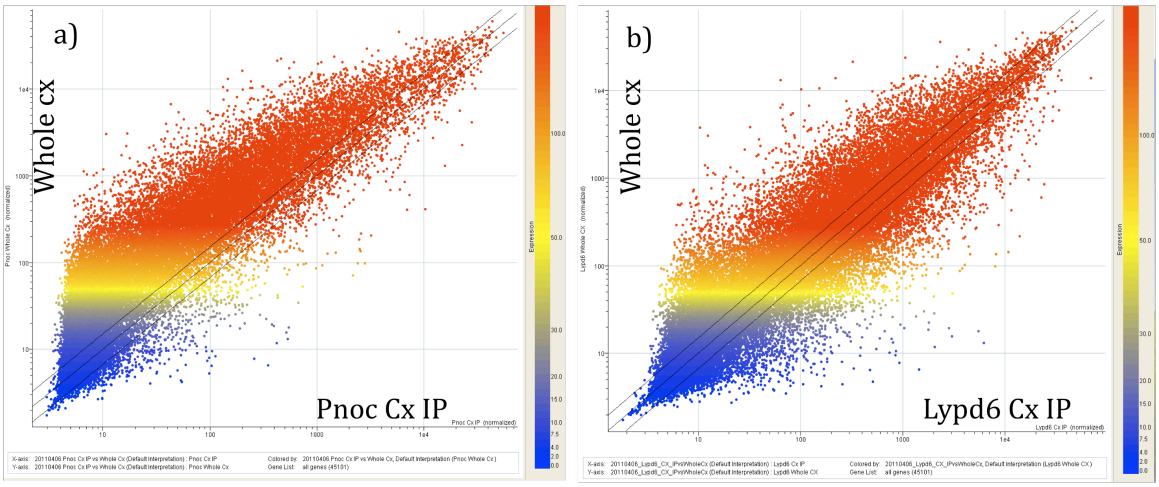

Figure 2.12: Translation profile of representative interneuron cortex cell types. Fluorescence signals of all 40,000 probesests for Pnoc GM64 and Lypd6 JP48 cortex IP replicates were averaged and plotted against total cortex input (whole cx) in an X-Y scatterplot (a) and (b) respectively.

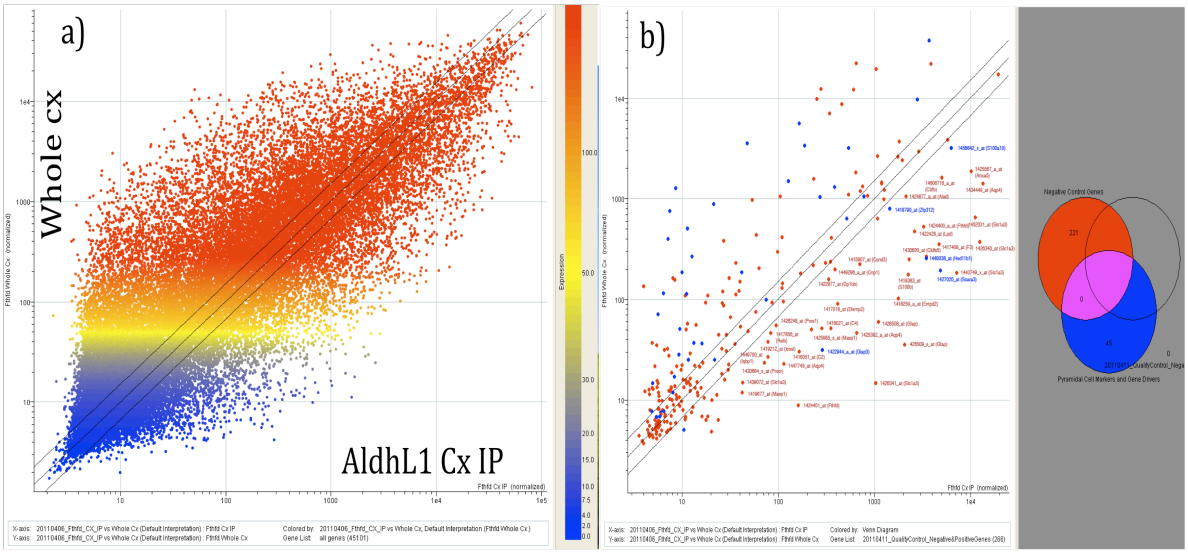

Figure 2.13: Translation profile of Aldehyde dehydrogenase 1 member L1 (AldhL1) JD130 astrocyte cortex cell type. Fluorescence signals of all 40,000 probesests for AldhL1 JD130 cortex IP replicates were averaged and plotted against total cortex input (whole cx) in an X-Y scatterplot (a). Pyramidal cell marker probesets (in blue) were examined for their distribution in the scatterplot together with non-pyramidal cell type marker genes (in red) (b).

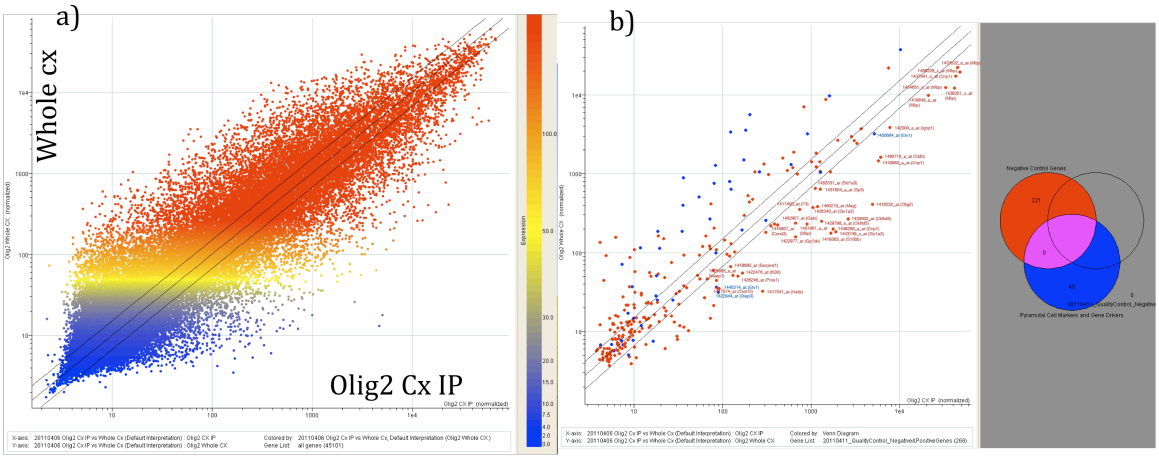

Figure 2.14: Translation profile of Oligodendrocyte gene 2 (Olig2) JD97 cortex cell type. Fluorescence signals of all 40,000 probesests for Olig2 JD97 cortex IP replicates were averaged and plotted against total cortex input (whole cx) in an X-Y scatterplot (a). Pyramidal cell marker probesets (in blue) were examined for their distribution in the scatterplot together with non-pyramidal cell type marker genes (in red) (b).

SI Analysis: Differentially expressed genes in Ntf3 PS1046 Cortex IP

Michigan Probe ID	Gene Symbol	Gene Description	SI	P value
5736	Tagln	Transgelin	5	4.10E-06
4129	Ntf3	neurotrophin 3	39.7142857	1.23E-05
6395	Tpm2	tropomyosin 2, beta	97.7142857	0.00020107
15127	Capsl	calcyphosine-like	119.714286	0.00032417
11089	Trim54	tripartite motif-containing 54	121.857143	0.00035084
15165	Rasl10a	RAS-like, family 10, member A	135.285714	0.00058063
9551	Wipf3	WAS/WASL interacting protein family, member 3	137.428571	0.0006032
10440	Kalrn	kalirin, RhoGEF kinase	152.142857	0.00080222
12347	Pkp2	plakophilin 2	152.571429	0.00080837
6813	Rin1	Ras and Rab interactor 1	157	0.00090685
4776	Rasd1	RAS, dexamethasone-induced 1	165	0.00105868
3295	Kcnh3	potassium voltage-gated channel, subfamily H (eag-related), member 3	166.428571	0.00109561
11019	Tesc	tescalcin	173.714286	0.00129668
1312	Arhgap6	Rho GTPase activating protein 6	184.142857	0.00151005
9822	Gm1337	predicted gene 1337	184.428571	0.00151826
1537	Capn3	calpain 3	186.428571	0.00155724
7821	Ankrd43	ankyrin repeat domain 43	192.857143	0.00170497
11331	Ngb	neuroglobin	211.142857	0.00226098
10051	Sh3bgr	SH3-binding domain glutamic acid-rich protein	219.142857	0.00249692
980	Palmd	palmdelphin	227.714286	0.0027144
9007	Trp53i11	transformation related protein 53 inducible protein 11	235.571429	0.00299754
5356	Yeats2	YEATS domain containing 2	248.714286	0.00357201
4137	Ntsr1	neurotensin receptor 1	253.571429	0.00375051
666	Baiap2	brain-specific angiogenesis inhibitor 1-associated protein 2	265.857143	0.00427165
8451	Rgs13	Regulator of G-protein signaling 13	268.142857	0.0043414
8713	Gprin1	G protein-regulated inducer of neurite outgrowth 1	272.571429	0.00453632
8885	Arsj	arylsulfatase J	276	0.00466557
10242	Nptx2	neuronal pentraxin 2	277.857143	0.00475174

Figure 2.15: Significantly enriched genes from the SI analysis for Ntf3 cell type. Cortex TRAP data for Ntf3 PS1046 was iteratively compared to the pyramidal cell types Etv1 PS476 and Syt6 PS3013, as well as interneuron cell types (Pnoc GM64 and Lypd6 JP48) and non-pyramidal glial cell types (AldhL1 JD130 and Olig2 JD97). Note that the driver Ntf3 is among the top significantly enriched gene (SI = 39.71, p = 1.23E-05).

a)

BiNGO Analysis for Ntf3 : Biological Pathway			
GO ID	Description	Corrected p-val	Genes
23052	Signaling	7.6420E -6	Nrp2, Grik5, Rasgef1c, Gpr88, Rgl1, Nov, Bdnf, Grin2b, Tiam2, Unc5a, Ppp1r1b
7399	Nervous System Development	2.2888E -4	Gprin1, Nrp2, Rtn4rl1, Ntf3, Klf16, Celsr3, Dapk3, Numbl, Ntrk3, Bdnf, Unc5a, Rac3,
23060	Signal Transmission	5.2711E -4	Nrp2, Cplx2, Grik5, Oxtr, Cacnb2, Rasgef1c, Gpr88, Rgl1, Rab40b, Nov, Rasal1, Arhga
23046	Signaling Process	5.2711E -4	Nrp2, Cplx2, Grik5, Oxtr, Cacnb2, Rasgef1c, Gpr88, Rgl1, Rab40b, Nov, Rasal1, Arhga
9966	Regulation of signal transduction	9.5291E -4	Arhgef17, Dgk1, Rasgef1c, Grm1, Rgl1, Rgs14, Rgs13, Ddiit4, Sgsm1, Grin2b, Tiam2,
50804	Regulation of synaptic transmission	1.6299E -3	Bdnf, Ncdn, Ntf3, Grin2b, Ptgs2, Grik5, Oxtr, Grm1
48699	Generation of neurons	1.6588E -3	Gprin1, Rtn4rl1, Ntf3, Celsr3, Dapk3, Numbl, Ntrk3, Bdnf, Rac3, Unc5a, Not, Bhlhb5,
51969	Regulation of transmission of nerve impul	2.0406E -3	Bdnf, Ncdn, Ntf3, Grin2b, Ptgs2, Grik5, Oxtr, Grm1
31175	Neuron projection development	2.0908E -3	Gprin1, Bdnf, Rtn4rl1, Ntf3, Unc5a, Rac3, Not, Celsr3, Kalrn, Numbl
30182	Neuron differentiation	2.0908E -3	Gprin1, Ntf3, Rtn4rl1, Celsr3, Dapk3, Numbl, Ntrk3, Bdnf, Rac3, Unc5a, Not, Bhlhb5,
6816	Calcium Ion Transport	2.2381E -3	Grin2b, Camk2b, Cacna1h, Cacnb2, Cacng3, Cacnb3, Trpm2
7264	Small GTPase mediated Signal Transductic	2.7528E -3	Rnd1, Rac3, Rasl10a, Baiap2, Rab15, Rasgef1c, Rasd1, Rgl1, Rab40b
51960	Regulation of nervous system developmer	5.9200E -3	Ntrk3, Bdnf, Ntf3, Akap5, Oxtr, Neurod1, Kalrn, Numbl, Islr2
51924	Regulation of Calcium Ion Transport	8.3037E -3	Ptgs2, Akap5, Cacna1h, Cacnb2, Cacnb3
6812	Cation Transport	3.5493E -2	Grin2b, Camk2d, Kctd1, Cacna1h, Cacnb2, Cacnb3, Kcnip2, Kcnh3, Trpm2, Kcnip4

b)

KEGG Pathway Analysis for Ntf3					
Term	Count	%	P Value	Benjamini FDR	Genes
Calcium Signaling Pathway	8	3.8	3.5E -3	8.3E -2	Cacna1h, Camk2d, Itpka Mylk, Oxtr, Prkcc, Grm1, Ntsr1
MAPK Signaling Pathway	9	4.2	5.9E -3	1.0E -1	Rac3, Bdnf, Cacna1h, Cacng3, Mapk8ip1, Ntf3, Prkcc
Axon Guidance	6	2.8	1.2E -2	1.2E -1	Gabra2, Grin2b, Grik5, Oxtr, Mas1, Adra2c, Grm1, Ntsr1
Long Term Potentiation	4	1.9	3.6E -2	2.0E -1	Camk2, Grin2b, Prkcc, Grm1

Figure 2.16: Overrepresented Gene Ontology (GO) categories and KEGG pathways for Ntf3 cortex cell type. Representative GO categories (a) and KEGG pathways (b) are significantly overrepresented in Ntf3 PS1046 cortex TRAP data when compared with other cell types using SI algorithm.

SI Analysis: Differentially expressed genes in Etv1 PS476 Cortex IP

Michigan Probe ID	Gene Symbol	Gene Description	SI	P value
1589	Cbr2	carbonyl reductase 2	68.85714286	3.40E-06
11373	Scube1	signal peptide, CUB domain, EGF-like 1	58.57142857	3.40E-06
3429	Lamc2	laminin, gamma 2	97.57142857	2.38E-05
3646	Lyz2	lysozyme 2	101.8571429	2.72E-05
10014	Dkkl1	dickkopf-like 1	107.7142857	4.08E-05
2202	Egr4	early growth response 4	125.1428571	7.48E-05
3306	Kcnj8	potassium inwardly-rectifying channel, subfamily J, mer	143	0.000129252
14411	Cnih3	cornichon homolog 3 (Drosophila)	143	0.000129252
1890	Crhr1	corticotropin releasing hormone receptor 1	146.7142857	0.000142857
7436	Cyp26b1	cytochrome P450, family 26, subfamily b, polypeptide 1	155	0.000166667
8954	Sh2d3c	SH2 domain containing 3C	176.4285714	0.000278912
7801	Lrrc3	leucine rich repeat containing 3	185.7142857	0.000341837
8632	Krt12	keratin 12	198	0.00044898
405	Pik3r6	phosphoinositide-3-kinase, regulatory subunit 6	209	0.000583333
2233	Emx1	empty spiracles homolog 1 (Drosophila)	219.2857143	0.000705782
11290	Zfp296	zinc finger protein 296	227.8571429	0.000840136
14715	Gtsf1	gametocyte specific factor 1	229	0.00085034
1818	Coch	coagulation factor C homolog (Limulus polyphemus)	236.8571429	0.00095068
651	Grm2	glutamate receptor, metabotropic 2	241.5714286	0.001017007
4599	Ptger3	prostaglandin E receptor 3 (subtype EP3)	244.5714286	0.001032313
3093	Indo	indoleamine 2,3-dioxygenase 1	247.8571429	0.001095238
10085	Slc7a8	solute carrier family 7 (cationic amino acid transporter,	249.1428571	0.001108844
16242	Depdc6	DEP domain containing MTOR-interacting protein	250.7142857	0.00112585
6427	Trpc3	transient receptor potential cation channel, subfamily C	255.5714286	0.001187075
4461	Pp11r	endonuclease, polyU-specific	262.8571429	0.001284014
14756	Atg7	autophagy-related 7 (yeast)	272.4285714	0.001465986
14213	Lsm11	U7 snRNP-specific Sm-like protein LSM11	278.4285714	0.001561224
766	Ms4a7	membrane-spanning 4-domains, subfamily A, member	278.7142857	0.001562925

Figure 2.17: Significantly enriched genes from the SI analysis for Etv1 cell type. Cortex TRAP data for Etv1 PS476 was iteratively compared to the pyramidal cell types Ntf3 PS1046 and Syt6 PS3013, as well as interneuron cell types (Pnoc GM64 and Lypd6 JP48) and non-pyramidal glial cell types (AldhL1 JD130 and Olig2 JD97).

a)

BiNGO Analysis for Etv1 : Biological Pathway

GO ID	Description	Corrected p-val	Genes
7268	Synaptic transmission	3.6863E -6	Tacr3, Slc12a5, Stxbp1, Adcyap1, Slc17a7, Sstr2, Slc17a6, Grm2, Camk4, Syn1,
31175	Neuron Projection Development	5.9635E -5	B2galt6, Stxbp1, Slit3, Epha4, Lingo1, Epha7, Ptk2b, Not, Atg7, B2gnt2, Boc, Tu
6811	Ion Transport	6.5133E -5	Kcnh1, Trpc4, Ptger3, Clcn2, Trpc3, Slc9a5, Slc12a5, Stim2, Cacna2d3, Kcnk2, K
48666	Neuron Development	5.2929E -4	B3galt6, Stxbp1, Slit3, Epha4, Lingo1, Epha7, Ptk2b, Not, Atg7, B3gnt2, Box, Tu
48812	Neuron Projection Morphogenesis	6.8884E -4	Epha4, Epha7, B3galt6, Not, Stxbp1, B3gnt2, Boc, Cacna1a, Tubb3, Slit3
6816	Calcium Ion Transport	6.8884E -4	Coro1a, Trpc4, Trpc3, Slc24a3, Stim2, Cacna1h, Cacna2d3, Cacna1a
7409	Axonogenesis	1.1837E -3	Epha4, Epha7, B3galt6, Not, Stxbp1, B3gnt2, Boc, Cacna1a, Tubb3, Slit3
30182	Neuron Differentiation	1.2953E -3	B3galt6, Emx1, Stxbp1, Slit3, Lingo1, Epha4, Epha7, Ptk2b, Not, Atg7, B3gnt2,
7411	Axon Guidance	1.3112E -3	Epha4, Epha7, B3galt6, B3gnt2, Boc, Tubb3, Slit3
7610	Behavior	1.3112E -3	Cckbr, Hmgcr, Pf4, Cx3cl1, Indo, Adcyap1, Crhr1, Epha4, Epha7, Coro1a, Hrh3,

b)

KEGG Pathway Analysis for Etv1

Term	Count	%	P Value	Benjamini FDR	Genes
Calcium Signaling Pathway	10	4.2	3.3E -4	2.5E -2	Htr7, Ptk2b, Cacna1a, Cacna1h, Camk4, Cckbr, Chrm1,
Neuroactive Ligand-receptor Interaction	9	3.8	1.0E -2	3.2E -1	Htr7, Cckbr, Chrm1, Crhr1, Grm2, Hrh3, Ptger3, Sstr2, T
MAPK Signaling Pathway	8	3.3	3.4E -2	5.8E -1	Cacna1a, Cacna1h, Cacna2d3, Dusp1, Dusp5, Map3k6,
Sphingolipid Metabolism	3	1.2	8.6E -2	8.1E -1	Glb1, Neu2, Sgpp2

Figure 2.18: Overrepresented Gene Ontology (GO) categories and KEGG pathways for Etv1 cortex cell type. Representative GO categories (a) and KEGG pathways (b) are significantly overrepresented in Etv1 PS476 cortex TRAP data when compared with other cell types using SI algorithm.

SI Analysis: Differentially expressed genes in Syt6 PS3013 Cortex IP

Michigan Probe ID	Gene Symbol	Gene Description	SI	P value
14346	Lime1	Lck interacting transmembrane adaptor 1	79.57142857	1.21E-05
342	Zfp692	zinc finger protein 692	92.14285714	1.45E-05
7439	Arhgap25	Rho GTPase activating protein 25	143.7142857	8.24E-05
3782	Meg3	maternally expressed 3	162	9.93E-05
6194	Wdr60	WD repeat domain 60	227.7142857	0.000280974
9348	Lba1	tetratricopeptide repeat and ankyrin repeat containing 1	260	0.000439627
15784	Tnrc4	VCUGBP, Elav-like family member 3	275.1428571	0.000530459
2603	Gas5	growth arrest specific 5	287	0.000612813
3286	Kcnab3	potassium voltage-gated channel, shaker-related subfamily, beta member	287.5714286	0.000617658
964	Foxp2	forkhead box P2	330.4285714	0.000997941
13222	Tmem89	transmembrane protein 89	372.1428571	0.001463001
5028	Sema3a	sema domain, immunoglobulin domain (Ig), short basic domain, secreted	397.1428571	0.00177183
5619	Fancd2	Fanconi anemia, complementation group D2	425.4285714	0.002171491
2075	Dffb	DNA fragmentation factor, beta subunit	457.7142857	0.002715272
12104	Rbm25	RNA binding motif protein 25	462.4285714	0.002770982
7146	Ncoa5	nuclear receptor coactivator 5	470.5714286	0.002899358
8111	Sulf1	sulfatase 1	512	0.003735013
10518	Fnbp4	formin binding protein 4	514.8571429	0.00379799
8364	Prss35	protease, serine, 35	527.4285714	0.004024464
2056	Ddx4	DEAD (Asp-Glu-Ala-Asp) box polypeptide 4	536.1428571	0.004231561
15608	Prdm8	PR domain containing 8	537.5714286	0.004264261
11093	Pmaip1	phorbol-12-myristate-13-acetate-induced protein 1	567.1428571	0.004976384
8695	Ddx3y	DEAD (Asp-Glu-Ala-Asp) box polypeptide 3, Y-linked	575.8571429	0.005213758
1676	Cdc7	cell division cycle 7 (S. cerevisiae)	577	0.005254935
6925	Atf6	activating transcription factor 6	584.1428571	0.005462032
4512	Mapk11	mitogen-activated protein kinase 11	586.7142857	0.005528642
9615	Fkbp15	FK506 binding protein 15	594.2857143	0.005756328
5598	Cpne9	copine family member IX	602.5714286	0.005990069
4433	Pnn	pinin	643.8571429	0.007260506
15045	Etnk1	ethanolamine kinase 1	661.4285714	0.007832142

Figure 2.19: Significantly enriched genes from the SI analysis for Syt6 cell type. Cortex TRAP data for Syt6 PS3013 was iteratively compared to the pyramidal cell types Ntf3 PS1046 and Etv1 PS476, as well as interneuron cell types (Pnoc GM64 and Lypd6 JP48) and non-pyramidal glial cell types (AldhL1 JD130 and Olig2 JD97).

a)

BiNGO Analysis for Syt6 : Biological Pathway			
GO ID	Description	Corrected p-val	Genes
7399	Nervous System Development	1.431E -3	Klk6, Sclt1, Cobl, Stx3, Efnb2, Tbr1, Foxp2, Ctnna2, Prdm8, Bbs2, B
48854	Brain Morphogenesis	93658E -3	Reck, Dock9, Cacnb2, Hk1, Hspa1b, Anxa3, Camkk1, Cish, Rgs11, S
50804	Regulation of synaptic transmission	2.8502E -2	Bdnf, Grm8, Slc24a2, Spr, Rapgef4, Npy5r
6350	Transcription	3.7440E -4	Fosl2, Fhl2, Pnn, Zc3h8, Esf1, Top1, Zfp668, 1810007M14Rik, Not,

b)

KEGG Pathway Analysis for Syt6					
Term	Count	%	P Value	Benjamini FDR	Genes
Axon Guidance	5	2	3.5E -2	9.6E -1	Rock2, Efnb2, Sema3a, Sema3e, Sema4c
MAPK Signaling Pathway	7	2.9	5.7E -2	8.4E -1	Bdnf, Cacnb2, Chuk, Fgf14, Hspa1a, Mapt, Mapk11

Figure 2.20: Overrepresented Gene Ontology (GO) categories and KEGG pathways for Syt6 cortex cell type. Representative GO categories (a) and KEGG pathways (b) are significantly overrepresented in Syt6 PS3013 cortex TRAP data when compared with other cell types using SI algorithm.

Figure 2.21: Hierarchical clustering of differentially expressed genes in Ntf3 cell type. Genelists of Top 500 enriched and depleted genes for Ntf3 cell type was obtained and among them, biologically relevant molecules, i.e. transcription factors, ion channels and receptors, were displayed in the unsupervised hierarchical cluster comprising of 5 cell types (Etv1, Ntf3, Syt6 and negative cell types: AldhL1/ Fthfd and Olig2) using a condition tree.

Figure 2.22: Hierarchical clustering of differentially expressed genes in Etv1 cell type. Genelists of Top 500 enriched and depleted genes for Etv1 cell type was obtained and among them, biologically relevant molecules, i.e. transcription factors, ion channels and receptors, were displayed in the unsupervised hierarchical cluster comprising of 5 cell types (Etv1, Ntf3, Syt6 and negative cell types: AldhL1/ Fthfd and Olig2) using a condition tree.

Figure 2.23: Hierarchical clustering of differentially expressed genes in Syt6 cell type. Genelists of Top 500 enriched and depleted genes for Syt6 cell type was obtained and among them, biologically relevant molecules, i.e. transcription factors, ion channels and receptors, were displayed in the unsupervised hierarchical cluster comprising of 5 cell types (Etv1, Ntf3, Syt6 and negative cell types: AldhL1/ Fthfd and Olig2) using a condition tree.

CHAPTER 3: NEUROANATOMY AND TRANSLATIONAL PROFILE OF DISTINCT CORTICOTHALAMIC PYRAMIDAL CELL TYPES

Among the cortical layers, layer 6 is the first neocortical layer to develop during embryogenesis (Rakic, 2009; Shepherd, 2004). Despite being one of the most prominent layers in the neocortex, it is much less well studied compared to layers 3, 4 and 5. The cellular heterogeneity within layer 6 has made it more difficult to classify cell types within this layer. For instance, in many prior in vivo extracellular recording studies, the types of neurons could not be identified pushing back the functional characterization, even though there have been anatomical studies performed to classify different groups of neurons within this layer (Thomson, 2010). Chen et al (Chen et al., 2009) reconstructed cortical neurons from layer 6 of mouse barrel cortex and measured different morphological parameters such as somatic shape and dendritic structure to classify six distinct groups of neurons in the region. These six groups of neurons included three groups of pyramidal cells – pyramidal cells with elaborate dendrites, pyramidal cells with moderate apical and basilar dendritic pattern and pyramidal cells with short overall dendrites.

Cortical pyramidal cells in layer 6 have also been classified according to hodology, i.e. projections of their axons (Thomson, 2010). By this measure, there are three types of pyramidal cells in layer 6: corticocortical (CC), corticothalamic (CT) and corticoclaustral cells (CL) (Fig 3.1). As evident by their terminologies, CC cells project to the cortex and may cross the corpus callosum, CT cells project to different nuclei in the thalamus and CL cells project to the claustrum (Thomson, 2010). Arimatsu and Ishida (Arimatsu and Ishida, 2002) showed that the CC cells are born later (on or after embryonic day 15, E15) than CT cells (on or before E14). Morphologically, the CC cells were described to be fairly short, upright pyramids with narrow local axonal arbors that project up towards more superficial layers. By contrast, CC cells were

described to have long, horizontally oriented axons that remain confined to the deep layers. Corticoclaustral cells have not been defined in morphological parameters yet.

3.1 Heterogeneity of Corticothalamic Pyramidal (CT) Cells in Neocortex

The hodologically-defined class of pyramidal cells, corticothalamic cells (CT), reside in layer 5 (L5) and 6 (L6) of neocortex. These two classes of CT cells – L5 and L6 – are characterized by different intrathalamic distribution of axonal fields and morphology of their terminations (Deschenes et al., 1998). Within the thalamus, there are two major categories of nuclei, namely first order and higher order nuclei (Fig 3.1). First order nuclei relay information from periphery to the cortex, whereas higher order nuclei relay information from one cortical area to another. L5 CT cells project to higher order thalamic nuclei and have major influence on the function and physiology of the thalamic neurons (driver) that they form Type II synapses with – hence they are a type of 'feedforward' pyramidal cells (Chen et al., 2009; Deschenes et al., 1998). On the other hand, L6 CT cells project to both first order and higher order thalamic nuclei and have the physiological characteristics of 'modulator' synapses that are of both Type I and II kinds. These L6 CT cells provide cortical 'feedback' to the thalamic neurons. It has been shown that L6 CT cells provide strong excitatory input to the inhibitory reticular neurons (TRN) and disynaptic inhibitory input to the relay neurons (Briggs and Usrey, 2008; McAlonan et al., 2006). Depending on the thalamic target, the L6 CT cells have been shown to have sublaminar topology within the cortex. For example, in rodent somatosensory cortex, L6 CT cells that project to the first order thalamic nucleus ventral posteromedial nucleus (VPm), are found in upper layer 6 (Bourassa et al., 1995) and have a well developed apical dendritic tuft and a

narrow, vertically oriented axonal arbor with appendages that terminate in layer 4 (Zhang and Deschenes, 1997). L6 CT cells in the somatosensory cortex that project to the higher order thalamic nucleus, posterior thalamic nucleus (Pom), are located in deep layer 6 and have shorter upright dendrites with both apical dendrites and axons ramifying in layer 6. This sublayer specificity in CT morphology and target selection has been reported in different species and in all primary sensory cortical regions (Thomson, 2010).

CT projections to the thalamus vastly outnumber the thalamic projections into the cortex. The excitatory synapses from CT pyramidal cells form the major afferent input into the thalamus. CT projections function to sharpen the receptive field of the apposing thalamic nuclei and also contribute to egocentric enhancement of sensory signals from primary afferents during sensory processing (Briggs and Usrey, 2008). At the global level, CT feedback contributes to the neuronal circuitry involved in adjusting the responsiveness of thalamic neurons and activity patterns during sleep and wakefulness (Lam and Sherman; Steriade, 2001; Steriade and Amzica, 1998; Steriade et al., 2001). In effect, CT feedback generates large scale coherent oscillations in the thalamus and during sleep, it is very prominent in eliciting a synchronized state. During wakefulness, the cholinergic input from the brain stem counteracts the CT input hence this state is characterized by lower levels of synchrony. There are neuropathological conditions associated with the malfunctioning of the CT circuit. Hyper synchronization of the thalamic circuit leads to the condition called absence epilepsy and is presented as abnormal large-scale synchronization of neuronal populations in cortex and thalamus (Kostopoulos, 2000; Paz et al., 2007). In electroencephalogram, high amplitude bilateral and rhythmic (~3 Hz) spike wave discharge (SWD) is detectable. By contrast, hyposynchronization of corticothalamic circuitry is

symptomatic of sleep disorder (Hill and Tononi, 2005; Steriade, 2003). It is also remarkable that decorticated cats were reported to continue to produce spindle oscillations (inhibitory rhythms on relay nuclei) in the thalamus but without large scale coherence, for which CT network needs to remain intact (Contreras et al., 1996).

The first order thalamic nuclei are distinct according to the sensory modality (Briggs and Usrey, 2008). L6 CT cells that synapse onto the first order nuclei affect the ensuing sensory responses and receptive field properties, as well as the firing mode and/or the activity state. The first order thalamic nuclei involved in the processing of visual, auditory and somatosensory are – lateral geniculate nucleus (LGN), medial geniculate body (MGB) and ventrobasal complex (VB). These primary sensory nuclei relay sensory information from the peripheral system to the relevant cortical area such as visual cortex, auditory cortex and somatosensory cortex respectively. On the other hand, higher order thalamic nuclei such as intralaminar nuclei, posteromedial nuclei (Pom) etc. receive input from cortical areas and they in turn project to other association areas in the cortex.

The notion of topographic reciprocity in thalamo-cortico-thalamic circuitry was first introduced in neuroanatomy by Diamond and colleagues (Conley et al., 1991) when they described the spatial distribution of CT projections from the auditory cortical areas in cats. The principal of reciprocity states that a cortical area returns axons to the thalamic nucleus from which it receives afferents. Deschenes (Deschenes et al., 1998) proposed that the spatial organization of corticothalamic connections complies with a more fundamental rule, the rule of parity, from which reciprocity follows as a general, but not obligatory consequence. The rule of

parity posits that the distribution of corticothalamic projections across and within the thalamic nuclei is determined by the branching patterns of different classes of prethalamic afferents. Reciprocity is evident in many corticothalamic connections. As revealed by early axonal transport techniques, this reciprocity applies to relay neurons in distinct sensory nuclei and their corresponding projection columns in the cortex. But even in association and intralaminar thalamic nuclei, where cells projecting to a given cortical area are more dispersed, reciprocal patterns of CT connectivity have been found (Deschenes et al., 1998).

3.2 Targeting Distinct Corticothalamic Cell Types with BAC Transgenesis

Heterogeneity among CT cell types is difficult to address with conventional immunostaining and in situ hybridization techniques, since these methods usually label cell bodies or processes. The BAC transgenesis strategy allows reproducible access to endogenous cell types by incorporating the necessary gene specific regulatory sequences in the BAC and thus enables cell type specific expression of effector molecules such as EGFP. The advantage of using soluble EGFP as a reporter is that it localizes to the cytoplasm throughout the cell body and the processes, thus we can identify specific gene drivers for different classes of corticofugal neurons. We screened the GENSAT database for specific markers for different types of CT cells and found at least four markers that specified seemingly mutually exclusive CT projection neurons: Syt6, Ntsr1, Chrna5 and Dsp (Fig 3.2). Among these, Syt6 and Chrna5 have a high rostral low caudal gradient whereas Ntsr1 has the opposite low rostral high caudal gradient. Dsp defines a sparse aggregate of CT cells in the retrospenial cortex that sends projections to the dorsal thalamic nuclei. We have pursued Syt6 and Ntsr1 gene drivers to characterize the cell

types defined by these genes in detail using other effector molecules, such as EGFP-L10 and Cre recombinase.

RESULTS:

3.3 Genetic Access to Neurotensin Receptor 1 (Ntsr1) CT Cell Type

Neurotensin Receptor 1 (Ntsr1) is a high affinity receptor for the trideceptide Neurotensin (Nts) with 7 transmembrane spanning regions. It has been shown that Nts by binding to its receptor can selectively modulate dopaminergic neurotransmission, and this has led to the hypothesis that Ntsr1 is implicated in Schizophrenia and other psychoses since postmortem studies revealed that the density of Ntsr1 receptors is reduced in schizophrenics. Ntsr1 null mice have been reported to have altered expression of dopamine receptor Drd2 and exhibited reduced activity in the forced swimming test (Austin et al., 2000; Maeno et al., 2004). Ntsr1 gene (ID: 18216) is located in chromosome 2 and is flanked by neighboring genes Slco4a1 on the 5' end and 1600027N09Rik on the 3' end. The in situ hybridization images in the Allen Brain Atlas database showed a strong expression of Ntsr1 mRNA in Layer VI cells in the neocortex with a low rostral high caudal gradient (Fig 3.3). Expression profile for Ntsr1-EGFP BAC transgenic mice at the GENSAT database concurred with the ISH data and additionally, projections of the CT cells expressing Ntsr1 and projecting to the thalamus was evident (Fig 3.3).

The Ntsr1 BAC RP23-314D14 was used for Cre modification by GENSAT (Gong et al., 2007). This was the same BAC as that used for generating Ntsr1 EGFP BAC transgenic mice (Gong et

al., 2003). The Cre protein is a site-specific recombinase (SSR) that catalyzes the recombination between specific DNA target sequences, namely loxP sites (Hoess et al., 1982). By combining the Cre transgenic line with a floxed allele introduced either by breeding to a mouse harboring it in its genome or by viral mediated transduction, we can selectively apply different genetic strategies to the same population of neurons reproducibly. For initial neuroanatomical characterization, the Ntsr1 Cre founder line GN220 was bred to the reporter line Rosa26-flSTOPfl-EGFP so that EGFP is expressed in the Ntsr1 cells starting from early embryonic days when Rosa26, a ubiquitous promoter (Zambrowicz et al., 1997), is transcribed. Thus Ntsr1 $GN220^{+/-}$ /$EGFP^{+/-}$ double transgenic mice presented an expression pattern that represented the cumulative development history of Ntsr1 gene (Fig 3.4). DAB staining with EGFP antibody revealed that the Ntsr1 EGFP cells in this line inhabit layer 6 of the neocortex with both high caudal low rostral, and high lateral low medial gradient of expression, and that these cells project to the sensory nucleus in the thalamus – the ventral posteromedial nucleus (VPM). The marker Ntsr1 has a very restricted pattern of expression throughout development and thus serves as a good choice for studying a specific class of CT cells.

3.4 Translational Profile of Ntsr1 CT Cell Type in the Neocortex

Our lab generated mice harboring the conditional allele of EGFP-L10 EF1alpha-flSTOPfl-EGFPL10 (described in Chapter 4) that allowed us to perform translational profile of specific cre-expressing cell types in the cortex in the Cre transgenic mice. We mated Ntsr1 GN220 Cre line to EF1alpha-flSTOPfl-EGFPL10 line and obtained double transgenic Ntsr1 $GN220^{+/-}$ /$EGFP^{+/-}$ mice with normal Mendelian ratio. Analysis of the neuroanatomy of these mice using EGFP and NeuN immunostains revealed a similar expression pattern as the previously

characterized Ntsr1 GN220$^{+/-}$ /EGFP$^{+/-}$ mice (Fig 3.5). However, the reporter EGFP-L10 is restricted to the cell soma and does not label the axons hence the CT projections of Ntsr1 cell type are not visible but can be inferred from the EGFP line. The rostrocaudal and mediolateral gradients are evident in this line as well.

The polysomal immunoprecipitation strategy, as described in Chapter 2, was applied to generate the translational profile of the cortical Ntsr1 cell type. We pooled together 6 cortices from a cohort of 3 adult mice to enrich the polysomes specific for the Ntsr1 cell type. We obtained an average yield of 8.21 ng/ul from each of the three biological replicates referred to as IPs. The Ntsr1 IP replicates were amplified and applied to the microarray chips. Using the Genespring software, Ntsr1 cortex IP samples were then plotted against the cortex background (Fig 3.6). The IP replicates had a high correlation with an average Pearson correlation coefficient of 0.95.

The Ntsr1 probe (1420799_at) was enriched in the Ntsr1 cortex IP by a fold change (FC) of 2.65? compared to the cortical input. For data quality assessment, known negative non-pyramidal cell markers were plotted on the Ntsr1 IP vs whole cortex graph which were mostly either depleted or not-enriched in the Ntsr1 IP. We also examined expression levels of annotated pyramidal cell markers and found that Crym (1416776_at), Wfs1 (1448411_at), Zfp312 (1418790_at) and vGlut1 or Slc17a6 (1418610_at) were enriched in Ntsr1 IP. The enrichment of vesicular glutamate transporter 1 (vGlut1), a marker for glutamatergic projection neurons (Fremeau et al., 2004), indicates that Ntsr1 cell type is pyramidal and glutamatergic. Other pyramidal cell markers that were depleted in the Ntsr1 cell type include: S100a10

(145666642_x_at and 1416762_at), Drd1a (14556629_at and 1456051_at) and Npnt (1452107_a_at). Among these markers, Drd1a defines a layer 6 cortical pyramidal cell type that projects to the striatum, so it is further evidence of heterogeneity of pyramidal cells residing in layer 6 of neocortex.

3.5 Genetic Access to Syt6 CT cell type in the Neocortex

As described in Chapter 1 and 2, the bacTRAP transgenic line for Syt6 was generated by modifying the Syt6 BAC with EGFP-L10 transgene. The reporter EGFP-L10 was restricted to the Syt6 cell soma located in layer 6 of neocortex, so the axonal trajectory was not directly traceable in this line. We thus used retrograde tracer Cholera Toxin-B (Llewellyn-Smith et al., 1990) conjugated to a fluorophore to determine that Syt6 cells were indeed corticothalamic. We could also infer the thalamic connections of Syt6 cell type from the Syt6 EGFP BAC transgenic line made by GENSAT. The translational profiles of Syt6 bacTRAP lines PS3011 and PS3013 were generated using the polysomal IP methodology.

We used the same Syt6 BAC RP23-184N6 for introducing Cre modification. Several BAC transgenic founder lines for Syt6 Cre were generated and analyzed for cortical expression of tdTomato reporter after being mated to Rosa26-flSTOPfl-tdTomato. Three founder lines KI130 and KI109 had low and high levels respectively of EGFP expression, both in intensity and total count of EGFP positive cells (Fig 3.7). Since Syt6 Cre KI109$^{+/-}$ /tdTomato$^{+/-}$ most closely resembled Syt6 bacTRAP PS3013, we decided to carry out further neuroanatomical and circuit level analysis on this particular Cre line.

3.6 Comparative Quantitative Translational Profile of CT cell types in Neocortex

We applied the Specificity Index (SI) algorithm, as described in Chapter 2, to quantitatively compare the translational profiles of Ntsr1 and Syt6 CT cell types. For background correction, we used translational profiles of the following cell types: Pnoc GM67 (interneuron cell type1), Lypd6 JP48 (interneuron cell type 2), AldhL1 JD130 (pan-neuronal astrocytes) and Olig2 JD67 (oligodendrocytes). As described in Chapter 2, translational profiles of these 4 negative cell types, 2 CT cell types (Ntsr1 and Syt6) and the cortical input, for a total of 7 different TRAP datasets, were iteratively compared to each other using the R based algorithm.

3.6.1 Comparative Quantitative Translational Profile of Ntsr1 CT cell type in Neocortex

Comparative SI analysis for Ntsr1 GN220$^{+/-}$ /EGFP$^{+/-}$ Cortex IP revealed 248 genes that were significantly enriched ($p < 0.05$) compared to the other cell types. Some of the biologically and statistically significant genes are described in Figure 3.8. Among the significantly enriched, there were some interesting genes that include Foxp2 (SI = 73, p = 8.40E-05), Camk2b (SI = 380.67, p = 0.0084) and Snap25 (SI = 674, p = 0.030). While Camk2b and Snap25 are known markers for pyramidal cells in the cortex, Foxp2 is reported to be expressed in a class of Tbr1+ CT projection neurons (Hisaoka 2009). To determine the functional classes of genes distinguishing the Ntsr1 cell type, we performed an over-representation analysis using the Gene Ontology (GO) database. Some of the GO terms pertinent to Biological Pathways that were overrepresented in the Ntsr1 cell type are: nervous system development, vesicle mediated transport, synaptic transmission, regulation of transcription, learning and memory, calcium ion

transport. These biologically relevant GO categories and the list of genes under each category are listed in Fig 3.9.

We then used the web-based DAVID software to analyze the biologically relevant KEGG pathways unique to Ntsr1 cell type. The statistically overrepresented KEGG pathways include (Fig 3.9): MAPK signaling pathway (Rasgrp1, Cacna2d1, Cacnb4, Gadd45a, Pak1, Pla2g4b, Prkcc and Rps6ka5), Neurotrophin signaling pathway (Camk2b, Camk2d, Rps6ka5, Ywhag and Ywhaz) and Axon guidance (Rnd1, Rock2, Pak1, Sema3e and Unc5c).

3.6.2 Comparative Quantitative Translational Profile of Syt6 CT cell type in Neocortex

Comparative SI analysis of Syt6 PS3013 cortex IP revealed 226 genes that were significantly enriched ($p < 0.05$) compared to other cell types including Ntsr1 GN220. Some of the biologically and statistically significant genes are described in Fig 3.10. The BiNGO GO analysis for overrepresented gene ontologies for Syt6 cell type revealed the following: nervous system development, neurogenesis, neuron projection morphogenesis, regulation of calcium ion transport, regulation of transmission of nerve impulse, synaptic transmission and calcium ion transport (Fig 3.11). The overrepresented KEGG pathways in Syt6 cell type compared to Ntsr1 cell type include: MAPK signaling pathway (Bdnf, Cacna1a, Cacna1h, Cacnb2, Dusp14, Hspa1a, Mapk11, Mapk9ip3 and Pla2g4e), axon guidance (Efnb2, Pak6, Sema3a, Slit3 and Unc5a) and VEGF signaling pathway (Mapk11, Pik3cb, Pla2q4e and Ptgs2) as shown in Fig 3.11.

3.6.3 Comparative Venn diagram of the Top enriched genes in Ntsr1 and Syt6 CT cell types

The list of Top 1000 highly enriched genes in Ntsr1 GN220 cortex IP and Syt6 PS3013 cortex IP, with respect to the cortical input, were directly compared using a Venn Diagram (Fig 3.12). The comparative Venn diagram analysis revealed that there are 385 genes in common between GN220 IP and PS3013 IP. By contrast, there are 647 genes that are exclusively enriched in Syt6 PS3013 cortex IP and 633 genes exclusively enriched in Ntsr1 GN220 cortex IP. This is an alternate way to analyze the TRAP data for the two CT cell types. The common genes (385) between Ntsr1 and Syt6 cell types probably represent genes that specify all pyramidal cells or all CT cell types in the cortex. Our results indicate that the Ntsr1 and Syt6 represent two different CT cell types with distinct translational profiles.

3.7 Circuit mapping of CT cell types

Circuit tracing of sparse population of pyramidal cells can reveal the topology of projection as well as whether the projections bifurcate along the way. When the Cre mice are crossed to a cre-dependent reporter line with a ubiquitous promoter, all the Cre expressing cells undergo recombination early in development. While this approach gives us a global picture of the cumulative trajectory of Cre cells over the developmental history, it is important to use alternative methods to trace the circuitry of a focal sparse group of cells in order to follow their axons completely and to ensure the circuitry is representative of adult stage.

3.7.1 Anterograde Circuit Mapping of Ntsr1 CT cell type with pAAV-doublefloxed-Reporter

Using viral gene transfer methods (described in detail in Chapter 4.3.1), we can trace the axonal trajectory of a focal population within a cell type, thus allowing us further specificity. We used the recombinant AAV virus: pAAV-EF1a-double floxed ChR2 (E123A)-mCherry-WPRE (Cardin et al.)– to transduce reporter expression in a focal subset of Ntsr1 cell type in the visual cortex. This version of AAV is less leaky compared to the earlier versions due to the two dissimilar loxP sites (loxP and lox2722) that flank mCherry. We stereotaxically injected 0.5 ul of pAAV-ChR2-mCherry into the secondary visual cortex (V2) of heterozygous Ntsr1 GN220 Cre +/- mice. We find that the focal population of Ntsr1 CT cells from V2 project to the dorsal region of the sensory lateral posteromedial nucleus (LPM) (Fig 3.13). Compared to the Ntsr1 $GN220^{+/-}$ /$Rosa26\text{-}EGFP^{+/-}$ line where all the Ntsr1 cells were labeled with EGFP and sent their projections to all of VPM/ LPM, we find that the focal population of Ntsr1 cell type transduced in the V2 project discretely to the dorsal LPM. Hence, this suggests that there might be a topographical relationship between the origin of the CT afferents i.e. where the cell bodies are located in the cortex and their target within the thalamic nucleus. The coherent projection to LPM also indicates that Ntsr1 cell type defines a class of CT neurons with afferents to first order sensory nucleus in the thalamus. The Ntsr1 CT afferents may play a role in sharpening the basic receptive field properties of thalamic neurons (Alitto and Usrey, 2003). A recent study by Lopez-Armanda (Lopez-Aranda et al., 2009) found that layer 6 CT cells of V2 are crucial for the processing of object-recognition memory (ORM). Hence, it will be useful in future to functionally manipulate the Ntsr1 cell type in V2 and study its effect

3.7.2 Anterograde Circuit Mapping of Syt6 CT cell type with pAAV-doublefloxed-Reporter

As described earlier, Syt6 KI109 Cre line was used for tracing the circuit of the Syt6 cell type. The Syt6 cells are distributed in a high rostral low caudal gradient along the neocortex. We wanted to ask the following questions: 1) Where in the thalamus do Syt6 CT cell type project to? and 2) Is there a topographical relationship between the somatic location of the Syt6 CT cells and the targets of their projections? In order to answer these questions, we decided to apply a dual AAV reporter strategy. We injected AAV-EF1a-dfl-ChR2-EYFP-dfl into the dorsal prelimbic cortex (PL) and AAV-EF1a-dfl-ChR2-mCherry-dfl into the anterior cingulate cortex (M2) of Syt6 KI109 cre mice. After 3 weeks the brains were analyzed for histology. The results of the anterograde tracing of the Syt6 CT projections are shown in Fig 3.14. In the case of PL injection, the EGFP labeled Syt6 CT axons traced all the way from PL to posterior thalamic nucleus (Po) and ventrolateral nucleus (VL) in the ipsilateral hemisphere. The EGFP filled up the apical dendrites of the Syt6 cell type as well, which revealed that the Syt6 cell type in PF send dendrites up to layer 2/3. The results for PL injection in Syt6 cell type conformed to our expectations. However, the M2 injection in the same mouse led to a surprising discovery as shown in Fig 3.14. The red mCherry reporter was expressed by a focal population of cells in layer 6 of M2 contralateral to the PL injection. What was surprising was that the mCherry labeled Syt6 cells not only projected to the ipsilateral thalamus, they also project to layer 6 in the contralateral cortex by crossing the corpus callosum. It is not clear whether the same Syt6 cells in M2 bifurcate and project both to thalamus and contralateral cortex, or there are two subpopulations of Syt6 cell type in M2 that project to the two targets mutually exclusively. It is also interesting to note that the M2 Syt6 CT cell type project only to the posterior thalamic nucleus (Po) in the ipsilateral hemisphere.

Perspective:

In this chapter, we have characterized two different BAC transgenic lines of corticothalamic (CT) pyramidal cells, defined by the expression of Ntsr1 and Syt6. While Ntsr1 CT cell type represents a sensory type CT projection from primary sensory areas to first order thalamic nuclei, Syt6 CT cell type represents an association type CT projection from higher association cortical areas to higher order thalamic nuclei. We presented evidence that these two CT cell types differ in neuroanatomy and cytoarchitectonics, as well as in the repertoire of molecules that they express. Comparative translational profile using specificity index (SI) algorithm revealed specific genes, gene ontology categories and KEGG pathways that are uniquely enriched in the two CT cell types. Finally, viral transduction of EGFP or mCherry reporter(s) in focal populations of Ntsr1 cell type in the visual cortex and Syt6 cell type in the prelimbic cortex and anterior cingulate cortex reveal that there is a topographic code to the cortical location of CT cells and their corresponding axonal connections in specific regions within the thalamic nuclei. We have thus identified parameters by which these two CT cell types differ from each other and hence define distinct cell types of corticothalamic projection neurons. The cortical layer 6 is endowed with cellular heterogeneity and there are possibly many more distinct corticothalamic cell types in this layer with distinct molecular profile, function and connectivity. Delineating the complexity of corticothalamic cell types will help us understand how the thalamic nuclei are modulated during sensory perception and cognition and may lead us to better therapeutic strategies towards treating diseases such as absence epilepsy and sleep disorders.

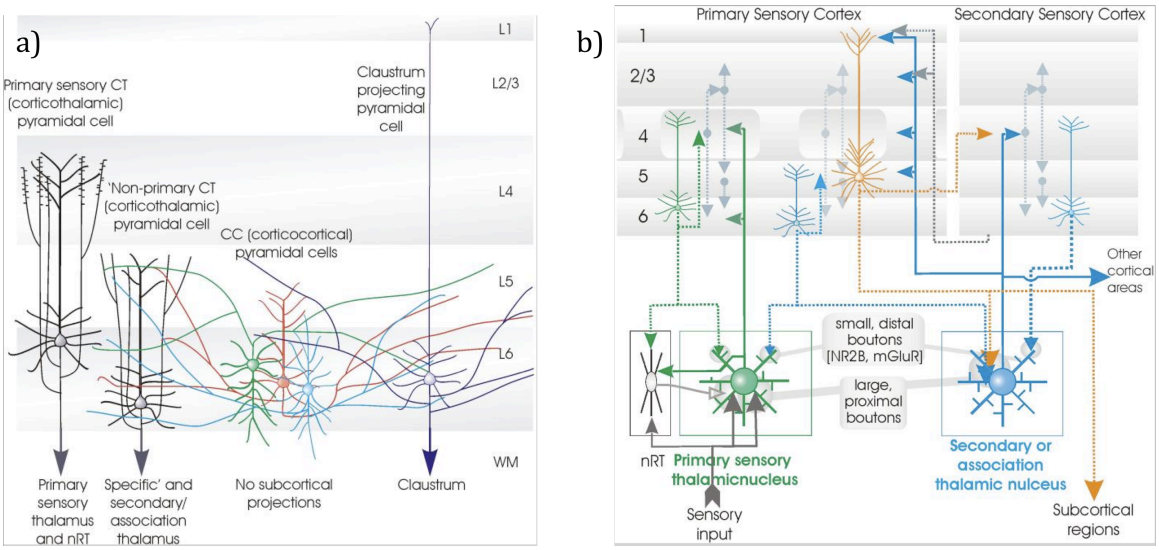

Thomson, 2010

Figure 3.1: Major classes of layer 6 pyramidal cells and diagram of thalamo-cortico-thalamic connectivity. (a) Layer 6 pyramidal cells can be classified by hodology into corticothalamic (CT), corticocortical (CC) and claustrum projecting pyramidal cells. Corticothalamic pyramidal cells can be further divided into primary sensory CT and non-primary CT cells according to their projections to primary sensory thalamus and higher-order association thalamus respectively. (b) CT cells in layer 6 send modulatory to thalamic nuclei. Primary sensory CT cells receive input from primary sensory thalamic nucleus that relay sensory input from periphery to cortex. Non-primary CT cells receive input from secondary (higher) or association thalamic nucleus which relay input from other cortical areas. Both kinds of CT cells in turn provide reciprocal glutamatergic signal to the respective thalamic nuclei. (Adapted from Thomson 2010)

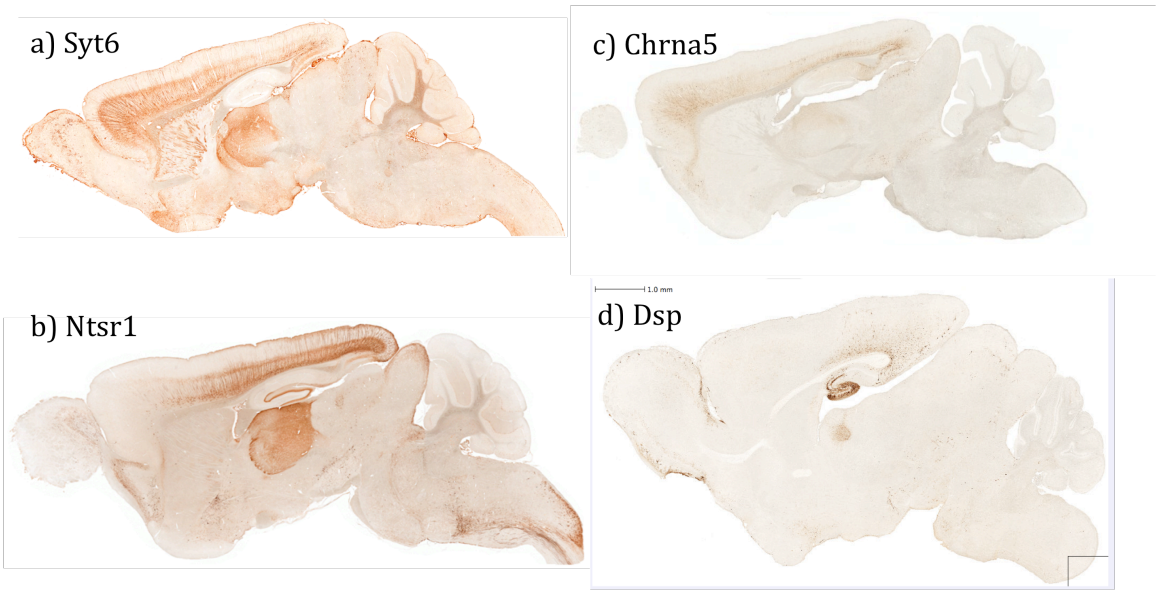

Figure 3.2: Diversity of corticothalamic (CT) pyramidal cell types in GENSAT GFP reporter mice. At least four different types of CT pyramidal cell types were identified using the GENSAT database. They include (a) anterior CT cells expressing Syt6, (b) posterior CT cells expressing Ntsr1, (c) frontal CT cells expressing Chrna5 and (d) retrospenial CT cells expressing Dsp.

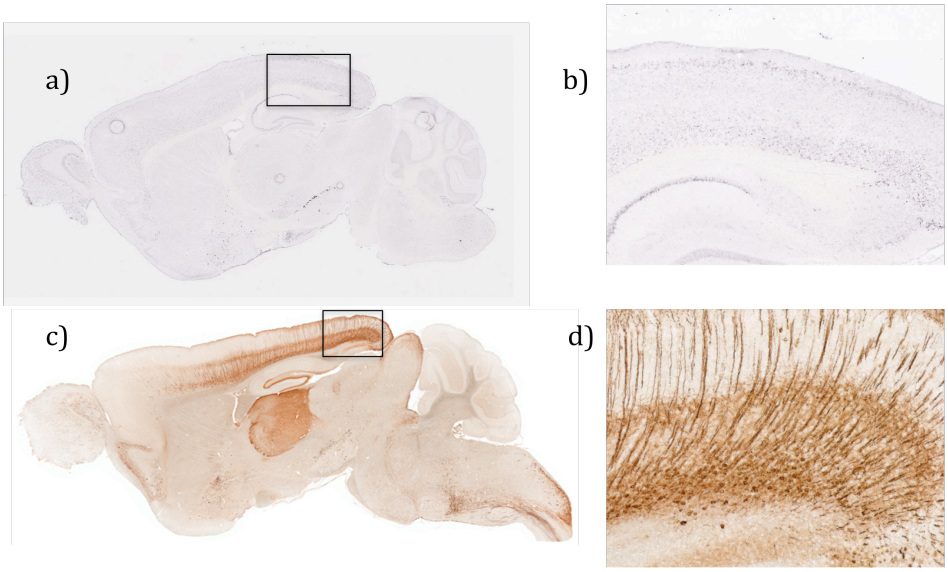

Figure 3.3: Expression pattern of Neurotensin Receptor 1 (Ntsr1) in the mouse brain. Digital *in situ* hybridization data in Allen Brain Atlas (ABA) reveals slight enrichment of Ntsr1 RNA in layer 6 of neocortex (a; enlarged inset: b) in coronal section. GENSAT BAC transgenic mice for Ntsr1 EGFP reporter concurred with Ntsr1 expression in layer 6 of neocortex (with a high caudal low rostral gradient) and additionally indicated corticothalamic projection (c; enlarged insetd: d).

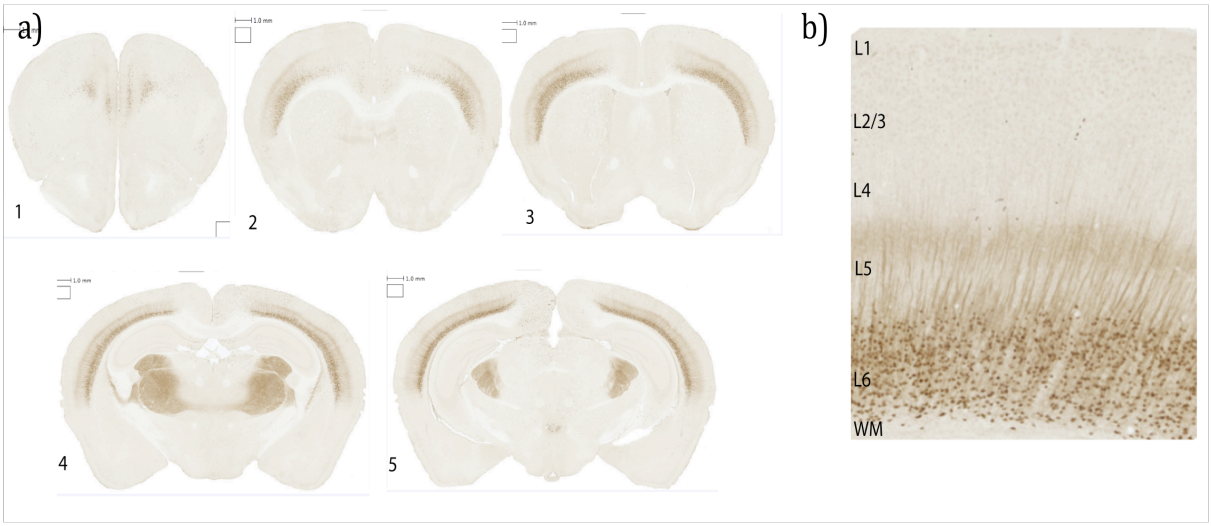

Figure 3.4: Cumulative developmental expression of Ntsr1 GN220 X Rosa26-EGFP. The EGFP reporter is expressed in Ntsr1+ cells during embryonic development when both Ntsr1 and Rosa26 promoters are active, and allow cre-mediated recombination. Cre is inherited by the progeny and all the cells with a history of Ntsr1 and Rosa26 expression are labeled with EGFP in the layer 6 of neocortex with a high caudal low rostral gradient (a: 1-5). At higher magnification, the morphology of Ntsr1+ cells was detectable with the apical dendrites reaching layer 4.

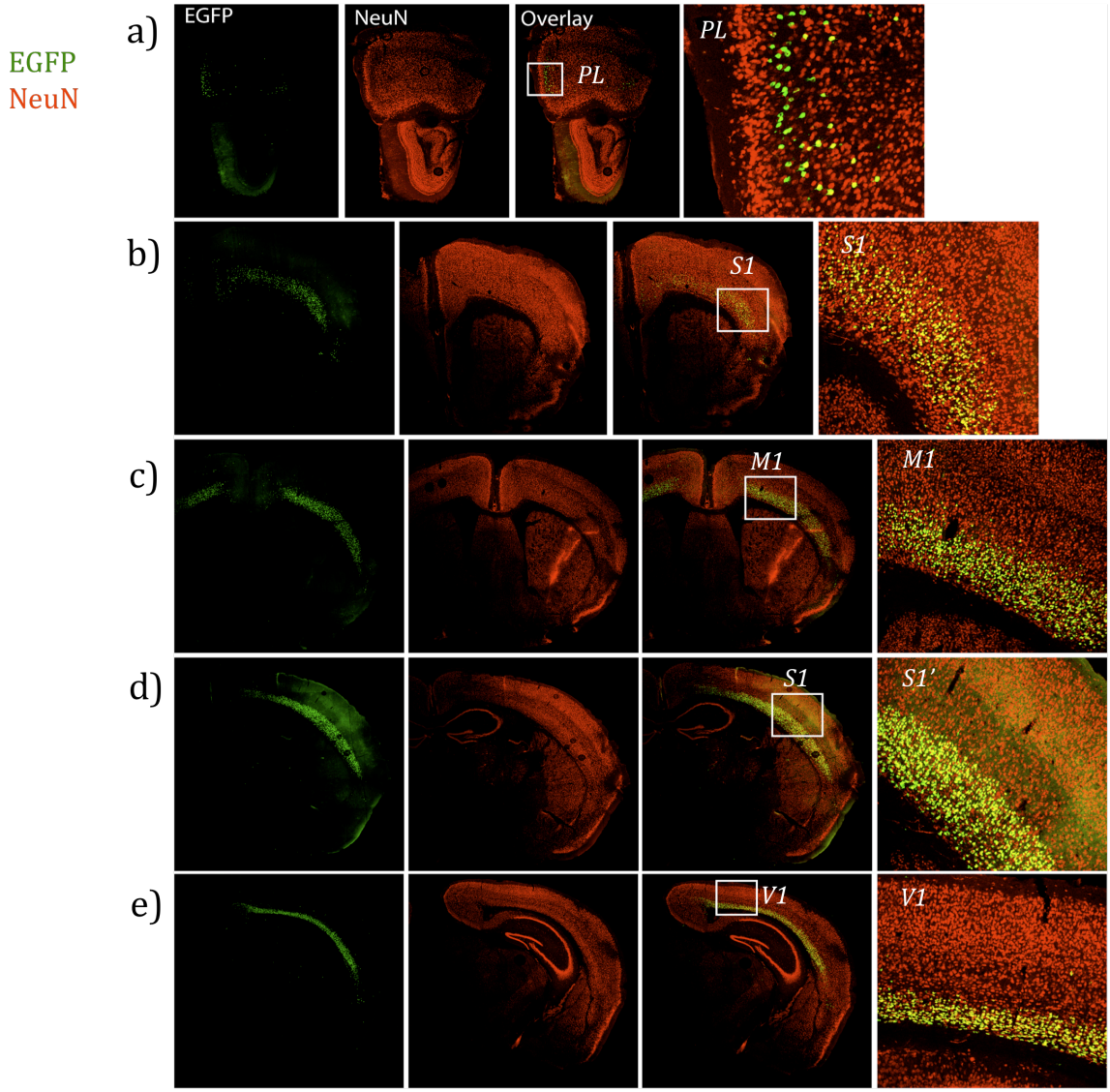

Figure 3.5: IHC of conditional TRAP line Ntsr1 GN220XEF1a-EGFPL10. EGFP and NeuN co-immunostaining reveal complete colocalization of EGFP with NeuN, indicating a neuronal identity (a- e). Strong EGFP/NeuN staining is detected in the layer 6 of neocortex with a high caudal low rostral gradient (a, b, c, d, e; enlarged insets: PL, S1, M1, S1' and V2).

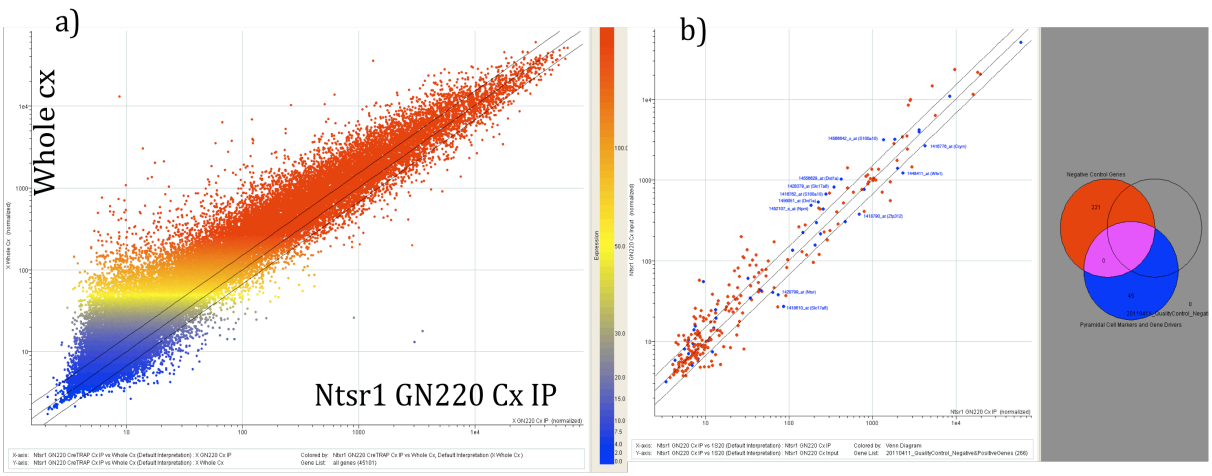

Figure 3.6: Translation profile of Neurotensin Receptor 1 Ntsr1 GN220 cortex cell type. Fluorescence signals of all 40,000 probesests for Ntsr1 GN220 cortex IP replicates were averaged and plotted against total cortex input (whole cx) in an X-Y scatterplot (a). Pyramidal cell marker probesets (in blue) were examined for their distribution in the scatterplot together with non-pyramidal cell type marker genes (in red) (b).

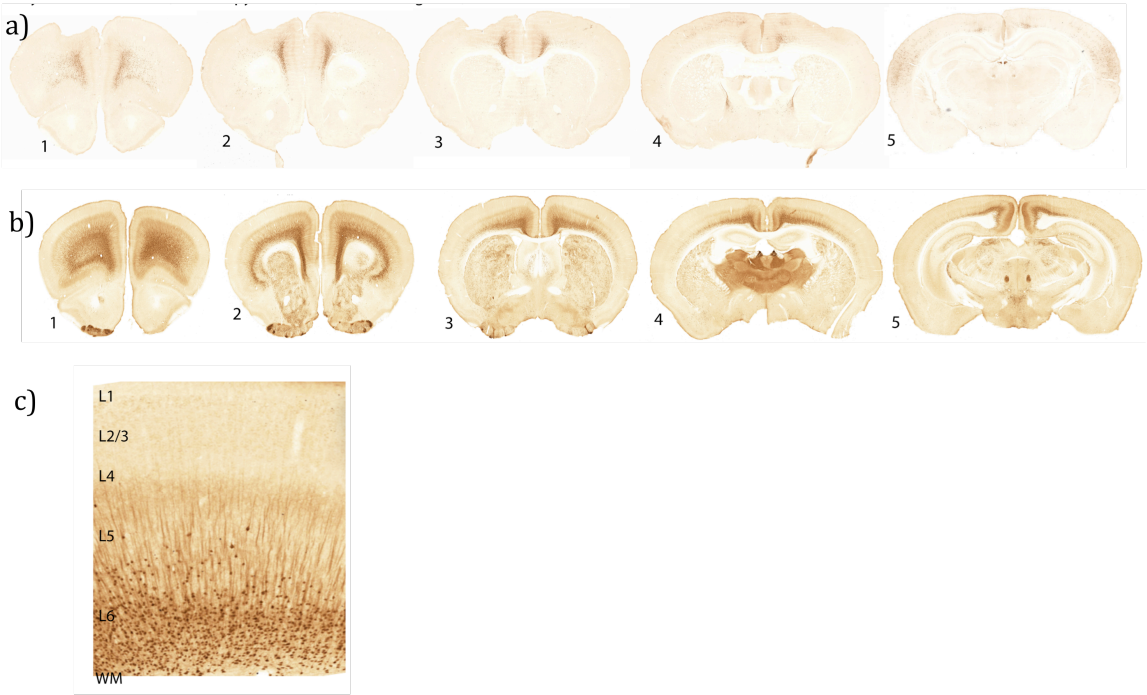

Figure 3.7: Cumulative developmental expression of Sy6 Cre X Rosa26-EGFP. DAB staining for EGFP revealed expression in partial population of Syt6+ cell type in KI130 (a) and complete population in KI109 (b). The EGFP reporter is expressed in Syt6+ cells during embryonic development when both Syt6 and Rosa26 promoters are active, and allow cre-mediated recombination. Cre is inherited by the progeny and all the cells with a history of Syt6 and Rosa26 expression are labeled with EGFP in the layer 6 of neocortex with a high rostral low caudal gradient (a, b: 1-5). At higher magnification (c), the morphology of Syt6+ cells was detectable with the apical dendrites reaching layer 4.

CT SI Analysis: Differentially expressed genes in Ntsr1 GN220 Cortex IP

Michigan Probe ID	Gene Symbol	Gene Description	SI	P value
4037	Nefm	neurofilament, medium polypeptide	69.6666667	7.90E-05
964	Foxp2	forkhead box P2	73	8.40E-05
3129	Igfbp4	insulin-like growth factor binding protein 4	199.166667	0.00176777
10001	Spag6	sperm associated antigen 6	219.166667	0.00225172
6651	Wfs1	Wolfram syndrome 1	225.333333	0.00240464
6258	Klf10	Kruppel-like factor 10	266.833333	0.00370862
1244	Ap2a2	adaptor protein complex AP-2, alpha 2 subunit	298.5	0.00488825
4036	Nefl	neurofilament, light polypeptide	299	0.00490674
2049	Gadd45a	growth arrest and DNA-damage-inducible 45 alpha	334.833333	0.00623761
11420	Clstn1	calsyntenin 1	360	0.0074206
9297	Olfml2b	olfactomedin-like 2B	360.5	0.00745085
11326	Sv2b	synaptic vesicle glycoprotein 2 b	372.666667	0.00805075
1528	Camk2b	calcium/calmodulin-dependent protein kinase II, beta	380.666667	0.00844564
7963	Tspyl5	testis-specific protein, Y-encoded-like 5	381.333333	0.00848429
10889	Necab3	N-terminal EF-hand calcium binding protein 3	386.333333	0.00872458
5606	Pla2g4b	phospholipase A2, group IVB	392.833333	0.00912284
12104	Rbm25	RNA binding motif protein 25	421.5	0.01074105
4028	Nfil3	nuclear factor, interleukin 3, regulated	443.666667	0.01206184
7742	Camkv	CaM kinase-like vesicle-associated	484.333333	0.01451353
5538	Syp	synaptophysin	488.166667	0.01480423
1509	Cacnb4	calcium channel, voltage-dependent, beta 4 subunit	550	0.01931608
5031	Sema3e	sema domain, immunoglobulin domain (Ig), short basic domain, secreted,	585.833333	0.02220467
5200	Snap25	synaptosomal-associated protein 25	674	0.0299311
648	Camk2d	calcium/calmodulin-dependent protein kinase II, delta	714.666667	0.03369854
1504	Cacna2d1	calcium channel, voltage-dependent, alpha2/delta subunit 1	718.166667	0.03400605
3285	Kcnab2	potassium voltage-gated channel, shaker-related subfamily, beta member 2	788.5	0.04100823

Figure 3.8: Significantly enriched genes from the SI analysis for Ntsr1 cell type. Cortex TRAP data for CT Ntsr1 GN220 was iteratively compared to the other CT pyramidal cell type Syt6 PS3013, as well as interneuron cell types (Pnoc GM64 and Lypd6 JP48) and non-pyramidal glial cell types (AldhL1 JD130 and Olig2 JD97).

a)

BiNGO Analysis for Ntsr1 : Biological Pathway

GO ID	Description	Corrected p-val	Genes
7399	Nervous system development	5.53E-06	Dlc1, Gprin1, Snap91, Hprt1, Syp, Ptk2b, Not, Atg7, Sema3e, Actl6b, Unc5c, Pak1, Nefl, Nefm, Aars, Klf16, Tbr1, Fc
31175	Neuron projection development	1.78E-05	Gprin1, Snap91, Hprt1, Tbr1, Syp, Ptk2b, Not, Atg7, Hpca, Pak1, Apbb1, Nefl, Kalrn
7610	Behavior	1.13E-04	Egr1, Gabrg2, Penk1, Hmgcr, Cacnb2, Cx3cl1, Hprt1, Prkcc, Foxp2, Pde18, Not, Atg7, Hpca, Sna25, Apbb1
16192	Vesicle mediated transport	1.37E-04	Ywhaz, Snap91, Napg, Kif17, Icam5, Syp, Ap2b1, Ap2a2, Cttn, Hpca, Rin1, Sv2b, Ap1gbp1, Snap25, Kalrn
7268	Synaptic transmission	3.51E-04	Syp, Gabrg2, Snap91, Hnmt, Clstn1, Hpca, Sv2b, Cacnb4, Snap25, Usp14
45449	Regulation of transcription	6.91E-04	Pdlim1, Stip1, Trim66, Mcm8, Sqstm1, Safb, Not, Yeats2, Leo1, Actl6b, Pak1, Emb, Ddx20, Nfil3, Egr1, Klf10, Klf16,
7611	Learning or memory	3.89E-03	Egr1, Pde1b, Hmgcr, Apbb1, Snap25, Foxp2
6816	Calcium ion transport	4.59E-03	Anxa6, Cacna2d1, Hpca, Camk2d, Camk2b, Cacnb4
6836	Neurotransmitter transport	4.72E-03	Snap91, Hpca, Sv2b, Slc6a17, Snap25

b)

KEGG Pathway Analysis for Syt6 CT cell type

Term	Count	%	P Value	Benjamini FDR	Genes
MAPK signaling pathway	8	3.6	5.70E-02	8.00E-01	Rasgrp1, Cacna2d1, Cacnb4, Gadd45a, Pak1, Pla2g4b, Prkcc, Rps6ka5
Neurotrophin signaling pathw	5	2.3	9.00E-02	7.70E-01	Camk2b, Camk2d, Rps6ka5, Ywhag, Ywhaz
Axon guidance	5	2.3	9.10E-02	7.30E-01	Rnd1, Rock2, Pak1, Sema3e, Unc5c

Figure 3.9: Overrepresented Gene Ontology (GO) categories and KEGG pathways for Ntsr1 cortex cell type. Representative GO categories (a) and KEGG pathways (b) are significantly overrepresented in Ntsr1 GN220 cortex TRAP data when compared with other cell types using SI algorithm.

CT SI Analysis: Differentially expressed genes in Syt6 PS3013 Cortex IP

Michigan Probe II	Gene Symbol	Gene Description	SI	P value
342	Zfp692	zinc finger protein 692	87	1.70E-05
14346	Lime1	Lck interacting transmembrane adaptor 1	91.3333333	1.70E-05
15784	Tnrc4	trinucleotide repeat containing 4	163.833333	0.00016713
3782	Meg3	maternally expressed 3	188.166667	0.00025433
10030	Atp9b	ATPase, class II, type 9B	190.833333	0.00025917
6194	Wdr60	WD repeat domain 60	247	0.00058132
9348	Lba1	lupus brain antigen 1	283.5	0.00080659
2603	Gas5	growth arrest specific 5	330.666667	0.00125712
1507	Cacnb2	calcium channel, voltage-dependent, beta 2 subunit	367.833333	0.00171491
10853	Psrc1	proline/serine-rich coiled-coil 1	403	0.00223689
3286	Kcnab3	potassium voltage-gated channel, shaker-related subfamily, beta member 3	447.833333	0.00299503
8610	Dpysl4	dihydropyrimidinase-like 4	493.666667	0.00391304
2075	Dffb	DNA fragmentation factor, beta subunit	540.5	0.00494732
1498	Cacna1a	calcium channel, voltage-dependent, P/Q type, alpha 1A subunit	548.166667	0.00515805
7146	Ncoa5	nuclear receptor coactivator 5	573.5	0.00580962
2233	Emx1	empty spiracles homeobox 1	629.833333	0.00743611
7167	Gpr103	G protein-coupled receptor 103	661.833333	0.00848492
5028	Sema3a	sema domain, immunoglobulin domain (Ig), short basic domain, secreted	695.333333	0.00966816
11066	Cacna1h	calcium channel, voltage-dependent, T type, alpha 1H subunit	701.166667	0.00989827
4674	Ptprk	protein tyrosine phosphatase, receptor type, K	703	0.00998062
9309	Zdhhc17	zinc finger, DHHC domain containing 17	784.5	0.0131985
4105	Npy5r	neuropeptide Y receptor Y5	818.833333	0.01464697
2193	Efnb2	ephrin-B2	824	0.01488434
3049	Hspa1b	heat shock protein 1B	841.333333	0.01570425
6428	Trpc4	transient receptor potential cation channel, subfamily C, member 4	887.666667	0.0180344
15773	Zc3h6	zinc finger CCCH type containing 6	888.833333	0.01808163

Figure 3.10: Significantly enriched genes from the SI analysis for Syt6 cell type. Cortex TRAP data for CT Syt6 PS3013 was iteratively compared to the other CT pyramidal cell type Ntsr1 GN220, as well as interneuron cell types (Pnoc GM64 and Lypd6 JP48) and non-pyramidal glial cell types (AldhL1 JD130 and Olig2 JD97).

a)

BiNGO Analysis for Syt6 : Biological Pathway

GO ID	Description	Corrected p-val	Genes
7399	Nervous system development	2.58E-08	Gprin1, Cobl, Adcyap1, Bdnf, Unc5a, Not, Atg7, Rapgef4, Sem3a, Emx1, Efnb2, Tbce, Racgap1, Afg3l2, Tbr1, Slit3,
22008	Neurogenesis	2.91E-08	Gprin1, Emx1, Tbce, Racgap1, Afg3l2, Tbr1, Adcyap1, Slit3, Prdm8, Ntrk3, Bdnf, Unc5a, Atg7, Not, Hpca, Akap5, M
48812	Neuron projection morphogenesis	2.53E-07	Tbce, Afg3l2, Tbr1, Slit3, Bdnf, Unc5a, Not, Hpca, Mapk8ip3, Sema3a, Dst, Slitrk5, Cacna1a
51924	Regulation of calcium ion transport	4.29E-05	Trpc4, Ptgs2, Hpca, Akap5, Cacna1h, Cacnb2, Cacna1a
51969	Regulation of transmission of nerve	4.18E-04	Bdnf, Ptgs2, Slc24a2, Hpca, Rapgef4, Cacna1a, Npy5r, Adcyap1
7268	Synaptic transmission	2.67E-03	Slc17a7, Bdnf, Hpca, Cacnb2, Ntsr1, Cacna1a, Npy5r, Adcyap1
6816	Calcium ion transport	2.92E-03	Trpc4, Slc24a2, Hpca, Cacna1h, Cacnb2, Cacna1a

b)

KEGG Pathway Analysis for Syt6 CT cell type

Term	Count	%	P Value	Benjamini FDR	Genes
MAPK signaling Pathway	9	4.5	3.00E-03	2.60E-01	Bdnf, Cacna1a, Cacna1h, Cacnb2, Dusp14, Hspa1a, Mapk11, Mapk9ip3, Pla2g4e
Axon Guidance	5	2.5	3.40E-02	8.10E-01	Efnb2, Pak6, Sema3a, Slit3, Unc5a
VEGF signaling pathway	4	2	3.40E-02	6.80E-01	Mapk11, Pik3cb, Pla2q4e, Ptgs2

Figure 3.11: Overrepresented Gene Ontology (GO) categories and KEGG pathways for Syt6 cortex cell type. Representative GO categories (a) and KEGG pathways (b) are significantly overrepresented in Syt6 PS3013 cortex TRAP data when compared with other cell types (Ntsr1 GN220, Pnoc, Lypd6, AldhL1 an Olig2) using SI algorithm.

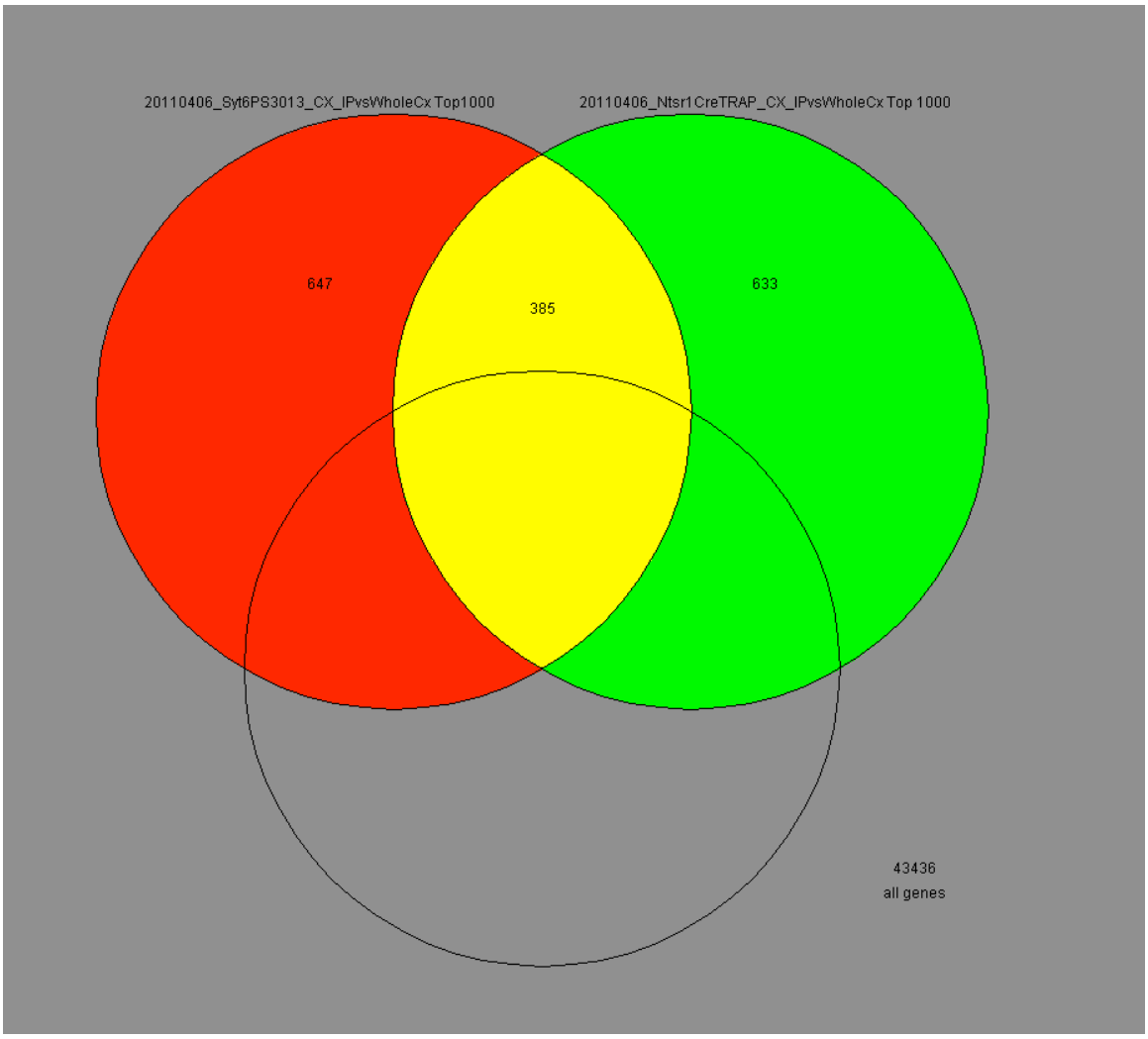

Figure 3.12: Venn Diagram comparing corticothalamic cell types: Ntsr1 and Syt6. Top 1000 most highly enriched genes in cortex IP (vs whole cx) of Syt6 PS3013 and Ntsr1 GN220 were compared to each other. There were 385 genes common between the two lists whereas 647 genes and 633 genes were exclusive to Syt6 PS3013 and Ntsr1 GN220 TRAP lines respectively.

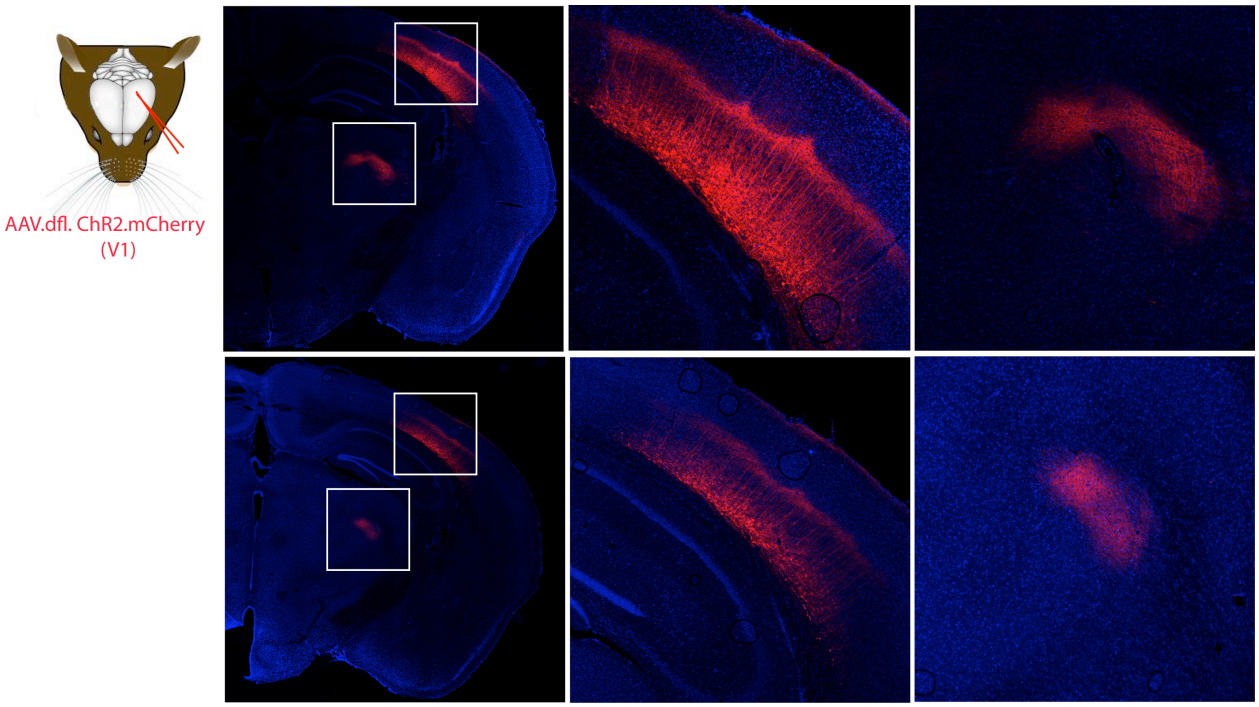

Figure 3.13: Circuit mapping of corticothalamic Ntsr1 Cell type. Anterograde viral tracer AAV-dfl-ChR2-mCherry-dfl was stereotactically injected into the primary visual cortex (V1) as shown in (a). Viral transduction of mCherry under the control of Cre recombinase revealed that Ntsr1 cells in V1 project to lateral posterior thalamic nucleus (LPM) in the thalamus.

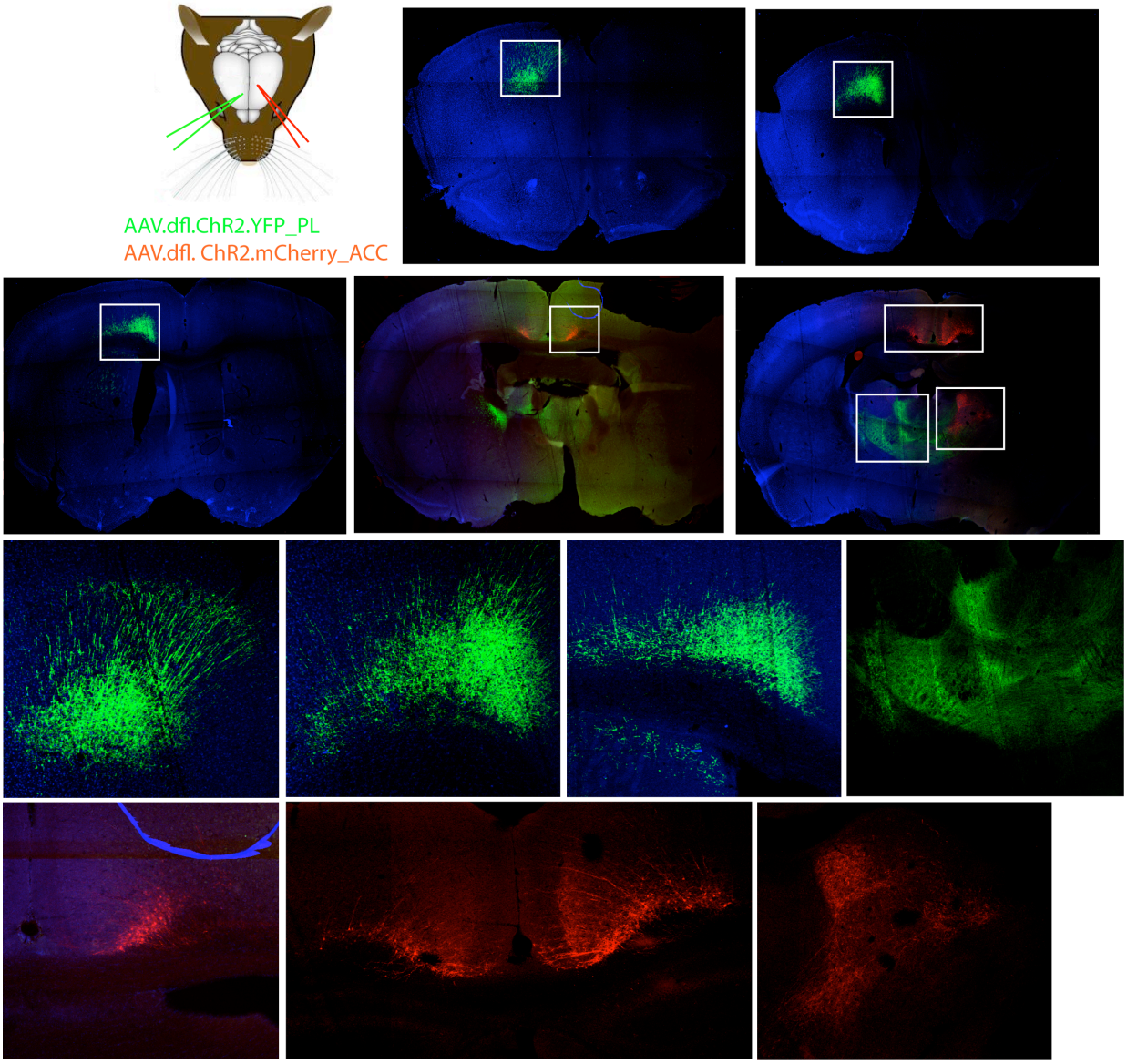

Figure 3.14: Circuit mapping of corticothalamic Syt6 Cell type. Anterograde viral tracers were stereotactically injected into prelimbic cortex (PL) and secondary motor cortex (M2) with AAV-dfl-ChR2-GFP (green) and AAV-dfl-ChR2-mCherry-dfl (red) respectively as shown in (a). Focal viral transduction of EGFP and mCherry revealed that Syt6 cell type in PL send their projections to posterior thalamic nucleus (Po) and ventrolateral thalamus in the ipsilateral hemisphere, whereas Syt6 cell type in M2 send projections both to the contralateral cortex layer 6 and ipsilateral posterior thalamic nucleus (Po).

CHAPTER 4: GENETIC ACCESS TO WFS1 CELL TYPE USING CRE TRANSGENIC MICE - MOLECULAR PROFILE, CIRCUIT TRACING AND LOCAL SILENCING

4.1 Genetic Access to Wfs1 Cell Type using Cre Transgenic Mice

The Cre/LoxP based binary expression strategy provides a premise to reproducibly access genetically defined cell type in the CNS. Reproducible access to the same cohort of cells is key in ensuring that the results from different functional manipulations are directly comparable. Genetic access has been defined as the ability to introduce into selected cells in the brain a genetically encoded molecule that, when expressed, can visualize, assay or perturb those neurons' development, connectivity or function (Dymecki and Kim, 2007). The Cre recombinase is a site-specific recombinase (SSR) that catalyzes recombination between specific DNA target sequences, namely loxP sites (Abremski et al., 1986; Hoess et al., 1986) that are otherwise absent in the mouse genome. Strategic placement of loxP sites into the mouse genome can be used to effectively engineer different predetermined modifications, including gene deletions, insertions, inversions or exchanges (Dymecki and Kim, 2007; Luo et al., 2008). The strength of BAC transgenesis to target genetically coherent cell types when combined with the Cre/LoxP binary expression strategy allows us to utilize the plethora of mouse responder resources in achieving specific cell type autonomous modulation (Heintz, 2001). In other words, there are already a host of cre-dependent responder line knock-ins that are designed mostly either to delete a gene or to express a reporter and/or modulator upon cre mediated recombination. These resources can be used effectively for cell type specific modulation via intersectional genetics using BAC transgenic mice that express Cre recombinase in genetically defined cell types (Gong et al., 2007; Madisen et al., 2010).

Wolframin (Wfs1) is a calcium sensor in the lumen of endoplasmic reticulum (ER) predicted to be important for calcium homeostasis in the ER (Luuk et al., 2008). The Wfs1 gene

(ID: 22393) is located in the minus strand of chromosome 5 and is flanked by the immediate neighboring genes Jakmip1 at 5' end and Ppp2r2c at 3' end. The *in situ* hybridization images in the Allen Brain Atlas database showed a strong expression of Wfs1 in Layer II cells in the neocortex with a notable gradient in the rostrocaudal (high rostral, low caudal) axis (Fig 4.1). Apart from the cortical expression, Wfs1 mRNA was also highly enriched in the Caudate Putamen, CA1 of hippocampus, Central Amygdala and Olfactory Bulb. This pattern of Wfs1 gene expression concurs with the literature as well as the Wfs1 EGFP BAC transgenic mice at the GENSAT database. The latter is further informative about the morphology of Wfs1 cell type in the neocortex – Wfs1 cell type is pyramidal and appears to define corticocortical projection neurons. The Wfs1 BAC RP23-405O19 was used for the generation of Wfs1-Cre ERT2 BAC transgenic mice by Allen Institute for Brain Science (Madisen et al., 2010). The exogenous transgene introduced into the BAC is a drug activatable Cre recombinase. Administration of tamoxifen, the drug homolog of estrogen hormone, leads to nuclear translocation of Cre from the cytoplasm, and thus makes Cre active in mediating recombination at the LoxP sites (Hayashi and McMahon, 2002). Tamoxifen Citrate can be incorporated in the rodent diet in order to induce Cre activation in a defined temporal window. Thus, the combination of BAC transgenesis, Cre/LoxP recombination and Tamoxifen inducibility of Cre allows a powerful approach to control cell-type specific transgene expression in a spatiotemporal manner.

Wfs1 Cre ERT2 BAC transgenic mice were mated with an EGFP-L10 knock-in line generated in the lab (Domingos, 2010 unpublished). The EGFP-L10 knock-in mice were created by knocking in the fusion construct carried by the targeting construct into the EF-1 alpha locus in mouse ES cells. EF-1 alpha is a ubiquitously expressed gene that encodes the alpha subunit of

the Elongation Factor 1 complex, which is responsible for the enzymatic delivery of aminoacyl tRNAs to the ribosome. The EGFP-L10 fusion construct is preceded by a floxed STOP codon that prevents the expression of the reporter in spite of being present in all tissues. Transgenic expression or viral transfer of Cre recombinase would excise the STOP codon and lead to expression of the EGFP-L10 reporter in cells expressing the active form of Cre. A two-week regimen of Tamoxifen enriched diet was sufficient to induce the activation of Cre in double transgenic Wfs1 CreER$^{T2+/-}$/ EGFPL10$^{+/-}$ mice. The transgenic mice used in the neuroanatomical analysis as well as TRAP studies were all maintained as trans-heterozygotes.

RESULTS:

4.2 Neuroanatomy and Translational Profile of the Wfs1 Cortical Cell Type in Wfs1 CreER$^{T2+/-}$/ EGFPL10$^{+/-}$ double transgenic mice

4.2.1 Neuroanatomy of Wfs1 Cre-ERT2/ EH-EGFPL10 double transgenic mice

The Wfs1-Tg2-CreERT2 founder line crossed with EF1a-EGFP-L10 produced the endogenous pattern of the transgene expression in Layer II cells of the neocortex, after Tamoxifen administration (Fig 4.2). The EGFP labeled pyramidal cells are present in the superficial layer II of neocortex with a high rostral low caudal gradient. Few scattered cells in the neocortex also express the reporter, which could be either from the ectopic expression related to site of integration or from low endogenous levels of expression in sparse cells in the middle layers. It is important to note that the regular Cre recombinase line when crossed with a

transgenic responder line would express the responder as soon as the gene promoters preceding Cre and the responder are induced during development. Once induced, Cre recombinase is inherited in all daughter cells of the progenitors, which is why the Cre lines are used for genetic fate mapping of cells. This could be a problem, however, for Cre transgenic lines driven by promoters that are active early during development in many progenitors but become selectively active or inactive in adulthood. If such genes were used as markers to target specific cell types based on adult brain expression pattern, then the resulting double transgenic Cre and responder line would lose the specificity of transgene expression. But the use of Cre-ERT2 circumvents this problem because the Cre is not active until Tamoxifen is administered to the mice and we control the temporal window precisely by introducing the drug only after the mice reach adult age (at least 6 weeks). The Cre expression in the Wfs1-Tg2-CreERT2/EF1a-EGFP-L10 is hence adult pattern of Wfs1 expression recapitulated in the transgenic mice. Besides the neocortex, the transgene is expressed in subcortical areas such as CEA (Central nucleus of Amygdala), CA1 (Hippocampus) and Arcuate nucleus of Hypothalamus.

We generated a rabbit polyclonal antibody to a custom synthesized peptide (CEPPRAPRPQADPSAG) of Wfs1. The antigen was purified to 90% by HPLC and coupled to a carrier before being injected to rabbits. The antibody titer from the rabbit blood was measured and later the effective concentration of the antibody for immunohistochemistry was determined empirically. The EGFP-L10 label and Wfs1 antibody staining coincided well for the most part in the Wfs1 Cre-ERT2/ EHGFP-L10 transgenic mice (Fig 4.2), although there appears to be some EGFP negative Wfs1 stained cells in the CNS. This could either be from the peptide being recognized by the antibody in non-Wfs1 positive cells such as the close family member Wfs2; or

it could be from the lack of Cre and/or cre induced EGFP expression in some of the Wfs1 positive cells. Overall, however, the double transgenic mouse serves as a good representation of Wfs1 promoter activity in the CNS and is thus useful for TRAP analysis of Wfs1 Cell Type in the neocortex.

4.2.2 Translational Profile of Cortical Wfs1 Cell Type: Wfs1 bacTRAP Analysis

For enrichment of transcripts autonomous to cortical Wfs1 Cell Type, we pooled together 6 cortices from 3 adult double-transgenic mice, which were gender balanced. We obtained an average RNA yield of 6.5 ng/ul from each biological replicate and subjected the purified RNA to two-cycle RNA amplification procedure. In the final step, the Biotin labeled cRNA was fragmented and applied to the Mouse Genome 430 2.0 Microarray chips for hybridization and subsequent scanning. Replicate Wfs1 IP samples gave nearly identical genome wide translational profiles (average Pearson correlation coeffficient of 0.93. Using the Genespring software, Wfs1 Cortex IP samples were then plotted against an average of the pooled whole cortex RNA (Fig 4.3). The Wfs1 probe (1448411_at) was enriched in the Wfs1 Cortex IP by a fold change (FC) of 4.053 compared to the whole cortex RNA. For the data quality assessment, known negative non-pyramidal cell markers were plotted on the Wfs1 IP vs Whole cortex graph (Fig 4.3). Most negative markers were not enriched or depleted in the Wfs1 Cortex IP except for two probesets – H2-Q1 (1418734_at) and Slc1a3 (1426341_at). Among the annotated pyramidal cell markers, the genes that were enriched in Wfs1 IP, besides the driver probe, are – Ntf3 (1434802_a_at) and Pdyn (1416266_at). This result agrees perfectly with our array results for both Ntf3 and Pdyn. It is noteworthy that certain pyramidal cell markers are depleted in Wfs1 Cortex IP such as S100a10 (14566642_x_at), Etv1 (14560684_at and 1422607_at), Zfp312

(1418790_at), Drd1a (14568051_at), Npnt (1452107_a_at) and Pdim1 (1416554_at). We next looked at the Top 1000 genes that were highly enriched in the Wfs1 Cortex IP and scored for specific or enriched expression in layer II of neocortex by consulting the digital ISH database at Allen Brain Atlas (ABA). Some of the Layer II enriched genes based on the ABA data include Penk1, Smoc2, Ntf3, Pdyn and low level enrichment (1 < FC < 2): Otof, AW125753, Kctd4 and Ptgs2. Among the ABA annotated Layer II genes that were depleted from Wfs1 Cortex IP were – Dusp18, Acvr1c, Pip5k1a, Pvrl3, Ddit4l, D8Ertd82e, Calb1, Pde7b, Kitl, Pdzrn3, Enpp2, Pak6 and Igsf11. These results indicate that within layer II, there are multiple cell types that express genes in a mutually exclusive manner.

4.2.3 Comparative Analysis of Three Cortical Layer II Cell Types: Wfs1, Ntf3 and Pdyn

We then compared the previous array results that we obtained for cortical IP of Pdyn CP12 and Ntf3 PS1046 with Wfs1 Tg2. Neuroanatomical studies indicated that the Wfs1 antibody staining overlapped with a subset of Ntf3 Cell Type in the medial and dorsal PFC but not in the ventral OFC. Even though we did not co-immunostain Pdyn CP12 brain sections with Wfs1 antibody, the restricted EGFP expression in ACC in Pdyn CP12 line suggests that there might be only partial overlap with the Wfs1 cortex IP data. We hence selected Top 1000 genes that were enriched in all three cortical IPs for Layer II pyramidal cells including Wfs1, Ntf3 and Pdyn, and then compared them to each other with a Venn diagram (Fig 4.4). We found that there were 24 probesets common among the three gene lists, 8 that were common between Wfs1 and Pdyn, 244 that were common between Pdyn and Ntf3, and 92 that were common between Ntf3 and Wfs1. By this comparison, it is evident that Wfs1 cell type shares more genes in common

with Ntf3 cell type but much less so with Pdyn cell type. Also, Pdyn cell type shares more genes with Ntf3 cell type than Wfs1. Still there are a lot of genes that are mutually exclusive and enriched only in a single cell type – such as 882 genes in Wfs1, 724 genes in Pdyn and 649 genes in Ntf3 cell types are uniquely expressed in the particular cell type.

For quantitative comparative analysis, we ran the SI algorithm on Wfs1, Ntf3 and Pdyn Cortex (Cx) IPs together with the negative cell types including Pnoc Cx, Lypd6 Cx (interneuron cell types) and Fthfd Cx and Olig2 Cx (glial cell types). The statistically significant ($p < 0.05$) genes in the Layer II cell types were then analyzed further for overrepresented GO ontologies and biological pathways. Some of the biologically and statistically significant genes are described in Figure 4.5. The overrepresented KEGG pathways (Fig 4.6) in Ntf3 cell type include MAPK signaling pathway (Bdnf, Cacnb2, Cacnb3, Cacng2, Mapk8ip1, Ntf3 and Prkcc), calcium signaling pathway (Camk2d, Itpka, Mylk, Prkcc and Grm1) and long-term potentiation (Camk2d, Prkcc and Grm1). Pdyn cell type has the following KEGG pathways overrepresented – calcium signaling pathway (Ptk2b, Adcy3, Cacna1a, Cacna1g, Cacna1h, Cckbr, Chrm1, Grin1, Itpr1, Pde1a, Plcb1, Plcb4 and Prkcc), long term depression (Cacna1a, Crhr1, Gria1, Itpr1, Plcb1, Plcb4 and Prkcc), long term potentiation (Gria1, Grin1, Itpr1, Plcb1, Plcb4 and Prkcc), axon guidance (Epha4, Ephb6, L1cam, Sema5b, Slit1, Slit3 and Unc5a), MAPK signaling pathway (Rasgrp1, Cacna1a, Cacna1g, Cacna1h, Cacna2d1, Cacn2d3, Cacng3, Mapk8ip3, Map4k2 and Prkcc), neuroactive ligand-receptor interaction (Cckbr, Chrm1, Crhr1, Gabrd, Gria1, Grin1, Grm2, Grm8 and Pth2r) and GnRH signaling pathway (Ptk2b, Adcy3, Itpr1, Plcb1 and Plcb4). Finally, the overrepresented KEGG pathways in Wfs1 cell type included just axon guidance (Cxcl12, Ppp3r1, Sema3a and Unc5c).

4.3 Circuit Mapping of Cortical Wfs1 Cell Type:

4.3.1 Anterograde Circuit Mapping of Cortical Wfs1 Cell Type with pAAV-double floxed-Reporter

Viral tools offer remarkable ability to probe into the local circuitry of neurons by transduction of either reporter and/or modulator genes. Mouse transgenesis offers efficient and reproducible access to genetic cohort of cells, however, even the most specific gene drivers are expressed by hundreds of cells in the neocortex, which in turn makes it difficult to target very local subset of neurons with a coherent function. Transduction vectors, like lentiviruses and adeno-associated viruses, have been shown to provide additional tools for localized and controlled genetic manipulation (Aronoff and Petersen, 2006). Viruses can be genetically engineered for tropism and transfer of genes of interest into a variety of cell types. Because of their multi-copy transfection of a single neuron and the use of strong and ubiquitous transcription promoters, viral mediated gene delivery can obtain high level gene expression and also bright labeling of fine structures such as neuronal synapses (Kuhlman and Huang, 2008). We have used the recombinant AAV viruses: pAAV-EF1a-double floxed ChR2 (E123A)-EYFP-WPRE and pAAV-EF1a-double floxed ChR2 (E123A)-mCherry-WPRE – mCherry to transduce reporter expression in a focal subset of Wfs1 Cell Type in the neocortex (Cardin et al., 2010). The Channelrhodopsin (ChR2) gene encodes a light gated ion channel that has become a major tool for achieving optical control of neuronal activity (Zhang et al., 2006). However, even though we have used the AAV virus carrying the ChR2 gene, we have only used the reporter

YFP or mCherry fused to ChR2 for tracing the circuitry. But it opens a possibility of optically activating a focal population of specific cell types to assess the effects on behavior and physiology of the cells. For cell type specific targeting by utilizing cre driver lines, we used the stringent version of cre-inducible ChR2-reporter that is flanked on either side with two dissimilar Lox sites, loxP and lox2722 (Lauth et al., 2002).

We carried out bilateral stereotaxic injections of the pAAV-ChR2-EYFP and pAAV-ChR2-mCherry into the Prelimbic Cortex (PL) and Anterior Cingulate Cortex (ACC) respectively. The bilateral injection of distinct fluorescent tracer in two different cortical areas alllowed us to compare directly if there were areal distinctions within the same genetically defined cell type in terms of sending long distance projections. The reporters EYFP and mCherry fill up the entire cell including the dendritic arbor, cell body and axons, so we can trace the circuit of the Wfs1 Cell Type in the anterograde direction (Fig 4.7). Additionally, empirical determination of optimal volume of the viral tracer combined with low diffusion and infectability of cells by the virus further from the injection site (200 um) helped us achieve a relatively sparse labeling of Wfs1 Cell Type in the PL and ACC cortices. The virally transduced genes have been shown to be stable for at least few months post delivery, and the recommended duration for cre-inducible viral transduction of genes is over 3 weeks. Hence, we returned the surgerized mice injected with the viral tracers back to the home cage for three weeks before we harvested the brain for neuroanatomical analysis. As shown in the figure, PL (Prelimbic Cortex) Wfs1 Cell Type send dual projections, first to Layer V in the ipsilateral cortex and also to layer V in the contralateral cortex after crossing the corpus callosum. Since there were several Wfs1 cells labeled with the EYFP reporter, it cannot be determined from current results whether axons

of the same population of Wfs1 cell type bifurcate and have one axonal branch project to the ipsilateral cortex and the other axonal branch to the contralateral cortex, or whether there are two subsets of Wfs1 cell type in the PL that project to the ipsilateral cortex and contralateral cortex mutually exclusively. In the case of ACC Wfs1 Cell Type labeled with mCherry, we found that mCherry labeled cells project to layer V within the ACC and also to the contralateral cortex upon crossing the corpus callosum. Surprisingly, a small subset of axonal fibers traverses to the dorsal striatum, which was not reported before.

4.3.2 Retrograde Transsynaptic Circuit Mapping of Cortical Wfs1 Cell Type with pseudorabies virus pPRV-ME185

The swine pathogen, pseudorabies virus (PRV), human pathogen, herpes simplex virus type 1 (HSV-1) and the rabies virus (RV) are the three transsynaptic viral strains used for defining circuitry of neurons in mouse CNS. Unlike most conventional chemical retrograde tracers such as Cholera Toxin B, the viral retrograde tracers reliably move from one neuron to another neuron via synapses, hence are the only true transsynaptic tracers. In particular, an attenuated form of PRV identified by Bartha (Bartha, 1961) has been applied extensively for transsynaptic definition of multisynaptic circuitry in a number of systems (Billig et al., 2000). The PRV-Bartha strain is transported exclusively in a retrograde transsynaptic fashion. The mechanisms responsible for the restriction of PRV to transport itself only across synapses are not fully understood. A possible contributor is that receptors for the rabies glycoprotein may be restricted to the presynaptic nerve terminals (Callaway, 2008). The recombinant PRV-ME185 that we used here for transsynaptic tracing was developed by Mats Ekstrand (2011 –

unpublished). The PRV is designed to be cre-inducible by constructing the viral vector with STOP codons flanked by LoxP sites that precede and follow the cassette of transgenes. The cassette includes the ORF of Thymidine Kinase (UL23), an essential gene for replication of PRV, Internal Ribosome Entry Site (IRES) promoter, and EGFP under the transcriptional regulation of IRES (Fig 4.8). Upon cre-mediated excision of STOP codons, the PRV can replicate and cross synapses and EGFP is expressed concurrently via transcriptional activity of IRES (Fig 4.8). Hence both PRV replication and EGFP expression are Cre dependent, which makes it possible to trace the circuitry of a focal population of strictly Wfs1 Cell Type in the neocortex.

We injected 500 nl of PRV-ME185 in the Anterior Cingulate Cortex of Wfs1 Tg2-Cre ERT2 mice (Coordinates: AP - 0.7 mm, ML -0.4 mm, DV +1.2 mm) unilaterally in the left hemisphere. After injection, the mice were returned to the home cage with ad libitum access to food and water for either 2 days or 5 days. PRV does not transport itself just monosynaptically but continues to cross synapses almost indefinitely, so with two different temporal windows, we might be able to stop the PRV from transporting itself at first order synapse and a higher order synapse. The temporal window for stopping PRV after first order synapse needs to be empirically determined since it depends on factors such as the titer of the virus, the infectability of the neurons, length of the axonal projection and most importantly the strength of synapses. It has been shown that tracing viruses and trans-synaptic tracers more generally cross stronger, more densely innervating connections faster than weaker and sparser ones (Wickersham et al.). We determined that the time length of 2 days was just enough for the PRV to cross first order synapse as the EGFP label was observed only in layer II/III and layer V of the contralateral

anterior cingulate cortex in the right hemisphere (Fig 4.8). Higher magnification revealed the retrogradely synaptically connected cells were pyramidal in morphology with apical dendrites (Fig 4.8). On the other hand, harvesting the tissue at the time point of 5 days revealed that there were many more neurons in other parts of the brain besides the focal population of contralateral cortex seen in Day 2. EGFP labeled cells were present in Layer V of lateral orbital cortex, Layer II/ III of contralateral infralimbic cortex, and layer II/ V of dorsal Prelimbic Cortex. Subcortically, there were sparse cells labeled in the basolateral amygdala (BLA) and hypothalamus (Fig 4.8), which together indicate that the Wfs1 cells in the ACC receive synaptic input several orders away from other pyramidal cells in the superficial and middle layers in the cortex and from neurons in the BLA and hypothalamus. Even though we can infer from the restricted pattern of expression of EGFP labeled neurons in the contralateral ACC on Day 2, we do not have definitive evidence on whether these neurons are a single or multiple synapses across from the Wfs1 cell type. And likewise, we cannot ascertain in the second experiment of Day 5, how many further synapses the EGFP labeled neurons in different CNS areas are from the Wfs1 cell type? Existing methods do not have the capability to address the second question, but to figure out the immediate first order synaptic partner of Wfs1 cell type, we can use the monosynaptic G-deleted rabies based viral tracer developed by Callaway and colleagues (unpublished, 2011) – the G-deleted virus is a replication deficient vector that will not spread beyond the initially infected neurons, unless the glycoprotein is supplied within them by the helper virus.

4.5 Localized Silencing of Wfs1 Cell Type in ACC with Viral Mediated Transfer of Tethered Toxins

4.5.1 Structure and Function of Anterior Cingulate Cortex

The Anterior Cingulate Cortex (ACC) is the dorsomedial region in the frontal cortex that forms the rostral end of the cingulate. While the ACC is involved in emotion and motor function, the posterior cingulate also known as retrospenial cortex s involve in visuospatial and memory function. The ACC constitutes two components that subserve affect and cognition. In human patients, elevated activity in the anterior cingulate cortex may contribute to tics, obsessive compulsive behaviors and aberrant social behavior (Devinsky et al., 1995). The cingulate epilepsy syndrome gave further insight into the role of the ACC in movement, affect and social behaviors. In other words, seizures in ACC lead to impairment of consciousness, affective state, and skeletomotor and autonomic activity (Devinsky et al., 1995). Among the two functional components of ACC – affect and cognition – the affect division modulates autonomic activity and emotional responses where as the cognitive division is involved in response selection associated with motor activity i.e. motor sequencing of behavior, motivation and responses to noxious stimuli. Human Positron Emission Tomography studies have shown that the ACC is activated during the application of acute noxious stimuli to the body surface (Casey et al., 1994; Jones et al., 1991; Talbot et al., 1991). Further human studies involving electroencephalogram, PET and fMRI have implicated the ACC in both normal and dysfunctional emotional self-control as well as tasks requiring executive control and evaluation of both stimuli and behavioral response.

ACC receives and sends projections to different motor and sensory areas of the brain. ACC is known to receive sensory input from the somatosensory cortices and other cortical areas, including the anterior insular cortex (Jeon 2010). Human studies have shown that during observation of other people experiencing fear or facially expressing fear, neuronal activities are altered both in ACC and amygdala. In addition, animal studies have shown that the ACC is involved both in pain sensation and pain affection of emotional behavior. A recent study in mice showed that observational fear learning was substantially impaired following inactivation of the ACC and parafascicular or mediodorsal thalamic nuclei, both of which are components of medial pain system representing pain affection. However, inactivation of the sensory thalamic nuclei had no effect (Jeon et al., 2010). Thus, prior literature indicates that ACC has an important role in regulation of emotional behavior in response to pain.

4.5.2 Anterior Cingulate Cortex and Affective Pain

According to the International Association for the Study of Pain (IASP), pain is defined as 'an unpleasant sensory and emotional experience associated with actual or potential tissue damage, or described in terms of such damage'. Pain has a dual role of being a key physiological function and a debilitating disease. Charles Darwin described pain as a 'homeostatic emotion', which is essential for the survival of species (Kuner, 2010). Physiological pain has a protective nature designed to warn an animal of danger from potential tissue damage. Acute pain serves as a warning mechanism and while it is caused upon injury to a specific site, it is completely abolished upon healing. On the other hand, chronic pain can persist long after the initial injury is healed and can arise even in the absence of any obvious pathological trigger. This form of pathological pain is manifested in conditions such as

inflammation, neuropathy, cancer, viral infections, chemotherapy and diabetes (Kuner, 2010). Additionally, individuals with chronic pain often show disease-induced, therapy-resistant deviations from normal tactile sensation, such as paraetheisias and dysethesias. In animals, the counterpart of these changes is referred to as tactile allodynia, which represents withdrawal behavior in response to innocuous stimuli (Eto et al.). People with chronic pathological pain syndromes such as phantom pain, chronic back pain, irritable bowel syndrome, fibromyalgia and headaches have been reported to have local morphological changes in the brain, mainly a decrease in the gray matter (Wang and Shyu, 2004). This decrease in brain gray matter is at least partially reversed when the pain is successfully treated, suggesting that the structural changes are a consequence of nociceptive inputs.

Nociception is defined as the set of mechanisms encompassing the triggering, sensing, transmitting and central perception of painful impulses (Sturzebecher et al.). Mammals possess the nociceptors, which are specialized sensory neurons, at free nerve endings in the periphery including skin, muscles and viscera. The nociceptors respond to different classes of noxious stimuli such as temperature, pressure and acids. The noxious stimuli of various modalities are sensed by a specialized set of nerve fibers: unmyelinated C fibers and thinly myelinated A-delta fibers, which are distinct from myelinated tactile sensors and proprioceptors (Fig 4.9). The physiochemical properties of noxious stimuli are converted in the sensory neurons to electrical activity by transient receptor potential channels (TRP) and purinergic channels, and this electrical activity is amplified by sodium channels to generate action potentials. These sensory neurons have their cell bodies located at the dorsal ganglion (DRG) which then send the axons to the dorsal horn of spinal cord within lamina I, II and V (Braz et al., 2005). The sensory inputs

are integrated and processed to some degree at the spinal cord whence they are carried by several pathways to distinct projection sites in the brain (Fig 4.9). From there on, the second order neurons constitute mainly two central pain pathways -1. Pain Sensation, and 2. Pain Perception or Affection (Kuner, 2010; Sturzebecher et al.). The pain sensation pathway involves the lateral spinothalamic tract (LST). The first order neuons in the DRG make synaptic connections with Rexed Layer I neurons in spinal cord and axons from these second order neurons decussate at the anterior white commissure and ascend in the contralateral anterolateral quadrant. Most of the pain fibers in this pathway terminate in the sensory thalamus in ventroposterolateral (VPL) nucleus and ventroposteromedial (VPM) nucleus of thalamus, which serves as a relay station that sends afferents to the primary somatosensory cortex (Fig 4.9). This LST tract is important for encoding the stimulus parameters and processing of the sensory and discriminative aspects of pain. By contrast, the second pathway, which is the pain perception of affection, involves the medial spinothalamic tract and medial spinoparabrachial tract (MST). The MST tract sensory neurons make synaptic contact to Rexed layer II neurons in the spinal cord and these second order neurons make synaptic connections in layer IV-VIII. Most of their axons cross and ascend in the spinal cord mainly in the anterior region and project to few different areas in the brain including reticular formation in the periaqueductal gray (PAG), tectum and intralaminar nucleus (PF-CM complex) in the thalamus (Devinsky et al., 1995). The innervation of this tract is bilateral because some of the fibers do not cross the opposite side of the cord. From the intralaminar nucleus, the thalamocortical relay neurons send their projections to the anterior cingulate cortex (ACC) and somatosensory cortex. This pathway is implicated in encoding the affect of pain, that is, the emotional and aversive component of pain.

Prior studies have reported that the pyramidal cells in the ACC are responsive to application of peripheral noxious stimuli. Koga et al (Koga et al.) presented the first evidence using in vivo whole cell patch-clamp recording that the noxious stimuli induces evoked spike responses in Layer II/III pyramidal neurons of mouse ACC in all three types of cells: regular spiking, intermediate and intrinsic bursting cells. These results concur with previous in vitro studies electrophysiological studies of ACC in cortical slices. Xu et al (Xu et al., 2008) showed that within ACC, pyramidal cells in Layer II/III and not deeper layers showed increased synaptic transmission in response to peripheral injury. They showed that peripheral L5 sciatic nerve ligation, a neuropathic pain model, triggers long-term changes in excitatory synaptic transmission in the superficial layer cells. The presynaptic release probability of glutamate and postsynaptic glutamate AMPA receptor-mediated responses were enhanced after injury, in addition to the upregulation of phosphorylated metabotropic glutamate receptor mGluR1 in the ACC. Pyramidal cells in ACC send their long range axonal projections to subcortical limbic regions such as the amygdala, ventral striatum and hypothalamus (Johansen et al., 2001). Jeon et al (Jeon et al., 2010) showed that the ACC and amygdala are functionally connected by comparing the local field potentials in the ACC and lateral amygdala simultaneously in mice subjected to observational fear learning. Colored power spectra analysis revealed that the moderate and dispersed neuronal activities in the ACC and lateral amygdala during habituation became intense and synchronized at theta frequency during observational fear learning, which is a conditioning paradigm attributed to the role of ACC in regulating emotional responses.

4.5.3 Cell autonomous blockade of neurotransmission with Tethered Toxins

Functional perturbation of cell types can give us valuable information on the contribution of these cells to the neuronal circuitry and overall organismal behavior. Knock out strategies and RNA interference are designed to delete or knock down a single gene and its product so as to analyze the phenotypic effects of loss of function of the particular gene in question. However, here we were more interested in the role of the ACC Wfs1 cells in the context of the affective pain circuitry. Different methods have been applied to achieve functional silencing of cells in the CNS. Traditionally, target regions in the cortex were surgically removed by laser ablation or microinfusion of cytotoxic reagents. Selective neuronal death has been carried out with targeted delivery of Chromophore Chlorin e6 (Worgotter et al., 2002), Diptheria Toxin A (DT-A) (Buch et al., 2005), Herpes Simplex Virus 1 Thymidine Kinase (HSV1-TK) and nucleoside analogs (Borrelli et al., 1988). For inducible cell silencing, there have been different strategies, such as Molecules for Inactivation of Synaptic Transmission (MIST) (Karpova et al., 2005), Allatostatin Receptor (Tan et al., 2006), optically activated ion pump Halrhodopsin NpHR (Zhang et al., 2008) and ion channel specific Tethered Toxins (Ibanez-Tallon et al., 2004). We have collaborated with Ibanez Talon and her team to obtain cell autonomous silencing of Wfs1 cell type in the ACC.

Tethered toxins are fundamentally based on the selectivity of venomous toxins found in nature that target specific ion channels in mammalian cells. In particular, ω-conotoxin MVIIA binds to $Ca_v2.2$ channels and effectively blocks N-type currents, and ω-agatoxin IVA inhibits P/Q type currents by interacting with $Ca_v2.1$ channels. These two channels $Ca_v2.2$ and $Ca_v2.1$ are the major voltage gated calcium channels in neurons and are responsible for driving the

presynaptic neurotransmitter release in response to neuronal depolarization (Auer et al.). The soluble toxins bind to the respective ion channels in all cells indiscriminately and also exhaust over a short period of time. Ibanez-Talon and her colleagues (Auer et al.) developed an innovative strategy of tailoring the membrane tether to the toxin(s) and attaching a fluorescent reporter on the cytoplasmic tail of the toxin. The recombinant membrane tethered toxin approach allows the cell-autonomous expression and inhibitory action of the toxins. Additionally the fusion of fluorescent reporter allows monitoring of the cellular expression as well as the subcellular localization of the tethered toxins within the cells. To confer cell type specificity, cre-dependent tethered toxins were constructed and packaged into adeno-associated viruses (AAV2).

RESULTS:

4.5.4 Focal silencing of Wfs1 Cell Type in ACC using Cre-dependent Tethered Toxins

We used three optimized t-toxins that were incorporated into the AAVs: MVIIA-PE, AgaIV-PE and the control no toxin-PE. In order to maximize neuronal silencing by blockade of both kinds of VGCCs, equimolar suspension of AAV-dfl-MVIIA-PC-mCherry and AAV-dfl-Aga-PC-EGFP was injected bilaterally into the ACC (Coordinates: AP -0.7 mm, ML -0.4 mm, DV +1.2 mm) of Wfs1-Tg2-Cre-ERT2 mice(Fig 4.10). These tethered toxins were previously tested for blockade of the calcium currents in hippocampal cultures as well as *in vivo* (Auer et al.). Prior to the injection, Wfs1 Cre ERT2 mice were fed with Tamoxifen diet for 2 weeks after weaning to induce the activation of Cre. Three weeks after the injection, we assessed the efficiency of the viral transduction of the toxins by confocal imaging of the brain tissue. We

detected bright green fluorescence associated with Agatoxin and bright red fluorescence associated with MVIIA in the neurons of ACC that underwent Cre mediated recombination (Fig 4.10). The EGFP fluorescence is brighter than the mCherry fluorescence in these mice, possibly because of the enhanced fluorophore, and hence more pyramidal cells especially in the medial ACC seem to express EGFP than mCherry. However, since the viral strain and titer were comparable and the viral suspension had a 1:1 ratio of MVIIA to Agatoxin, the difference in fluorescence seen with MVIIA (red) might suggest a lower rate of diffusion from the site of injection and/or the reduced brightness of mCherry compared to EGFP in the medial region of ACC. However, the mCherry positive cells completely overlap with EGFP positive cells, suggesting that the focal population of ACC Wfs1 pyramidal cells express both the MVIIA and AgaIV toxins effective against the P type and N type Voltage Gated Calcium Channels.

4.5.5 Behavioral assays for ACC Wfs1 Silenced Mice (SIACC.Wfs1)

The SIACC Wfs1 transgenic mice together that were injected with MVIIA and AgaIV in the ACC were subjected to behavioral tests for spontaneous locomotion and anxiety. A cohort of control Wfs1 transgenic mice injected with empty vector was also subjected to the same behavioral measures as a control. Following these experiments, the test subjects were then assessed for acute physiological pain in response to thermal and mechanical stimuli. And finally, the mice were tested for affective pain using the formalin induced conditioned place aversion paradigm.

4.5.6 Overt appearance and Body Weight

Analysis of *ad libitum* body weight of Tamoxifen treated transgenic mice compared with the regular diet fed mice indicated that the drug slightly decreased the body weight by ~5% (Tamoxifen+ Mice: average 22 g vs. No Tam Mice: average 24 g). Hence, a regimen was followed whereupon the Wfs1 Cre ERT2 mice were continually administered Tamoxifen Citrate in the diet, with *ad libitum access,* starting at the weaning age (21 days) for two weeks. Mice were then weaned to regular diet, which led to normal body weight within a week. The intracranial stereotactic injections of AAV2-MVIIA-PC and AAV2-AgaIV-PC were carried out after the mice were 6 weeks old and the mice were allowed to recover with free access to food and water for the next 3 weeks. So, after the mice were 4 weeks old, there was no overt difference in the appearance and body weight of the Wfs1 Cre ERT2 mice.

4.5.7 Spontaneous locomotor activity in Open Field Boxes

Locomotor activity of SIACC WFS1 and PE WFS1 control mice were compared in a semi brightly lit (~400 lx) room (Fig 4.11) using open field arena for 60 min. Two way repeated measures ANOVA revealed that there was no genotype based difference between SIACC WFS1 mice and control mice in their activity over 60 min for all the locomotion parameters including horizontal activity: $F(6,13) = 0.126$, $p = 0.876$; vertical activity: $F(6,13) = 0.908$, $p = 0.340$ and total distance: $F(6,13) = 0.469$, $p = 0.507$. There was a time related decrease in horizontal activity as well as total distance over the 60 min block with measurements made in 10 min bins. Both SIACC WFS1 and control mice had acclimation manifested as reduced activity over time in terms of their horizontal activity: $F(6,13) = 48.94$, $p < 0.0001$ and total distance: $F(6,13) =$

48.73, $p < 0.0001$. Even the vertical activity or rearing behavior for both groups alters with time: $F(6,13) = 9.926$, $p < 0.0001$. When assessed for anxiety by looking at the distance travelled in the center with respect to distance travelled in the periphery, also known as thigmotaxis, the mice did not have a significant difference based on genotype: $F(6,13) = 2.837$, $p = 0.118$, but exhibited a significant increase in thigmotaxis with time: $F(6,13) = 7.765$, $p < 0.0001$. These results indicate that focal silencing of the Wfs1 cell type in ACC did not affect locomotor behavior and anxiety in the mice.

4.5.8 Acute Physiological Pain in SIACC WFS1 mice in response to Noxious Thermal and Mechanical Stimuli

Subsequent to the tests for locomotor activity, the SIACC Wfs1 mice and the controls were tested for sensitivity to acute physiological pain. Nociceptors in the periphery express a wide variety of molecular markers including ion channels and receptors. Depending on whether they express a receptor for plant isolectin, they are classified as either peptidergic (IB4+) or nonpeptidergic (IB4-) nociceptors. IB4+ nociceptor neurons are further identified by molecular markers GDNF and the receptor Ret, whereas the IB4- nociceptors are defined by NGF and its receptor TrkA. It has been established that IB4+ nociceptors play an important role for transmission of mechanical and neuropathic pain (Braz et al., 2005). On the other hand, IB4- nociceptors are critical for thermal pain transmission (Marmigere and Ernfors, 2007; Stucky and Lewin, 1999). So at the level of first order neurons itself, the neural transmission of thermal and mechanical noxious stimuli are demarcated.

We used two independent tests to measure sensitivity to acute thermal and acute mechanical pain. The first was Plantar Test for thermal pain, which involves an Infra-red (IR) beam emitter connected to an automated module. The IR intensity was set at 50 and using the emitter, the IR beam was directed to center of the hindpaw of each experimental animal and the latency to the paw withdrawal in response to the noxious heat stimulus was recorded by the module. This procedure was repeated for the left and right hindpaw of the mice for a total of 5 times. We found that the SIACC Wfs1 mice and control mice had equivalent threshold for thermal pain (Fig 4.12). Their left and right paws had similar thermal pain thresholds with the following means - SIACC: 6.629±0.369 s for left paw and 7.171±0.584 s for right paw; Control: 7.071±0.560 s for left paw and 6.229±0.385 s for right paw respectively. There were no statistically significant differences between the mice both by toxin administration: $F(6,13) = 0.266$, $p = 0.611$ and by paw laterality (right vs left paw): $F(6,13) = 0.095$, $p = 0.760$.

We then tested the mice for latency to paw withdrawal upon the application of acute mechanical stimulus. We used the Plantar Aesthesiometer Test for this purpose, which consists of an actuator component with a Von Frey like filament adjusted to be lifted with a defined gradient of force. The actuator is connected to a module that allows assignment of the maximum force and gradient with which the filament is to be lifted to impinge on the hindpaw of the mice. The force of the filament increases at 1 g/s until the maximum value, which was set at 20 g, or when the mouse lifts the hindpaw off the filament. The mean paw withdrawal latency for SIACC WFS1 was 5.143±0.131 s for left paw and 5.471±0.190 s for right paw; and for control group it was 4.871±0.231 s and 5.014±0.283 s for left and right paws respectively. We found that there was no significant difference between the two groups of mice (SIACC WFS1 and control) in

paw withdrawal latency: F (6,13) = 1.191, p = 0.105. Also, there was no significant different in pain threshold for either left or right paw: F (6,13) = 0.185, p = 0.286. Similarly, measurements of a related parameter, mechanical force, revealed that the force of paw withdrawal was equivalent for both SIACC WFS1 and control mice: F (6,13) = 1.435, p = 0.243. The mean force of paw withdrawal for SIACC WFS1 mice was 5.457±0.138 g for left paw and 5.786±0.192 g for right paw, whereas for the control group it was 5.100±0.253 g for left paw and 5.629±0.254 g for right paw.

4.5.9 Affective response to Inflammatory Pain: Formalin induced Conditioned Place Aversion

Dubuisson and Dennis (Dubuisson and Dennis, 1977) first introduced the use of formalin to generate nociception in the hindpaw. Intraplantar injection of formalin into the hindpaw of rodent elicits a biphasic pattern of pain behavior: an early short lasting neurogenic phase, which has been attributed to a direct activation of the C-fiber nociceptors followed by a second and more sustained inflammatory phase, generally associated with local release of inflammatory mediators. The first phase lasts for approximately 5 min immediately after injection, whereas the second phase usually begins around 15 min and terminates within 1 hour. Formalin was combined with the conditioned place aversion paradigm (CPA) for the first time by Johansen (Johansen et al., 2001), whereupon they showed that the neural substrates underlying the affective-motivational component of pain can be dissociated from the neural substrates encoding other features of sensory experience such as the spatial parameters and intensity of the noxious stimulus. Their approach to investigate the circuitry of affective pain involved modification of the Pavlovian conditioning paradigm. As a sensory cue, formalin was used to inflict inflammatory pain in the hindpaw, followed by quick placement of the rodent in the

conditioning chamber. The rodent associates the context of the chamber, which is distinctive, with the inflicted pain and thus develops an aversion to the pain-associated context, referred to as CPA. We have employed the same strategy in SIACC WFS1 and control group of mice. Johansen (2001) used rat as an experimental organism, so this is the first time for applying the formalin-CPA model to assess affective pain in mice.

As described earlier, we subjected both SIACC WFS1 and control mice to formalin-CPA. Our protocol for this task involved two days of habituation in the CPA boxes, a third day of Saline conditioning, a fourth day of Formalin conditioning and on the last day, the mice are allowed unrestricted access to both chambers in the CPA box and their aversion to the Formalin conditioned chamber is assessed. For either Saline or Formalin conditioning, the agent was injected into the intraplantar surface of the hindpaw and immediately after, the mice were confined to a contextual chamber in the CPA box, which was either a black or a white box with different kinds of floor and walls. Our pilot experiments with different dosages of Formalin led us to settle on 3% Formalin as the nociceptive stimulus since it elicited detectable inflammation (swelling and redness) of the hindpaw, pain response behavior (flicking and licking of paw) and also was sufficient to elicit CPA to the formalin paired context. A higher concentration of formalin (5%) produced long lasting inflammation (over a month) and gradually led to necrosis of individual toes from the paw, which was avoided with 3% formalin (Data not shown). At the same time, 3% formalin was salient enough to elicit CPA with just a single injection-paired session. The conditioning sessions were 1 hour long in order to allow completion of the biphasic response to formalin within the same context, so as to strengthen the association. The bias

against the formalin-paired context on the post-conditioning day was corrected for nonspecific pre-conditioning bias towards either chamber.

Our results are presented in the graph (Fig 4.12) where we plotted the net bias (post-conditioning minus pre-conditioning bias) against the paired agents and tethered toxin groups. We show that the control mice (N = 7) that were intracranially administered with empty PE vector developed a strong aversion to formalin and spent significantly more time in the saline-paired context after conditioning. The mean net time spent in the saline paired context for control group was 91.98±49.36 s and for SIACC WFS1 group it was 11.26±57.39 s. On the other hand the mean net time spent in the formalin paired context for control group was -149.0±35.12 s and for SIACC WFS1 group it was -5.064±15.20 s. The difference of time that was not spent in either the saline paired or formalin-paired context was spent in the grey passage between the two chambers. It is possible that since saline is also injected into the hindpaw without anesthesia, the mice associate saline-paired context to be also aversive, although the aversion to formalin paired context would be more salient. The unpaired two tailed T-test for net bias for saline context showed no significant difference between the two groups (SIACC WFS1 and control) owing to the wide variability ($p = 0.336$, $df = 7$). The same T-test for net bias against formalin context showed highly significant difference between the two groups ($p = 0.0047$, $df = 7$). These results indicate that focal silencing of Layer II Wfs1 cell type in the ACC leads to a significant reduction in affective pain, as inferred from reduced contextual aversion to the noxious stimuli.

One might argue that silencing of Wfs1 Cell Type in ACC produced a deficit in contextual memory and that the subjects were not able to make the contextual association. If this were the case, mice should not have a bias for saline or against formalin paired contexts, but in our experiments, mice chose to spend more time either in the saline-paired context or the grey passage between the two contexts. The second argument could be that the SIACC WFS1 mice are deficient in Formalin-CPA but the aversive effect may be aversion to an external agent rather than to a nociceptive stimulus. This is a less likely explanation, since formalin has been established as a salient inflammatory agent that causes painful responses in the mice and activates specific nociceptors in the hindpaw. Although we cannot directly confirm that the amygdalar connections to the Wfs1 Cell Type might be responsible for producing affective pain, we can infer from our retrograde circuit mapping studies using PRV that the Wfs1 Cells in ACC receive synaptic input from the basolateral amygdala even though the synapse might be multi-order. In addition, besides amygdala, the Wfs1 cell type also receives synaptic input from neurons in the hypothalamus, which are also implicated in affective pain.

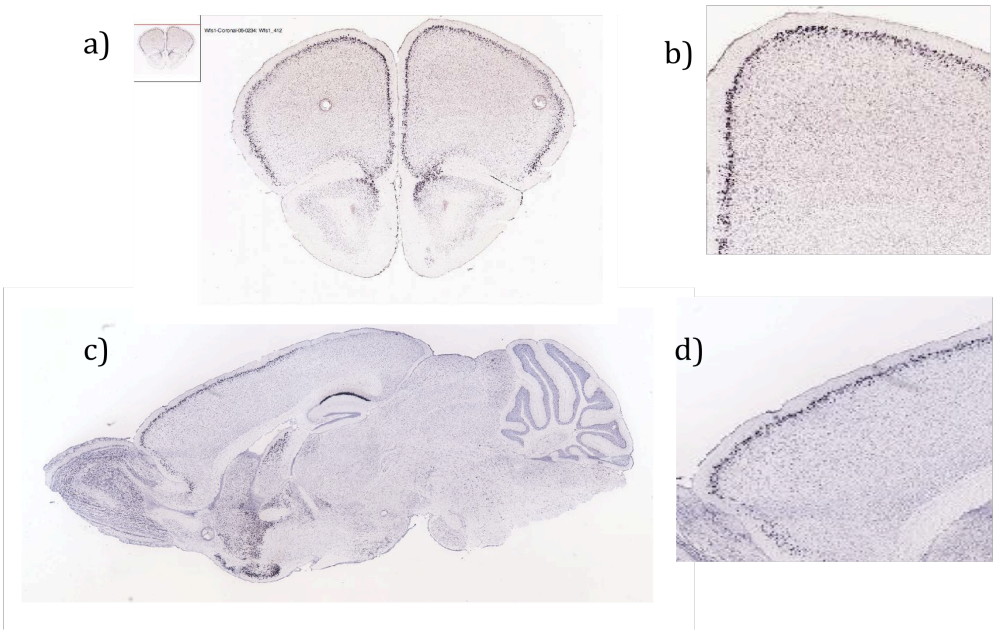

Figure 4.1: Expression pattern of Wolframin (Wfs1) in the mouse brain. Digital *in situ* hybridization data in Allen Brain Atlas (ABA) reveals enrichment of Wfs1 RNA in layer 2 of PFC in coronal section (a; enlarged inset: b). Sagittal ISH section shows high rostral low caudal gradient of Wfs1 expression in neocortex as well as subcortical expression in ventral striatum and CA1 (c; enlarged inset: d)

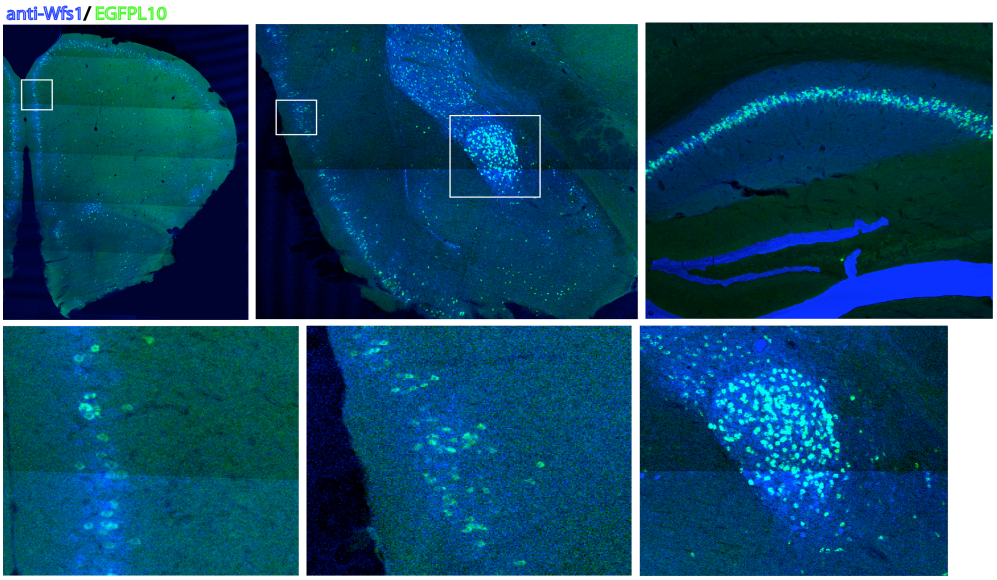

Figure 4.2: IHC of conditional TRAP line Wfs1 Tg2 CreERT2XEF1a-EGFPL10. EGFP/ Wfs1 co- immunostaining reveal complete colocalization of EGFP (green) with Wfs1 (blue), indicating targeting of the endogenous Wfs1 population(a- f). Strong EGFP/Wfs1 staining is detected in the layer 2 of PFC (a; enlarged inset:d), auditory cortex (A1: b, enlarged inset: e), central extended amygdala (CEA: b, enlarged inset: f) and CA1 of hippocampus (c).

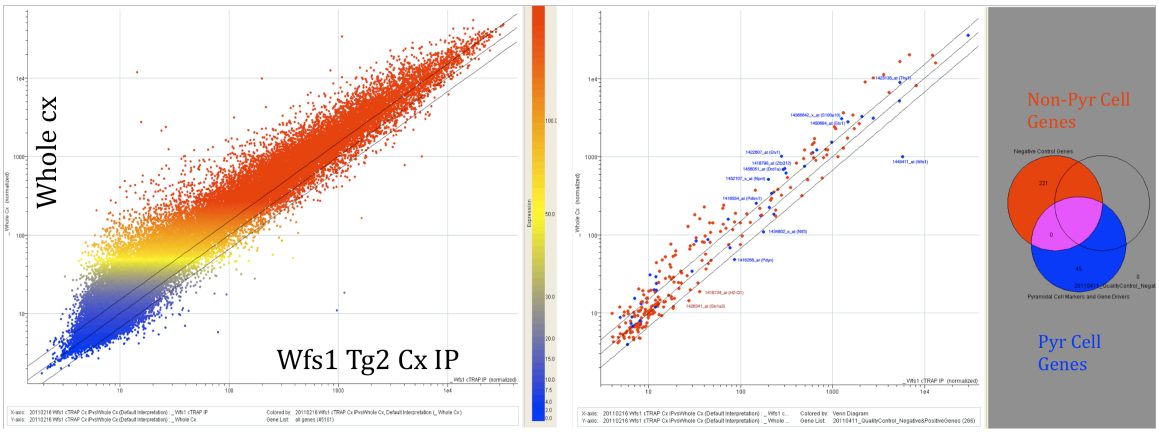

Figure 4.3: Translation profile of Wolframin Wfs1 Tg2 cortex cell type. Fluorescence signals of all 40,000 probesests for Wfs1 Tg2 cortex IP replicates were averaged and plotted against total cortex input (whole cx) in an X-Y scatterplot (a). Pyramidal cell marker probesets (in blue) were examined for their distribution in the scatterplot together with non-pyramidal cell type marker genes (in red) (b).

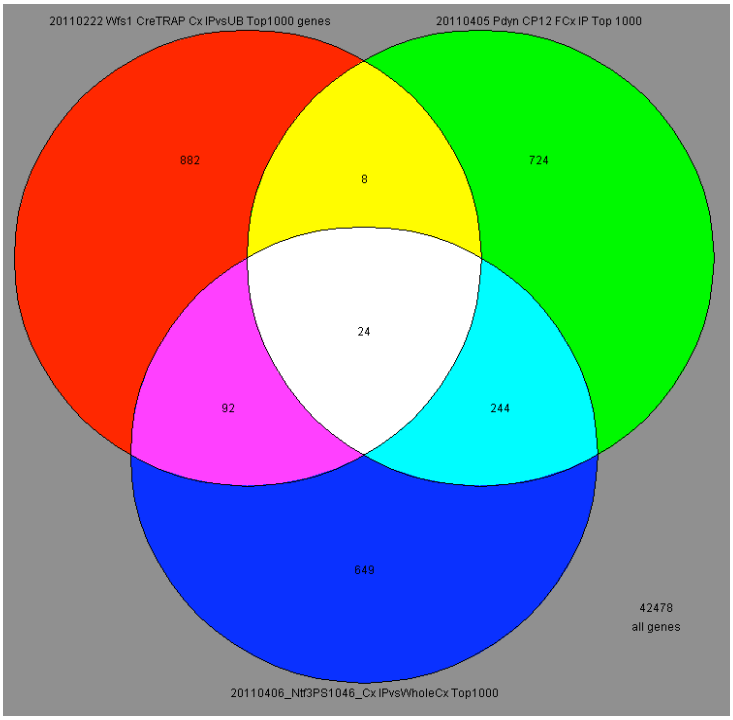

Figure 4.4: Venn Diagram comparing layer 2 cortical pyramidal cell types: Wfs1, Pdyn and Ntf3. Top 1000 most highly enriched genes in cortex IP (vs whole cx) of Wfs1 Tg2, Pdyn CP12 and Ntf3 PS1046 were compared to each other. There were 24 genes common among the three lists, 8 genes common between Wfs1 and Pdyn lists, 92 genes common between Wfs1 and Ntf3 lists and 244 genes common between Pdyn and Ntf3 lists. The number of exclusive genes present in the genelists were: 882 genes (Wfs1 Tg2), 649 genes (Ntf3 PS1046) and 724 genes (Pdyn CP12).

Top enriched genes in Wfs1 Tg2 cortex

Affymetrix Probeset ID	Fold Change	Common	Description
1421244_at	15.31	Esr1	estrogen receptor 1 (alpha)
1426313_at	4.791	Bre	brain and reproductive organ-expressed protein
1448411_at	4.053	Wfs1	Wolfram syndrome 1 homolog (human)
1427038_at	4.019	Penk1	preproenkephalin 1
1422860_at	3.725	Nts	neurotensin
1425833_a_at	3.689	Hpca	hippocalcin
1423653_at	3.184	Atp1a1	ATPase, Na+/K+ transporting, alpha 1 polypeptide
1453928_a_at	3.069	Ssb	Sjogren syndrome antigen B
1422948_s_at	3.064	Hist1h4h	histone 1, H3a
1447647_at	3.04	Wnt7a	wingless-related MMTV integration site 7A
1434525_at	2.58	Pkn3	zinc finger, DHHC domain containing 12
1422531_at	2.571	Syt5	troponin T1, skeletal, slow
1435626_a_at	2.39	Herpud1	homocysteine-inducible, endoplasmic reticulum stress-inducible, ubiquiti
1434802_s_at	2.388	Ntf3	neurotrophin 3
1422459_a_at	2.116	Psmd13	proteasome (prosome, macropain) 26S subunit, non-ATPase, 13
1431295_a_at	2.108	Stx18	syntaxin 18
1427548_a_at	2.102	Clns1a	chloride channel, nucleotide-sensitive, 1A
1417388_at	2.09	Bex2	brain expressed X-linked 2
1415998_at	2.084	Vdac1	voltage-dependent anion channel 1
1451822_a_at	2.08	Scrn2	secernin 2
1423152_at	2.033	Vapb	vesicle-associated membrane protein, associated protein B and C
1441906_x_at	2.03	Syap1	synapse associated protein 1
1423566_a_at	2.021	Hsp105	heat shock protein 105
1456934_at	2.013	Calb1	calbindin-28K
1435788_at	1.973	2900086B20Rik	Adult male hippocampus cDNA, RIKEN full-length enriched library, clone:2
1422520_at	1.969	Nef3	neurofilament 3, medium
1422522_at	1.911	Fxr2h	fragile X mental retardation gene 2, autosomal homolog
1420772_a_at	1.904	Dsip1	delta sleep inducing peptide, immunoreactor

Figure 4.5: Top enriched genes for Wfs1 cell type in neocortex. Cortex TRAP data for Wfs1 Tg2 line was compared against the whole cortex RNA data in Genespring 7.2 and with a threshold of >50 on expression level, top 1000 genes enriched in the Wfs1 IP were enlisted. Selected genes from this list are shown.

KEGG Pathway Analysis for Ntf3 layer 2 cell type

Term	Count	%	P value	Benjamini FDI	Genes
MAPK signaling pathway	7	4	8.30E-03	9.60E-02	Bdnf, Cacnb2, Cacnb3, Cacng2, Mapk8ip1, Ntf3, Prkcc
Calcium signaling pathway	5	2.9	3.90E-02	2.40E-01	Camk2d, Itpka, Mylk, Prkcc, Grm1
Long term potentiation	3	1.7	8.10E-02	4.00E-01	Camk2d, Prkcc, Grm1

KEGG Pathway Analysis for Pdyn layer 2 cell type

Term	Count	%	P value	Benjamini FDI	Genes
Calcium signaling pathway	13	5.2	4.60E-05	4.80E-03	Ptk2b, Adcy3, Cacna1a, Cacna1g, Cacna1h, Cckbr, Chrm1, Grin1, Itpr1, Pde1a, Plcb1, Prkcc
Long term depression	7	2.8	9.60E-04	2.50E-02	Cacna1a, Crhr1, Gria1, Itpr1, Plcb1, Prkcc
Long term potentiation	6	2.4	5.10E-03	1.00E-01	Gria1, Grin1, Itpr1, Plcb1, Plcb4, Prkcc
Axon guidance	7	2.8	1.80E-02	2.40E-01	Epha4, Ephb6, L1cam, Sema5b, Slit1, Slit3, Unc5a
MAPK signaling pathway	10	4	2.50E-02	2.60E-01	Rasgrp1, Cacna1a, Cacna1g, Cacna1h, Cacna2d1, Cacna2d3, Cacng3, Mapk8ip3, Map4k2, Prkcc
Neuroactive ligand-recepto	9	3.6	5.60E-02	3.70E-01	Cckbr, Chrm1, Crhr1, Gabrd, Gria1, Grin1, Grm2, Grm8, Pth2r
GnRH signaling pathway	5	2	7.00E-02	3.90E-01	Ptk2b, Adcy3, Itpr1, Plcb1, Plcb4

KEGG Pathway Analysis for Wfs1 layer 2 cell type

Term	Count	%	P value	Benjamini FDI	Genes
Axon guidance	4	2.1	7.00E-02	7.30E-01	Cxcl12, Ppp3r1, Sema3a, Unc5c

Figure 4.6: Overrepresented KEGG pathways for layer 2 cortical cell types.: Ntf3, Pdyn and Wfs1. Listed KEGG pathways (a, b, c) are significantly overrepresented in the TRAP data for Ntf3 PS1046, Pdyn CP12 and Wfs1 Tg2 when compared with each other and non-pyramidal cell types (Pnoc, Lypd6, AldhL1 an Olig2) using SI algorithm.

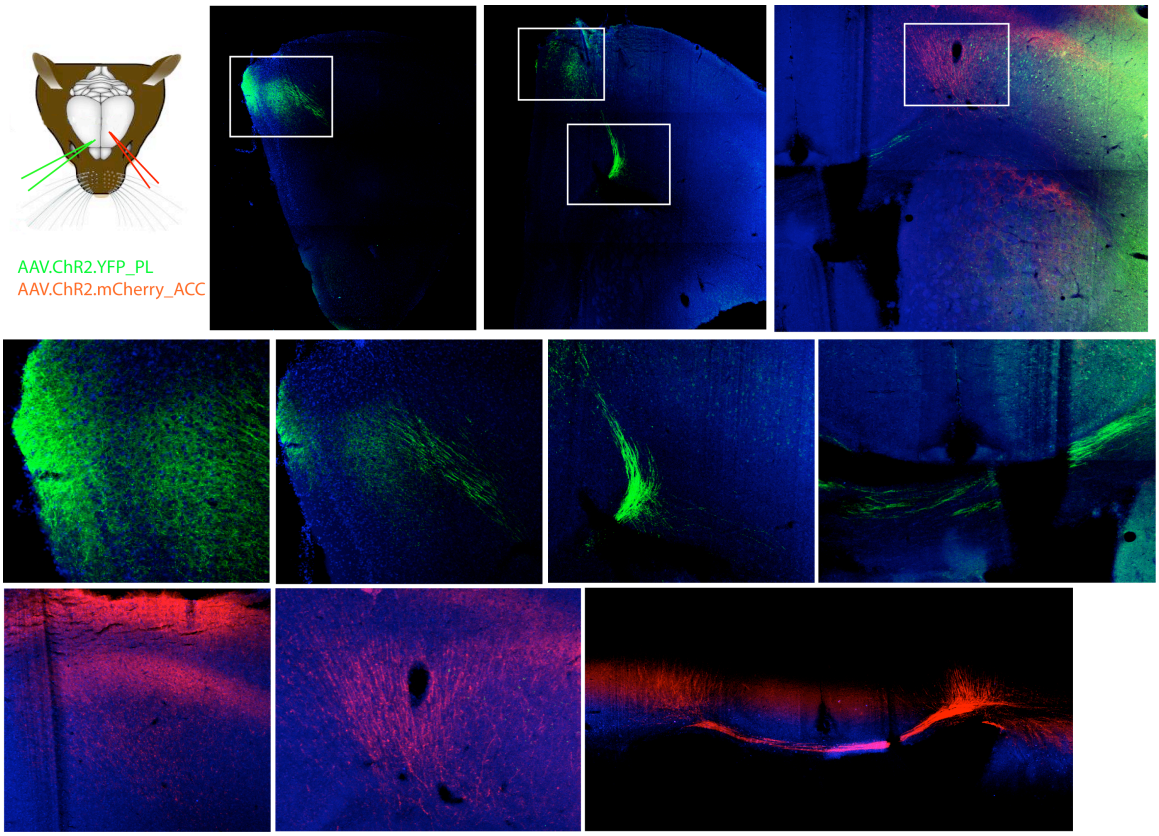

Figure 4.7: Circuit mapping of cortical layer 2 Wfs1 cell type. Anterograde viral tracer AAV-dfl-ChR2-EGFP-dfl was stereotactically injected into the prelimbic cortex (PL) and AAV-dfl-ChR2-mCherry-dfl into anterior cingulate cortex (ACC) of Wfs1 Cre-ERT2 mice as shown in (a). Viral transduction of mCherry under the control of Cre recombinase revealed that Wfs1 cells in PFC (a,c, h enlarged insets: e, f, g) and ACC (d, i, j, k) both project callosally to the contralateral cortex.

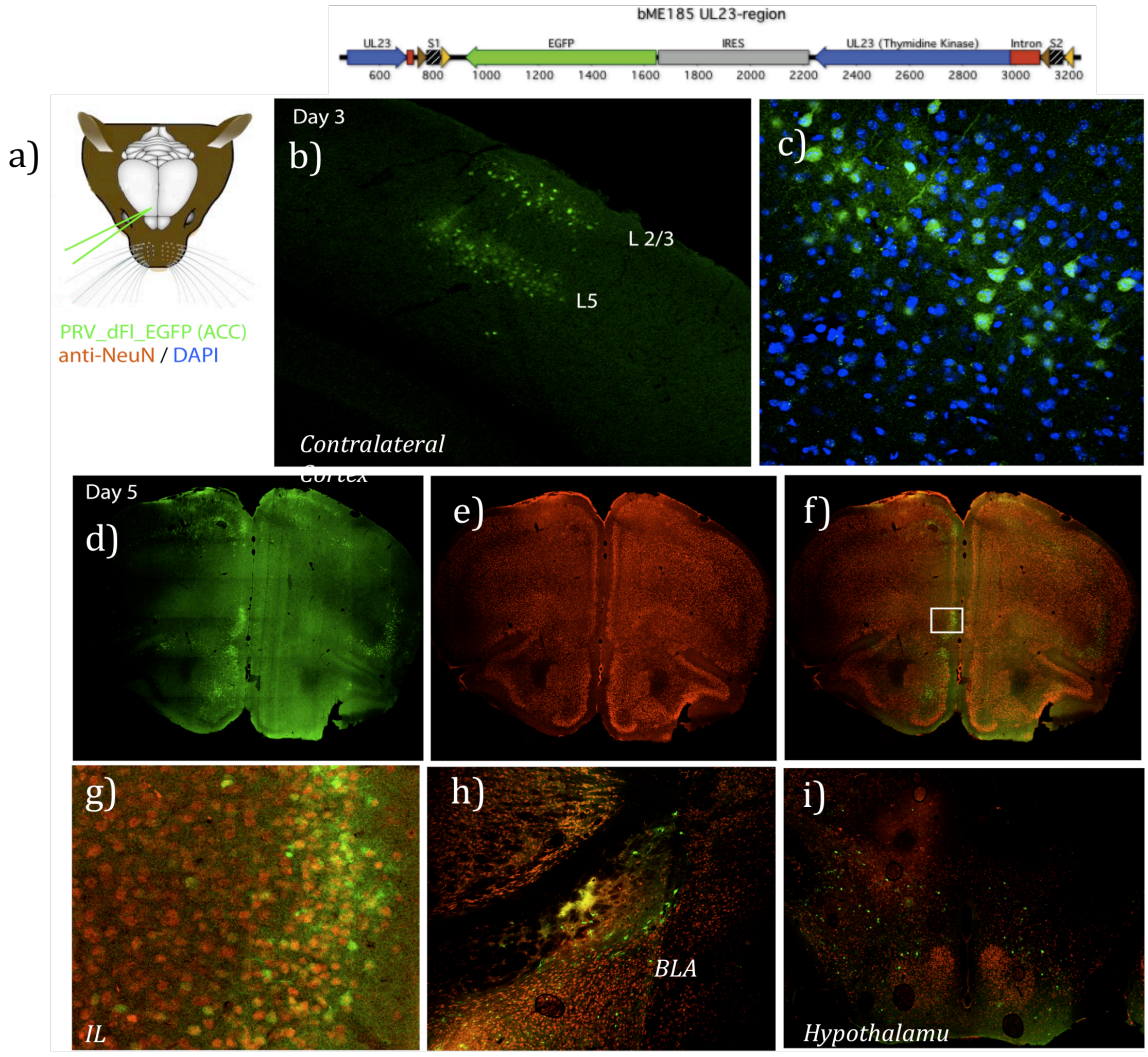

Figure 4.8: Retrograde circuit mapping of cortical layer 2 Wfs1 cell type. Retrograde transsynapatic viral tracer PRV-ME185 (top panel) was stereotactically injected into the anterior cingulate cortex (ACC) of Wfs1 Cre-ERT2 mice as shown in (a). Viral transduction of EGFP under the control of Cre recombinase for 3 days revealed that Wfs1 cells in ACC receive synaptic input from cortical pyramidal cells in layer 2/3 and 5 (b; enlarged inset with DAPI counterstain: c). Since there was no other labeling seen in other areas of cortex or subcortical brain regions, these cells are monosynaptically connected to Wfs1 ACC cell type. At day 5, PRV-ME185 labeled many cells in both ipsilateral and contralateral cortex as revealed by EGFP/NeuN co-immunostaining (d, e, f; enlarged inset: g). There were scattered cells labeled also in basolateral amygdala (BLA) and hypothalamus.

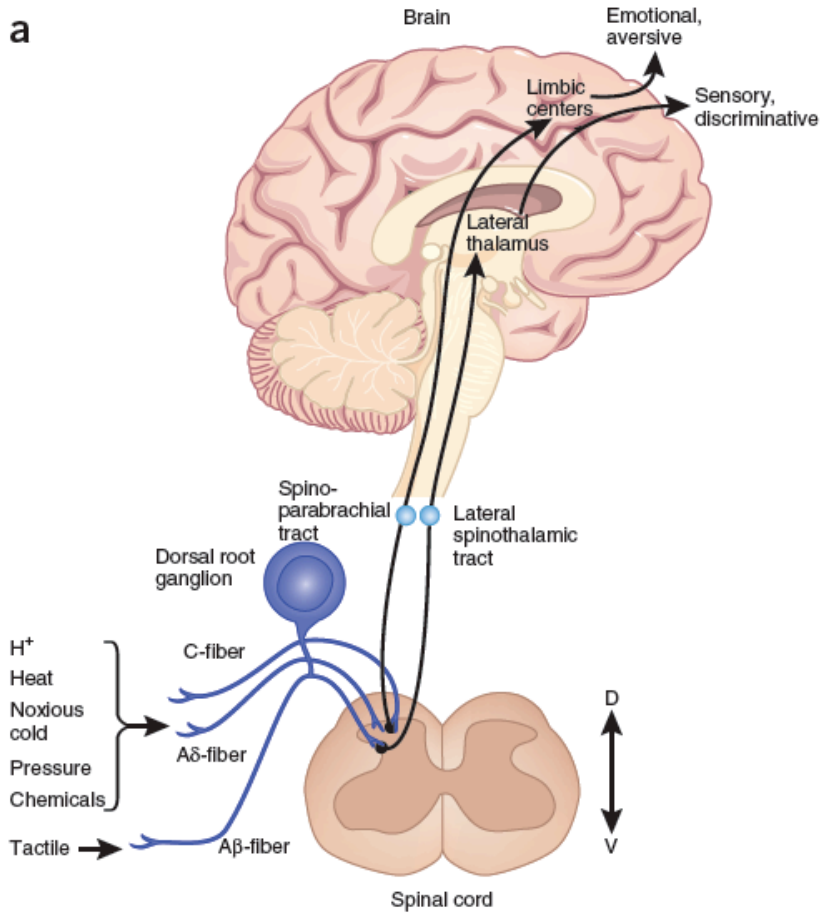

Figure 4.9: Pain circuitry in Mammals. Noxious stimuli from the periphery are sensed by specialized sensory neurons which send their axons to the dorsal root ganglion of spinal cord. The second order neurons constitute two central pathways: pain sensation pathway involving the lateral spinothalamic tract (LST)and pain affection pathway involving medial spinoparabrachial tract (MST). The LST tract, important for encoding stimulus parameters, sends projections to the lateral thalamus which then relay sensory information to the somatosensory cortex. By contrast, the MST tract relays information related to affection of pain by sending projections to the limbic regions including anterior cingulate cortex and amygdala. (picture adapted from Konig 2010)

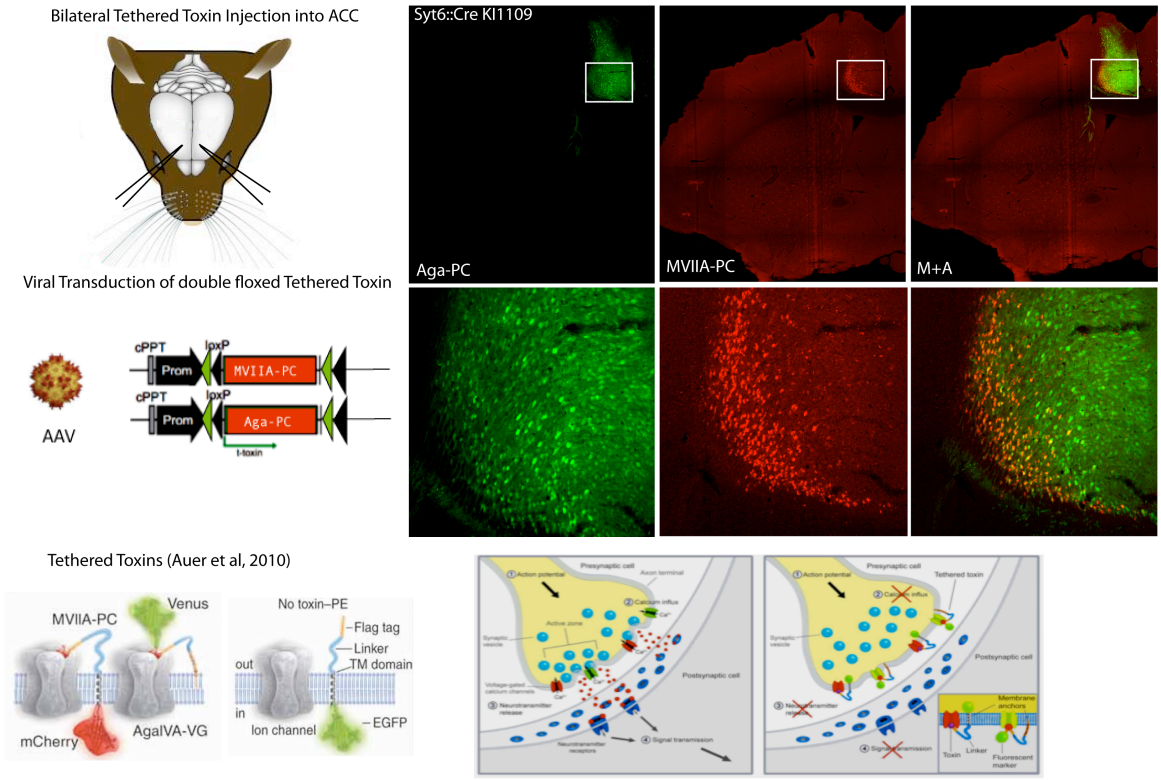

Figure 4.10: Cell autonomous silencing with viral transduction of tethered toxins. Wfs1 Cre ERT2 mice were stereotactically injected (a) with equimolar suspension of AAV-dfl-MVIIA-mCherry-PC-dfl (red) and AAV-dfl-AgaIV-EGFP-PC (green) or control AAV-dfl-PE-dfl (b) into the anterior cingulate cortex. These tethered toxins are cell-autonomonous by being anchored to the membrane with a transmembrane domain (c) and bind voltage gated calcium channels (Cav2.1 and Cav2.2) effectively blocking synaptic transmission (d). Tethered toxin expression can be monitored with EGFP and mCherry expression (e, f, g and enlarged insets: h, I, j)

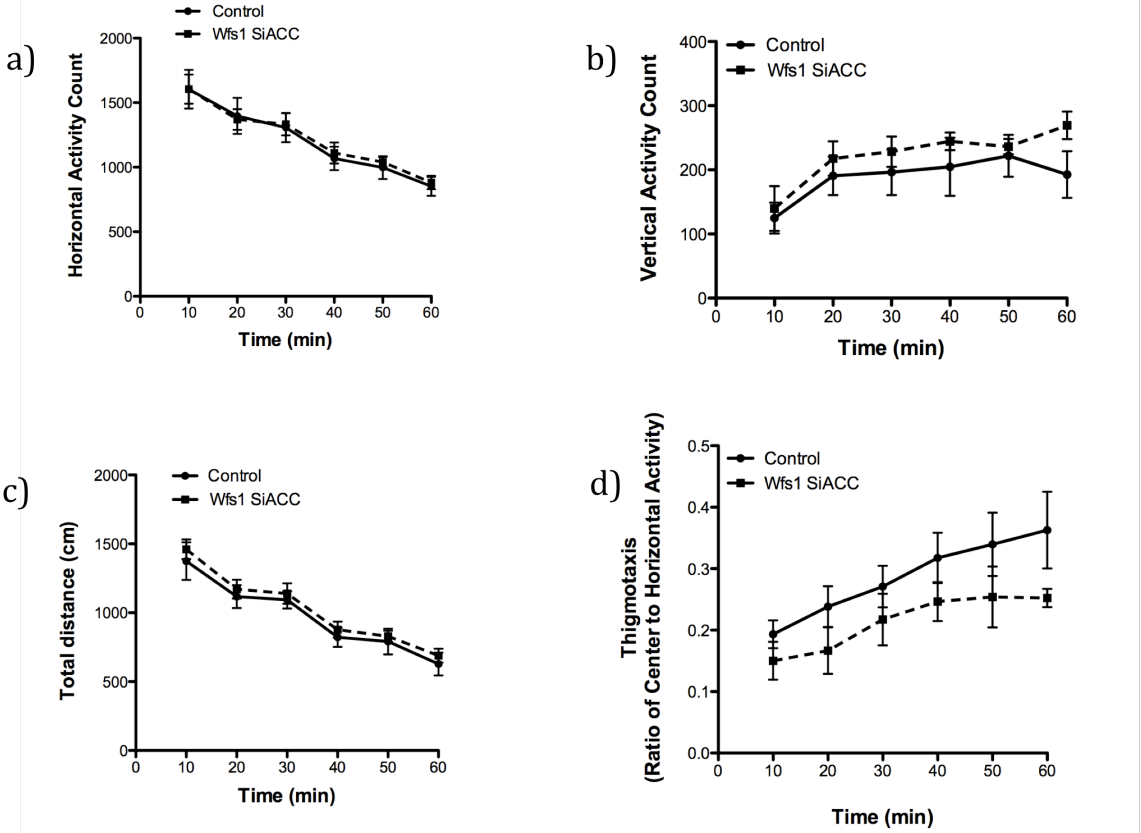

Figure 4.11: Spontaneous locomotor activity of SIACC Wfs1 and PE WFS1 (control) mice in open field boxes. Mice were tested for 60 min of activity in open arena. Two way RM ANOVA comparing SIACC Wfs1 with PE WFS1 showed no difference in horizontal activity (a: $F(6,13) = 0.126$, $p = 0.876$), vertical activity (b): $F(6,13) = 0.908$, $p = 0.340$ and total distance (c): $F(6,13) = 0.469$, $p = 0.507$. Thigmotaxis was also not significantly different between the two groups ($F(6,13) = 2.837$, $p = 0.118$).

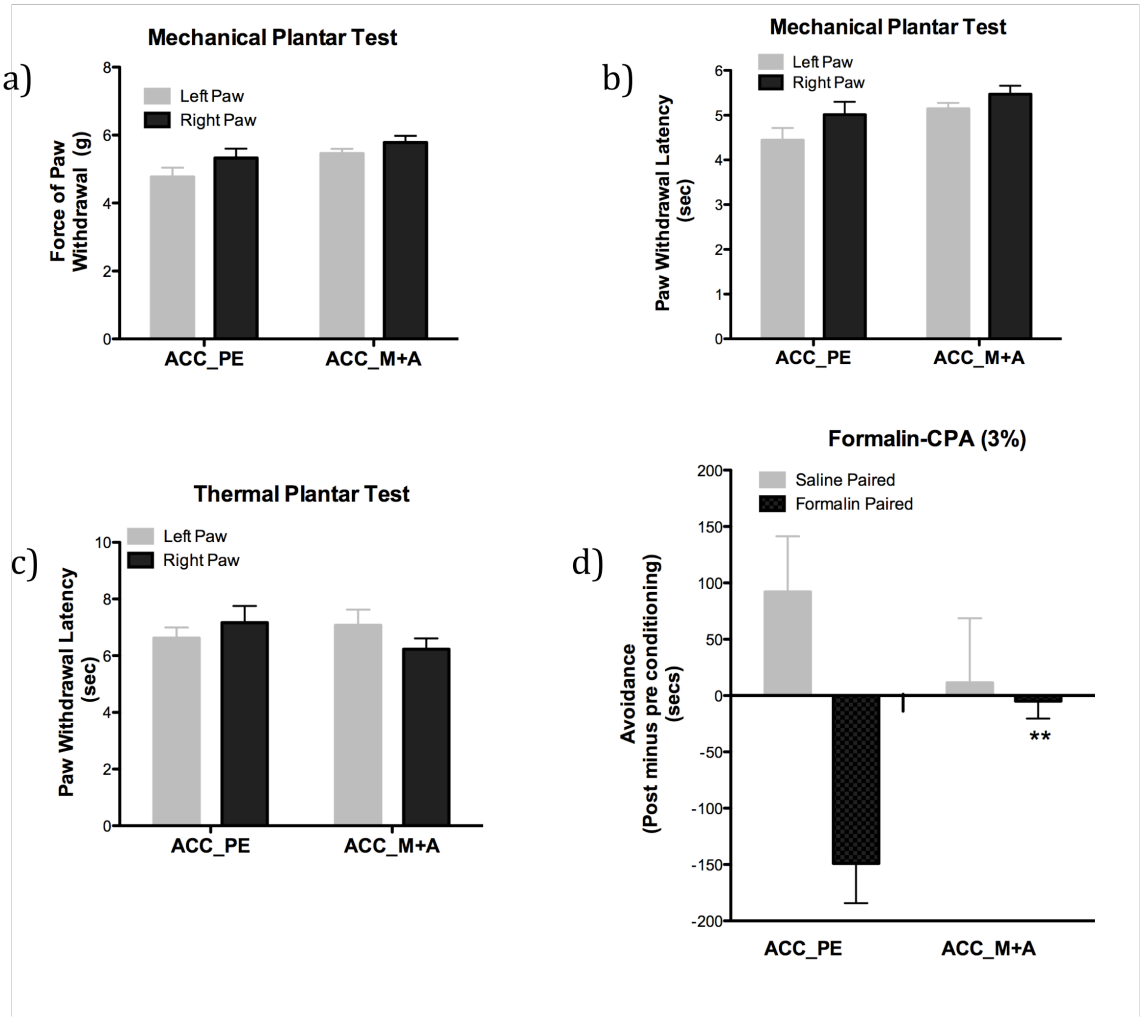

Figure 4.12: Pain sensation and affection in SIACC Wfs1 and PE Wfs1 control mice. Mice were tested for sensitivity to noxious mechanical and thermal stimuli, and then for affective pain using formalin-conditioned place aversion module. Pain sensitivity for mechanical pain for both groups of mice did not differ from each other in measures like force of paw withdrawal (a; $F(6,13) = 0.185$, $p = 0.286$) and latency to paw withrawal (b: $F(6,13) = 1.191$, $p = 0.105$). Likewise physiological pain sensitivity to thermal stimulus also did not significantly differ between the groups ($F(6,13) = 1.191$, $p = 0.105$). By contrast, when the mice were tested for formalin induced CPA, SIACC Wfs1 were significantly impaired in averting the formalin paired context compared to PE control ($p = 0.0047$, $df = 7$).

CHAPTER 5: CELLULAR AND BEHAVIORAL CHARACTERIZATION OF CORTEX SPECIFIC DELETION OF WOLFRAMIN (WFS1)

The strength of cell type specific translational profile using TRAP methodology lies in the access to the list of candidate genes specifically enriched in the given cell type. The candidate genes may encompass ion channels, membrane bound G-protein coupled receptors (GPCRs), transcription factors or genes that are implicated in neurodegenerative disorders. When we analyzed the translational profiles of Layer II pyramidal cells as genetically defined by the drivers Ntf3 and Pdyn, a candidate gene Wfs1 that was enriched in both TRAP data stood out for high enrichment as well as implication in the etiology of a human neurodegenerative disorder. We decided to take a candidate gene approach on Wfs1 by conditionally deleting the gene in pyramidal cells of neocortex. Wfs1 is the causative gene for Wolfram syndrome, a multisystem neurodegenerative disease that is accompanied by pathologies of the pancreatic islets, hearing system, optic atrophy and neuronal degeneration in various areas of the brain.

5.1 Wolfram syndrome, a multisystem neurological disorder

In 1938, Wolfram and Wagener described a family in which four siblings developed bilateral optic atrophy and diabetes mellitus, followed by deafness, incontinence and ataxia, thus presenting the first report of Wolfram Syndrome (Fonseca et al., 2005). Frequent association of the disease with diabetes insipidus, diabetes mellitus, optic atrophy and deafness led to the acronym DIDMOAD, referring to the four cardinal symptoms. Wolfram Syndrome is a rare autosomal recessive disorder complicated by both genetic and clinical heterogeneity. In other words, WS patients present with part or the entire host of symptoms for Wolfram Syndrome and among the WS patients, they may harbor different genetic mutations in the causative gene Wolframin (Wfs1). Meta-analysis of genotype-phenotype correlation in Wolfram Syndrome revealed that nonsense or frame-shift mutations cause more severe phenotypes compared with

missense mutations in the Wfs1 gene (Cano et al., 2007). Besides metabolic and non-CNS symptoms, mutations in the Wfs1 gene are associated with diverse behavioral and cognitive abnormalities. Neuropathological manifestations of WS include atrophy of the optic nerves, hypothalamic region, posterior pituitary, pontocerebellar region and brain stem. Psychiatric findings in WS patients have included progressive dementia, severe depression, attempted suicides, paranoid delusions, hallucinations, mental retardation, anorexia and insomnia (Luuk, 2009). Swift et al (Swift et al., 1990) investigated medical histories of 68 WS patients in US and reported that 60% of them had experienced psychiatric manifestations, most notably depression. In many cases, antidepressants alone or in combination with antipsychotics were effective in ameliorating the psychiatric symptoms. The prevalence of WS has been estimated to be 1 in 770,000 in UK and 1 in 100,000 in North America, whereas the carrier frequency is 1 in 345 in UK and approx. 1% in the US. The median age of death in WS patients is 30 years, with the most common causes of mortality being neurological manifestations and complications of urinary tract atony (Luuk, 2009; Swift and Swift, 2005).

5.2 Wolframin (Wfs1), the causative gene for Wolfram Syndrome

Wolfram (Wfs1) was first identified as a causative gene for WS in 1996, when Collier et al linked WS to chromosome 4p16.1 using linkage analysis of multiple UK families with WS. In WS patients, mutations in Wfs1 are distributed along the length of the coding sequence although mutations in the largest exon, exon 8, occur in highest frequency. The Wfs1 mutations have included deletions, insertions, nonsense and missense mutations (Khanim et al., 2001). The chromosomal location 4p16.1 is interesting because a number of hereditary diseases have been mapped to the 4p16 region in humans, such as Huntington's disease (4p16.3), ADHD, bipolar

disorder and food relation obsessions (Khanim et al., 2001; Luuk et al., 2008). It is possible that the chromosomal region 4p16 is a general hot spot for mutations pertaining to psychiatric disorders and the specific location where mutations occur determine the specific nature of the disorder.

In mice, Wfs1 is located in the chromosomal location 5qB3. Wfs1 gene, as earlier mentioned, is composed of eight exons spanning about 30 kb of genomic DNA. The Wfs1 transcript is approx. 3.6 kb long with the translation start site located in the beginning of second exon. About 60% of the coding sequence (2.6 kb) is located in the largest exon, exon 8. The WFS1 protein is composed of 890 amino acids, with 9-10 transmembrane domains, and has a molecular weight of about 100 kDa. In native conditions, WFS1 exists as a 400 kDa structure, presumably formed by a homotetrameric complex. WFS1 has been shown to localize to the membrane of Endoplasmic Reticulum (ER) via its transmembrane domains. The WFS1 protein is unstable when the post-translational N-glycosylation is inhibited. Although the precise molecular function of WFS1 has not been established, it has been suggested to play a role in maintaining Calcium homeostasis in the ER (Luuk et al., 2008; Takeda et al., 2001; Takei et al., 2006). Previous studies have shown that Wfs1 deficient pancreatic B cells have impaired glucose stimulated insulin secretion and cell cycle progression, coupled to activation of the ER stress/ unfolded protein response (UPR) pathways and ultimately enhanced susceptibility to apoptosis (Fonseca et al., 2005; Ishihara et al., 2004; Yamada et al., 2006). The ER is an important cellular compartment for the folding of newly synthesized secretory proteins and imbalance in Ca2+ homeostasis within the organelle leads to ER stress. The UPR pathway counteracts ER stress by

eliciting gene expression, reduction in translation and degradation of proteins associated with the ER (Fonseca et al., 2005).

Transgenic mice have been utilized as models to understand the function of Wfs1 in the pathophysiology of pancreatic B cells and behavioral abnormalities. Different research groups have generated Wfs1 deficient mice by targeting either the second exon or the eighth exon. Ishihara (Ishihara et al., 2004) generated Wfs1 deficient mice lacking the second exon and studied the impaired metabolic phenotype in pancreatic B cells, whereas Kato (Kato et al., 2008) studied the behavioral phenotype of the same mice and concluded that the Knock Out (KO) mice had reduced escape latency in passive avoidance tasks and subtle impairments in social interaction. Riggs et al (Riggs et al., 2005) generated a Wfs1 deficient mice lacking the eighth exon and reported that these mice displayed glucose intolerance by 4 months of age and elevated ER stress and apoptotic pathways. However they did not study cognitive and affective impairments in these KO mice. Luuk et al (Luuk, 2009) used a similar strategy and targeted the eighth exon of Wfs1, but they also knocked in reporter B-gal in place of eighth exon (i.e. Wfs1 Bgal/Bgal mice) enabling them to track where the normally Wfs1 expressing cells. They found that Wfs1 Bgal/Bgal mice appeared normal in overt appearance but occasionally the males were smaller in size. They found that the KO mice, both males and females, occasionally (15-50% of cases) produced audible vocalizations in the 10 kHz range, which was blocked with anxiolytic diazepam. Due to stronger metabolic phenotype in the male KO mice, they used female transgenic mice for their subsequent behavior studies, which pose a few complications in behavioral analysis owing to the hormonal estrus cycle that has been shown to influence behavior. They found that the KO mice had significantly elevated levels of corticosterone in

their blood plasma in response to stress although the baseline levels were identical compared to their wildtype littermates. Also the KOs exhibited anxiety like phenotype, both in exploratory behavior and hyponeophagia tests, which was ameliorated with diazepam (Luuk, 2009).

The multisystem pathophysiology characteristic of Wolfram Syndrome complicates the analysis of how the loss of Wfs1 in the brain is contributing to its clinical phenotype. Even within the brain, Wfs1 gene is expressed in a host of regions including cerebral cortex, striatum, amygdala, hypothalamus, brainstem and pons. Constitutive deletion of Wfs1 in all the tissue that express the gene results in a heterogeneous blend of phenotypes resulting from functional impairment in any or all of those regions. In particular, the strong metabolic phenotype ensuing from pancreatic B cell loss makes it difficult to compare the behavioral outcome with their healthy wildtype littermates. In order to circumvent the metabolic disturbances as well as to elucidate the role of cerebral cortex in cognitive impairments associated with WS, we have applied a strategy to specifically delete the gene in pyramidal cells of cerebral cortex.

RESULTS:

5.3 Generation of Transgenic mice with Cortex restricted deletion of Wfs1

Mice harboring conditional allele of Wfs1 were generated as described in Materials and Methods. Briefly, conditional targeting vector with LoxP sites flanking the eighth exon of Wfs1 gene was used to electroporate into 129/SvEvBrd ES cells (Fig 5.1). Correctly integrated ES clones were identified by Southern Blot and microinjected into C57Bl/6 (albino) blastocysts. The resulting chimera were mated to C57Bl/6 (albino) females to generate mice that were heterozygous for the Wfs1 conditional mutation, referred to as Wfs1 fl/+ from here onwards.

The Wfs1 fl/+ heterozygotes were crossed to C57Bl/6 mice for at least 2 generations before mating them to each other in order to obtain Wfs1 fl/fl homozygote mice for the conditional allele. Next, we utilized a Knock-In Cre transgenic line that renders expression specificity to the pyramidal cells in the cerebral cortex – the Emx1 IRES.Cre. This line is generated by homologous recombination of an internal ribosome entry site (IRES) and Cre recombinase coding region into the 3' untranslated region of the mouse Emx1 gene. Due to the use of IRES for transcription of Cre, this strategy prevents reduction in Emx1 gene/protein in Emx1 IRES.Cre/Emx1 IRES.Cre transgenic mice. Emx1 encodes a homeodomain protein whose expression is restricted primarily to cortical subdivisions of the telencephalon (Gorski et al., 2002). Cortical excitatory neurons and glia but not GABAergic neurons are generated in the Emx1 expressing lineage. Our breeding strategy involves mating Wfs1 fl/fl conditional allele to Emx1-IRESCre mice to generate Emx1 IRES.Cre$^{+/-}$/ Wfs1 fl/+ heterozygote mice which were then breed again to Wfs1 fl/fl homozygote mice, in order to get Emx1 IRES.Cre$^{+/-}$/ Wfs1 fl/fl mice (referred to as Wfs1 CxKO from here onwards) and their wildtype control littermates harboring just the conditional allele Wfs1 fl/fl. The Emx1 IRES.Cre mice were generated in129sv background but backcrossed to C57Bl/6 for at least 8 generations. Our breeding strategy for obtaining triple allele transgenic mice for Emx1 IRES.Cre and Wfs1 fl/fl makes it somewhat difficult to state the background strain with confidence, however it might be accurate to describe it as (129/SvEvBrd X C57Bl/6) X C57Bl/6 mixed strain, with major contribution from C57Bl/6.

5.4 Neuroanatomical characterization of Cortex specific deletion of Wfs1

Adult Wfs1 CxKO mice and their wildtype littermates, at 8 weeks of age, were used for neuroanatomical analysis. Both male and female mice were analyzed for neuroanatomy; there were no gender-related differences in the CNS expression of Wfs1. The Wfs1 antibody, raised against a peptide corresponding to a region within Exon 8 of WFS1 as described in Chapter 4, was used to immunologically determine the pattern of Wfs1 expression in the CNS of the KO mice and their wildtype control littermates. The subcellular distribution of WFS1, as determined by the antibody staining, includes neuronal perikarya, processes and nerve fibers. In the wildtype brain, WFS1 protein is detected in the superficial layer II of neocortex, with a progressive decrease in expression in the rostrocaudal axis. Outside of neocortex, WFS1 is detected in the olfactory bulb (OB), hippocampal CA1 region, olfactory tubercle, caudate putamen (CPu), central extended amygdala (CEA) and hypothalamus (Fig 5.2). In the Wfs1 CxKO mice, WFS1 is completely missing from the neocortex but is present in equal abundance in most of the subcortical regions including OB, CPu, CEA and hypothalamus. WFS1 is not detected, however, in the hippocampal CA1 region in the Wfs1 CxKO mice. Prior literature on Emx1 expression revealed that this gene is expressed in pyramidal cells in both neocortex and hippocampus. Hence, the lack of WFS1 detection in the hippocampus alongside the neocortex concurs with the reported findings on Emx1 expression. Next, in order to determine whether the Wfs1 cells in the neocortex are subjected to neurodegeneration, we used Fluoro-Jade C, an established stain for degenerating neurons. Bian et al (Bian et al., 2007) showed that Fluoro-Jade C is a useful marker for staining the dopaminergic neurons in substantia nigra while they degenerate in response to

MPTP induced insult. Fluoro-Jade C positive cells emit green color and are mostly shrunken or smaller sized compared to normal analogous cells in controls. Fluoro-Jade C staining on the Wfs1 CxKO brain did not reveal any staining of the neocortex similar to the wildtype brain, indicating that the Wfs1 cells in layer II are not degenerating neurons (Data not shown). NeuN immunostaining and DAPI nuclear counterstain of brain sections of the Wfs1 CxKO mice revealed no discernible differences in the thickness of cortical layers as well as distance from pia to the superficial layer II, suggesting that the Wfs1 cells are not missing from the cortex (data not shown).

5.5 Reproduction, Overt appearance and Body Weight

The Wfs1 CxKO mice were born in normal Mendelian ratio and had normal *ad libitum* body weight compared to their wildtype littermates. The KO mice had normal glucose levels by urinalysis in non-fasting conditions (data not shown), which suggested that the pancreatic B cells were spared in these mice and that we were able to avoid the metabolic phenotype of Wolfram Syndrome. Both male and female Wfs1 CxKO mice appeared normal in appearance with similar body size compared to each other as well as the wildtype controls. The female Wfs1 CxKO mice were fertile and bred with other male transgenic mice giving progeny in a normal Mendelian ratio, indicating that the reproductive system in the Wfs1 CxKO mice was functioning normally. Occasionally, whisker trimming, a social dominance behavior, was observed among the littermates regardless of the genotype, which has been attributed to the mixed strain background of 129/SvEvBrd X C57Bl/6. Only male mice were used for subsequent behavior analysis in order to avoid the hormonal influences of the female estrus cycle.

5.6 Battery of Behavioral Tests for Phenotyping Wfs1 CxKO mice

Adult male Wfs1 CxKO mice and their wildtype littermates, starting at 10 weeks of age, were tested in a battery of behavioral tests in order to assess the phenotypic effects of deleting Wfs1 in the cerebral cortex. It is difficult to model endophenotypes of any psychiatric disease, since many symptomatic aberrant behaviors may be uniquely human and/or difficult to assay in rodents, such as melancholy and suicidal tendency. However, by defining a disease as individual components of symptoms, causes and treatment responses, it may be possible to model components of human disease in mice, without undue anthropomorphism (Chadman et al., 2009). We took a similar approach to breaking down the symptoms of Wolfram Syndrome (WS) into its individual components. Since our Wfs1 CxKO mouse model of WS is deficient of the gene only in the neocortex sparing brain regions such as amygdala and hypothalamus, we chose behavioral test batteries to elucidate cortical contributions to the endophenotype of the disease. The neocortex has been implicated in a range of executive functions including emotional and cognitive behavior. Hence, we tested Wfs1 CxKO mice in assays for spontaneous locomotion, motor coordination, pain sensation, anxiety, depressive behavior and operant conditioning. Cohorts of mutant mice and their wildtype littermates were tested in a series that begins with the least stressful tests such as the open field tests, followed by more complex stressful tasks such as elevated plus maze, sucrose preference test and three-choice operant conditioning tasks. The order of the behavioral tests carried out for the Wfs1 CxKO and wildtype mice are listed in the table (Fig 5.3).

5.7 Spontaneous Locomotor Activity in the Open Field Arena

A cohort of ten mice each of genetic backgrounds, Wfs1 CxKO and wildtype, were first tested for open field activity at 10 weeks of age. They were provided free access to food and water in their home cage prior to the test. They were allowed to habituate to the behavior room under the test lighting conditions (~400 lx) for 1 hour before being placed in the open field arena. We found that the Wfs1 CxKO mice were generally hypoactive in open field arena compared to the wildtype littermates in all three measures including horizontal activity, vertical activity and total distance. Both groups of mice acclimatized to the open field over the experimental period of 60 min i.e. they both displayed high levels of exploration when the arena was novel, but the activity tapered off as time progressed from 0 to 60 min (in 10 min bins) and the novelty wore off (Fig 5.4). Two way RM ANOVA revealed that the horizontal activity for KO mice was significantly lower than that of wildtype: $F(1,19) = 4.57$, $p = 0.047$. However, when individual time points were compared with Bonferroni multiple comparisons post hoc test, it was revealed that the difference was only significant at time point 40 min ($t = 2.73$, $p < 0.05$). In the case of vertical activity, which is a measure of grooming behavior, Two way RM ANOVA showed that the KO mice had a significantly reduced vertical activity compared to controls: $F(1,19) = 6.342$, $p = 0.022$. Again, when individual time points were considered, the difference in vertical activity of the two groups was significant only at time point 40 min ($t = 3.055$, $p < 0.05$). The third measure of locomotion, total distance travelled, was not significantly different between the two groups. Also the two groups of mice did not display any difference in thigmotaxis, measured as the relative distance travelled in the central quadrant compared to the periphery.

For later studies of cognitive function, the Wfs1 CxKO mice and wildtype controls were food restricted to 85% of their *ad libitum* body weight. The stress induced by food restriction could affect their locomotor behavior and anxiety. Hence, we ran the food restricted KO and WT mice in the open field tests with the exact same parameters. Surprisingly, it was revealed that under stress, both KO and WT mice do not acclimatize to the open field arena over the 60 min experimental session and their activity remains at high level throughout the session (Fig 5.4). Secondly, there is no difference in the locomotor behavior of the food restricted KO vs WT in all three parameters, including horizontal activity, vertical activity and total distance travelled. These results indicate that the reduction in motor behavior observed in the open field in KO mice is not from impairment in motor skill but instead might indicate a lack of motivation to explore the arena. Alternately, it is possible that the bright lighting conditions (~400 lx) increased their anxiety and thus led to reduction in the exploratory behavior. However, since thigmotaxis was not affected in these two groups, it is less likely that the KO mice are hypoactive due to anxiety related behavior.

5.8 Motor Coordination and Balance

Rotarod is used to assess the ability of an animal to balance on a rotating rod, which is set to accelerate at a set speed (Carter 2001). We tested Wfs1 CxKO and their wildtype littermates (N=10) in the accelerating rotarod for 3 times a day for 3 consecutive days (Fig 5.5). There was no significant difference between the two groups of mice as measured by Two Way RM ANOVA. This indicates that the Wfs1 CxKO mice had no impairments in motor coordination and balance.

5.9 Sucrose preference Test: A measure of Anhedonia

Anhedonia, the inability to experience pleasure from activities formerly found enjoyable, is a prominent feature of depression. In rodents, anhedonia is commonly assessed with a sucrose preference test, which provides good face validity. Sucrose has an inherent hedonic value and given a choice between sucrose and water, mice prefer sucrose to water. In our experiment, the Wfs1 CxKO mice had a significant reduced preference for sucrose compared to wildtypes (Fig 5.6). The sucrose preference Isa calculated as the ratio of volume of sucrose to volume of water imbibed. The wildtype mice displayed a sucrose preference (Mean±SEM = 0.647±0.066, N=7) where as the Wfs1 CxKO mice did not exhibit it (Mean±SEM = 0.447±0.049, N=9). The difference between the two groups was significant with unpaired Two-tailed ttest ($p = 0.0265$, $t = 2.479$, $df = 14$). Thus our results indicate that the Wfs1 CxKO mice present one major feature of depression. Other commonly used assays to evaluate the depression like phenotype in mice include tail-suspension test (TST), forced swim test (FST). Both tests measure immobility and response to an inescapable stressor. Unfortunately, Wfs1 CxKO are hypoactive compared to the wildtype mice (as revealed by the open field tests), hence measures of immobility for assaying depression phenotype would be confounded by low pre-existing levels of activity. On the other hand, we could aim for predictive validity by treating Wfs1 CxKO mice with anti-depressants. The antidepressant treatment would be hypothesized to relieve the anhedonia symptoms and possibly immobility in the TST and FST assays.

5.10 Light-Dark Transition Test

Light-Dark (LD) Transition Test is an unconditioned test of anxiety-like behavior designed for mice. Anxious mice generally tend to spend more time in the dark arena and do not make as many transitions to the light arena as wildtype mice. Constitutive deletion of Wfs1 in the whole body (and brain) was reported to cause anxiety related behavior in the Light-Dark Transition Test. But in constitutive KO mice, the Wfs1 gene is deleted also in Amygdala, the emotional center of the brain. Hence, we wanted to determine if cortical deficiency of Wfs1 would lead to anxiety related behavior. So, we tested Wfs1 CxKO and wildtypes in LD-Transition test (Fig 5.7). The two groups do not significantly differ from one another in most parameters of the test including staytimes in dark side and light side, entries to the dark side, distance moved in dark side and light side and total distance moved. The only parameter where the two groups differ is entries to the light side (unpaired Two tailed ttest: $t=2.306$, $df = 20$, $p =0.0319$). This deficit in transitions to the light side could be explained by hypoactivity since the staytimes in light side are not different between the mutants and the wildtypes.

5.11 Elevated Plus Maze Test

This test employs a naturalistic conflict in mice between the tendency to explore a novel environment and aversive properties of a brightly lit, open area. Thus it is a test for anxiety related behavior in mice and provides internal controls such as total arm entries to detect potential confounds of sedation and hyperactivity. In this test, the two groups Wfs1 CxKO mice and wildtypes did not significantly differ from each other in any of the parameters including total distance moved, staytime in closed arms, staytime in open arms, closed arm entries, open

arm entries and most importantly, percent open arm entries (with respect to total arm entries) (Fig 5.8).

5.12 Hyponeophagia

Hyponeophagia, also referred to as novelty-induced food suppression, is another test for anxiety. Mice were subjected to a bright arena with a food pellet in the center, and their latency to approach the food and make their first nibble was recorded. The Wfs1 CxKO mice did not display any deficit in hyponeophagia – the latency to start eating was 292.1±45.17 s for control mice (N=10) and 251.6±44.73 s for the KO mice (N=10); the unpaired two-tailed ttest was not significant (t=0.6371, df=18, p=0.532) (Fig 5.9). Thus all three tests for anxiety indicate that Wfs1 CxKO mice do not have an anxiety phenotype.

5.13 Appetitive Operant Conditioning

5.13.1 Parsing Prefrontal Cortex Function(s) with Wfs1 loss-of-function

Within the mouse PFC, Wfs1 is expressed in the superficial layer II of infralimbic cortex, prelimbic cortex and anterior cingulate. These regions within the PFC have been implicated in higher cognitive functions involved in goal directed behavior and habit formation. As discussed in Chapter 1, the medial PFC that includes prelimbic and infralimbic cortices is important for working memory, consolidation of fear extinction and extradimensional shift of attention. The anterior cingulate cortex (ACC) on the other hand is implicated in motor sequencing of behavior and behavioral disinhibition. Instead of focusing on subregions of PFC, we wanted to ask the

question: What role do frontal layer II pyramidal cells defined by Wfs1 play in contributing to the PFC function? Loss-of-function approach by deleting Wfs1 in the neocortex allows us unprecedented access to cell type specific contribution to pathophysiology and cognitive impairment with a PFC basis. With this approach, we obviate the cellular complexity of subregions within PFC and instead delineate subtle functional aspects of PFC attributable to the Wfs1 cell type.

5.13.2 Operant Conditioning: An overview

Operant conditioning is a paradigm first investigated by E. L. Thorndike (1898) (Thorndike, 1898) and later refined and extended by B.F. Skinner (1938) (Skinner, 1938). The term, operant conditioning, was coined by Skinner in the context of reflexive physiology, to differentiate behavior that affects or acts upon the environment from the reflex related behavior inherent to Pavlovian conditioning. Although Skinner's definition of operant conditioning bore high similarity to Thorndike's 'Instrumental learning', it was Skinner who devised a method for automated training with intermittent reinforcement that could be modified to accommodate different schedules of reinforcement. A reinforcement schedule is any procedure that delivers a reinforcer to the subject according to some well-defined rule. The usual reinforcer is food for diet-restricted rodents and the usual schedule is one that delivers the reinforcer in a beam break or switch closure caused by nose poke at the aperture or a lever press. Two types of reinforcement schedules are commonly applied: the first type is time based schedules such as fixed and variable interval, in which the reinforcer is delivered after a fixed or variable time period after a time marker, usually the preceding reinforcer. The second type is ratio schedule

which requires a fixed or variable number of responses before a reinforcer is delivered (Malkki et al., 2011).

Rodent behavior in operant conditioning paradigm is characterized by two components: a goal-directed behavior and an action-outcome habit mechanism (Balleine and Dickinson, 1998). These two components represent two different forms of learning. The goal directed behavior consists of acquiring an incentive value for an action by association with a reward. After prolonged training, this reward seeking behavior turns to a habit and may persist in the absence of any reward (Balleine and Dickinson, 1998; Malkki et al., 2011). Behavioral perseveration and inflexibility are symptomatic of human psychiatric conditions such as schizophrenia or obsessive-compulsive disorder (OCD), whereupon anxiety is coupled to carrying out non-functional rituals and habits (Elliott et al., 1995; Luuk, 2009; Malkki et al., 2011; Veale et al., 1996). It is interesting to note that the compulsive behavior in OCD is attenuated by administering a particular class of antidepressants – the selective serotonin reuptake inhibitors (SSRIs), but not tricyclic antidepressants or anxiolytic drugs. This anecdotal finding has bolstered the serotonin hypothesis of OCD. In models of addiction, the drug seeking behavior may persist even when there is a negative reinforcer, i.e. punishment (Latagliata et al., 2010; Vanderschuren and Everitt, 2004). Perseveration can be detrimental for adaptive behavior in real life circumstances such as foraging. In other words, extinction of instrumental responses is necessary to adapt well to the changing environment that rewards a new strategy as well as to avoid the cost of an unrewarded action. Due to the transition of the goal directed behavior to a compulsive habit-like behavior, animals take several trials before they are able to extinguish the unrewarded response completely (Malkki et al., 2011).

Extinction in rodents has mostly been studied in the context of fear conditioning and conditioned taste aversion (Crabbe et al., 1982; Ingram, 1982; Santini et al., 2008). It has been established that extinction does not involve deletion or removal of earlier memory, but instead is a new memory itself. Like other forms of learning, extinction occurs in three phases: acquisition, consolidation and retrieval (Malkki et al., 2011). Extinction is distributed across different structures in the brain. Acquisition of extinction is the initial phase during which conditioned responses decline within an extinction training session. The second phase is consolidation of extinction, which happens over several hours and involves molecular and physiological processes that stabilize the long-term memory of extinction. Finally, presenting the extinguished conditioned stimulus elicits retrieval of extinction, manifested in low levels of conditioned responding. These different phases and components of extinction are distributed across a network of structures. For instance, in the case of extinction of fear memory, the amygdala is involved in fear expression whereas plasticity in the hippocampus and prefrontal cortex are implicated in contextual modulation and consolidation of the fear extinction memory (Quirk et al., 2007). Within the prefrontal cortex, ventromedial PFC, mainly infralimbic cortex, has been shown by microinfusion experiments to play an important role in extinction of fear conditioning in rats (Santini et al., 2008).

An established learning paradigm for evaluating the behavioral flexibility is reversal learning, which involves an intra- or extra-dimensional shift of strategy (Gourley et al., 2010). In other words, mice have to extinguish a previously reinforced action and learn a new action that is associated with reward. Reversal learning requires updating action-outcome associations.

Previous lesion studies in rodents have shown that lateral orbitofrontal cortex (lOFC) is important for reversal learning whereas prelimbic cortex is not necessary for the intradimensional shift in strategy (Gourley et al., 2009; Gourley et al., 2010). Extradimensional shift in strategy, which involves cross-modal switch in stimulus-outcome associations, however, have been shown to depend on medial PFC in rat studies (Veale et al., 1996).

Most functional studies of rodent operant conditioning behavior have been carried out by microinfusing the defined subregion within PFC with agents such as protein synthesis inhibitors, NMDA receptor agonists and GABA receptor agonists. While these studies have shed light on the role of PFC in different aspects of learning and memory, the cellular complexity – encompassing various cohorts of pyramidal cells, interneurons, glia, astrocytes, microglia and even blood cells - in the lesioned region makes it very difficult to understand the underlying molecular and cellular correlates of prefrontal cortical function(s). This is the first study to our knowledge on cell type specific deficits in PFC related cognitive function of mice. We have used the three-choice operant conditioning module to train mice for acquisition, consolidation, reversal and extinction of appetitive instrumental responses.

5.13.3 Three-choice operant conditioning

Cohorts of Wfs1 CxKO mice and their wildtype littermates were trained in the operant/ instrumental action-outcome associations. Since food is used as reinforcer in the appetitive operant conditioning paradigm, mice were food restricted to ~85% of their *ad libitum* body weight and maintained at that body weight for the duration of the experiment (about 20 days). The operant conditioning box consists of three nose poke apertures on one side of the wall and

the food magazine, where the food is dispensed, at the opposite side. Mice were initially trained to associate the food magazine with the food reward, followed by a series of 10 training sessions to make the action-outcome associations (acquisition phase). Subsequent to this, the location of the reinforced aperture within the chamber was changed from northeastern to northwestern corner or vice-versa, representing the reversal phase. Mice were required to shift responding to the newly reinforced aperture even though they did not receive any punishment for perseverative responding to the previously reinforced but no longer reinforced aperture. A variable ratio (VR) schedule was used, with no discrete cues for signaling reinforcement delivery since we wanted to avoid Pavlovian form of conditioning that involves stimulus-outcome associations. The reversal learning was carried out for 5 days and the perseverative responses at the previously reinforced aperture as well as the adaptation to the newly rewarded aperture were evaluated to infer behavioral flexibility in the knockout mice. Finally, the last phase of the behavioral training involved extinction of the learned associations between action and outcome (reinforcer). In this phase, all three apertures in the operant conditioning chamber were inert and did not associate with delivery of the reinforcer. Mice have to learn to inhibit their responses at previously reinforced apertures and the food magazine and evaluate the behavioral cost of their actions, which are no longer associated with any outcome. The extinction sessions are carried out for 5 days at the same time every day for 25 min. Immediately following extinction session (any operant conditioning session), mice are returned to their home cage and provided rodent chow for 90 min, in order to maintain their optimal body weight (~85%) for the experiment. Over many repeated sessions of operant conditioning, it is reasonable to assume that mice will build an expectation of receiving food in the home cage after the experimental session is over. During extinction, mice will have to make the decision to withhold their responses at the apertures

which are no longer rewarded and save their energy for foraging in anticipation of the food that will be provided to them in their home cage post session.

RESULTS

5.13.3 Acquisition of instrumental response

During initial acquisition phase, that lasted for 12 days, both Wfs1 CxKO mice and their wildtype littermates started out responding almost nil to the reinforced nosepoke but gradually learned to make the association of active nosepokes to reinforcer. Hence, both groups of mice increased responding with a steep slope until day 6 and then their responses increased with a lower slope until day 12 (Fig 5.10). Thus both groups of mice had a significant increase in responding with time $F(1, 18) = 50.5$; $p < 0.0001$. They did not differ however by genotype in terms of increase in instrumental response $F(1,18) = 3.01$; $p = 0.0997$ and the time X genotype interaction was also not significant $F(1,18) = 1.07$; $p = 0.384$. Both groups of mice responded negligibly at the inactive nosepokes, which indicated that the mice were able to discriminate the reinforced aperture and were not just being hyperactive. In terms of magazine entries, both groups of mice exhibited high level of entries or beam-breaks at the magazine, since they were already magazine trained before the start of the acquisition phase. The magazine entries for both groups increased over time, as they got more motivated to retrieve the reinforcers; $F(1,18) = 1.96$, $p = 0.0417$, but they did not differ in magazine entries by genotype; $F(1,18) = 0.599$, $p = 0452$. The quantity of reinforcers delivered in response to correct nosepokes followed the pattern mirroring active nosepokes. There was a steady increase in rewarded pellets over time in both groups; $F(1,18) = 39.31$, $p < 0.0001$ but there was no significant effect of genotype; $F(1,18) = 0.335$, $p = 0.572$. These results indicate that both Wfs1 CxKO and wildtype mice learned to

make action-outcome associations and also that the cortex specific deletion of Wfs1 does not interfere with the learning ability of mice at the acquisition phase.

5.13.4 Reversal of learned instrumental response

The action-outcomes were reversed to new aperture within a single session 5 min into the session. We found that both groups of mice learned to shift to a new strategy very quickly – by day 2, they were responding to the newly active aperture at high levels similar to the acquisition phase. There was a small effect of time on the active nose pokes $F(1,18) = 3.832$, $p = 0.0566$) but no effect of genotype. The perseverative responses were evaluated by looking at number of responses to the previously reinforced aperture. Perseveration was significantly reduced after day 1 in both groups and decreased steeply to zero from day 2 to 5 (Fig 5.11); time: $F(1,18) = 16.95$, $p < 0.0001$. The two groups did not differ from each other in inactive nosepokes by genotype; $F(1,18) = 0.580$, $p = 0456$. Magazine entries for both groups were high on day 1 of reversal and reduced slightly and plateaued from day 2 to 5 (Fig 5.11), the difference by genotype is not significant. The reinforcers obtained by the mice follows a similar trend as active nosepokes, starting at low levels on day 1 and quickly rising to high levels on day 2 after which they plateau (Fig 5.11); time $F(1,18) = 17.25$, $p < 0.0001$. There is no difference in reinforcers by genotype. These results indicate that Wfs1 CxKO and wildtype mice were both able to reverse and adapt their behavior to the new intra-dimensional shift in strategy.

5.13.5 Extinction of learned Instrumental response

Subsequent to reversal learning, mice were tested in a different reinforcement schedule based on a progressive ratio (PR) of 5. This reinforcement schedule is a test for motivational aspects of learning, whereupon the mouse has to progressively multiplicate nosepokes at the correct aperture to get the same reward. In our experiment, we used a PR schedule of 5, so the mice had to perform 5 nosepokes for the first food pellet, 10 for the next, 15 for the following and so on. The Wfs1 CxKO and wildtype mice did not display any difference in breakpoint ratio (BR) (data not shown). BR is the schedule ratio when the mouse terminates responding to the active nosepoke because of high cost of the reward.

Following the PR schedule of reinforcement, mice were subjected to extinction of learned instrumental response (Fig 5.12). All the three apertures (center, left and right) did not have any value to them, as in nosepoke action at any of the three apertures did not entail an outcome i.e. the food reinforcer. We found that the Wfs1 CxKO and wildtype controls are both able to reduce their response at the previously reinforced aperture gradually over the days (time: $F(1,18) = 50.31$, $p < 0.0001$). These two groups however do not differ in the trend of their decreasing response at the active nosepoke by genotype. ($F(1,18) = 1.689$, $p = 0.661$) and there is no significant interaction between time and genotype ($F(1,18) = 1.689$, $p = 0.162$).

Surprisingly, even though Wfs1 CxKO mice were able to inhibit responses at the nosepoke that was previously active, they exhibited a strong compulsive responding behavior at the food magazine, in anticipation of the reinforcer. The start at the same low level as wildtype in the number of entries they make to the magazine but from day 2, they diverge out radically. The

wildtype controls maintain low level responding at the magazine throughout the experimental sessions over 5 days, whereas the KO mice significantly increase responding at the magazine (Fig 5.12). Over time, the magazine entries gradually decreased but the difference between wildtype controls and KO mice are still significant (time: $F(1,18) = 2.252$, $p = 0.0731$, genotype: $F(1,18) = 11.67$, $p = 0.0035$, Interaction (time x genotype): $F(1,18) = 5.030$, $p = 0.0014$). Bonferroni post hoc test for multiple comparisons revealed that when individual data points were analyzed, significant differences between KO and Control mice were evident for day 2 ($p < 0.0001$) and day 3 ($p < 0.01$). These results indicate that the Wfs1 CxKO mice have deficits in inhibiting their habitual behavior of making magazine entries despite the lack of reinforcers.

5.14 Summary of Behavioral Research on Wfs1 Cortex KO

Our behavioral studies reveal that the intersectional strategy of using Emx1-Cre to delete Wfs1 gene from cortical pyramidal cells allows us to delineate cell type specific contribution to PFC function. By restricting Wfs1 deletion to neocortex, we are able to avoid complicating behavioral phenotype that would result from malfunctioning of the amygdala, hypothalamus, brain stem and striatum. In addition, Wfs1 is widely expressed outside of CNS such as cochlea, optic nerve and pancreatic B cells, and especially the B cells are vulnerable to Wfs1 deletion and undergo apoptosis in its absence. Our approach thus circumvents the multiplexity of phenotype seen in constitutive null of Wfs1 gene. We showed that Wfs1 cortex KO mice had normal appearance, body weight and fertility, and did not exhibit symptoms of diabetes. We found that the KO mice were hypoactive in the open field tests, but this hypoactivity was absent when the mice were under stress and food-restricted. The hypoactivity was not a result of deficit in motor

coordination and balance, since the KO mice performed just as well as the wildtype controls in the accelerating rotarod test. Because of the baseline hypoactivity, we could not test the mice in the established immobility based tests for depression such as tail suspension test and forced swimming test. We however assayed another prominent feature of depression – anhedonia – using sucrose preference test and found that the KO mice were anhedonic and did not display a preference for sucrose as wildtype controls do. Anxiety is sometimes comorbid with depression, and constitutive null mutant of Wfs1 was shown by other researchers to exhibit anxiety related behavior, hence we tested the Wfs1 cortex KO mice for anxiety in a series of tests including light-dark transition test, elevated plus maze test and novelty induced food suppression test. The Wfs1 cortex KO mice did not have any anxiety phenotype as revealed by all three assays. These results indicate that the anxiety phenotype in the constitutive Wfs1 KO was due to amygdalar deletion of the gene, and since it is not affected in the Wfs1 cortex KO, these mice do not display anxiety like behavior.

The Wfs1 cortex KO mice were tested for cognitive function in appetitive operant conditioning paradigm. The KO mice performed just as well as the wildtype control in the acquisition and reversal phases, indicating that they had intact goal directed behavior and could make action-outcome associations. However, the KOs had persistent compulsive response at the magazine where they made elevated responses after the reinforcer was dissociated from the magazine. This indicates that the Wfs1 cortex KO mice might model an aspect of obsessive-compulsive disorder (OCD). One of the most salient features of OCD is its selective response to treatment with SSRIs that led to the serotonin hypothesis of OCD. Thus for future research, it would be informative to treat the mice with the SSRI and evaluate whether the compulsive

magazine entries are attenuated. Additionally, since the KOs exhibit the anhedonia aspect of depression, we can test the effectiveness of the SSRIs in relieving anhedonia, and it is possible that the SSRIs might also help with the hypoactivity displayed by the KOs. Depression has been frequently comorbid with OCD, so it is possible that our Wfs1 cortex KO is a case of comorbid depression and OCD.

5.15 Candidate Molecular Players underlying the Pathophysiology in Wfs1 Cortex KO mice

Molecules define the function and pathophysiology of cell types in the brain. Hence we wanted to investigate molecular players that are either implicated in prior literature by association with WFS1 or are coexpressed in the Wfs1 cell type as revealed by the cortex TRAP data for Wfs1 Cre-ERT2/ EF1alpha-TRAP. Figure 5.13 has the list of shortlisted candidates that could have relevance to the cortical pathophysiology and behavioral phenotype of the Wfs1 cortex KO mice. Briefly, we made a list of following candidate molecules that were enriched in the TRAP data and coexpressed by digital expression data (ISH and GENSAT): Ntf3 (Pae et al., 2008), Nts (Cervo et al., 1992) and Penk (Kung et al., 2010), all three of which are also implicated in depression and anxiety. We selected Bdnf, a known protein implicated in depression, that is also highly enriched in the Wfs1 cortex TRAP data (Warner-Schmidt et al.). Other molecules include GABA receptors GABARa1 and GABARa2, that have been known to be regulated by Wfs1 and are implicated in anxiety (Raud et al., 2009) and Carboxypeptidase (Cpe) the known interactor of Wfs1. Finally, since Wfs1 is an ER bound protein known to play a role in ER Stress, we picked candidates such as Atp1b1 (Zatyka et al., 2008), Bip (Bown et al.,

2002), Atf6alpha, Grp94, Hrd1 (Fonseca et al.), IRE1alpha and PERK (Kakiuchi et al., 2009), all known ER stress markers that have been shown to be regulated by Wfs1. Among these proteins, Cpe and Atp1b1 are the only two proteins that have been shown to interact directly with Wfs1. In the case of carboxypeptidase (Cpe1), it has been shown to interact with Wfs1 *in vivo* (Hiebsch 2006).

Based on the expression pattern, Penk1 and Ntf3 are two candidates to have high likelihood in being involved in the cortical pathophysiology of Wolfram Syndrome (Fig 5.14). The co-expression of Penk1 and Wfs1 is inferred from the digital ISH images at Allen Brain Atlas whereas the evidence for coexpression of Ntf3 and Wfs1 is direct from Wfs1 immunostaining results for the Ntf3 TRAP line(s). However, coexpression does not mean that the genes are also coregulated. Based on prior literature, Bdnf is a good candidate for depressive phenotype in Wfs1 cortex KO.

Understanding the pathophysiology of depression is difficult due to heterogeneity in syndromes and etiological diversity. About 1 in 6 individuals in the US is diagnosed with clinical depression during their lifetime (Krishnan 2008). Core symptoms of depression include anhedonia, difficulty in concentrating and abnormalities in appetite and sleep. It is interesting that depressed patients have an increased risk for coronary artery disease and type 2 diabetes. One of the defining clinical symptoms of Wolfram Syndrome is diabetes mellitus. Brain derived Neurotrophic Factor (BDNF) has been extensively studied in the context of depression. BDNF is expressed widely in the limbic structures and while BDNF in hippocampus is associated with anti-depressant effects, it has the opposite pro-depressant effect when infused into the ventral

tegmental area – nucleus accumbens (VTA-NAC). So while BDNF-mediate signaling is involved in neuroplastic responses to stress and antidepressants, these effects are both region-specific and antidepressant specific and function in the background of other potent genetic and environmental modifiers (Krishnan and Nestler, 2008). BDNF enrichment in the Wfs1 cell type indicates its potential role in contributing to the depressive phenotype in Wfs1 cortex KO mice. Another neurotrophic factor, Ntf3, has also been implicated in depression. Exposure to long term immobilization stress increases Ntf3 levels in the hippocampus (Nickl-Jockschat and Michel).

Penk1, the precursor for enkephalins, is also highly enriched in the Wfs1 cell type and is expressed by layer II pyramidal cells in the neocortex. Enkephalins are endogenous opioid peptides that are thought to be vital in regulating many physiological functions, including pain perception and analgesia, response to stress, aggression and dominance (Konig et al., 1996). Penk1 KO mice have altered supraspinal pain responses even though the spinal level responses are intact. As demonstrated in Chapter 4, focal silencing of Wfs1 cell type in the ACC led to deficits in affective pain response, while keeping the physiological pain sensation intact. Even though the cellular phenotype would be stronger by silencing neurotransmission than deleting Wfs1 gene, it is possible that we may get the same affective pain phenotype with Wfs1 cortex KO mice. In addition, Wfs1 has been shown to interact directly with carboxypeptidase e, which is an enkephalin convertase enzyme that converts proenkephalin to enkephalin by cleaving the end amino acid residue. We have thus hypothesized that either of the following two models are possible in the context of Wfs1 cell type (Fig 5.15). In the first model, we propose that in control animals, Wfs1 binds to Cpe and makes it enzymatically active in the conversion of Penk1 to its mature peptides Leu-Enkephalin and Met-Enkephalin. Thus in Wfs1 KO cells, in the absence of

Wfs1 Cpe is not as efficient in converting Penk1 to the enkephalins, leading to an increase in the cellular concentration of Penk1 and depletion of the Enkephalins. This reduction in levels of Enkephalins in the cortex might lead to deficits in pain perception and related symptoms. In the second model, we propose that in default state, Wfs1 binds and sequesters Cpe inhibiting its enzymatic action hence Wfs1 downregulates the conversion of Penk1 to its mature peptides. In the absence of Wfs1, Cpe is disinhibited and facilitates the conversion of Penk1 to Enkephalins. In this case, Wfs1 cortex KO mice would have a decreased pool of Penk1 and increased pool of the mature Enkephalins. In order to test which of these two models holds true, we plan to run a Western blot assay of the cortical tissue extracts of Wfs1 KO mice and the wildtype controls. Using antibody against the enkephalins, we should be able to detect the change in the relative ratio of Penk1:Enkephalins in the two conditions.

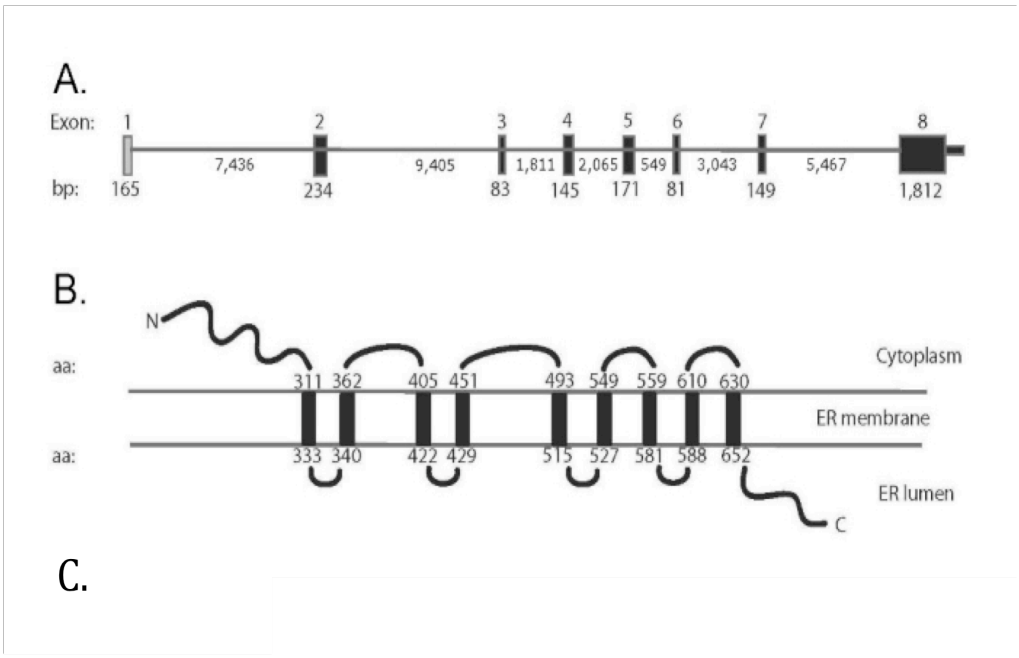

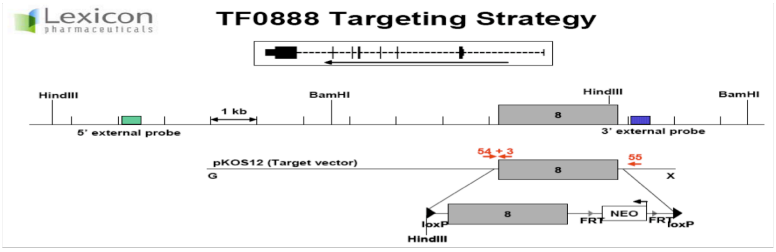

Figure 5.1: Structure of Wolframin (Wfs1) gene/protein and targeting strategy. The Wfs1 gene (A) is composed of 8 exons spanning about 30 kb of genomic DNA. The Wfs1 transcript is approx. 3.6 kb long with the translation start site located in the beginning of second exon. The WFS1protein (B) is composed of 890 amino acids, with 9-10 transmembrane domains, with which WFS1 is anchored in the ER membrane. The Wfs1 targeting vector for generating conditional allele of Wfs1 consists of loxP sites flanking the 8th exon, which was recombined into the ES cells and screened for Neomycin resistance. The recombined ES cells were screened and implanted into blastocysts of 129sv mice.

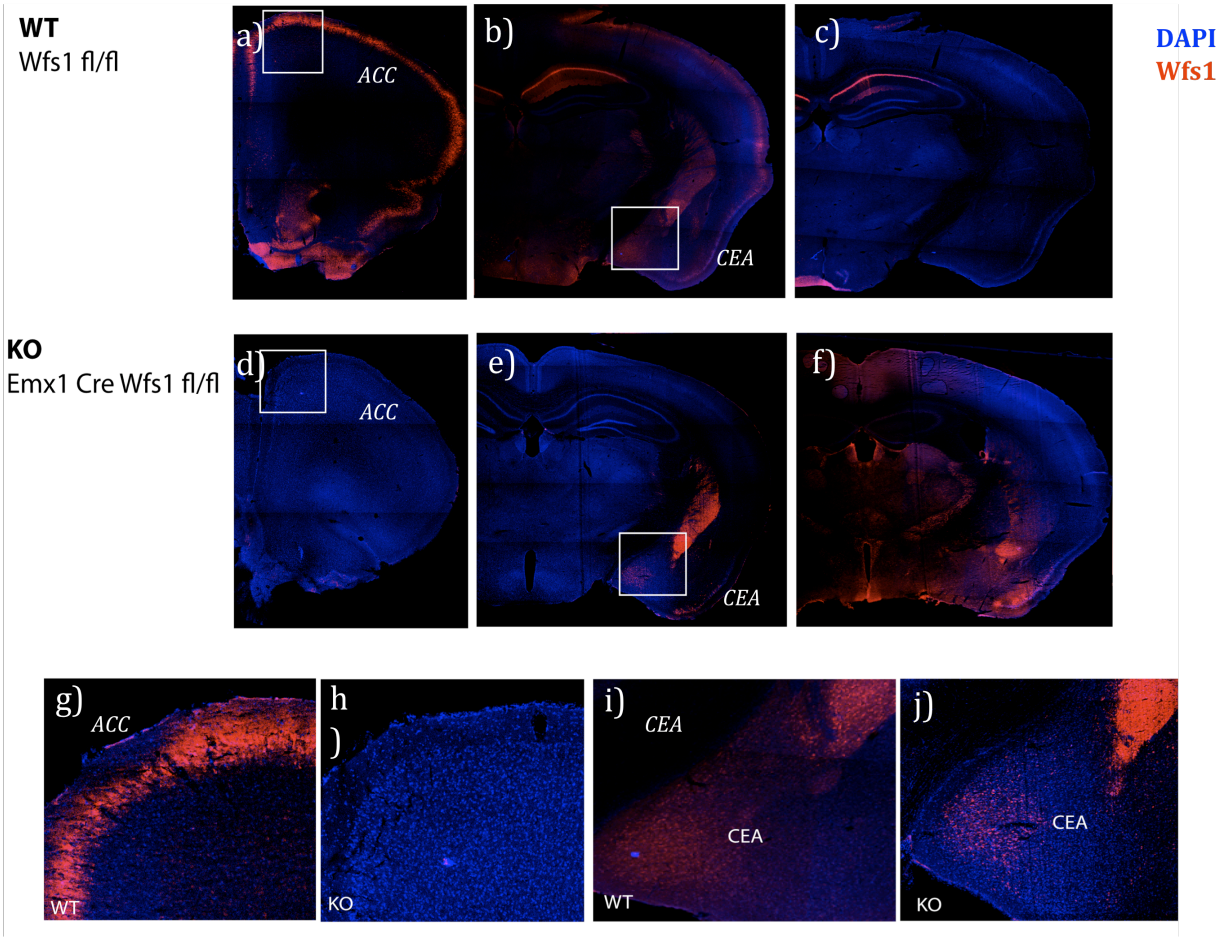

Figure 5.2: Histology of Wfs1 cortex KO and wildtype mice. IHC with Wfs1 antibody and DAPI nuclear counterstain reveals restricted expression of WFS1 protein in superficial layer 2 of neocortex with high rostral low caudal gradient (a, b, c; enlarged inset in a: g). Subcortical expression in wildtype mice is detected in olfactory bulb (a), central extended amygdala (CEA: b; enlarged inset: i) and CA1 (c). Emx1 Cre+/-/ Wfs1 fl/fl mice, the Wfs1 cortex KO, completely lacks the cortical expression of Wfs1 (d, e, f; enlarged inset: h). However subcortical expression of Wfs1 in striatum (f) and amygdala (CEA: e; enlarged inset: i) are preserved in the KO mice.

a) Order of Behavioral Tests

Behavioral Test	Behavior Assessed	Number in Order
Open Field	Spontaneous locomotion, Anxiety	1
Light-Dark Transition	Anxiety	2
Elevated Plus Maze	Anxiety	3
Hyponeophagia	Anxiety	3
Sucrose Preference Test	Anhedonia (Depression)	3
Rotarod	Motor Coordination	4
	, Perseverance, Extinction	4

b)

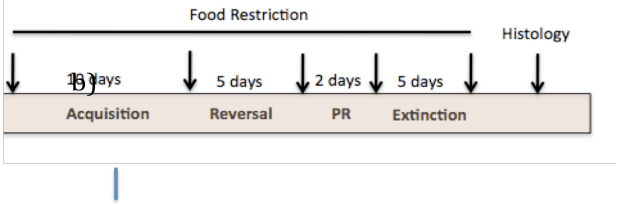

c)

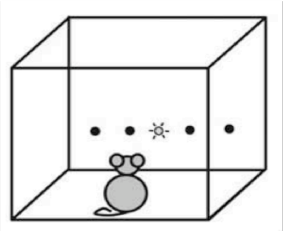

Figure 5.3: Order of behavioral tests for Wfs1 cortex KO mice. (a) The behavioral tests for the Wfs1 cortex KO mice and their wildtype littermates were undertaken in the chronological order of least stressful to more stressful tests. (b) Operant conditioning paradigm involved initial magazine training followed with 10 days of acquisition of instrumental response. After acquisition, animals underwent reversal learning where the value of the aperture was switched for 5 days followed by 2 days of progressive ratio responding. Finally 5 days were allotted for extinguishing the response (extinction) before mice were analyzed for histology. The operant conditioning chamber contains three apertures or nosepokes at one wall and the food magazine at the opposite wall.

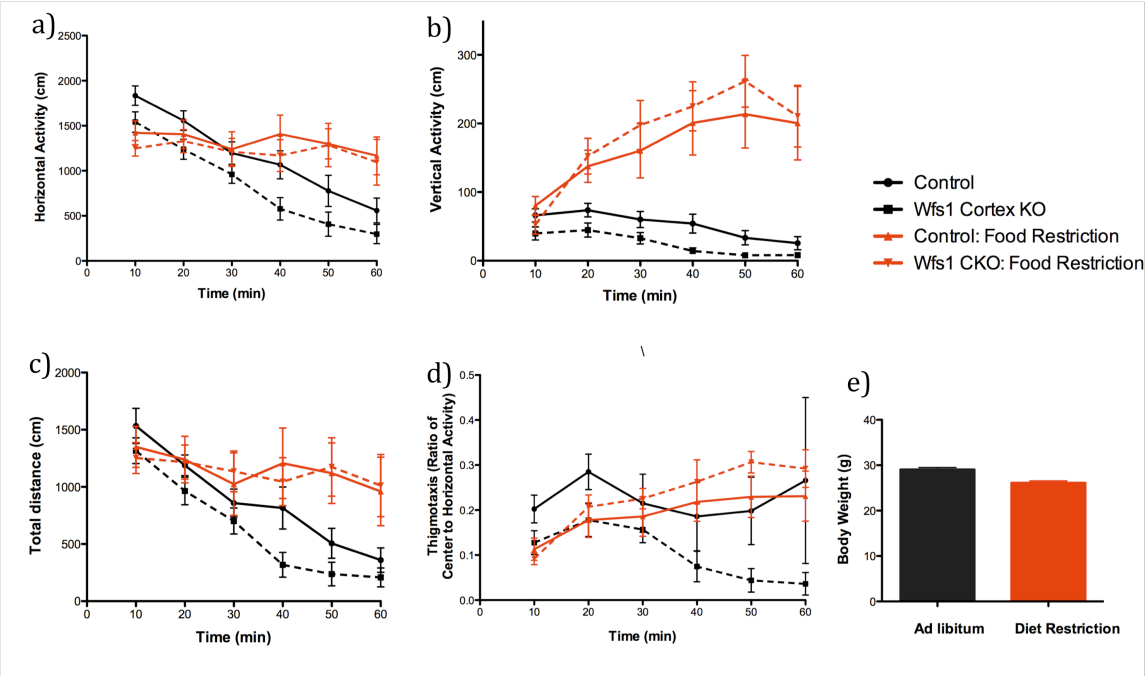

Figure 5.4: Spontaneous locomotion of Wfs1 cortex KO mice before and after food restriction. The KO mice (black dotted line) are significantly hypoactive compared to wildtypes (black solid line) in measures of horizontal activity (a) (RM ANOVA: $F(1,19) = 4.57$, $p = 0.047$) and vertical activity (b) (RM ANOVA: $F(1,19) = 6.342$, $p = 0.022$) but the total distance was not different. Thigmotaxis was not significantly different between KO and WT (d). Under conditions of food restriction KOs and WTs did not differ from each other in all measures of activity (KO: red dotted line, WT: red solid line). The KO mice were food restricted to 85% of their *ad libitum* body weight (e).

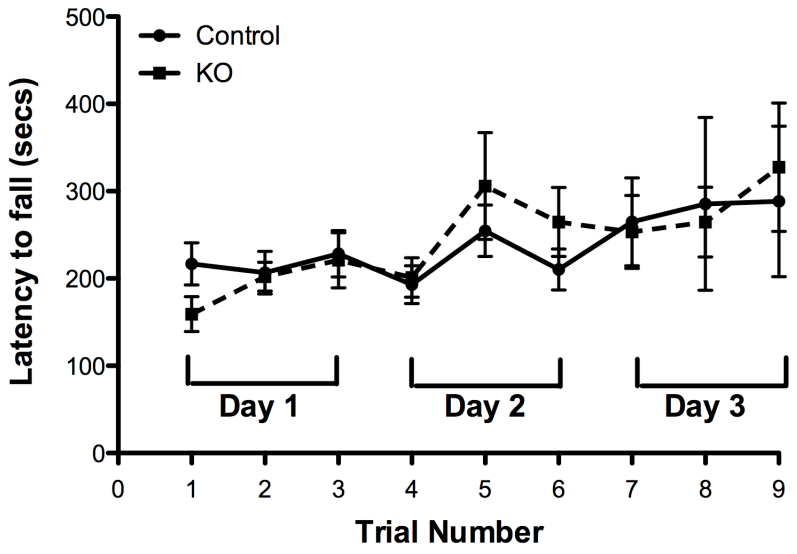

Figure 5.5: Motor coordination and balance in Wfs1 cortex KO mice. Two way RM ANOVA reveals no significant difference between the KO and WT mice in accelerating rotarod tested for 3 consecutive days with 3 sessions per day.

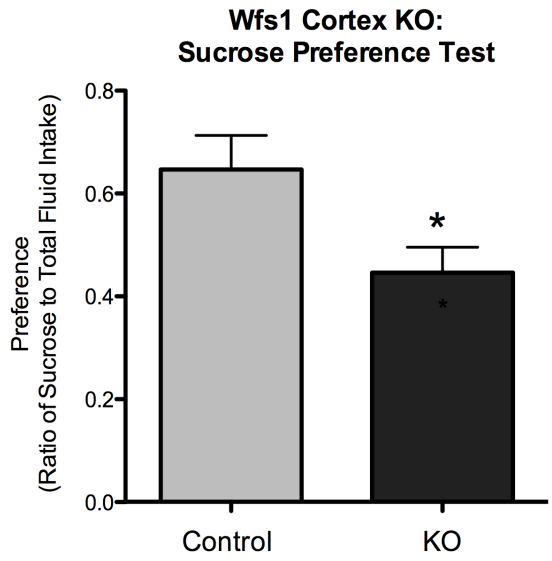

Figure 5.6: Anhedonia in Wfs1 cortex KO mice. There is significant decrease in sucrose preference (ratio of sucrose to total fluid intake) of the KO mice (Mean±SEM = 0.447±0.049, N=9) compared to the WT controls (Mean±SEM = 0.647±0.066, N=7). Two tailed ttest: p = 0.0265, t = 2.479, df = 14

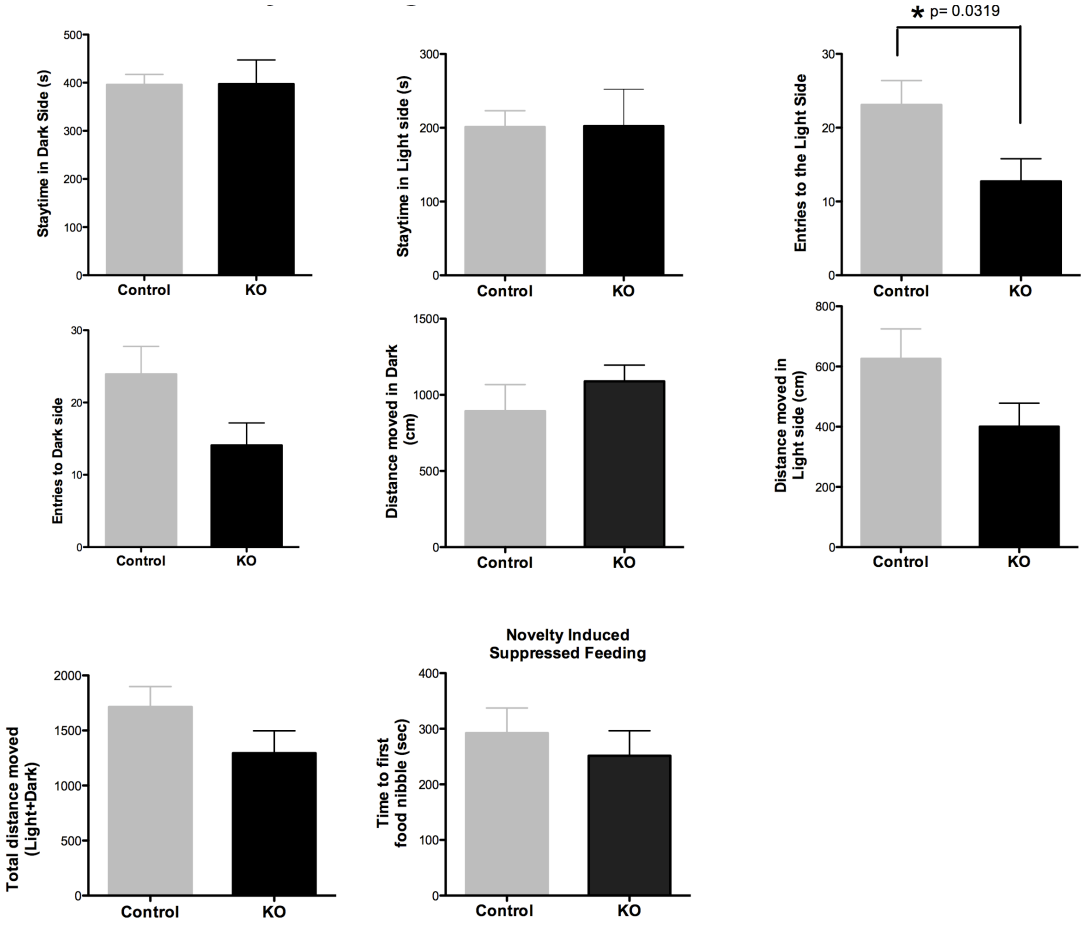

Figure 5.7: Light:Dark Transition test for Wfs1 cortex KO. The KO and WT control mice did not differ from each other in most parameters of the test including staytimes in dark side and light side, entries to the dark side, distance moved in dark side and light side and total distance moved. KO mice make significantly fewer entries to the light side compared to WT controls (unpaired Two tailed ttest: t=2.306, df = 20, p =0.0319), which can be attributed to hypoactivity.

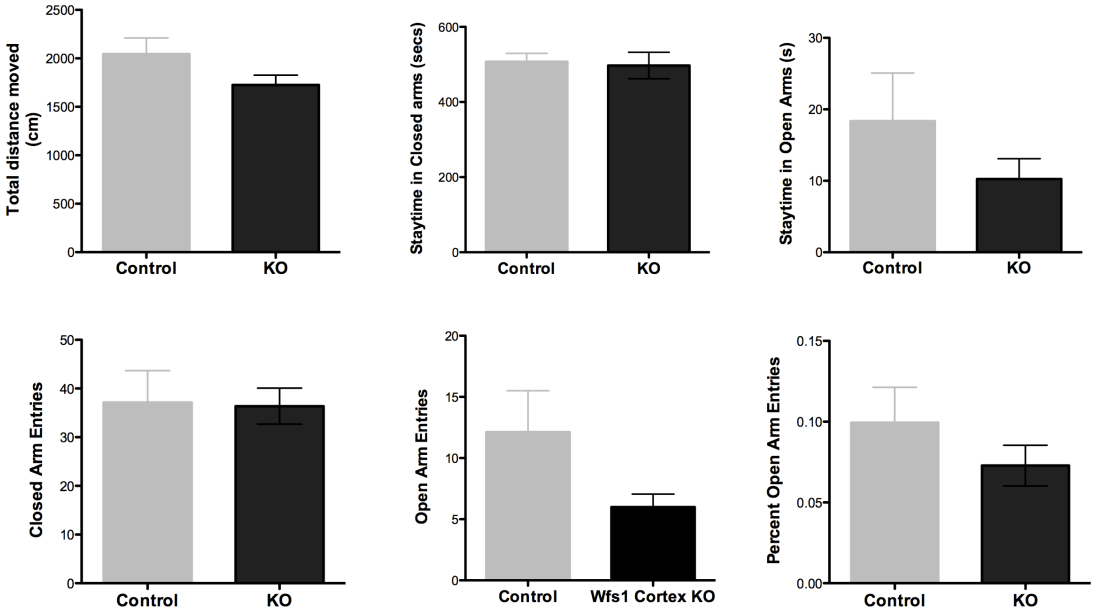

Figure 5.8: Elevated plus maze performance in Wfs1 cortex KO. The KO and WT control groups did not significantly differ in any parameters measured in this test such as: total distance moved, staytime in closed arms, staytime in open arms, closed arm entries, open arm entries and percent open arm entries.

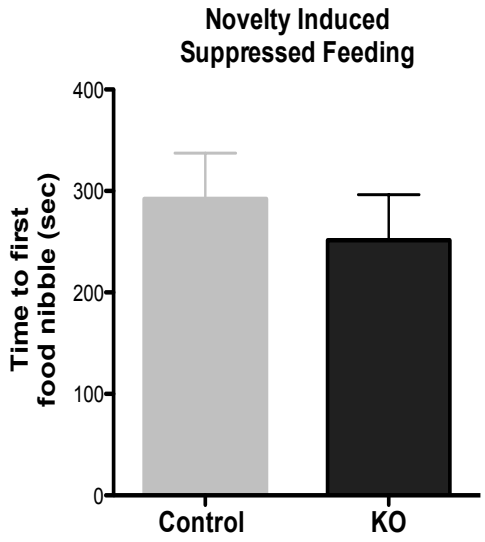

Figure 5.9: Hyponeophagia test in Wfs1 cortex KO. The KOs and WT controls do not significantly differ from each other in latency to nibble the food pellet placed in the central quadrant of open arena.

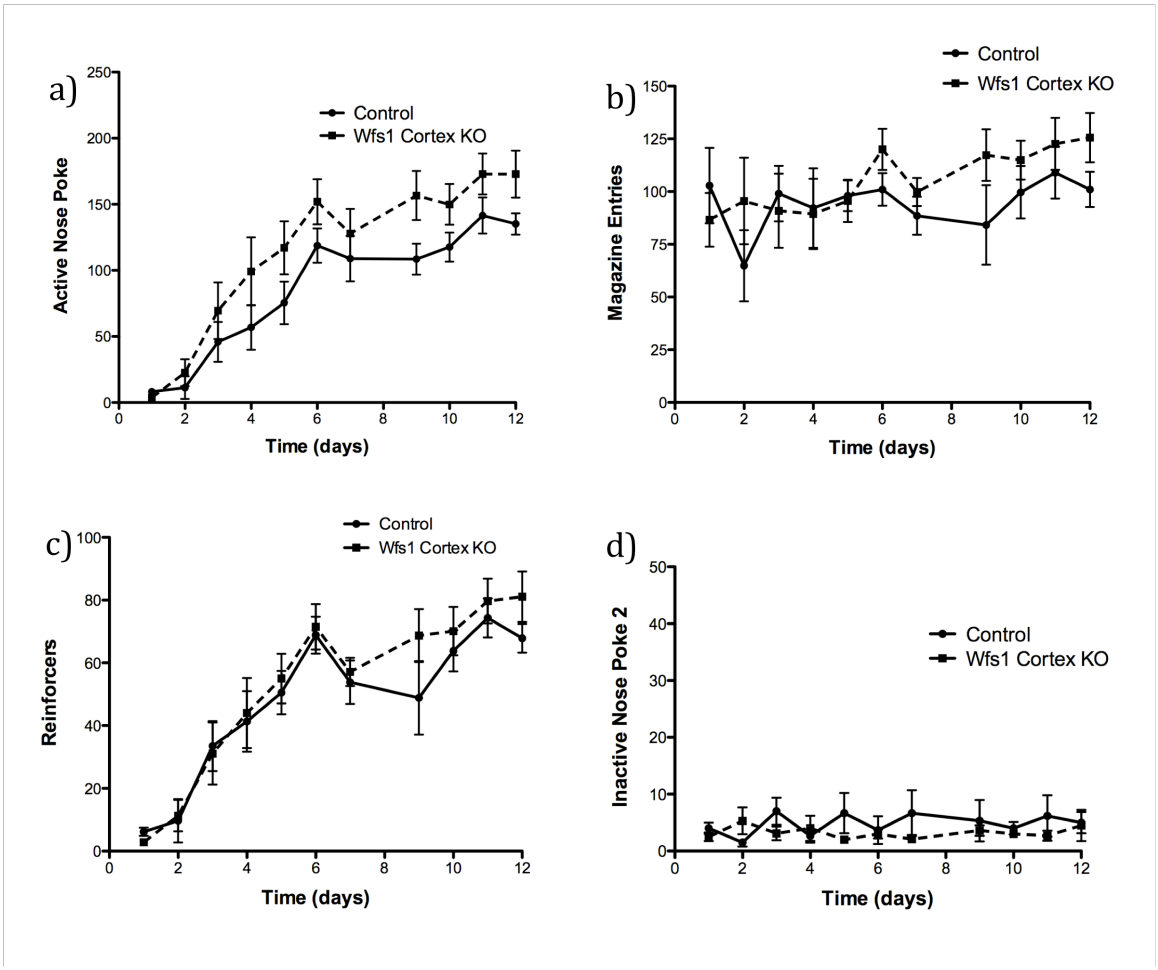

Figure 5.10: Acquisition of instrumental response in Wfs1 cortex KO. During 12 days of acquisition (a), KO and WT mice both gradually learn to make the action-outcome associations with a significant increase in responding at the active nosepoke with time ($F(1, 18) = 50.5$; $p < 0.0001$). There is however no effect of genotype on active nosepoke (a), magazine entries (b), reinforcers (c) and inactive nosepokes (d). N=10

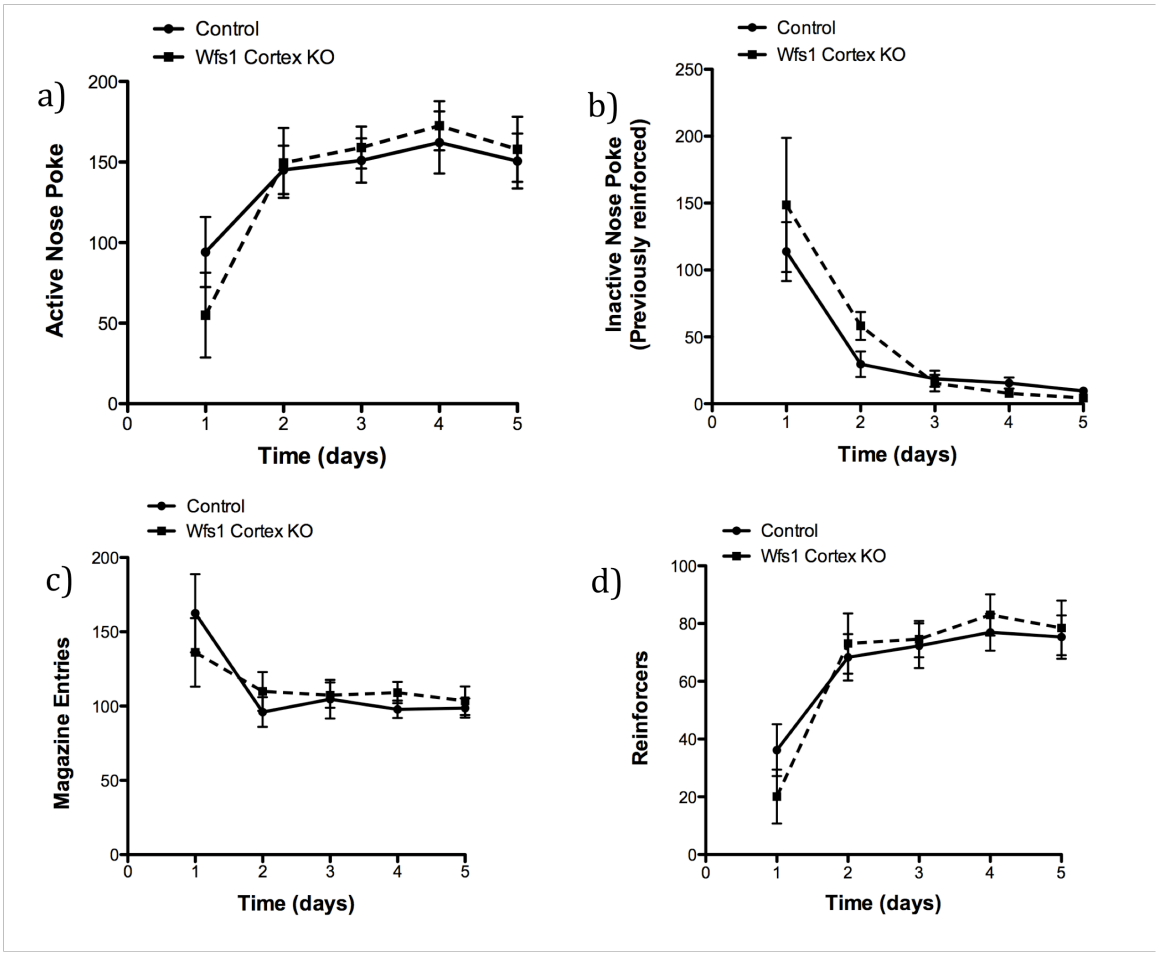

Figure 5.11: Reversal of instrumental response in Wfs1 cortex KO. Following acquisition, the action-outcome was reversed to a new aperture within a single session 5 min after the start. There was a small, but not significant, effect of time on active nosepoke responses $F(1,18) = 3.832$, $p = 0.0566$). The KO and WT groups do not differ from each other in active nosepokes (a), nosepokes at previously reinforced nosepoke (b), magazine entries (c) and reinforcers (d).

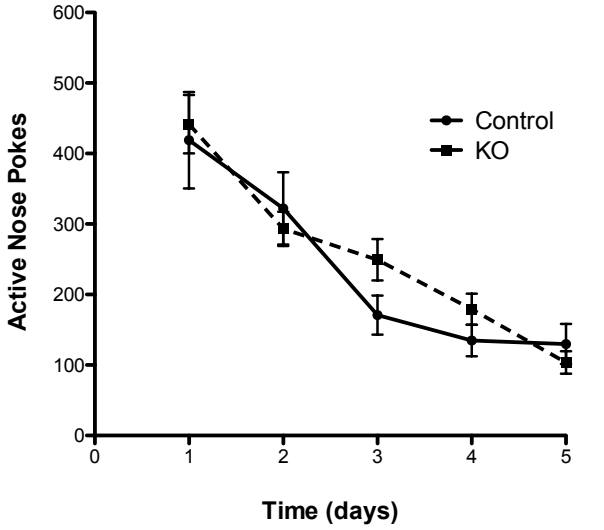

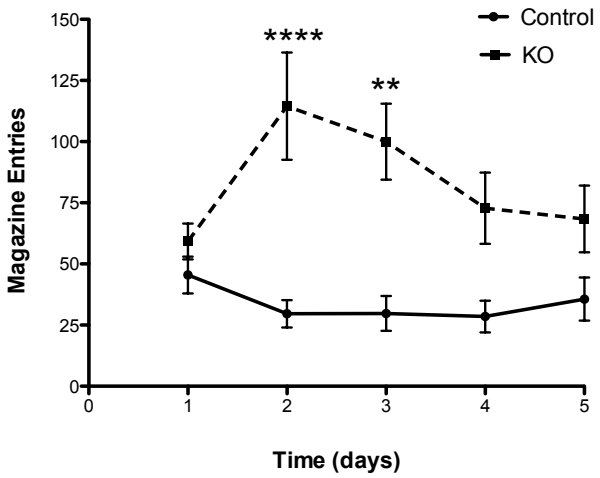

Figure 5.12: Extinction of previously reinforced instrumental response in Wfs1 cortex KO. During 5 days of extinction following reversal, both KO and WT control mice are able to reduce their responses at the previously reinforced 'active' nosepoke significantly over time: $F(1,18) = 50.31$, $p < 0.0001$ (a), but there was no effect of genotype. However, the KO exhibit a strong compulsive response at the magazine whereas the WT mice plateau for magazine entries throughout the phase. Genotype has a significant effect on magazine entries ($F(1,18) = 50.31$, $p < 0.0001$) and the interaction of timeXgenotype is also significant $F(1,18) = 5.030$, $p = 0.0014$). N=10

Gene ID	Coexpression (TRAP)	Coexpression (Anatomy)	Direct Interaction	Regulation by Wfs1	Depression/ Anxiety	ER Stress	Gene Description	Reference
Ntf3							neurotrophic factor 3	TRAP, ABA, GENSAT, Pae 2008
Bdnf							brain derived nerve growth factor	TRAP data, Warner-Schmidt 2010
Nts							neurotensin	TRAP, GENSAT, Cervo 1992
Penk							proenkephalin	TRAP data, ABA, Kung 2010
GABARα1							GABA (A) receptor α 1	Raud 2009
GABARα2							GABA (A) receptor α 2	Raud 2009
Cpe							carboxypeptidase E	Hiebsch 2006
Atp1b1							ATPase Beta 1	Zatyaka 2007
Bip							heat shock protein 5	TRAP data, Bown 2002
Atf6α							acting transcription factor 6 α	Fonesca 2010
Grp94							glucose regulated protein 94	Bown 2002
Hrd1							synovial apoptosis inhibitor 1, synoviolin	Fonesca 2010
IRE1α							endoplasmic reticulum (ER) to nucleus signalling 1	Kakiuchi 2009
PERK							eukaryotic translation initiation factor 2 alpha kinase 3	Kakiuchi 2009

Figure 5.13: Candidate molecules for Wolfram syndrome cortical phenotype. Prior literature, TRAP data for Wfs1 in cortex, and existing gene expression databases such as Allen Brain Atlas ISH database and GENSAT were consulted to shortlist candidates with potential role in contributing to Wfs1 cortex KO phenotype related to depression and deficit in cognition.

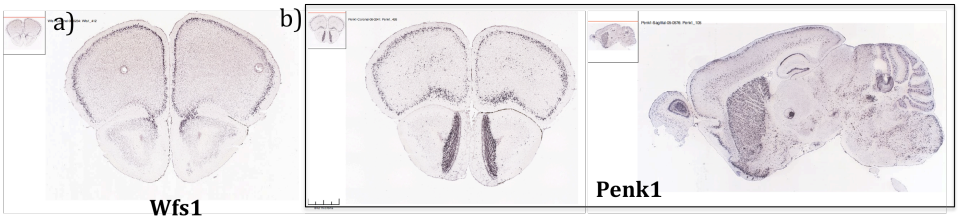

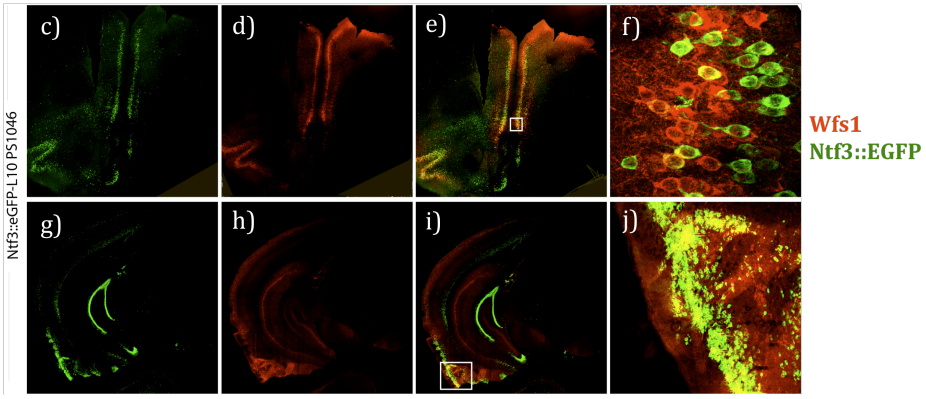

Figure 5.14: Candidate genes with relevant expression pattern and function: Penk1 and Ntf3. Compared to ISH pattern of Wfs1 (a), Penk1 is also expressed in layer 2 cells in the cortex as Wfs1, even though Penk1 is not as specific as Wfs1 to layer 2 and is also expressed by sparse layer 5 cells in the cortex, and subcortically in striatum (b). Direct evidence is available for coexpression of Ntf3 and Wfs1 since anti-Wfs1 stains EGFP positive pyramidal cells in medial PFC of Ntf3 TRAP line PS1046 (c, d, e; enlarged inset: f) and piriform cortex (i; enlarged inset: j). Interestingly Ntf3 and Wfs1 are expressed in different areas of hippocampus in a nonoverlapping manner (g, h, i).

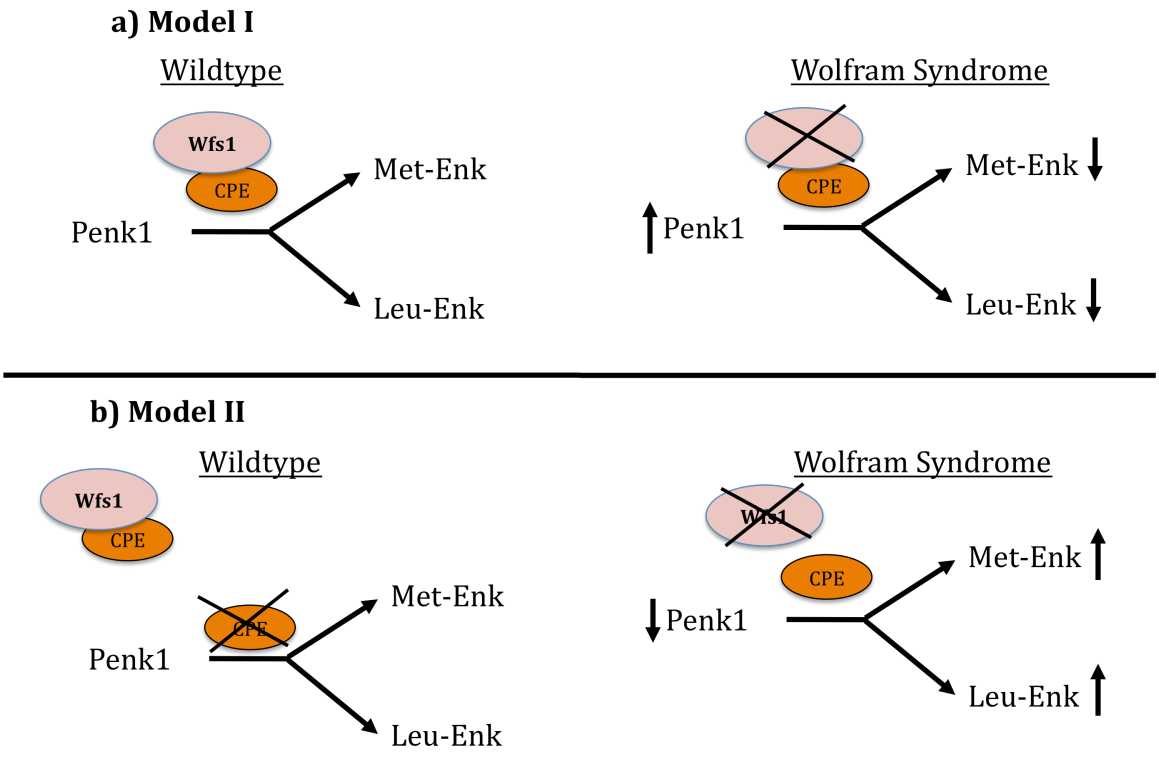

Figure 5.15: Two alternate models for Wfs1 and Carboxypeptidase E (Cpe) interaction. In model 1 (a), Wfs1 binds to Cpe and makes it enzymatically active in converting Penk1 to it mature peptides Leu-enkephalin and Met-enkephalin. In Wolfram syndrome, deletion of Wfs1 leads to reduced rate of Penk1 conversion to its mature peptides thus leading to increased pool of Penk1 and decreased pool of Met-Enk and Leu-Enk. In model (b), Wfs1 binds to Cpe and inhibits the enzymatic activity of Cpe in converting Penk1 to Met-Enk and Leu-Enk. In Wolfram syndrome, Cpe is free to process Penk1 thus leading to increase in pool of Met-Enk and Leu-Enk and Penk1 is depleted.

CONCLUSION

Mammalian neocortex is evolutionarily the most recent albeit also the most complex structure in the brain. Considered the seat of executive function, neocortex subserves diverse higher cognitive processes including decision-making, motor planning, sensory discrimination and memory consolidation. The complexity of neocortical function is paralleled by the inherent cellular heterogeneity. Classical studies of cortical neuroanatomy in the early 1900s established the neuron doctrine, i.e. neuron as the basic element of central nervous system, and also elucidated the diversity of cell types in the neocortex. However it was only in the last decade that significant leaps were made in characterizing cell types within the neocortex, mainly due to advances in genome sequencing and mouse transgenesis.

Large scale brain atlases, such as GENSAT and Allen Brain Atlas, have provided digital access to the pattern of expression of thousands of genes in the CNS, enabling us to screen for structurally annotate genes for further analysis. We used these databases to select candidate drivers for genetically accessing distinct pyramidal cell types in the neocortex. Bacterial artificial chromosomes (BACs) carrying regulatory sequences for these genes were modified by homologous recombination and engineered to incorporate either EGFP tagged ribosomal subunit L10 (EGFP-L10) or Cre recombinase enzyme under the transcriptional control of gene specific promoter. The EGFP-L10 transgene was the basis for the translating ribosome affinity purification (TRAP) strategy developed in our lab. Polysomal pulldown from genetically defined cell types followed by affinity purification of the translating messenger RNAs serve in producing a translational profile of the targeted cell types. We have generated transgenic mice as well as translational profiles of six pyramidal cell types in the neocortex, which are distinguished not only by marker expression, but also areal/laminar topography, hodology and cell morphology;

these cell types are defined by genes: Ntf3, Pdyn, Wfs1, Etv1, Syt6 and Ntsr1 respectively. Among these genes, Ntf3, Pdyn and Wfs1 define cell types in layer 2 of prefrontal cortex, Etv1 defines a cell type in layer 5 of lateral neocortex, whereas Syt6 and Ntsr1 define two different corticothalamic cell types in layer 6 with an opposite gradient of expression along the rostrocaudal gradient.

The initial characterization led to bigger questions pertaining to connectivity, function and global behavioral output. We thus implemented three different strategies to analyze cortical cell types. First, we applied cre-inducible viral transduction of reporter genes to map the circuit of three cell types: Ntsr1, Syt6 and Wfs1 using their respective Cre BAC transgenic lines. Using stereotactic injections of adeno-associated virus carrying floxed fluorophore, we showed that focal population of the cell type in prefrontal cortical subregions can have slightly distinct projection patterns, as revealed for Syt6 PFC and ACC populations, or can be topographically uniform, for instance Wfs1 and Ntsr1. Transsynaptic retrograde tracer, a cre dependent pseudorabies virus carrying EGFP, was stereotaxically injected into the anterior cingulate of Wfs1 cre transgenic mice, which revealed presumably monosynaptic connections from layer 2 and 5 cells in the contralateral cortex.

Our second strategy involved viral mediated silencing of neural transmission using tethered toxins that target voltage gated calcium channels (VGCCs) Cav2.1 and Cav2.2. Cell autonomous blockade of VGCCs was achieved by - 1. cre-inducible viral constructs for tethered toxins, 2. cell type specific expression by using BAC transgenic mice that express cre in distinct cell type (Wfs1) and 3. the tethering transmembrane domain of the tailored toxins, which restrict

the toxins to cells expressing them and prevent diffusion into the extracellular space. The tethered toxins carried by AAV constructs were stereotaxically injected into the anterior cingulate cortex of Wfs1 Cre ERT2 transgenic mice and expression of the toxins was confirmed by histology. We found that focal silencing of the ACC (SIACC) Wfs1 cell type leads to impairment in the affective pain circuitry. Compared to controls, the SIACC Wfs1 mice exhibit a significantly reduced aversion to formalin-paired context in the formalin-conditioned place aversion paradigm. However, the SIACC Wfs1 mice have intact pain sensitivity as measured by latency of their paw withdrawal from acute thermal or mechanical stimulus. ACC has been shown in prior studies to have connectivity with emotional center of the brain, the amygdala, and neural responses in ACC have been recorded during pain perception. Hence, our results support the role of ACC in mediating affective pain and additionally present evidence for cell type specific contribution to this phenomenon for layer 2 Wfs1 cells in the ACC.

Our third strategy was to investigate cell type specific contribution to a neurological disorder by picking a candidate from the TRAP data for our BAC transgenic lines. Wfs1, a gene responsible for the human neurological disorder Wolfram Syndrome, was highly enriched in the Ntf3 cell type, as revealed by the TRAP data. Reciprocally, Wfs1 TRAP data revealed enrichment for Ntf3 and to further confirm co-expression, immunohistochemistry with Wfs1 antibody in Ntf3 TRAP brain sections revealed partial overlap in the medial prefrontal cortex. We generated conditional allele of Wfs1 gene and bred it to Emx1 cre knock-in line to delete Wfs1 only in pyramidal cells of neocortex, which we confirmed with Wfs1 histology.

We ran a battery of behavioral tests on Wfs1 cortex KO mice mainly testing for motor behavior, anxiety, depression and cognitive function. We found that Wfs1 cortex KO were hypoactive in open field but this hypoactivity was not due to motor coordination problems and was corrected under diet restriction, indicating that the hypoactivity might be from reduced motivation or heightened anxiety. We tested mice for anxiety in elevated plus maze, light dark transition and hyponeophagia, all of which revealed no difference between the Wfs1 cortex KO and their wildtype littermates. We then tested these mice in depression assay for anhedonia and found that the KOs have a significantly reduced preference for sucrose, which is normally considered more pleasurable than water. Due to the pre-existing hypoactivity phenotype, we could not test these mice in the common depression tests that measure immobility such as tail suspension test and forced swimming test.

We further tested the mice for prefrontal cortex related cognitive functions since Wolfram syndrome patients present with depressive behavior as well as mental retardation. Wfs1 cortex KO mice were tested for appetitive operant conditioning paradigm where they first have to learn to make action-outcome association with one of the three apertures in the conditioning box in order to receive a food reward. After 12 days of acquisition learning, mice then have to switch to a different aperture, which is now associated with the reward, and inhibit responding at the previously reinforced aperture. This 'reversal' phase lasts for 5 days and measures perseveration and accuracy of mice in making correct action-outcome associations. We found that the Wfs1 cortex KO mice did not exhibit any deficit in both phases and thus could learn and reverse the choice as easily as the wildtype controls. However, in the next phase of 'extinction' learning, mice had to inhibit responding altogether since the apertures were no longer associated

with food reward, and we found that Wfs1 cortex KO displayed a strong phenotype in compulsive responding at the magazine compared to the wildtype even though the magazine did not deliver any reinforcer. This phenotype is similar to compulsive behavior seen in obsessive-compulsive disorder (OCD) patients who keep repeating habits and rituals in spite of there being no value to the action.

To sum it altogether, this dissertation presents evidence that BAC transgenesis can be applied to genetically access pyramidal cell types in the neocortex for molecular profiling as well as functional characterization using silencing viruses and conditional alleles. We also showed direct utility of TRAP data in elucidating cortex specific contribution to the complex neurological disorder, Wolfram Syndrome. Therefore, a combination of specific gene driver selection, BAC transgenesis methods and functional modulatory strategies can give us valuable insight into the underlying neuronal circuitry in the cortex responsible for distinct behavioral outputs, physiology and pathophysiology.

MATERIALS AND METHODS

6.1 Generation of BAC Transgenic Mice

6.1.1 Molecular Cloning, BAC modification and Transgenesis

The BAC modification and transgenesis were carried out as previously established (Gong 2003). For each driver, an optimal BAC was selected using CloneFinder (Homology regions 'A boxes' were PCR amplified from the BAC containing the gene of interest using 5' and 3' primers designed using Primer-Blast program (http://www.ncbi.nlm.nih.gov/tools/primer-blast/). The A boxes were then cloned into the AscI/NotI sites in the shuttle vector pS296 (bacTRAP) or pS175 (Cre). The pS296 vector has EGFP-L10 incorporated into its backbone immediately after the A box, whereas the R6kY-ORI promoter drives the pi protein dependent replication of the shuttle vector in the pir1 cells. The cloned shuttle vector is then used to electroporate BAC competent cells for the respective gene relevant BAC. The BAC competent cells have been rendered recombination competent by introduction of RecA gene from a carrier vector.

Once electroporation is done, proper BAC cointegrates that underwent homologous recombination and incorporated the A box along with the transgene (EGFP-L10) are selected for by using a combination of three antibiotics: ampicillin (S296), chloramphenicol (BAC) and tetracycline (RecA plasmid). Further, BAC cointegration is confirmed in two steps: first by carrying out cointegrate PCR, where primers for the region further 5' from the A box and EGFP reverse primer are used to screen colonies, and then by carrying out a Southern blot on frequently cutting enzyme-restricted BAC DNA using radiolabeled A box as a probe. The modified BAC, thus confirmed, is then purified using cesium chloride gradient and ran on the

pulse field gel to ensure BAC integrity, size and concentration. The purified supercoiled BAC is subsequently linearized and injected into the fertilized oocytes of FVB/N female mice.

6.1.2 Animal Husbandry

All animal protocols were carried out in accordance with the US National Institutes of Health Guide for the Care and Use of Laboratory Animals and were approved by the Rockefeller University Institutional Animal Care and Use Committee. All mice were raised at 78 ^{0}C in 12h light: 12h dark conditions with food and water provided *ad libitum* except when noted, for experiments requiring food restriction. Wfs1 cre ERT2 mice, at weaning age, were put on a Tamoxifen-diet (Teklad diet) which had a composition of 0.8% Tamoxifen citrate by mass in order to induce the activation of cre.

Once the FVB/N pregnant females injected with the BAC gave birth, their progeny were screened for germline transmission of the modified BAC by PCR genotyping for EGFP. Mice that carry the modified BAC in their genome, inferred by the presence of EGFP, are referred to as BAC founders (FF). EGFP genotyping was carried out using the primers CCTACGGCGTGCAGTGCTTCAGC and CGGCGAGCTGCACGCTGCGTCCTC. The BAC founders are bred to C57Bl/6J mice to produce F1 litters which are then characterized for neuroanatomy i.e. expression of EGFP in the cell types of interest in the neocortex. The BAC founders that recapitulate the endogenous gene expression pattern in the CNS and express the reporter EGFP at high enough levels are then used to start breeding scheme in order to generate enough age-matched BAC transgenic mice for reporter expression, functional modulation of gene expression analysis.

6.2 Generation of Wfs1 conditional null allele

The Wfs1 mutant mice were generated at Lexicon Pharmaceuticals, Inc. (The Woodlands, TX). The conditional targeting vector was derived using the Lambda KOS system (Wattler et. al. BioTechniques 26:1150-1160, 1999). The Lambda KOS phage library, arrayed into 96 superpools, was screened by PCR using exon 8-specific primers Wfs-2 [5'-GTGAAGTACCCTTTACACGC-3'] and Wfs-3 [5'-GCAGCAGGTCGGTGAGAG-3']. The PCR-positive phage superpools were plated and screened by filter hybridization using the 280 bp amplicon derived from primers Wfs-2 and Wfs-3 as a probe. Three pKOS genomic clones, pKOS-12, pKOS-39, and pKOS-58 were isolated from the library screen and confirmed by sequence and restriction analysis. Gene-specific arms (5'-

GAGGCCCAGGAGTGGGAAAGTCTAGGGTGTG-3') and (5'-GACAAGGCTCCCTGTAATCAAACCAGAAGG-3') were appended by PCR to a yeast selection cassette containing the URA3 marker. The yeast selection cassette and pKOS-12 were co-transformed into yeast, and clones that had undergone homologous recombination to replace a 2706 bp region containing exon 8 with the yeast selection cassette were isolated. This 2706 bp fragment was independently amplified by PCR and cloned into the intermediate vector pLF-Neo introducing flanking LoxP sites and a Neo selection cassette (Wfs1-pLFNeo). The yeast cassette was subsequently replaced with the Wfs1-pLFNeo selection cassette to complete the conditional Wfs1 targeting vector that has exon 8 flanked by LoxP sites.

The Not I linearized targeting vector was electroporated into 129/SvEv^{Brd} (Lex-1) ES cells. G418/FIAU resistant ES cell clones were isolated, and correctly targeted clones were identified and confirmed by Southern analysis using a 485 bp 5' external probe (9/50), generated by PCR using primers Wfs-9 [5'-CTGCCTTGCTTGCAATGTTG-3'] and Wfs-50 [5'-CATGTCCAAGACAGGATGTG-3'], and a 443 bp 3' external probe (37/53), amplified by PCR using primers Wfs-37 [5'-CAACATTTCTCAGAGCTTCC-3'] and Wfs-53 [5'-CGTGTTAGAGTGCTGTACAG-3']. Southern analysis using probe 9/50 detected a 12.1 Kb wild type band and 9.6 Kb mutant band in Hind III digested genomic DNA while probe 37/53 detected a 8.8 Kb wild type band and 10.8 Kb mutant band in Bam HI digested genomic DNA. Three targeted ES cell clones were microinjected into C57BL/6 (albino) blastocysts. The resulting chimeras were mated to C57BL/6 (albino) females to generate mice that were heterozygous for the Wfs1 conditional mutation (Wfs1 fl/+).

The Wfs1 fl/+ heterozygotes were crossed to C57Bl/6 mice for at least 2 generations before mating them to each other in order to obtain Wfs1 fl/fl homozygote mice for the conditional allele. The Wfs1 fl/+ mice were bred to Emx1-IRES.Cre knock-in mice in order to generate cortex specific knockout of Wfs1.

6.3 Quantitative real-time PCR for BAC copy number analysis

Tail pieces (about 1 mm) from different BAC founder lines were lysed and DNA was retrieved from them by isopropanol extraction and ethanol precipitation. EGFP PCR was performed on the tail DNAs with Bio-Rad iQ5 syber green supermix in accordance with the manufacturer's protocols (Bio-Rad, Hercules, CA), with 500 nm final concentration of the EGFP primers. Cycling and quantitation were performed with Bio-Rad iQ5 multiplex real-time detection hardware. PCR was carried out for 45 cycles (94oC 30 s, 63oC 30 s, 72oC 30s) followed by a melt curve. Each replicate was assayed in triplicate. Conditions yielding significant dimmers, as demonstrated by melt curve, were excluded from further analysis. Products that did not yield a product in at least 2 out of 3 replicates prior to 35 cycles were also excluded from further analysis. Data were normalized to Actin B with the ddCT method, via iQ5's optical system software version 2, and averaged across replicates. Tail DNA from the knock in mouse (heterozygotes) harboring the conditional allele for EGFP-L10 was taken as a control for representing a single copy of BAC and thus EGFP. All other tail DNA samples from different EGFP BAC transgenic founder lines were compared to the control to determine the BAC dosage or copy number in each line.

6.4 Generation of rabbit polyclonal antibody to WFS1

Rabbit polyclonal antibody was generated against a custom synthesized peptide (CEPPRAPRPQADPSAG) of Wfs1. The antigen was purified to 90% by HPLC and coupled to a carrier before being injected to rabbits. The antibody titer from the rabbit blood was measured and effective concentration of the antibody for immunohistochemistry was determined empirically.

6.5 Histology

Brains were processed identically with MultiBrain Technology (NSA, NeuroScience Associates, Knoxville, TN) for DAB IHC with a 1:75,000 dilution of Goat anti-EGF serum (Heiman et al, 2008) according to the Vectastain elite protocol (Vector Labs, Burlingame, CA). Serial sections were digitized with a Zeiss Axiosko2 microscope at 10X magnification. For immunofluorescence, mice were deeply anesthetized using CO2 chamber and transcardially perfused with 10 ml of phosphate buffered saline (PBS) followed by 30 ml of 4% paraformaldehyde (PFA) in PBS. Brains were post-fixed in 4% PFA for 1 h and cryoprotected by sequential sinking in 5% weight/volume (w/v) sucrose in PBS at 4oC for 24h with gentle agitation followed by 30% w/v sucrose in PBS for the next 24 h. Brains were then attached to the stage of Leica SM200R Freezing Microtome using water as the adhesive and covered with powdered dry ice. 40 um coronal sections were cut with the microtome and the brains were transferred to cryoprotection buffer (phosphate buffer, pH 7.4 with 25% glycerol and 25% ethylene glycol). For immunohistochemistry, sections were blocked in 5% Normal Donkey

Serum (NDS) in PBS/0.1% Triton X-100 for 30 min and incubated overnight at 4oC with primary antibody against EGFP (Chicken monoclonal Ab, ab13970, diluted 1:500, Abcam), Wfs1 (Rabbit polyclonal Ab, diluted 1:250, Green Mountain Antibodies) or NeuN (Mouse monoclonal Ab, MAB377, diluted 1:500, Millipore) in the blocking buffer. On the next day, sections were washed 3 times with 1X PBS for 5 min and then incubated with the appropriate Alexa dye-conjugated secondary antibodies diluted 1:400 in the blocking buffer. The sections were then washed 3 times with 1X PBS and counterstained with DAPI for nuclear staining at 1:10,000 dilution. Sections were mounted on the Superfrost slides (VWR) and sealed with Fluorogel (EMS).

6.6 Stereotactic Intracranial Injections

All animals were anesthetized by intraperitoneal injection of a cocktail of ketamine (100 mg/ml) and xylazine (1 mg/ml), at a volume equivalent to 10% of their body weight. The stereotactic coordinates for different areas of mouse brain were determined using Paxinos/Franklin mouse atlas (Paxinos and Franklin, 2004); all stereotaxic measurements were taken relative to Bregma and with the depth determined from the brain surface. Following coordinates were used for different areas of the brain: anterior cingulate cortex (ACC:), prelimbic cortex (PL), secondary motor cortex (M2), secondary visual cortex (V2), posterior thalamic nucleus (Po) and caudate putamen (CPu). The retrograde transneuronal tracer, cholera toxin-B (CT-B – 0.5 ul) conjugated to Alexa fluor 568, was injected into the PL, CPu and Po of Ntf3 PS1046, Etv1 PS476 and Syt6 PS3013 bacTRAP lines respectively in order to determine whether the cortical cell types defined by each of these lines project to the expected target brain

region. Following the CT-B injection, mice were returned to their home cage for 3 days after which they were euthanized and brain tissue was harvested for immunohistochemistry.

6.6.1 Anterograde viral tracer

Cre dependent AAV viral tracers were used to delineate the neuronal processes of distinct cortical cell types in the anterograde direction. Specifically, the corticothalamic pyramidal cell cre lines Ntsr1 GN220 and Syt6 KI109 were stereotaxically injected with 0.5 ul of AAV-dfl-ChR2-EYFP-WPRE-dfl and/or AAV-dfl-ChR2-mCherry-WPRE-dfl (Deisseroth 2010) in V2 (Ntsr1), PL and M2 (Syt6) respectively. Callosal pyramidal cell cre line Wfs1 cre-ERT2 were fed with Tamoxifen diet for 2 weeks before being subjected to the AAV surgery. The AAV anterograde tracer was injected into the ACC of the Wfs1 cre mice. After the AAV surgery, mice were returned to their home cage for 21 days and provided access to food and water *ad libitum*. This duration was sufficient to elicit cre-dependent expression of the reporter in the focal population around the injection site. After 21 days, mice were euthanized and transcardially perfused with 4% paraformaldehyde to analyze the reporter expression in the neuronal axodendritic processes.

6.6.2 Retrograde viral tracer

For retrograde transsynaptic tracing, we used Cre dependent pseudorabies (PRV) viral tracer, PRV-ME185, developed by Ekstrand et al (2011, unpublished). The PRV-ME185 construct consists of the essential viral protein UL23, IRES and EGFP, with 2 floxed STOP codons before UL23 and after EGFP, i.e. PRV-flSTOPfl-UL23-IRES-EGFP-flSTOPfl. We

injected 0.5 ul of PRV-ME185 into the ACC of Wfs1 Cre-ERT2 mice unilaterally in the left hemisphere. Following surgery, mice were returned to their home cages with *ad libitum* access to food and water. Two temporal windows, 2 days and 5 days, were tested in order to attempt to harvest the brain right after crossing the first order synapse and multi order synapses respectively.

6.6.3 Viral tethered toxins

Cre dependent tethered toxins (t-toxins) that block specific voltage gated calcium channels Cav2.1 and Cav2.2 – MVIIA and AgaIV – were generated and optimized by Ibanez-Tallon and colleagues (Auer and Ferrarese, unpublished). AAV viruses were constructed to carry these t-toxins i.e. AAV-dfl-MVIIA-PC-mCherry-dfl, AAV-dfl-AgaIV-PC-EGFP-dfl and AAV-dfl-PE-EGFP-dfl. The last viral construct was a control virus that transduces the expression of just EGFP. Equimolar suspension of AAV-MVIIA and AAV-AgaIV was prepared to inject 0.5 ul of this mix into the ACC of Wfs1 Cre ERT2 transgenic mice. In control mice AAV-PE was injected in the same volume. Mice were returned to the home cage following surgery. Three weeks after the surgery, they were tested on various behavioral assays. At the end of the behavioral experiments, mice were euthanized and transcardially perfused with paraformaldehyde for subsequent neuroanatomical analysis.

6.7 Affinity purification of translating ribosomes

All immunoprecipitations were performed with a mix of two custom generated GFP monoclonal antibodies (19C8, 19F7). Three to six adult mice (7-10 weeks old) for each replicate sample were euthanized with CO2 and the whole or frontal part of cerebral cortex was dissected

out using HEPES buffer. In each case, males and female mice were used, evenly balanced in each replicate. Each cell population was assayed in triplicate. The cortical tissue was homogenized and centrifuged at 2000 X g for 10 min. The supernatant from the homogenate was then supplemented with a mix of detergents DHPC and NP-40 before a second centrifugation at 20,000 X g for 15 min. The supernatant after the second spin was incubated overnight at 4oC with pre-washed Streptavidin My-One Dynabeads conjugated with Protein-L and a mix of monoclonal anti-EGFP 19C8 and 19F7 antibodies. On the following day, the RNAs bound to the beads, referred to as immunoprecipitate (IP), were washed with high salt buffer (0.35M KCl) three times and RNA was extracted and purified using Absolutely NanoPrep RNA purification kit (Stratagene). RNA quantity and quality were determined using a Nanodrop 1000 spectrophotometer (Wilmington, DE) and Agilent 2100 Bioanalyzer (Foster City, CA). For each sample, 15 ng of total RNA was amplified with Affymetrix two-cycle amplification kit and hybridized to Affymetrix 430 2.0 microarrays according to the manufacturer's instructions.

6.8 Microarray normalization and analysis

All RNA samples were first normalized with GCRMA. The IP replicates for each cell type were imported together and so were the Whole Cx RNA pools. For each cell type, three biological replicates of IP were averaged and compared to the Whole Cx using an X-Y scatter plot for all 40,000 probesets. Thresholds for expression (50) and fold change (variable) were applied in order to get a list of Top 1000 genes that are most highly enriched in the IP for a given cell type. The Top 1000 genes in the IP were compared between different cell types in the appropriate context: three different cortical pyramidal cell types (Ntf3 PS1046, Etv1 PS46 and Syt6 PS3013), layer II cortical pyramidal cell types (Pdyn CP12, Ntf3 PS1046 and Wfs1 Tg2) and

layer VI corticothalamic pyramidal cell types (Ntsr1 GN220 and Syt6 PS3013). Pearson's correlations were carried out in Genespring 7.0 on the replicates in order to evaluate how closely they are similar to each other. Unsupervised hierarchical clustering was performed on the cell types relevant to the context together with the negative glial cell types (AldhL1 and Olig2) and whole cortex. Both condition tree and gene tree were applied on the cluster and the heat map colored arbitrarily using 300 for high, 150 for normal and 50 for low levels of expression of any given probeset. Lists of biologically relevant molecules – transcription factors, receptors and ion channels – were created and displayed on the hierarchical cluster in order to facilitate selection of differentially expressed and biologically relevant molecules.

6.9 Statistical Analysis of Microarray Data

R- based Specificity Index (SI) algorithm was used to quantitatively compare the translational profile of different cell types in the given context. Following GCRMA normalization within replicates and global normalization across samples, IP was compared to the total to filter out non-specific background by setting a threshold based on negative controls. The filtered IP was iteratively compared to each other and a ratio is calculated for each probeset. The probesets are ranked in accordance with the ratio and a statistical measure, p value, is calculated based on how likely it is for a given probeset to have the rank by chance.

Lists of statistically significant genes ($p < 0.05$) for each cell type in the given context of comparison (cortical cell types, corticothalamic cells or layer 2 pyramidal cells) were generated after the SI analysis and analyzed for overrepresented gene ontology (GO) categories using

BiNGO plugin for the Cytoscape software (Maere 2005). Statistically overrepresented KEGG pathways were revealed by the online DAVID software.

6.10 Quantitative real-time RT PCR for independent candidate verification

cDNA was synthesized from 15 ng of total RNA from three replicate IP and UB or S20 samples using NUGEN WT-Ovation RNA Amplification kit and then purified with the QIAGEN Quick PCR cleanup, according to the manufacturer's instructions (QIAGEN, Valencia, CA). PCR was performed with Bio-Rad iQ5 syber green supermix in accordance with the manufacturer's protocols (Bio-Rad, Hercules, CA), with 500 nm final concentration of each primer. Cycling and quantitation were performed with Bio-Rad iQ5 multiplex real-time detection hardware. PCR was carried out for 45 cycles (94oC 30 s, 63oC 30 s, 72oC 30s) followed by a melt curve. Each replicate was assayed in triplicate. Conditions yielding significant dimmers, as demonstrated by melt curve, were excluded from further analysis. Products that did not yield a product in at least 2 out of 3 replicates prior to 35 cycles were also excluded from further analysis. Data were normalized to Actin B with the ddCT method, via iQ5's optical system software version 2, and averaged across replicates.

6.11 Behavior Assays and Analysis

6.11.1 Spontaneous locomotion and Open field Activity

Locomotor and exploratory behaviors were recorded for each individual mouse for 60 min using eight Dig scan open field (OF) apparatus and Fusion software (Accessing Instruments, Inc., Columbus, OH). Mice were habituated in the testing room for 30 min before the start of the

experiment. A large arena (42 cm X 42 cm) with infrared beams at three different levels was used to record horizontal locomotor activity (total distance), vertical movement (rearing) and thigmotaxis (time spent in the center vs. total distance). Two fluorescent lamps positioned on two sides of the room provided light levels of about 450 lux in the open field arenas. Each animal was placed in the center of the open field and its activity was measured for 60 min. The floor of the arena was cleaned with Clidox sterilizer and dried thoroughly after each mouse.

6.11.2 Motor coordination and Balance

Mice were individually placed on a rotating rod and the time each animal was able to maintain its balance walking on top of the rod was recorded. The speed of the rotarod was 4 rpm on the first day of training or accelerated from 4 to 40 rpm over a 5 min period. Mice were tested on the rotarod three times in a day for three consecutive days.

6.11.3 Light:Dark Transition Test

The light-dark transition test is an unconditioned test of anxiety-like behavior designed for mice. Mice were habituated to the testing room for 30 min. The Open field Plexiglas boxes (Accuscan-USA) were modified to analyze the mice in the light-dark transition test. Briefly, the dark enclosure measuring 16 inch X 8 inch X 5 inch was placed against the rear wall of the arena. The enclosure has an animal entry opening of 4 inch X 1.25 inch and has holes on all four sides to allow the beams in the horizontal and vertical sensors to monitor the animal's activity. Each mouse was placed in the center of the light compartment and the activity was recorded immediately after for 10 min. Fusion software was used to divide the arena into two equal zones marked light and dark, and data such as distance traveled in the light and dark areas, horizontal

activity, time spent in each side and frequency of transitions were recorded and analyzed.

6.11.4 Elevated Plus Maze

The plus maze consisted of two opposite open arms without sidewalls and two enclosed arms of the same size with 14-cm high sidewalls and an endwall. The arms extended from a common central square (5 sq cm X 5 sq cm) perpendicular to each other, making the shape of a plus sign. The entire plus-maze apparatus was elevated to a height of 30 cm. Testing began by placing an animal on the central platform of the maze facing the closed arm. An arm entry was counted only all the four limbs were within a given arm. Standard 10 min test duration was applied and the maze was wiped with 70% Ethanol in between trials. Test sessions were video-recorded with a camera in the center of the maze while ensuring minimal shadows. Ethovision software was used to record the time spent on open arms and closed arms, total distance moved, and number of open arm and closed arm entries.

6.11.5 Hyponeophagia

The experiment was carried out in a brightly lit (400 lx) room. The mice, food deprived for 24 h, were taken from their home cage and habituated in empty cages devoid of food, water and bedding for 30 min. They were then placed singly in a translucent plastic box (18cm°—22cm°—14 cm; actual measurement) filled with a single layer of food pellets (Lab Diet) to a depth of ca. 1 cm. To avoid social transmission of behavior, mice that had already been tested were placed in a separate box. The latency to start eating was measured from the time a mouse was placed in the box. Eating was defined as eating for at least 3 s consecutively. A cut-off score of 180 s was used.

6.11.6 Sucrose preference test

The sucrose preference test was performed with a two-bottle procedure, during which mice had free access to both water and sucrose solution. Group-housed animals were first habituated for 48 hours both to consume fluids from a small bottle and to adjust to the 2% sucrose solution. After habituation, the sucrose preference was measured over 3 days. Each day, group-housed mice were individually caged and two bottles were presented to them for 24 hours: one with tap water and one with 2% sucrose solution. Consumption of water or sucrose solution was measured by weighing the bottles before and after the sessions. Bottles were counterbalanced across the left and the right sides of the cage, and their position was alternated from test to test. Animals were weighed after the last day of test. Sucrose preference was calculated in two ways: Preference = (average sucrose solution intake (ml)/ animal weight (g)], and Preference (%) = (average sucrose solution intake (ml)/ average total fluid intake (ml) X 100.

6.11.7 Thermal Nociception

Thermal latency was determined using the plantar test (Ugo Basile) based on the method described by Hargreaves (Hargreaves et al., 1988). 15 min after placing the mice in the Plexiglas chamber (15 cm diameter, 22.5 cm in height) a high intensity light beam is directed at the plantar surface of the hindpaw. Movement of the paw stops the light beam and the latency will be indicated on a digital screen. Measurements will be done five times on each paw and mean values were used for statistical analysis. Criteria for inclusion are calm behavior of the mouse prior to testing and a clear paw withdrawal.

6.11.8 Mechanical Nociception

Mechanical sensitivity will be determined using a dynamic plantar aesthesiometer (Ugo Basile, Milan, Italy). All animals are first acclimatized to the behavioral testing apparatus for 15 min. A mechanical force is applied to the plantar surface of the mouse hindpaw. The force will be increased with a ramp by 1 g/s with a maximum of 20 g. Each paw is measured five times and mean values of the applied forces will be determined and used for statistical analysis. Criteria for inclusion are calm behavior of the mouse prior to testing and a clear paw withdrawal.

6.11.9 Formalin-Conditioned Place Aversion

Conditioned Place Aversion (CPA) boxes (Med Associates) were designed with three compartments and manual guillotine doors. The white and black compartments each have distinct colored wall and floor type (grid rod style vs mesh style) so that the animal can associate distinct context with the cue introduced while it is confined to the particular context. Infrared photobeam detectors on the chamber walls track the animal position during the course of the experiment. Mice were first habituated for 15 min in CPA boxes with free access to all three compartments on day 1. On day 2, the same procedure was repeated but this time mouse position within the CPA boxes was tracked during the 15 min habituation so that a pre-existing bias towards any chamber is detected. If the bias was above 65%, the mouse was excluded from the experiment. On day 3, the intraplantar surface of one of the mouse hindpaws was injected with saline and the mouse was confined to white or black chamber for 1 hr. On day 4, the intraplantar surface of contralateral hindpaw was injected with 3% formalin, a potent inflammatory agent, and immediately confined to either white or black chamber for 1 hour. The duration of 1 hr was chosen based on the temporal dimension of the formalin elicited biphasic response. The saline-

pairing and formalin-pairing to either white or black chamber was randomized. On day 5, the mice were allowed free access to all three chambers and the net bias for or against the formalin and saline-paired boxes was recorded.

6.12 Appetite Operant Conditioning

6.12.1 Determination of baseline body weight and food restriction

The behavioral study of reversal learning involves instrumental learning motivated by food reinforcement. Hence mice are food-restricted to 85-90% of their baseline body weight. The baseline body weight is determined over three days of free and unrestricted access to standard diet. The mice are then put on a restricted diet and allowed access to food for one hour daily during the light cycle in order to attain the optimal body weight necessary for their performance in the instrumental learning task. If the mice lose more body weight than optimal, the food access is prolonged for an additional 30 min. The food restriction is maintained during the three-week course of the experiment, which includes two weeks for acquisition and one week for reversal.

6.12.2 Magazine Training

Dust-free precision pellets (Bio-Serv) were used as reinforcers in the instrumental task, hence they were introduced into the home cage for a day before the experiments in order to eliminate the novelty associated with these pellets. The mice are then given two days of magazine training in which each entry into the food magazine is reinforced by dispensal of food pellets at variable interval 20 that is pellets were dispensed between 1 and 40 seconds or until 50

reinforcers were delivered. All experiments are performed during the afternoon in the light cycle between 7 a.m. and 7 p.m.

6.12.3 Acquisition and Reversal of Instrumental Learning

The reversal-learning task was carried out in operant conditioning chambers (Med Associates, USA) equipped with a food magazine, house light, stimulus light and tone generator and three nose poke apertures. Mice were trained to perform a food-reinforced operant nosepoke response. One of the three illuminated nose poke apertures was designated as active (left, center or right) in a pseudo-randomized and balanced manner for each genotype. A response in the active aperture ('correct response') resulted in delivery of a food pellet, accompanied by a 3 sec presentation of stimulus light above the magazine and tone. A response in the other two apertures ('incorrect response') had no effect. The food reinforcers were all delivered on a variable ratio-2 schedule (1, 2 or 3 correct responses were required to obtain reinforcement). Mice were tested for 25 min each day over 10 consecutive days of training (Acquisition) and the number of correct and incorrect responses were recorded. On day 11, the position of the active nose poke was switched (1^{st} reversal) after 5 min into the session, and the nosepoke responses in the next 25 min session were monitored for 5 daily sessions. Based on the role for the prefrontal cortex in reversal learning (Dalley et al, 2004), mice with impaired prefrontal cortical function would be expected to show increased perseverative responding, i.e. increased responding at the previously reinforced aperture following reversal.

6.12.4 Extinction of Learned Instrumental Action

Extinction was carried out by cessation of food delivery at the magazine from nosepoke at any of the three apertures. The mouse thus has to learn to inhibit itself from performing nosepokes at any of the three apertures because there is no longer any value associated with it. However, there is no negative reinforcement or punishment given for the persistent nosepoke responses. The extinction session is carried out for 25 min for 5 consecutive days. Immediately after the session is over, mice are returned to their home cages where they are provided with a pellet of food. So mice also have to evaluate the cost of their action in light of the food waiting for them in the home cage.

REFERENCES:

Abremski, K., Wierzbicki, A., Frommer, B., and Hoess, R.H. (1986). Bacteriophage P1 Cre-loxP site-specific recombination. Site-specific DNA topoisomerase activity of the Cre recombination protein. J Biol Chem *261*, 391-396.

Alitto, H.J., and Usrey, W.M. (2003). Corticothalamic feedback and sensory processing. Curr Opin Neurobiol *13*, 440-445.

Angevine, J.B., Jr., and Sidman, R.L. (1961). Autoradiographic study of cell migration during histogenesis of cerebral cortex in the mouse. Nature *192*, 766-768.

Arber, S., Ladle, D.R., Lin, J.H., Frank, E., and Jessell, T.M. (2000). ETS gene Er81 controls the formation of functional connections between group Ia sensory afferents and motor neurons. Cell *101*, 485-498.

Arimatsu, Y., and Ishida, M. (2002). Distinct neuronal populations specified to form corticocortical and corticothalamic projections from layer VI of developing cerebral cortex. Neuroscience *114*, 1033-1045.

Arion, D., Unger, T., Lewis, D.A., and Mirnics, K. (2007). Molecular markers distinguishing supragranular and infragranular layers in the human prefrontal cortex. Eur J Neurosci *25*, 1843-1854.

Arlotta, P., Molyneaux, B.J., Chen, J., Inoue, J., Kominami, R., and Macklis, J.D. (2005). Neuronal subtype-specific genes that control corticospinal motor neuron development in vivo. Neuron *45*, 207-221.

Aronoff, R., and Petersen, C.C. (2006). Controlled and localized genetic manipulation in the brain. J Cell Mol Med *10*, 333-352.

Auer, S., Sturzebecher, A.S., Juttner, R., Santos-Torres, J., Hanack, C., Frahm, S., Liehl, B., and Ibanez-Tallon, I. Silencing neurotransmission with membrane-tethered toxins. Nat Methods *7*, 229-236.

Austin, J., Buckland, P., Cardno, A.G., Williams, N., Spurlock, G., Hoogendoorn, B., Zammit, S., Jones, G., Sanders, R., Jones, L.*, et al.* (2000). The high affinity neurotensin receptor gene (NTSR1): comparative sequencing and association studies in schizophrenia. Mol Psychiatry *5*, 552-557.

Balleine, B.W., and Dickinson, A. (1998). Goal-directed instrumental action: contingency and incentive learning and their cortical substrates. Neuropharmacology *37*, 407-419.

Bannister, A.P. (2005). Inter- and intra-laminar connections of pyramidal cells in the neocortex. Neurosci Res *53*, 95-103.

Bartha, A. (1961). Experimental reduction of virulence of Aujeszky's disease virus. Ungarische Tieri~rztliche Monatsschrift *16*, 42-45.

Bian, G.L., Wei, L.C., Shi, M., Wang, Y.Q., Cao, R., and Chen, L.W. (2007). Fluoro-Jade C can specifically stain the degenerative neurons in the substantia nigra of the 1-methyl-4-phenyl-1,2,3,6-tetrahydro pyridine-treated C57BL/6 mice. Brain Res *1150*, 55-61.

Billig, I., Foris, J.M., Enquist, L.W., Card, J.P., and Yates, B.J. (2000). Definition of neuronal circuitry controlling the activity of phrenic and abdominal motoneurons in the ferret using recombinant strains of pseudorabies virus. J Neurosci *20*, 7446-7454.

Borrelli, E., Heyman, R., Hsi, M., and Evans, R.M. (1988). Targeting of an inducible toxic phenotype in animal cells. Proc Natl Acad Sci U S A *85*, 7572-7576.

Bourassa, J., Pinault, D., and Deschenes, M. (1995). Corticothalamic projections from the cortical barrel field to the somatosensory thalamus in rats: a single-fibre study using biocytin as an anterograde tracer. Eur J Neurosci *7*, 19-30.

Bown, C.D., Wang, J.F., Chen, B., and Young, L.T. (2002). Regulation of ER stress proteins by valproate: therapeutic implications. Bipolar Disord *4*, 145-151.

Braz, J.M., Nassar, M.A., Wood, J.N., and Basbaum, A.I. (2005). Parallel "pain" pathways arise from subpopulations of primary afferent nociceptor. Neuron *47*, 787-793.

Briggs, F., and Usrey, W.M. (2008). Emerging views of corticothalamic function. Curr Opin Neurobiol *18*, 403-407.

Buch, T., Heppner, F.L., Tertilt, C., Heinen, T.J., Kremer, M., Wunderlich, F.T., Jung, S., and Waisman, A. (2005). A Cre-inducible diphtheria toxin receptor mediates cell lineage ablation after toxin administration. Nat Methods *2*, 419-426.

Bunney, W.E., Bunney, B.G., Vawter, M.P., Tomita, H., Li, J., Evans, S.J., Choudary, P.V., Myers, R.M., Jones, E.G., Watson, S.J., and Akil, H. (2003). Microarray technology: a review of new strategies to discover candidate vulnerability genes in psychiatric disorders. Am J Psychiatry *160*, 657-666.

Bussey, T.J., Muir, J.L., Everitt, B.J., and Robbins, T.W. (1996). Dissociable effects of anterior and posterior cingulate cortex lesions on the acquisition of a conditional visual discrimination: facilitation of early learning vs. impairment of late learning. Behav Brain Res *82*, 45-56.

Butz, S., Fernandez-Chacon, R., Schmitz, F., Jahn, R., and Sudhof, T.C. (1999). The subcellular localizations of atypical synaptotagmins III and VI. Synaptotagmin III is enriched in synapses and synaptic plasma membranes but not in synaptic vesicles. J Biol Chem *274*, 18290-18296.

Cahoy, J.D., Emery, B., Kaushal, A., Foo, L.C., Zamanian, J.L., Christopherson, K.S., Xing, Y., Lubischer, J.L., Krieg, P.A., Krupenko, S.A., *et al.* (2008). A transcriptome database for astrocytes, neurons, and oligodendrocytes: a new resource for understanding brain development and function. J Neurosci *28*, 264-278.

Callaway, E.M. (2008). Transneuronal circuit tracing with neurotropic viruses. Curr Opin Neurobiol *18*, 617-623.

Cano, A., Rouzier, C., Monnot, S., Chabrol, B., Conrath, J., Lecomte, P., Delobel, B., Boileau, P., Valero, R., Procaccio, V., *et al.* (2007). Identification of novel mutations in WFS1 and genotype-phenotype correlation in Wolfram syndrome. Am J Med Genet A *143A*, 1605-1612.

Cardin, J.A., Carlen, M., Meletis, K., Knoblich, U., Zhang, F., Deisseroth, K., Tsai, L.H., and Moore, C.I. Targeted optogenetic stimulation and recording of neurons in vivo using cell-type-specific expression of Channelrhodopsin-2. Nat Protoc *5*, 247-254.

Cardin, J.A., Carlen, M., Meletis, K., Knoblich, U., Zhang, F., Deisseroth, K., Tsai, L.H., and Moore, C.I. (2010). Targeted optogenetic stimulation and recording of neurons in vivo using cell-type-specific expression of Channelrhodopsin-2. Nat Protoc *5*, 247-254.

Casey, K.L., Minoshima, S., Berger, K.L., Koeppe, R.A., Morrow, T.J., and Frey, K.A. (1994). Positron emission tomographic analysis of cerebral structures activated specifically by repetitive noxious heat stimuli. J Neurophysiol *71*, 802-807.

Cervo, L., Rossi, C., Tatarczynska, E., and Samanin, R. (1992). Antidepressant-like effect of neurotensin administered in the ventral tegmental area in the forced swimming test. Psychopharmacology (Berl) *109*, 369-372.

Chadman, K.K., Yang, M., and Crawley, J.N. (2009). Criteria for validating mouse models of psychiatric diseases. Am J Med Genet B Neuropsychiatr Genet *150B*, 1-11.

Chen, C.C., Abrams, S., Pinhas, A., and Brumberg, J.C. (2009). Morphological heterogeneity of layer VI neurons in mouse barrel cortex. J Comp Neurol *512*, 726-746.

Chung, C.Y., Seo, H., Sonntag, K.C., Brooks, A., Lin, L., and Isacson, O. (2005). Cell type-specific gene expression of midbrain dopaminergic neurons reveals molecules involved in their vulnerability and protection. Hum Mol Genet *14*, 1709-1725.

Clarke, S., Zimmer, A., Zimmer, A.M., Hill, R.G., and Kitchen, I. (2003). Region selective up-regulation of micro-, delta- and kappa-opioid receptors but not opioid receptor-like 1 receptors in the brains of enkephalin and dynorphin knockout mice. Neuroscience *122*, 479-489.

Conley, M., Kupersmith, A.C., and Diamond, I.T. (1991). The Organization of Projections from Subdivisions of the Auditory Cortex and Thalamus to the Auditory Sector of the Thalamic Reticular Nucleus in Galago. Eur J Neurosci *3*, 1089-1103.

Contreras, D., Destexhe, A., Sejnowski, T.J., and Steriade, M. (1996). Control of spatiotemporal coherence of a thalamic oscillation by corticothalamic feedback. Science *274*, 771-774.

Coutte, L., Monte, D., Imai, K., Pouilly, L., Dewitte, F., Vidaud, M., Adamski, J., Baert, J.L., and de Launoit, Y. (1999). Characterization of the human and mouse ETV1/ER81 transcription factor genes: role of the two alternatively spliced isoforms in the human. Oncogene *18*, 6278-6286.

Coutureau, E., and Killcross, S. (2003). Inactivation of the infralimbic prefrontal cortex reinstates goal-directed responding in overtrained rats. Behav Brain Res *146*, 167-174.

Crabbe, J.C., Rigter, H., and Kerbusch, S. (1982). Analysis of behavioural responses to an ACTH analog in CXB/By recombinant inbred mice. Behav Brain Res *4*, 289-314.

Damasio, H., Grabowski, T., Frank, R., Galaburda, A.M., and Damasio, A.R. (1994). The return of Phineas Gage: clues about the brain from the skull of a famous patient. Science *264*, 1102-1105.

Deschenes, M., Veinante, P., and Zhang, Z.W. (1998). The organization of corticothalamic projections: reciprocity versus parity. Brain Res Brain Res Rev *28*, 286-308.

Devinsky, O., Morrell, M.J., and Vogt, B.A. (1995). Contributions of anterior cingulate cortex to behaviour. Brain *118 (Pt 1)*, 279-306.

Dougherty, J.D., Schmidt, E.F., Nakajima, M., and Heintz, N. (2010). Analytical approaches to RNA profiling data for the identification of genes enriched in specific cells. Nucleic Acids Res *38*, 4218-4230.

Doyle, J.P., Dougherty, J.D., Heiman, M., Schmidt, E.F., Stevens, T.R., Ma, G., Bupp, S., Shrestha, P., Shah, R.D., Doughty, M.L.*, et al.* (2008). Application of a translational profiling approach for the comparative analysis of CNS cell types. Cell *135*, 749-762.

Dubuisson, D., and Dennis, S.G. (1977). The formalin test: a quantitative study of the analgesic effects of morphine, meperidine, and brain stem stimulation in rats and cats. Pain *4*, 161-174.

Duman, R.S., and Monteggia, L.M. (2006). A neurotrophic model for stress-related mood disorders. Biol Psychiatry *59*, 1116-1127.

Dymecki, S.M., and Kim, J.C. (2007). Molecular neuroanatomy's "Three Gs": a primer. Neuron *54*, 17-34.

Elliott, R., McKenna, P.J., Robbins, T.W., and Sahakian, B.J. (1995). Neuropsychological evidence for frontostriatal dysfunction in schizophrenia. Psychol Med *25*, 619-630.

Eto, K., Wake, H., Watanabe, M., Ishibashi, H., Noda, M., Yanagawa, Y., and Nabekura, J. Inter-regional Contribution of Enhanced Activity of the Primary Somatosensory Cortex to the Anterior Cingulate Cortex Accelerates Chronic Pain Behavior. J Neurosci *31*, 7631-7636.

Farinas, I., Jones, K.R., Backus, C., Wang, X.Y., and Reichardt, L.F. (1994). Severe sensory and sympathetic deficits in mice lacking neurotrophin-3. Nature *369*, 658-661.

Fonseca, S.G., Fukuma, M., Lipson, K.L., Nguyen, L.X., Allen, J.R., Oka, Y., and Urano, F. (2005). WFS1 is a novel component of the unfolded protein response and maintains homeostasis of the endoplasmic reticulum in pancreatic beta-cells. J Biol Chem *280*, 39609-39615.

Fonseca, S.G., Ishigaki, S., Oslowski, C.M., Lu, S., Lipson, K.L., Ghosh, R., Hayashi, E., Ishihara, H., Oka, Y., Permutt, M.A., and Urano, F. Wolfram syndrome 1 gene negatively regulates ER stress signaling in rodent and human cells. J Clin Invest *120*, 744-755.

Fremeau, R.T., Jr., Voglmaier, S., Seal, R.P., and Edwards, R.H. (2004). VGLUTs define subsets of excitatory neurons and suggest novel roles for glutamate. Trends Neurosci *27*, 98-103.

Geschwind, D.H. (2000). Mice, microarrays, and the genetic diversity of the brain. Proc Natl Acad Sci U S A *97*, 10676-10678.

Gong, S., Doughty, M., Harbaugh, C.R., Cummins, A., Hatten, M.E., Heintz, N., and Gerfen, C.R. (2007). Targeting Cre recombinase to specific neuron populations with bacterial artificial chromosome constructs. J Neurosci *27*, 9817-9823.

Gong, S., Zheng, C., Doughty, M.L., Losos, K., Didkovsky, N., Schambra, U.B., Nowak, N.J., Joyner, A., Leblanc, G., Hatten, M.E., and Heintz, N. (2003). A gene expression atlas of the central nervous system based on bacterial artificial chromosomes. Nature *425*, 917-925.

Gorski, J.A., Talley, T., Qiu, M., Puelles, L., Rubenstein, J.L., and Jones, K.R. (2002). Cortical excitatory neurons and glia, but not GABAergic neurons, are produced in the Emx1-expressing lineage. J Neurosci *22*, 6309-6314.

Gourley, S.L., Howell, J.L., Rios, M., DiLeone, R.J., and Taylor, J.R. (2009). Prelimbic cortex bdnf knock-down reduces instrumental responding in extinction. Learn Mem *16*, 756-760.

Gourley, S.L., Lee, A.S., Howell, J.L., Pittenger, C., and Taylor, J.R. (2010). Dissociable regulation of instrumental action within mouse prefrontal cortex. Eur J Neurosci *32*, 1726-1734.

Groh, A., Meyer, H.S., Schmidt, E.F., Heintz, N., Sakmann, B., and Krieger, P. (2009). Cell-Type Specific Properties of Pyramidal Neurons in Neocortex Underlying a Layout that Is Modifiable Depending on the Cortical Area. Cereb Cortex.

Hargreaves, K., Dubner, R., Brown, F., Flores, C., and Joris, J. (1988). A new and sensitive method for measuring thermal nociception in cutaneous hyperalgesia. Pain *32*, 77-88.

Hatten, M.E., and Heintz, N. (2005). Large-scale genomic approaches to brain development and circuitry. Annu Rev Neurosci *28*, 89-108.

Hayashi, S., and McMahon, A.P. (2002). Efficient recombination in diverse tissues by a tamoxifen-inducible form of Cre: a tool for temporally regulated gene activation/inactivation in the mouse. Dev Biol *244*, 305-318.

Heiman, M., Schaefer, A., Gong, S., Peterson, J.D., Day, M., Ramsey, K.E., Suarez-Farinas, M., Schwarz, C., Stephan, D.A., Surmeier, D.J.*, et al.* (2008). A translational profiling approach for the molecular characterization of CNS cell types. Cell *135*, 738-748.

Heintz, N. (2000). Analysis of mammalian central nervous system gene expression and function using bacterial artificial chromosome-mediated transgenesis. Hum Mol Genet *9*, 937-943.

Heintz, N. (2001). BAC to the future: the use of bac transgenic mice for neuroscience research. Nat Rev Neurosci *2*, 861-870.

Hevner, R.F., Daza, R.A., Rubenstein, J.L., Stunnenberg, H., Olavarria, J.F., and Englund, C. (2003). Beyond laminar fate: toward a molecular classification of cortical projection/pyramidal neurons. Dev Neurosci *25*, 139-151.

Hill, S., and Tononi, G. (2005). Modeling sleep and wakefulness in the thalamocortical system. J Neurophysiol *93*, 1671-1698.

Hoess, R.H., Wierzbicki, A., and Abremski, K. (1986). The role of the loxP spacer region in P1 site-specific recombination. Nucleic Acids Res *14*, 2287-2300.

Hoess, R.H., Ziese, M., and Sternberg, N. (1982). P1 site-specific recombination: nucleotide sequence of the recombining sites. Proc Natl Acad Sci U S A *79*, 3398-3402.

Huang da, W., Sherman, B.T., Zheng, X., Yang, J., Imamichi, T., Stephens, R., and Lempicki, R.A. (2009). Extracting biological meaning from large gene lists with DAVID. Curr Protoc Bioinformatics *Chapter 13*, Unit 13 11.

Hurd, Y.L., Svensson, P., and Ponten, M. (1999). The role of dopamine, dynorphin, and CART systems in the ventral striatum and amygdala in cocaine abuse. Ann N Y Acad Sci *877*, 499-506.

Ibanez-Tallon, I., Wen, H., Miwa, J.M., Xing, J., Tekinay, A.B., Ono, F., Brehm, P., and Heintz, N. (2004). Tethering naturally occurring peptide toxins for cell-autonomous modulation of ion channels and receptors in vivo. Neuron *43*, 305-311.

Inada, T., Winstall, E., Tarun, S.Z., Jr., Yates, J.R., 3rd, Schieltz, D., and Sachs, A.B. (2002). One-step affinity purification of the yeast ribosome and its associated proteins and mRNAs. RNA *8*, 948-958.

Ingram, D.K. (1982). Lithium chloride-induced taste aversion in C57BL/6J and DBA/2J mice. J Gen Psychol *106*, 233-249.

Ishihara, H., Takeda, S., Tamura, A., Takahashi, R., Yamaguchi, S., Takei, D., Yamada, T., Inoue, H., Soga, H., Katagiri, H*., et al.* (2004). Disruption of the WFS1 gene in mice causes progressive beta-cell loss and impaired stimulus-secretion coupling in insulin secretion. Hum Mol Genet *13*, 1159-1170.

Jeon, D., Kim, S., Chetana, M., Jo, D., Ruley, H.E., Lin, S.Y., Rabah, D., Kinet, J.P., and Shin, H.S. (2010). Observational fear learning involves affective pain system and Cav1.2 Ca2+ channels in ACC. Nat Neurosci *13*, 482-488.

Jessell, T.M. (2000). Neuronal specification in the spinal cord: inductive signals and transcriptional codes. Nat Rev Genet *1*, 20-29.

Johansen, J.P., Fields, H.L., and Manning, B.H. (2001). The affective component of pain in rodents: direct evidence for a contribution of the anterior cingulate cortex. Proc Natl Acad Sci U S A *98*, 8077-8082.

Jones, A.K., Brown, W.D., Friston, K.J., Qi, L.Y., and Frackowiak, R.S. (1991). Cortical and subcortical localization of response to pain in man using positron emission tomography. Proc Biol Sci *244*, 39-44.

Kakiuchi, C., Ishigaki, S., Oslowski, C.M., Fonseca, S.G., Kato, T., and Urano, F. (2009). Valproate, a mood stabilizer, induces WFS1 expression and modulates its interaction with ER stress protein GRP94. PLoS One *4*, e4134.

Kanehisa, M., Goto, S., Kawashima, S., Okuno, Y., and Hattori, M. (2004). The KEGG resource for deciphering the genome. Nucleic Acids Res *32*, D277-280.

Karpova, A.Y., Tervo, D.G., Gray, N.W., and Svoboda, K. (2005). Rapid and reversible chemical inactivation of synaptic transmission in genetically targeted neurons. Neuron *48*, 727-735.

Kato, T., Ishiwata, M., Yamada, K., Kasahara, T., Kakiuchi, C., Iwamoto, K., Kawamura, K., Ishihara, H., and Oka, Y. (2008). Behavioral and gene expression analyses of Wfs1 knockout mice as a possible animal model of mood disorder. Neurosci Res *61*, 143-158.

Khanim, F., Kirk, J., Latif, F., and Barrett, T.G. (2001). WFS1/wolframin mutations, Wolfram syndrome, and associated diseases. Hum Mutat *17*, 357-367.

Killcross, S., and Coutureau, E. (2003). Coordination of actions and habits in the medial prefrontal cortex of rats. Cereb Cortex *13*, 400-408.

Klein, R. (1994). Role of neurotrophins in mouse neuronal development. FASEB J *8*, 738-744.

Koga, K., Li, X., Chen, T., Steenland, H.W., Descalzi, G., and Zhuo, M. In vivo whole-cell patch-clamp recording of sensory synaptic responses of cingulate pyramidal neurons to noxious mechanical stimuli in adult mice. Mol Pain *6*, 62.

Konig, M., Zimmer, A.M., Steiner, H., Holmes, P.V., Crawley, J.N., Brownstein, M.J., and Zimmer, A. (1996). Pain responses, anxiety and aggression in mice deficient in pre-proenkephalin. Nature *383*, 535-538.

Kostopoulos, G.K. (2000). Spike-and-wave discharges of absence seizures as a transformation of sleep spindles: the continuing development of a hypothesis. Clin Neurophysiol *111 Suppl 2*, S27-38.

Krishnan, V., and Nestler, E.J. (2008). The molecular neurobiology of depression. Nature *455*, 894-902.

Kuhlman, S.J., and Huang, Z.J. (2008). High-resolution labeling and functional manipulation of specific neuron types in mouse brain by Cre-activated viral gene expression. PLoS One *3*, e2005.

Kuner, R. (2010). Central mechanisms of pathological pain. Nat Med *16*, 1258-1266.

Kung, J.C., Chen, T.C., Shyu, B.C., Hsiao, S., and Huang, A.C. (2010). Anxiety- and depressive-like responses and c-fos activity in preproenkephalin knockout mice: oversensitivity hypothesis of enkephalin deficit-induced posttraumatic stress disorder. J Biomed Sci *17*, 29.

Kunitomo, H., Uesugi, H., Kohara, Y., and Iino, Y. (2005). Identification of ciliated sensory neuron-expressed genes in Caenorhabditis elegans using targeted pull-down of poly(A) tails. Genome Biol *6*, R17.

Lam, Y.W., and Sherman, S.M. Functional organization of the somatosensory cortical layer 6 feedback to the thalamus. Cereb Cortex *20*, 13-24.

Latagliata, E.C., Patrono, E., Puglisi-Allegra, S., and Ventura, R. (2010). Food seeking in spite of harmful consequences is under prefrontal cortical noradrenergic control. BMC Neurosci *11*, 15.

Lauth, M., Spreafico, F., Dethleffsen, K., and Meyer, M. (2002). Stable and efficient cassette exchange under non-selectable conditions by combined use of two site-specific recombinases. Nucleic Acids Res *30*, e115.

Lein, E.S., Hawrylycz, M.J., Ao, N., Ayres, M., Bensinger, A., Bernard, A., Boe, A.F., Boguski, M.S., Brockway, K.S., Byrnes, E.J., *et al.* (2007). Genome-wide atlas of gene expression in the adult mouse brain. Nature *445*, 168-176.

Livesey, F.J., and Cepko, C.L. (2001). Vertebrate neural cell-fate determination: lessons from the retina. Nat Rev Neurosci *2*, 109-118.

Llewellyn-Smith, I.J., Minson, J.B., Wright, A.P., and Hodgson, A.J. (1990). Cholera toxin B-gold, a retrograde tracer that can be used in light and electron microscopic immunocytochemical studies. J Comp Neurol *294*, 179-191.

Lopez-Aranda, M.F., Lopez-Tellez, J.F., Navarro-Lobato, I., Masmudi-Martin, M., Gutierrez, A., and Khan, Z.U. (2009). Role of layer 6 of V2 visual cortex in object-recognition memory. Science *325*, 87-89.

Lorente de No, R. (1933). Studies on the structure of the cerebral cortex. The area entorhinalis. . J Psychol Neurol *45*, 381-437.

Lorente de No, R. (1934). The cerebral cortex: Architecture, Intracortical connections and motor projections. In In: Physiology of the Nervous System (Oxford: Oxford University Press), pp. 291-339.

Lund, J.S., Lund, R.D., Hendrickson, A.E., Bunt, A.H., and Fuchs, A.F. (1975). The origin of efferent pathways from the primary visual cortex, area 17, of the macaque monkey as shown by retrograde transport of horseradish peroxidase. J Comp Neurol *164*, 287-303.

Luo, L., Callaway, E.M., and Svoboda, K. (2008). Genetic dissection of neural circuits. Neuron *57*, 634-660.

Luuk, H. (2009). Distribution and behavioral effects of Wfs1 in Central Nervous System. Ph.D. Dissertation.

Luuk, H., Koks, S., Plaas, M., Hannibal, J., Rehfeld, J.F., and Vasar, E. (2008). Distribution of Wfs1 protein in the central nervous system of the mouse and its relation to clinical symptoms of the Wolfram syndrome. J Comp Neurol *509*, 642-660.

Madisen, L., Zwingman, T.A., Sunkin, S.M., Oh, S.W., Zariwala, H.A., Gu, H., Ng, L.L., Palmiter, R.D., Hawrylycz, M.J., Jones, A.R., *et al.* (2010). A robust and high-throughput Cre reporting and characterization system for the whole mouse brain. Nat Neurosci *13*, 133-140.

Maeno, H., Yamada, K., Santo-Yamada, Y., Aoki, K., Sun, Y.J., Sato, E., Fukushima, T., Ogura, H., Araki, T., Kamichi, S., *et al.* (2004). Comparison of mice deficient in the high- or low-affinity neurotensin receptors, Ntsr1 or Ntsr2, reveals a novel function for Ntsr2 in thermal nociception. Brain Res *998*, 122-129.

Maere, S., Heymans, K., and Kuiper, M. (2005). BiNGO: a Cytoscape plugin to assess overrepresentation of gene ontology categories in biological networks. Bioinformatics *21*, 3448-3449.

Malkki, H.A., Donga, L.A., de Groot, S.E., Battaglia, F.P., and Pennartz, C.M. (2011). Towards mouse models of perseveration: A heritable component in extinction of operant behavior in fourteen standard and recombinant inbred mouse lines. Neurobiol Learn Mem.

Marin, O., and Rubenstein, J.L. (2001). A long, remarkable journey: tangential migration in the telencephalon. Nat Rev Neurosci *2*, 780-790.

Marmigere, F., and Ernfors, P. (2007). Specification and connectivity of neuronal subtypes in the sensory lineage. Nat Rev Neurosci *8*, 114-127.

McAlonan, K., Cavanaugh, J., and Wurtz, R.H. (2006). Attentional modulation of thalamic reticular neurons. J Neurosci *26*, 4444-4450.

Miyashita, T., Wintzer, M., Kurotani, T., Konishi, T., Ichinohe, N., and Rockland, K.S. Neurotrophin-3 is involved in the formation of apical dendritic bundles in cortical layer 2 of the rat. Cereb Cortex *20*, 229-240.

Molnar, Z., and Cheung, A.F. (2006). Towards the classification of subpopulations of layer V pyramidal projection neurons. Neurosci Res *55*, 105-115.

Mori, Y., Takada, N., Okada, T., Wakamori, M., Imoto, K., Wanifuchi, H., Oka, H., Oba, A., Ikenaka, K., and Kurosaki, T. (1998). Differential distribution of TRP Ca2+ channel isoforms in mouse brain. Neuroreport *9*, 507-515.

Mortazavi, A., Williams, B.A., McCue, K., Schaeffer, L., and Wold, B. (2008). Mapping and quantifying mammalian transcriptomes by RNA-Seq. Nat Methods *5*, 621-628.

Muir, J.L., Everitt, B.J., and Robbins, T.W. (1996). The cerebral cortex of the rat and visual attentional function: dissociable effects of mediofrontal, cingulate, anterior dorsolateral, and parietal cortex lesions on a five-choice serial reaction time task. Cereb Cortex *6*, 470-481.

Nickl-Jockschat, T., and Michel, T.M. The role of neurotrophic factors in autism. Mol Psychiatry *16*, 478-490.

Nickl-Jockschat, T., and Michel, T.M. (2011). The role of neurotrophic factors in autism. Mol Psychiatry *16*, 478-490.

Okaty, B.W., Sugino, K., and Nelson, S.B. (2011). A quantitative comparison of cell-type-specific microarray gene expression profiling methods in the mouse brain. PLoS One *6*, e16493.

Ostlund, S.B., and Balleine, B.W. (2007a). Orbitofrontal cortex mediates outcome encoding in Pavlovian but not instrumental conditioning. J Neurosci *27*, 4819-4825.

Ostlund, S.B., and Balleine, B.W. (2007b). The contribution of orbitofrontal cortex to action selection. Ann N Y Acad Sci *1121*, 174-192.

Pae, C.U., Marks, D.M., Han, C., Patkar, A.A., and Steffens, D. (2008). Does neurotropin-3 have a therapeutic implication in major depression? Int J Neurosci *118*, 1515-1522.

Parnavelas, J.G. (2000). The origin and migration of cortical neurones: new vistas. Trends Neurosci *23*, 126-131.

Paxinos, G., and Franklin, K.B.J. (2004). The mouse brain in stereotaxic coordinates, Compact 2nd edn (Amsterdam ; Boston: Elsevier Academic Press).

Paz, J.T., Chavez, M., Saillet, S., Deniau, J.M., and Charpier, S. (2007). Activity of ventral medial thalamic neurons during absence seizures and modulation of cortical paroxysms by the nigrothalamic pathway. J Neurosci *27*, 929-941.

Poo, M.M. (2001). Neurotrophins as synaptic modulators. Nat Rev Neurosci *2*, 24-32.

Quirk, G.J., Martinez, K.G., and Nazario Rodriguez, L.L. (2007). Translating findings from basic fear research to clinical psychiatry in Puerto Rico. P R Health Sci J *26*, 321-328.

Ragozzino, M.E., Detrick, S., and Kesner, R.P. (1999). Involvement of the prelimbic-infralimbic areas of the rodent prefrontal cortex in behavioral flexibility for place and response learning. J Neurosci *19*, 4585-4594.

Rakic, P. (1988). Specification of cerebral cortical areas. Science *241*, 170-176.

Rakic, P. (2009). Evolution of the neocortex: a perspective from developmental biology. Nat Rev Neurosci *10*, 724-735.

Ramon, Y.C. (1899). Histology of the nervous system of man and vertebrates (Editorial Moya, Madrid
).

Rash, B.G., and Grove, E.A. (2006). Area and layer patterning in the developing cerebral cortex. Curr Opin Neurobiol *16*, 25-34.

Raud, S., Sutt, S., Luuk, H., Plaas, M., Innos, J., Koks, S., and Vasar, E. (2009). Relation between increased anxiety and reduced expression of alpha1 and alpha2 subunits of GABA(A) receptors in Wfs1-deficient mice. Neurosci Lett *460*, 138-142.

Riggs, A.C., Bernal-Mizrachi, E., Ohsugi, M., Wasson, J., Fatrai, S., Welling, C., Murray, J., Schmidt, R.E., Herrera, P.L., and Permutt, M.A. (2005). Mice conditionally lacking the Wolfram gene in pancreatic islet beta cells exhibit diabetes as a result of enhanced endoplasmic reticulum stress and apoptosis. Diabetologia *48*, 2313-2321.

Rockland, K.S., and Pandya, D.N. (1979). Laminar origins and terminations of cortical connections of the occipital lobe in the rhesus monkey. Brain Res *179*, 3-20.

Romualdi, P., Bregola, G., Donatini, A., Capobianco, A., and Simonato, M. (1999a). Region-specific changes in prodynorphin mRNA and ir-dynorphin A levels after kindled seizures. J Mol Neurosci *13*, 69-75.

Romualdi, P., Donatini, A., Capobianco, A., and Ferri, S. (1999b). Methamphetamine alters prodynorphin gene expression and dynorphin A levels in rat hypothalamus. Eur J Pharmacol *365*, 183-186.

Rose, J.E., and Woolsey, C.N. (1949). The relations of thalamic connections, cellular structure and evocable electrical activity in the auditory region of the cat. J Comp Neurol *91*, 441-466.

Rossner, M.J., Hirrlinger, J., Wichert, S.P., Boehm, C., Newrzella, D., Hiemisch, H., Eisenhardt, G., Stuenkel, C., von Ahsen, O., and Nave, K.A. (2006). Global transcriptome analysis of genetically identified neurons in the adult cortex. J Neurosci *26*, 9956-9966.

Rushworth, M.F., and Behrens, T.E. (2008). Choice, uncertainty and value in prefrontal and cingulate cortex. Nat Neurosci *11*, 389-397.

Russo, S.J., Mazei-Robison, M.S., Ables, J.L., and Nestler, E.J. (2009). Neurotrophic factors and structural plasticity in addiction. Neuropharmacology *56 Suppl 1*, 73-82.

Santini, E., Quirk, G.J., and Porter, J.T. (2008). Fear conditioning and extinction differentially modify the intrinsic excitability of infralimbic neurons. J Neurosci *28*, 4028-4036.

Schnell, L., and Schwab, M.E. (1993). Sprouting and regeneration of lesioned corticospinal tract fibres in the adult rat spinal cord. Eur J Neurosci *5*, 1156-1171.

Segal, R.A. (2003). Selectivity in neurotrophin signaling: theme and variations. Annu Rev Neurosci *26*, 299-330.

Sharifi, N., Diehl, N., Yaswen, L., Brennan, M.B., and Hochgeschwender, U. (2001). Generation of dynorphin knockout mice. Brain Res Mol Brain Res *86*, 70-75.

Shepherd, G.M. (2004). The synaptic organization of the brain, 5th edn (Oxford ; New York: Oxford University Press).

Skinner, B.F. (1938). The behavior of organisms: an experimental analysis. . Oxford, England: Appleton-Century., 457.

Sotres-Bayon, F., Bush, D.E., and LeDoux, J.E. (2004). Emotional perseveration: an update on prefrontal-amygdala interactions in fear extinction. Learn Mem *11*, 525-535.

Steriade, M. (2001). Impact of network activities on neuronal properties in corticothalamic systems. J Neurophysiol *86*, 1-39.

Steriade, M. (2003). The corticothalamic system in sleep. Front Biosci *8*, d878-899.

Steriade, M., and Amzica, F. (1998). Coalescence of sleep rhythms and their chronology in corticothalamic networks. Sleep Res Online *1*, 1-10.

Steriade, M., Timofeev, I., and Grenier, F. (2001). Natural waking and sleep states: a view from inside neocortical neurons. J Neurophysiol *85*, 1969-1985.

Stucky, C.L., and Lewin, G.R. (1999). Isolectin B(4)-positive and -negative nociceptors are functionally distinct. J Neurosci *19*, 6497-6505.

Sturzebecher, A.S., Hu, J., Smith, E.S., Frahm, S., Santos-Torres, J., Kampfrath, B., Auer, S., Lewin, G.R., and Ibanez-Tallon, I. An in vivo tethered toxin approach for the cell-autonomous inactivation of voltage-gated sodium channel currents in nociceptors. J Physiol *588*, 1695-1707.

Sudhof, T.C. (2002). Synaptotagmins: why so many? J Biol Chem *277*, 7629-7632.

Sugino, K., Hempel, C.M., Miller, M.N., Hattox, A.M., Shapiro, P., Wu, C., Huang, Z.J., and Nelson, S.B. (2006). Molecular taxonomy of major neuronal classes in the adult mouse forebrain. Nat Neurosci *9*, 99-107.

Sur, M., and Leamey, C.A. (2001). Development and plasticity of cortical areas and networks. Nat Rev Neurosci *2*, 251-262.

Swift, M., and Swift, R.G. (2005). Wolframin mutations and hospitalization for psychiatric illness. Mol Psychiatry *10*, 799-803.

Swift, R.G., Sadler, D.B., and Swift, M. (1990). Psychiatric findings in Wolfram syndrome homozygotes. Lancet *336*, 667-669.

Takeda, K., Inoue, H., Tanizawa, Y., Matsuzaki, Y., Oba, J., Watanabe, Y., Shinoda, K., and Oka, Y. (2001). WFS1 (Wolfram syndrome 1) gene product: predominant subcellular localization to endoplasmic reticulum in cultured cells and neuronal expression in rat brain. Hum Mol Genet *10*, 477-484.

Takei, D., Ishihara, H., Yamaguchi, S., Yamada, T., Tamura, A., Katagiri, H., Maruyama, Y., and Oka, Y. (2006). WFS1 protein modulates the free Ca(2+) concentration in the endoplasmic reticulum. FEBS Lett *580*, 5635-5640.

Talbot, J.D., Marrett, S., Evans, A.C., Meyer, E., Bushnell, M.C., and Duncan, G.H. (1991). Multiple representations of pain in human cerebral cortex. Science *251*, 1355-1358.

Tan, E.M., Yamaguchi, Y., Horwitz, G.D., Gosgnach, S., Lein, E.S., Goulding, M., Albright, T.D., and Callaway, E.M. (2006). Selective and quickly reversible inactivation of mammalian neurons in vivo using the Drosophila allatostatin receptor. Neuron *51*, 157-170.

Thomson, A.M. (2010). Neocortical layer 6, a review. Front Neuroanat *4*, 13.
Thorndike, E. (1898). Some Experiments on Animal Intelligence. Science *7*, 818-824.

Topic, B., Huston, J.P., Namestkova, K., Zhu, S.W., Mohammed, A.H., and Schulz, D. (2008). Extinction-induced "despair" in aged and adult rats: links to neurotrophins in frontal cortex and hippocampus. Neurobiol Learn Mem *90*, 519-526.

Tsiola, A., Hamzei-Sichani, F., Peterlin, Z., and Yuste, R. (2003). Quantitative morphologic classification of layer 5 neurons from mouse primary visual cortex. J Comp Neurol *461*, 415-428.

Tuoc, T.C., and Stoykova, A. (2008). Er81 is a downstream target of Pax6 in cortical progenitors. BMC Dev Biol *8*, 23.

Uylings, H.B., Groenewegen, H.J., and Kolb, B. (2003). Do rats have a prefrontal cortex? Behav Brain Res *146*, 3-17.

Van De Werd, H.J., Rajkowska, G., Evers, P., and Uylings, H.B. (2010). Cytoarchitectonic and chemoarchitectonic characterization of the prefrontal cortical areas in the mouse. Brain Struct Funct *214*, 339-353.

Vanderschuren, L.J., and Everitt, B.J. (2004). Drug seeking becomes compulsive after prolonged cocaine self-administration. Science *305*, 1017-1019.

Veale, D.M., Sahakian, B.J., Owen, A.M., and Marks, I.M. (1996). Specific cognitive deficits in tests sensitive to frontal lobe dysfunction in obsessive-compulsive disorder. Psychol Med *26*, 1261-1269.

Wang, C.C., and Shyu, B.C. (2004). Differential projections from the mediodorsal and centrolateral thalamic nuclei to the frontal cortex in rats. Brain Res *995*, 226-235.

Wang, Z., Gerstein, M., and Snyder, M. (2009). RNA-Seq: a revolutionary tool for transcriptomics. Nat Rev Genet *10*, 57-63.

Warner-Schmidt, J.L., Chen, E.Y., Zhang, X., Marshall, J.J., Morozov, A., Svenningsson, P., and Greengard, P. A role for p11 in the antidepressant action of brain-derived neurotrophic factor. Biol Psychiatry *68*, 528-535.

Wickersham, I.R., Sullivan, H.A., and Seung, H.S. Production of glycoprotein-deleted rabies viruses for monosynaptic tracing and high-level gene expression in neurons. Nat Protoc *5*, 595-606.

Worgotter, F., Eyding, D., Macklis, J.D., and Funke, K. (2002). The influence of the corticothalamic projection on responses in thalamus and cortex. Philos Trans R Soc Lond B Biol Sci *357*, 1823-1834.

Xu, H., Wu, L.J., Wang, H., Zhang, X., Vadakkan, K.I., Kim, S.S., Steenland, H.W., and Zhuo, M. (2008). Presynaptic and postsynaptic amplifications of neuropathic pain in the anterior cingulate cortex. J Neurosci *28*, 7445-7453.

Xuei, X., Flury-Wetherill, L., Almasy, L., Bierut, L., Tischfield, J., Schuckit, M., Nurnberger, J.I., Jr., Foroud, T., and Edenberg, H.J. (2008). Association analysis of genes encoding the nociceptin receptor (OPRL1) and its endogenous ligand (PNOC) with alcohol or illicit drug dependence. Addict Biol *13*, 80-87.

Yamada, T., Ishihara, H., Tamura, A., Takahashi, R., Yamaguchi, S., Takei, D., Tokita, A., Satake, C., Tashiro, F., Katagiri, H.*, et al.* (2006). WFS1-deficiency increases endoplasmic reticulum stress, impairs cell cycle progression and triggers the apoptotic pathway specifically in pancreatic beta-cells. Hum Mol Genet *15*, 1600-1609.

Yang, X.W., Model, P., and Heintz, N. (1997). Homologous recombination based modification in Escherichia coli and germline transmission in transgenic mice of a bacterial artificial chromosome. Nat Biotechnol *15*, 859-865.

Yoneshima, H., Yamasaki, S., Voelker, C.C., Molnar, Z., Christophe, E., Audinat, E., Takemoto, M., Nishiwaki, M., Tsuji, S., Fujita, I., and Yamamoto, N. (2006). Er81 is expressed in a subpopulation of layer 5 neurons in rodent and primate neocortices. Neuroscience *137*, 401-412.

Zambrowicz, B.P., Imamoto, A., Fiering, S., Herzenberg, L.A., Kerr, W.G., and Soriano, P. (1997). Disruption of overlapping transcripts in the ROSA beta geo 26 gene trap strain leads to widespread expression of beta-galactosidase in mouse embryos and hematopoietic cells. Proc Natl Acad Sci U S A *94*, 3789-3794.

Zanetti, M.E., Chang, I.F., Gong, F., Galbraith, D.W., and Bailey-Serres, J. (2005). Immunopurification of polyribosomal complexes of Arabidopsis for global analysis of gene expression. Plant Physiol *138*, 624-635.

Zatyka, M., Ricketts, C., da Silva Xavier, G., Minton, J., Fenton, S., Hofmann-Thiel, S., Rutter, G.A., and Barrett, T.G. (2008). Sodium-potassium ATPase 1 subunit is a molecular partner of Wolframin, an endoplasmic reticulum protein involved in ER stress. Hum Mol Genet *17*, 190-200.

Zhang, F., Prigge, M., Beyriere, F., Tsunoda, S.P., Mattis, J., Yizhar, O., Hegemann, P., and Deisseroth, K. (2008). Red-shifted optogenetic excitation: a tool for fast neural control derived from Volvox carteri. Nat Neurosci *11*, 631-633.

Zhang, F., Wang, L.P., Boyden, E.S., and Deisseroth, K. (2006). Channelrhodopsin-2 and optical control of excitable cells. Nat Methods *3*, 785-792.

Zhang, Y., Lang, Q., Li, J., Xie, F., Wan, B., and Yu, L. Identification and characterization of human LYPD6, a new member of the Ly-6 superfamily. Mol Biol Rep *37*, 2055-2062.

Zhang, Z.W., and Deschenes, M. (1997). Intracortical axonal projections of lamina VI cells of the primary somatosensory cortex in the rat: a single-cell labeling study. J Neurosci *17*, 6365-6379.

Zhou, Q., and Anderson, D.J. (2002). The bHLH transcription factors OLIG2 and OLIG1 couple neuronal and glial subtype specification. Cell *109*, 61-73.